Novel ultrasound-assisted electrodeposited Ni-based coatings for bearing applications

Tudela-Montes, Ignacio

Award date:
2015

Awarding institution:
Coventry University

Novel ultrasound-assisted electrodeposited Ni-based coatings for bearing applications

By

Ignacio José Tudela Montés

PhD

May 2015

Novel ultrasound-assisted electrodeposited Ni-based coatings for bearing applications

By

Ignacio José Tudela Montés

May 2015

A thesis submitted in partial fulfilment of the University's requirements for the Degree of Doctor of Philosophy

To my parents, to whom I owe who I am

To José, to whom I owe the passion I have for research

To Maje, to whom I owe this thesis

Science is like sex: sometimes something useful comes out, but that is not the reason we are doing it

Attributed to Prof Richard Feynman

If only there was as much science in politics as there is politics in science

Read in Prof Frank C. Walsh's PhD thesis, Loughborough University, 1981

ABSTRACT

The purpose of the present PhD research project was to evaluate the feasibility of the electrodeposition of novel thin Ni composite coatings with lubricant particles from an additive-free Watts bath and their application as diffusion barrier layers in journal bearings for medium-speed diesel engines. Overall, the main objective was to develop thin Ni composite coatings with the following characteristics:

- Improved tribological performance.
- Good adhesion properties.
- Good 'anti-diffusion' performance.

Ultrasound was used in the preparation of pure Ni coatings and Ni composite coatings with lubricant particles under different conditions in order to understand how ultrasonic cavitation influences electrodeposition and characteristics of said Ni-based coatings. Two main studies were conducted related to this:

1. Study of the effect of ultrasonic power on the electrodeposition of pure Ni coatings to understand the influence of cavitation phenomena near the surface of the cathode on the properties of Ni deposits
2. Study of the effect of ultrasound on the production of Ni composite coatings to understand the influence of ultrasound in the dispersion of particles, the electrodeposition of Ni composite coatings and the properties of said Ni composite coatings.

The influence of ultrasound on the dispersion of particles in the Watts bath was evaluated by observing the visual appearance of the resulting dispersions and analysing the particle size distribution of diluted solutions by laser diffraction-based particle sizing methods. The effect of ultrasound on the characteristics of Ni deposits and Ni composite coatings electrodeposited from the additive-free Watts bath was evaluated by different material characterization techniques:

- X-Ray Diffraction (XRD) analysis was employed to observe the orientation of the Ni crystals that formed the coatings.
- Field Ion Beam – Scanning Electron Microscopy (FIB-SEM) was employed to analyse the surface morphology and microstructure of the coatings.
- Microhardness tests were performed to observe how the modification of the grain structure and the presence of particles may affect the hardness of the coatings.
- Glow Discharge – Optical Emission Spectroscopy (GD-OES) was also employed to estimate the particle content in the Ni composite coatings.

Pure Ni deposits and selected Ni/hBN and Ni/WS_2 composite coatings electrodeposited under ultrasound that exhibited promising features (e.g. more fragmented/refined structure, reasonable incorporation of uniformly-distributed particles, etc.) were selected for further tribological analysis. Scratch tests performed on these coatings under lubricated (mixed-film/boundary lubrication) and non-lubricated (dry boundary lubrication) conditions showed that the Ni/WS_2 composite coatings were the only newly developed Ni-based coating that exhibited enhanced tribological performance when compared with benchmark Ni coatings.

Finally, the performance of these novel Ni/WS_2 composite coatings with enhanced tribological performance acting as diffusion barrier layers in real bearing overlay systems was studied:

- In terms of adhesion, similar loads before bonding failure were measured for both Ni/WS_2 composite coating and the benchmark Ni deposit. No de-attachment was observed between the bronze lining and both diffusion barrier layers, and the bonding failure occurred mostly between the glue and the Sn-Cu overlay and within the Sn-Cu overlay.
- In terms of diffusion, an overall increase in diffusion phenomena (e.g. formation of intermetallic layer, reduction in thickness of the diffusion barrier layer, etc.) was

observed for the Ni/WS_2 composite coating when compared with the benchmark Ni deposit.

The overall increase in diffusion phenomena here reported for the novel Ni/WS_2 composite coatings with enhanced tribological performance may imply the unsuitability of said coatings for their use as diffusion barrier layers in plain bearings. Nevertheless, the growth rate and nature of the intermetallic layer formed in the bearing overlay system with the Ni/WS_2 diffusion barrier layer, along with the enhanced tribological performance of said composite coating, may open new possibilities in bearing overlay development where functional intermetallic phases are sought for different bearing applications.

Keywords: Nickel, composite coatings, lubricant particles, electrodeposition, Watts bath, bearings, tribology, diffusion.

ACKNOWLEDGEMENTS

I wish to express my deepest gratitude to my Director of Studies, Dr Andrew J. Cobley, and my Supervisors Dr John E. Graves and Dr Larisa Paniwnyk, for their guidance and assistance throughout the course of the investigation, and to Daido Metal and the 'Knowledge Transfer Partnership' scheme for providing the financial support for this research project.

Much of the work included in this thesis is owed to my Industrial Supervisor, Dr Yi Zhang, for his outstanding help and formal discussions during all these years, and for his loyal friendship in-and-out of the laboratory. I am also indebted to Mr Madan Pal and Mr Ian Kerr for their assistance and support, and to Mrs Grazina Burmistroviene and Mr Chris Howard for their technical aid. And I should also note the 'moral' support of Elena Banchelli, Dr Rolandas Verbickas, Dr Mayank Anand and Mr Guy Lowman. They made me feel part of the family that the Daido Metal EHQ R&D Department is, and that is far more than the highest expectation I had when I decided to commence this journey.

I want to acknowledge the contribution of Dr M. Lesley Wears (University of Exeter) and Dr Geoff West (Loughborough University) for their assistance with XRD and FIB-SEM analysis, respectively. I would also like to thank Prof Andreas Bund for inviting me to visit his research group at Technische Universität Ilmenau, where I have the pleasure to work with Dr Magali Camargo and Dr Rolf Griesler on characterizing some of the coatings developed during the present research project (GD-OES data included in the present thesis was obtained there with the assistance of Mr Markus Wilke). Much of the discussion regarding the preferred orientation of electrodeposited Ni is the result of the stimulating brainstorming talks I had with Magali and Rolf.

I need to acknowledge Maje for all her love, support and patience during all this time, especially in those weekends where I would remain absent in my own world, reading and writing this thesis, and my parents (Pedro and María Teresa), brother (Carlos) and sister

(Mariate), friends (David, Jorge, Pepan, Carlos, Pica, Pak, Mora, Juan Carlos…) and family for their constant encouragement during the research project… and their trips to UK!!

I also want to thank the late Dr José González-García and the rest of the people I worked with at the University of Alicante (Dr Pedro Bonete, Miss Verónica Sáez, Dr María Deseada Esclapez, Miss María Isabel Díez García, Dr Olivier Louisnard, Miss Bérénice Guinchard, Dr Angel Frías-Ferrer, Dr Teresa Lana Villarreal, Dr Roberto Gómez Torregrosa, etc.) for all the good times we all shared in Alicante, and for sharing with me their love for Electrochemistry, Acoustics and Science in general.

And finally, I thank my good friend Dr Néstor Guijarro-Carratalá for helping me with 'a few things' and for all the 'skyping' during all these years. Literature searching and thesis writing would be a lot less amusing, this thesis would *lack of scientific content* and papers would be less *elegant* without his friendship.

TABLE OF CONTENTS

List of Acronyms

AE ..... Acoustic Emission

BSE ..... Back-Scattered Electrons

CoF ..... Coefficient of Friction

CTAB ..... Cetyl Trimethyl Ammonium Bromide

D50 ..... median particle size

D90 ..... 90th percentile of the particle size

DIBE ..... Daido Industrial Bearings Europe

EBSD ..... Electron Back-Scattered Diffraction

EDS ..... Energy-Dispersive X-ray Spectroscopy

FEG-SEM ..... Field-Emission Gun– Scanning Electron Microscopy

FIB-SEM ..... Field Ion Beam – Scanning Electron Microscopy

GD-OES ..... Glow-Discharge Optical Emission Spectroscopy

hBN ..... hexagonal BN

HPB ..... Hexadecyl Pyridinium Bromide

PTFE ..... Polytetrafluoroethylene

RI ..... Refractive Index

RTC ..... Relative Texture Coefficient

SDS ..... Sodium Dodecyl Sulphate

SE ..... Secondary Electrons

SEM ..... Scanning Electron Microscope

XRD ..... X-Ray Diffraction

1. INTRODUCTION

1.1. CONTEXT OF THE RESEARCH PROJECT

This PhD project focused on the development of novel electroplated composite coatings and their potential applicability in bronze-based, multi-layer materials for bearing applications. Such materials are widely found in most of the bearings manufactured by Daido Industrial Bearing Europe Ltd. (DIBE), Coventry University's industrial partner in the present research project. DIBE, based in Ilminster, Somerset, manufactures plain and thrust bearings and bushings for medium-speed diesel engines such as those employed in the marine industry, and also for turbochargers and other industrial engines.

1.2. BEARINGS IN INTERNAL COMBUSTION ENGINES

1.2.1. INTRODUCTION

A bearing may be defined as *'a support or guide which at the same time allows relative movement to take place between two bodies'* [1]. Bearings are therefore critical components of internal combustion engines [2]. As mentioned by Kerr, *'without them, there is no relative motion between components, no transmission of forces and no power generation or conversion'* [3]. In any internal combustion engine, the most important bearings are those placed in the engine housing ('main' bearings) which allow the axial rotation of the crankshaft and those between the connecting rod, and crankshaft ('big-end' bearings) which are the ones responsible for translation of the up and down movement of the piston into the rotational motion of the crankshaft of the engine [4]. Both main and big-end bearings bear the load from the combustion process and inertial loads from the rotation of crankshaft. Nevertheless, more bearing elements are found in an engine such as piston-pin bushes or thrust washers, as shown in Figure 1.1 [5].

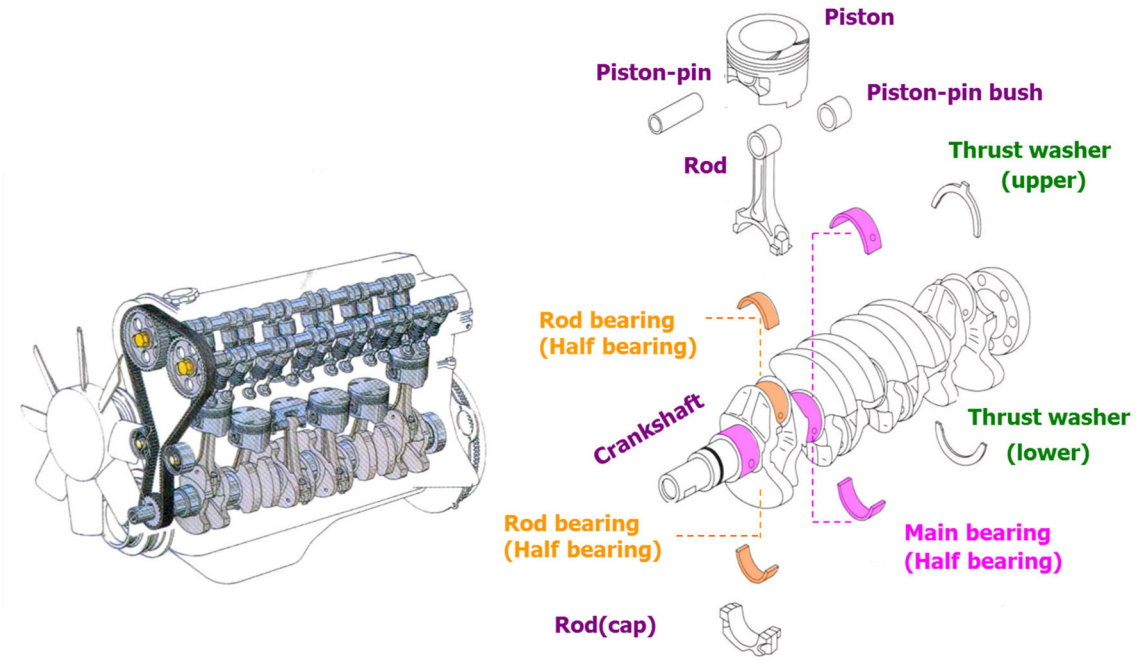

Figure 1.1. Diagram of an automotive engine showing different types of bearings. Adapted from [5].

A bearing system usually involves three different components: two sliding surfaces (e.g. those of the bearing and the crankshaft) and the lubricant between them. The resulting system is quite complex, as several interactions (Figure 1.2) are set between the different bearing components and the environment within which the bearing works [6]. When facing the design of a bearing system, the specifications of each component, not only the bearing, but also the crankshaft and the lubricant, must be evaluated as the surface of the crankshaft, the lubricant and even the working environment influence the performance of the bearing.

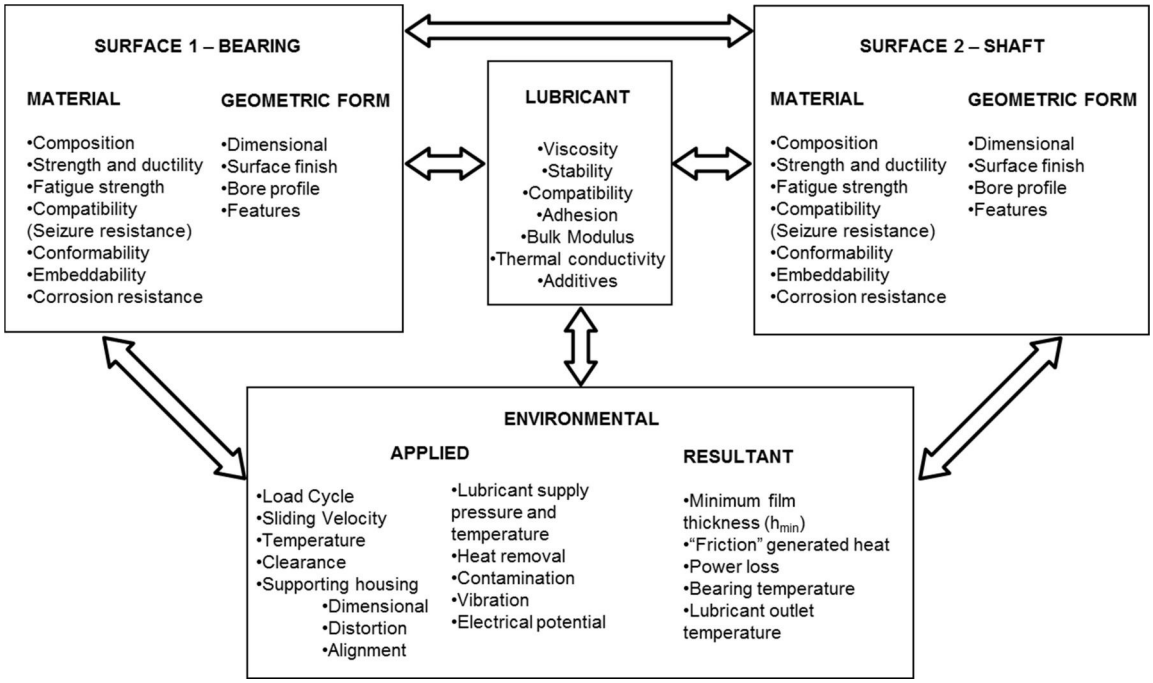

Figure 1.2. Interactions between components and environment in a bearing system. Adapted from [6].

1.2.2. BEARING DESIGN

Main and big-end bearings in internal combustion engines are generally designed to operate under 'hydrodynamic' lubrication where the surface of both the crankshaft and the bearings are fully separated by a lubricant film [7]. Regarding the bearing itself, its performance is mainly influenced by its material and geometry [1]. The materials used for bearing applications must not only be soft enough to give conformability, embeddability, and seizure resistance [8], but also strong enough to resist wear, fatigue, and cavitation [9]. As some of these requirements may conflict, a compromise between them is required when facing the

task of designing a bearing [10]. Hence, there is not a universal bearing material that completely satisfies all bearing applications [3]. The geometry is also crucial in the performance of a bearing, and depending on the application, it can be very complex as many variables and parameters such as the wall thickness, length and height, the lug or the oil hole and oil groove influence the working behaviour [4]. A good example of this could be the oil hole and oil groove in a half-shell bearing such as those used as main bearings or connection rod bearings in any internal combustion engine (Figure 1.3). The oil hole enables the introduction of lubricant into the bearing system, while the oil groove improves the distribution of the lubricant and the formation of the lubricant film between the bearing and the crankshaft. The required lubrication and the engine specifications determine the location, shape and dimensions of both the hole and groove, and the design must not only assure the proper lubrication of the bearing system, but also allow the oil to pass to other sections of the bearing [4].

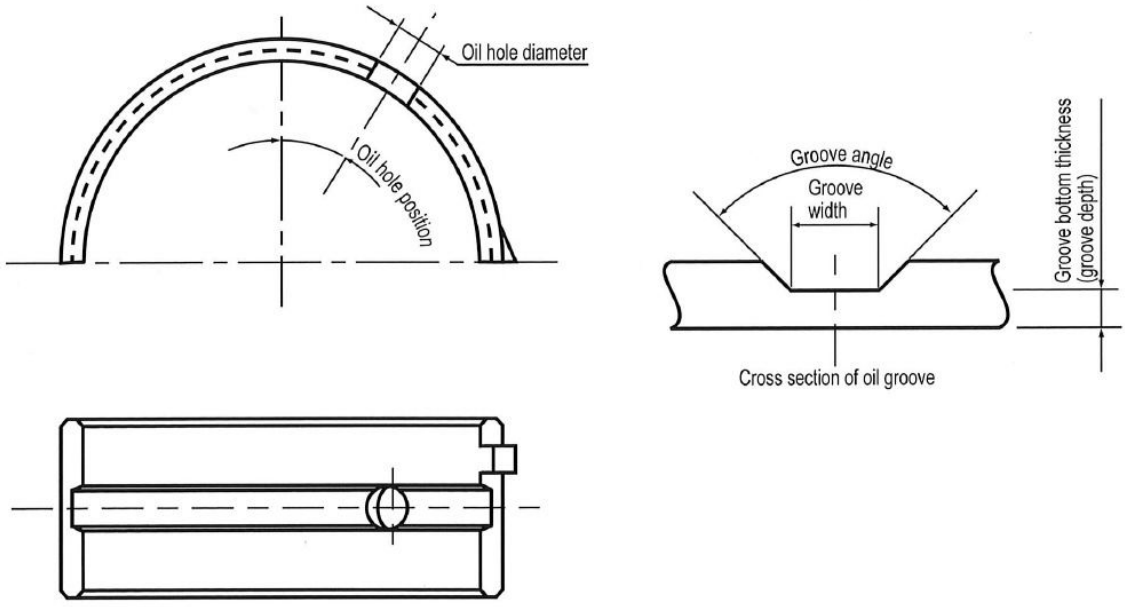

Figure 1.3. Definition of oil hole and oil groove in a half-shell bearing. Adapted from [4].

1.3. BEARING MATERIALS

Two main types of multilayer materials are employed in half-shell bearings such as those acting as main or big-end bearings in internal combustion engines [11]. These are two-layer materials, which are mainly Al-based materials, and three-layer materials, which consist of Cu/bronze-based alloys in most cases (Figure 1.4). The bearing material is commonly supported on a steel backing body in both cases, giving a solid fit and stability to the bearing. While Al-based bearings are mainly used in petrol combustion engines in the automotive market, bronze-based bearings are mainly designed for high load applications, mainly diesel engines in both automotive and industrial/marine markets.

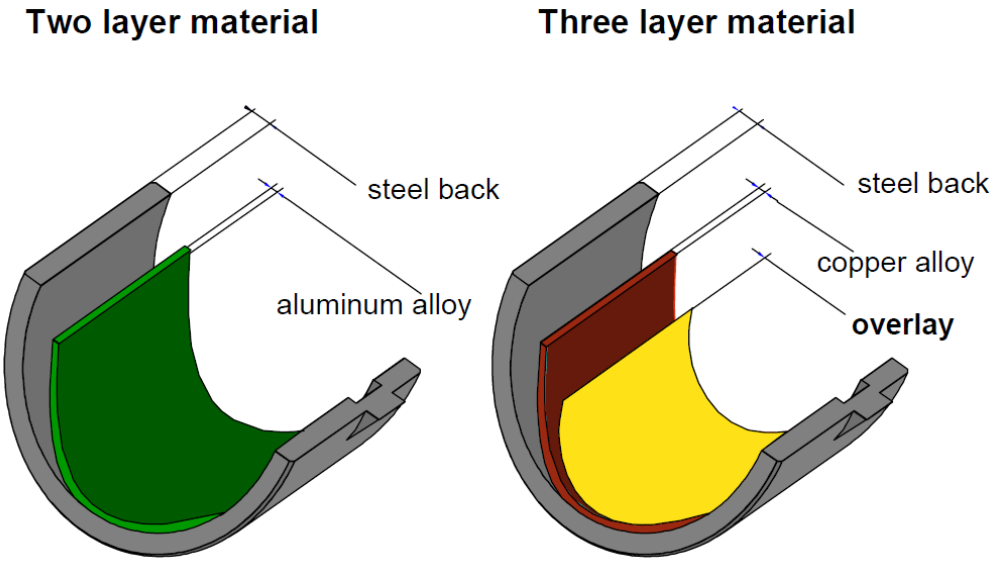

Figure 1.4. Layer construction of engine bearing materials. Adapted from [11].

1.3.1. BRONZE-BASED BEARING MATERIALS

Sintered or cast bronze is the most basic material for bearing applications (Figure 1.5 A). It has a long history as a bearing material [12] and it is still used in different applications (e.g. small-end bush bearings in the automotive market). Pb-bronze alloys have also been employed for a long time [13]. The addition of Pb (Figure 1.5 B) to bronze improves the seizure performance of the bearing. Such material is currently employed for bush bearings in different low load applications. As previously mentioned, a steel backing [14] is employed

to support the Pb-bronze lining (Figure 1.5 C), which not only gives additional strength and stiffness to the material, but also results in a decrease in the cost of the bearing due to the lower price of steel. Such material combination is currently employed in some types of thrust washer bearings.

It is worth mentioning, at this stage, some of the findings of Bowden and Tabor on the friction properties of Pb-Cu alloys such as those used for bearing applications [15]. They noticed that the friction of a Pb-Cu alloy was the same as that of a Cu surface on which a thin Pb film had been deposited. Their results supported the hypothesis that, in Pb-bronze alloys used for bearing applications, the anti-frictional and anti-seizure properties are mainly due to the spreading of thin films of Pb, which is softer and has a lower melting point, over the surface of the bronze lining (Figure 1.5 D). This observation was extremely significant, as it backed the development of Pb-based films electrodeposited on top of the bronze lining.

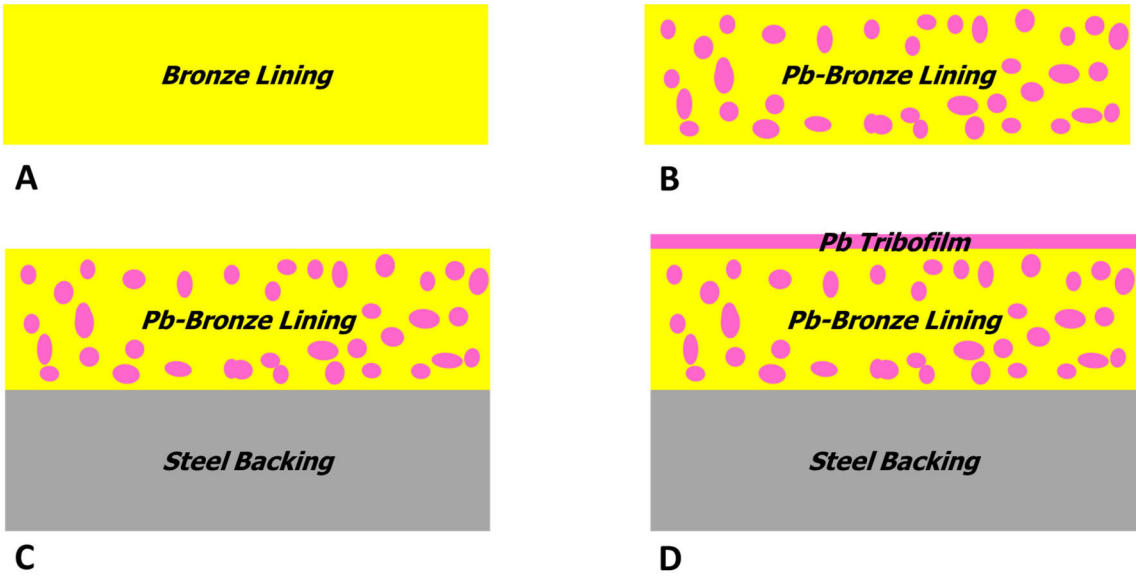

Figure 1.5. Evolution of basic bronze bearing materials: (A) bronze lining, (B) Pb-bronze lining, (C) Pb-bronze lining supported on steel, and (D) Pb-bronze lining supported on steel with a lead film formed on top. Adapted from [3].

1.3.2. Pb-based overlays for bronze-based bearing materials

Electroplated Pb-based overlays containing Sn have been applied to bronze bearings for many years [16,17]. In spite of its environmental toxicity, Pb is still widely used in bearings for large engines due to its good seizure resistance and lubrication properties [18]. Sn presents good compatibility and higher corrosion resistance to oil components and impurities than Pb [19], the latter being the main reason for its addition to electroplated Pb overlays. A minimum of 3% by weight of Sn is enough to improve the corrosion resistance of Pb overlays to oil and its additives/impurities [20]. Pb-Sn overlays (Figure 1.6 A) also enhance the embeddability and conformability of the bearings due to the soft nature of Sn and Pb, and they are currently used in half-shell bearings for medium/low load applications in medium-speed diesel engines.

One of the main issues of the use of Pb-Sn overlays is the partial loss of the Sn present in the overlay by diffusion into the substrate, leading to the formation and growth of Sn-Cu intermetallic compounds such as Cu_3Sn [21,22], which are commonly found in bronze-based bearings also containing Sn [11]. The formation of these intermetallic compounds in solder joints on electronic applications have been intensively studied due to their brittle nature [23,24] and the adhesion issues that may occur when these intermetallic layers form between the Sn coating and the copper substrate [25]. In addition, the loss in Sn content in the overlay due to its migration makes the overlay prone to oil corrosion if the Sn level falls below the 3% limit [1]. To minimize both issues, a Ni diffusion barrier layer [26] may be added between the lining and the Pb-Sn overlay (Figure 1.6 B), drastically reducing the diffusion of Sn from the overlay and minimising the formation and growth of undesired intermetallic compounds, mainly Cu_3Sn [1].

The incorporation of Cu to the Pb-Sn overlay (Figure 1.6 C) not only improves both the fatigue and wear resistance of the bearing, but also its anti-corrosion properties, as the Sn loss by diffusion is lower due to the formation of Sn-Cu intermetallic compounds within the

overlay [1]. Pb-Sn-Cu alloys are not only stronger than Pb-Sn alloys (e.g. the addition of 3% of Cu in the overlay would give, for a specific bearing load, a five times longer life to fatigue failure than that of the Pb-Sn overlay [27]), but also present a higher resistance to seizure [28]. Pb-Sn-Cu overlays are currently employed in moderately high load applications in markets where Pb has not been banned yet. Further addition of In to the Pb-Sn-Cu overlay (Figure 1.6 D) enhances the fatigue and wear resistance of the bearings [29]. Such Pb-Sn-In-Cu alloy is currently used in half shell bearings for engines in very high load applications where the resistance to fatigue is critical.

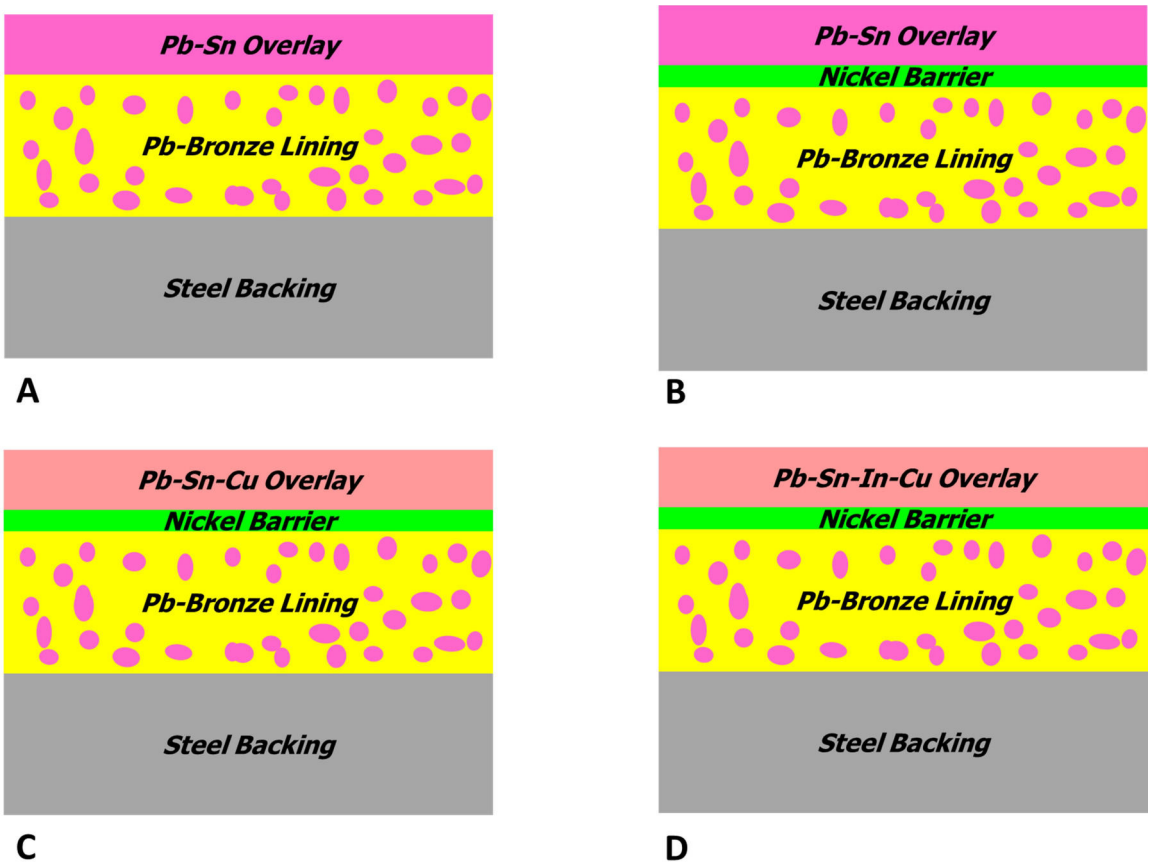

Figure 1.6. Evolution of Pb-based overlays electrodeposited on bronze-based bearing materials: (A) Pb-Sn overlay, (B) Pb-Sn overlay with a Ni interlayer, (C) addition of Cu to the Pb-Sn overlay, and (D) addition of In to the Pb-Sn-Cu overlay. Adapted from [3].

1.3.3. Sn-based overlays for bronze-based bearing materials

Sn-based materials have been used in bearing applications for many years, especially since Babbitt patented his famous Sn-Sb-Cu alloy for journal boxes more than 150 years ago [30].

Although the so-called Babbitt metals have therefore been well-known for a long time, the interest in these materials for bearing applications has grown in the last twenty years due to current needs to decrease the environmental impact of internal combustion engines. The release of harmful and toxic chemicals and materials into the environment is a major concern, not only from the combustion of the fuel in the engine [31], but also from the components of the engine itself [32]. This implies the removal of Pb as an overlay material for bearing applications and the urge to develop Pb-free overlay materials with lower toxicity and impact in the environment. Among other alternatives, Sn-based overlays with a small portion of Cu (Figure 1.7 A) have emerged as a good option for medium-speed diesel engines due to their good fatigue, wear, seizure and hydrodynamic cavitation resistance. However, Sn-based materials are prone to the formation of different intermetallic compounds, including brittle Cu_3Sn. These intermetallic structures tend to migrate towards the Sn-Cu-Ni intermetallic layer that forms between the overlay and the Ni diffusion barrier layer. The incorporation of a second Sn-Cu layer between the diffusion barrier layer and the Sn-Cu overlay (Figure 1.7 B) with higher Cu content retards such issues [33].

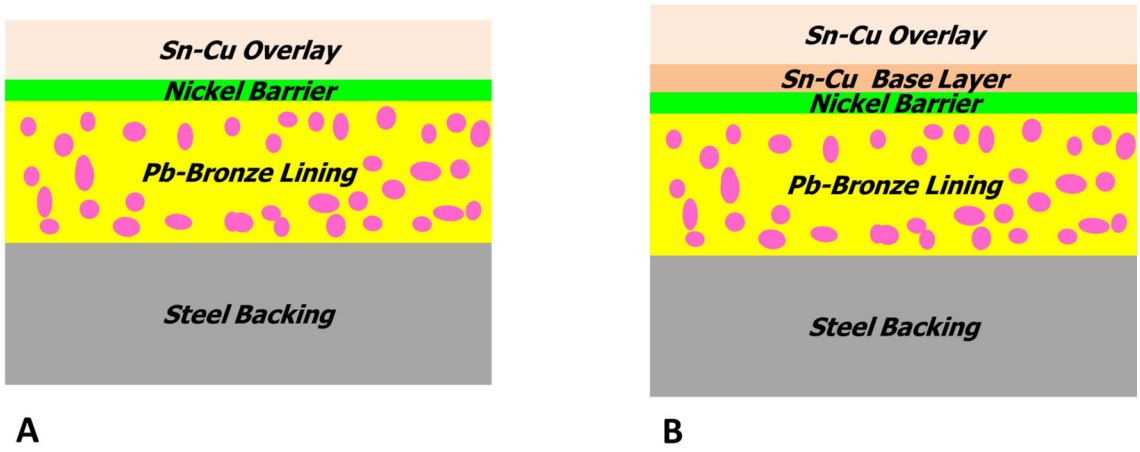

Figure 1.7. Pb-free, Sn-based overlays electrodeposited on bronze-based bearing materials: (A) Sn-Cu overlay, (B) Sn-Cu multilayer system. Adapted from [3].

1.4. NEED FOR IMPROVED NI-BASED BARRIER LAYERS IN BEARINGS

In modern engines, bearing specific loads and the intensity of fatigue loads are increasing as more power is obtained from ever smaller and lighter engines. Thinner viscosity lubricants are more often used in order to achieve greater efficiency by reducing parasitic losses from engine components, resulting in thinner oil films which may cause bearings to run under 'mixed-film' lubrication (sliding contacting bodies, i.e. crankshaft and bearing, are supported on a combination of asperity-asperity contact points and fluid regions between asperities [34]) and 'boundary' lubrication (asperity-asperity contact points become the main part of the load supporting system [35]). Combining this with other factors (e.g. engine downsizing) creates arduous conditions under which bearings must operate, causing in some cases the local loss and removal of the overlay by wear, corrosion or other mechanisms, resulting in the exposure of the Ni diffusion barrier layer. If the Ni diffusion barrier layer is exposed to the running crankshaft during operation of the bearing by wear, corrosion or other mechanisms, it may lead to the seizure of a bearing due to the poor tribological performance of Ni against steel crankshafts [36].

1.5. OBJECTIVES OF THE RESEARCH PROJECT

The aim of this PhD project was to study the feasibility of the electrodeposition of Ni composite coatings with embedded lubricant particles from a Ni Watts bath currently employed in DIBE's manufacturing line. The main goal was to develop Ni composite coatings to be used as diffusion barrier layers in journal bearings with the next properties:

- Enhanced tribological performance and resistance to seizure in those cases where the diffusion barrier may become tribologically active due to localised removal of the overlay.

- Good adhesion between the bronze lining and the thin Ni composite coating electrodeposited over the bronze lining, and between the thin Ni composite coating and the Sn-Cu overlay electrodeposited on top of the Ni composite coating.
- Good resistance to diffusion to prevent the loss of Cu from the Sn-Cu overlay and the formation of brittle SnCu intermetallic compounds that would lead to the failure of the bearing in the engine.

A fine and uniform dispersion of the particles in both the electroplating solutions and the deposits must be achieved to make Ni-based composite coatings suitable for this application, as the formation and co-deposition of large agglomerated particles may not only lead to an inefficient effect of the particles in the coating, but also to an eventual seizure of the coating. In order to achieve a uniform distribution of finely dispersed particles in the coating, ultrasound is used to prevent the agglomeration of particles and the incorporation of aggregates into the coating.

Based on this, the contents of this PhD thesis have been structured as follows:

- Recent developments in the manufacturing of Ni diffusion barrier layers with particles and the electrodeposition of Ni and Ni composite coatings from Watts bath formulations have been thoroughly reviewed in Chapter 2. This chapter also includes the use of ultrasound in electroplating in general and the electrodeposition of Ni composite coatings in particular.
- The experimental methodology followed to carry out the research here presented is included in Chapter 3. This chapter includes all the information related to the 'wet chemistry' experiments, the characterisation of the Ni-based coatings produced, the evaluation of selected Ni-based coatings acting as tribologically active layers, and the final evaluation of the novel Ni/WS_2 composite coating acting as a diffusion barrier layer in a bearing overlay coating system.

- The study of the effect of ultrasound on the electrodeposition of Ni from the Watts bath is included in Chapter 4. Specifically, this chapter is focused on the effect of ultrasonic power on the characteristics of Ni deposits.
- The study of the effect of ultrasound on the electrodeposition of Ni composite coatings with lubricant particles is included in Chapter 5. This chapter shows how the best conditions in terms of dispersing particles may not be good enough when electrodepositing the composite coatings. The characterization of the most promising Ni composite coatings is also included in this chapter.
- The study of the tribological performance of selected Ni deposits and Ni composite coatings is included in Chapter 6, showing that Ni/WS_2 was the only composite coating that exhibited a much better performance that the benchmark Ni coating under both lubricated and non-lubricated conditions.
- The evaluation of the performance of Ni/WS_2 diffusion barrier layers in bearing overlay systems is included in Chapter 7. This chapter consists of two main parts: (i) adhesion studies, and (ii) diffusion studies.
- Chapter 8 is a brief recapitulation of the main results, discussions and conclusions included in this thesis. This final chapter also described current and future lines of work related to the research here presented.
- Different appendices have been also included with more detailed information regarding some of the experimental procedures, as well as the list of publications and conference presentations prepared as a direct outcome of this PhD project.

1.7. REFERENCES

[1] C. Evans, J.F. Warriner, Bearings and bearing metals, in: R. Baranescu, B. Challen (Eds.), Diesel engine reference book, 2nd ed., Butterworth-Heinemann Ltd, Oxford, 1999.

[2] M. Pal, Advances in plain bearing technology for better fuel efficiency – does experience in the automotive market translate to the large engine market?, 4th CIMAC Cascades, March 2014.

[3] I. Kerr, Plain bearing condition – A barometer of engine health, Bearing service experience & material development (The first 100 years), Seminar at the Royal Institution of Naval Architects, February 2012.

[4] T. Shibayama, Y. Okamoto, A. Kimura, A. Okabe, N. Mabuchi, T. Egami, S. Asai, J. Onoue, T. Katagiri, Book of engineering data required to design plain bearings for automobile engines, 4th ed., Daido Metal, Nagoya, 2002.

[5] I. Kerr, Bearing technologies for automotive engines, Seminar at Loughborough University, November 2011.

[6] A. Hill, Trans. Inst. Mar. Eng. 88 (1976) 204.

[7] A. Kapoor, S.C. Tung, S.E. Schwartz, M. Priest, R.S. Dwyer-Joyce, Automotive Tribology, in: B. Bhushan (Ed.), Modern Tribology Handbook, CRC Press, Boca Raton-London-New York-Washington D.C., 2000.

[8] I.D. Massey, N.A. MacQuarrie, N.F. Coston, D.R. Eastham, Tribology S. 18 (1991) 43.

[9] W.P. Brown, M. Scott, J.F. Warriner, Development of a bi-metal bearing alloy for medium speed diesel engines, 21st International Congress on Combustion Engines, Interlaken, Switzerland, June 1995. Paper CIMA/CIMA/1995/001/21D74.

[10] J.A. Charles, F.A.A. Crane, J.A.G. Furness, Selection and use of engineering materials, 3rd ed., Reed Elsevier plc group, Oxford-Auckland-Boston-Johannesburg-Melbourne-New Delhi, 1997.

[11] A. Adam, G. Andler, G. Arnold, The progression of engine bearing overlays, SAE World Congress, Detroit, March 2002. Paper 2002-01-1316.

[12] A. Baker, The component contribution: Engine progress through the specialist manufacturers, Hutchinson Benham Ltd, London, 1979.

[13] S. Doubleday, US patent 160885, 1875.

[14] R.D. Pike, E.W. Carroll, US patent 1870867, 1932.

[15] F. P. Bowden, D. Tabor, The friction and lubrication of solids, Clarendon Press, Oxford, 1950.

[16] R. Schaefer, J. B. Mohler, US patent 2461350, 1949.

[17] W.H. Tait, GB patent 660904, 1951

[18] I. Kerr, M. Priest, Y. Okamoto, M. Fujita, P. I. Mech. Eng. J. – J. Eng. 221 (2007) 321.

[19] F.C. Campbell (Ed.), Elements of metallurgy and engineering alloys, ASM International, Materials Park OH, 2008

[20] R.W. Wilson, E.B. Shone, Anti-Corros. Method. M. 17 (1970) 9.

[21] K.N. Tu, Acta Metall. Mater. 21 (1973) 347.

[22] K.N. Tu, R.D. Thompson, Acta Metall. Mater. 30 (1982) 947.

[23] R.J. Fields, S.R. Low III, G.K. Lucey Jr, Physical and mechanical properties of intermetallic compounds commonly found in solder joints, Proceedings of TMS Symposium, Cincinnati, October 1991.

[24] R.R. Chromik, R.P. Vinci, S.L. Allen, M.R. Notis, J. Mater. Res. 18 (2003) 2251-2261.

[25] M. Jordan, The electrodeposition of tin and its alloys, Eugen G. Leuze Publishers, Saulgau-Ŵürtt, 1995.

[26] The Glacier Metal Company Limited, GB patent 755084, 1954

[27] G.C. Pratt, Int. Metall. Rev. 18 (1973) 62.

[28] D.R. Eastham, C.S. Crooks, Trans. Inst. Met. Finish. 60 (1982) 9.

[29] T. Tanaka, M. Sakamoto, M. Wada, K. Yamamoto, H. Ishikawa, Y. Nagai, K. Sakai, GB patent 2253016, 1992.

[30] I. Babbitt, US patent 1252, 1839.

[31] EU Directive 98/69/EC relating to measures to be taken against air pollution by emissions from motor vehicles and amending Council Directive 70/220/EEC, 1998.

[32] EU Directive 2000/53/EC on end-of life vehicles, 2000.

[33] H. Tsuji, H. Ishikawa, T. Shibayama, GB patent 2375801, 2002.

[34] K.C. Ludema, Friction, in: B. Bhushan (Ed.), Modern Tribology Handbook, CRC Press, Boca Raton-London-New York-Washington D.C., 2000.

[35] S.M. Hsu, R.S. Gates, Boundary lubrication and boundary lubriating films, in: B. Bhushan (Ed.), Modern Tribology Handbook, CRC Press, Boca Raton-London-New York-Washington D.C., 2000.

[36] K. Mihara, Y. Inada, T. Mashiko, Anti-seizure properties of bearing in heavy-duty diesel engines, SAE World Congress, Detroit, February 1991. Paper 910890.

2. LITERATURE REVIEW

2.1. OVERVIEW

The previous chapter served as a brief introduction to what bearings are, how many types may be found in an engine, and how bronze-bearings for medium-speed diesel engines have evolved in recent years. It also showed how important the role of a Ni diffusion barrier layer is in their performance by preventing the loss of Sn from the overlay in Pb-Sn-based overlays, which would make the overlay prone to corrosion, and slowing down diffusion and the formation and growth of undesired intermetallic compounds in Pb-free, Sn-Cu overlays.

As also stated in the previous chapter, the main objective of the present research project is to develop novel electrodeposited Ni-based composite coatings with embedded particles to be employed as diffusion barrier layers in bronze-based bearing materials. For this purpose, the electrodeposition of Ni composite coatings with particles is reviewed in the present chapter, which is divided into three main parts:

1. The first part of the chapter covers recent developments in the use of Ni composite coatings as diffusion barrier layers in overlay systems for bearing applications.
2. The second part of the chapter covers a brief introduction of what electrodeposition is, how industrial Ni electrodeposition processes were developed, what Ni Watts processes are and a brief review of electrodeposited Ni-based composite coatings with no ultrasound.
3. The third part of the chapter covers a brief introduction of the use of ultrasound in Chemistry and Electrochemistry, the use of ultrasound in the electrodeposition of Ni and a brief review of the recent developments in the use of ultrasound in the electrodeposition of Ni-based composite coatings.

2.2. NI COMPOSITE COATINGS USED AS DIFFUSION BARRIER LAYERS IN BEARING APPLICATIONS

Although the exposure of the Ni diffusion barrier layer in local areas of bearings is not common, it is becoming a concern due to the more demanding operational conditions suffered by bearings in modern engines. The incorporation of particles into the Ni diffusion barrier layer may therefore present a substantial benefit in prolonging the lifespan of the bearing by reducing the possibility of seizure of the overlay system due to the improvement of the tribological properties of the Ni interlayer. Moreover, the presence of inherently soft, lubricant particles would result in a better tribological performance of the Ni diffusion barrier layer, resulting in a significantly lower coefficient of friction in those points where

the Ni layer acts as the sliding surface. KS Geitlager, a bearing manufacturing company based in Germany, recently applied for two patents focused on the development of Ni-based composite coatings to be used as barrier diffusion layers in bearings with Cu-based lining [1,2]. Both inventions describe a bearing material made of Sn or Sn-Cu alloy, a Ni diffusion barrier and a Cu-based lining material, where the diffusion barrier is electroless plated. The novelty of the first invention remains in the diffusion barrier (thickness around 3-12 μm), which consists of a Ni-based composite coating with 5-30 % vol. of graphite, MoS_2, hexagonal BN (hBN) and/or polytetrafluoroethylene (PTFE) particles. This composite diffusion barrier would show a good tribological performance if it became tribologically active due to localised removal of the overlay and would result in a substantial improvement of the running behaviour in such case, significantly reducing the susceptibility to seizure failure of the bearing. The second invention deals with the improvement of the diffusion barrier by introducing 1-15 % vol. of hard particles such as metal carbides, cubic nitrides, oxides and/or silicides, which is likely to result in the reduction of wear and abrasion of the diffusion layer in case it is exposed. However, many disadvantages are associated with using Ni electroless plating processes for bearings: i) Ni electroless plating depends on reducing agents, which make the plating solution complex and difficult to control, ii) Ni electroless plating must be carried out at high temperatures, requiring much more energy to plate the coating than an electroplating process, iii) lifespan of chemicals used in Ni electroless plating processes is very limited compared to Ni Watts bath formulations, iv) the deposition rates are too slow, and v) effluent treatment is expensive due to the fast chemical renewal. All these factors increase the operational costs. In addition, as no dispersing method is mentioned by the inventors, the dispersed particles may be prone to agglomerate in the bath and in the deposited coating, giving a poor quality microstructure.

2.3. ELECTRODEPOSITION OF NI AND NI-BASED COMPOSITE COATINGS

2.3.1. Introduction

As defined by the IUPAC, 'electrodeposition' (or 'electroplating', as the two terms are often used interchangeably) is *'the deposition of dissolved or suspended material by an electric field on an electrode'* [3], meaning that it is the method of producing a deposit on a surface by the action of electric current [4]. For a metallic coating, electrodeposition is achieved by setting a negative charge on the object to be plated after being immersed into a solution containing a dissolved salt of the metal to be deposited. As the metal ions carry a positive charge, they are attracted to the negatively charged object, which provides electrons to reduce the positive metal ions. The result is the production of a metallic coating on the surface of the object, as shown in Figure 2.1.

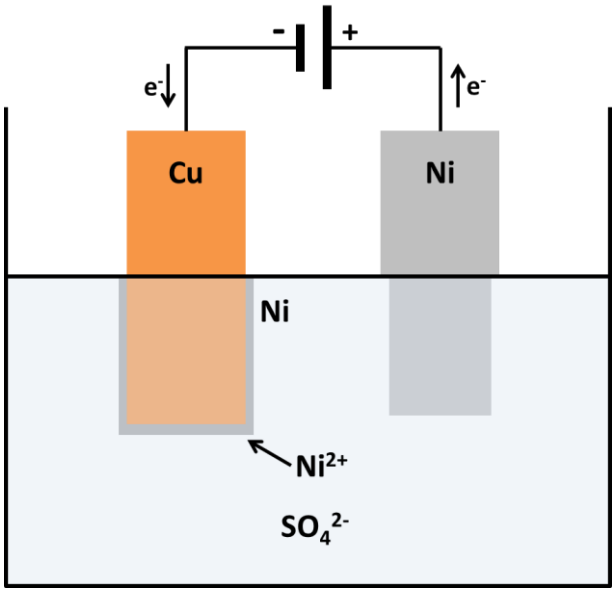

Figure 2.1. Electrodeposition of a metal (Ni) from a solution containing a metal salt ($NiSO_4$).

The electrodeposition of metals has been used in a wide variety of areas from metallurgy to electronics. Some examples are: electroplating of Au and Au-based alloys for electrical contacts in electronic circuits, electroplating of Cu for microelectronic interconnects,

electroplating of Ni-Fe alloys for magnetic recording heads, production of high purity metals and, more recently, microelectronics, sensors and microsystems for information and energy applications [5].

2.3.2. ELECTRODEPOSITION OF NI

Since Bird first described the formation of *'a crust of metallic nickel on the negative electrode, often of a silvery lustre on the surface immediately applied to the platinum'* using $NiCl_2$ and $NiSO_4$ solutions [6], a wide variety of studies have been focused on the electrodeposition of Ni, as it is one of the most common metal plating processes in industry [5]. Its importance in terms of economic and commercial impact in the form of metal and salts annually consumed by the electroplating industry was roughly estimated by Di Bari [7], being around 100,000 tonnes worldwide. In this sense, nearly 250 surface engineering companies in United Kingdom (and around 10% of the European plating industry) use Ni electroplating processes to some extent [8].

2.3.2.1. EARLY WORKS AND DEVELOPMENT

Different works and patents [9] followed Bird's initial study on the electrodeposition of Ni, including the paper by Bottger [10] that first mentioned the use of an acid $(NH_4)_2SO_4$ electrolyte that became the basis for the Ni plating industry for the next 70 years [7,11]. This publication was followed by others, including Gore's initial use of double salts [12] that was later improved and patented by Adams [13,14]. Different attempts to develop a similar process by Remington were not completely successful, although he was the first to propose a Ti basket containing Ni pieces as the anode [15], which still constitutes a major anode configuration in the Ni electroplating industry. Adams' work was followed by other researchers such as Weston, who came up with the idea of adding H_3BO_3 to plating solutions made of $NiSO_4$ and/or $NiCl_2$ [16] to act as buffering agent and prevent the deposition of sub-salts of Ni on the anode. This would eventually lead to the formulation of a bath by Watts [17] which, over the years, has grown to become the most widely spread Ni electroplating

method in the industry with little modification and is actually named after him. Watts' original formulation had to be used hot at higher current densities than those employed at that moment in the industry, and its original composition was 240 g/L of $NiSO_4.7H_2O$, 20 g/L of $NiCl_2.6H_2O$ and 20 g/L of H_3BO_3.

2.3.2.2. Ni Watts bath

The Watts bath processes constitute the vast majority in the Ni electroplating industry. This type of bath not only produces high quality deposits, but it also is a highly efficient process, as the cathode current efficiency for general Ni Watts bath formulations usually remains around 90-97 %, while the anode efficiency for Ni dissolution is nearly 100 % [7].

The composition of most commercial Ni Watts bath formulations is [11]:

- $NiSO_4.6H_2O$: 150 to 400 g/L.
- $NiCl_2.6H_2O$: 20 to 80 g/L.
- H_3BO_3: 15 to 50 g/L.

And the plating parameters are [7]:

- Temperature: 44 to 66 °C.
- Agitation: air or mechanical.
- Cathode current density: 3 to 11 A/dm^2.
- Anodes: Ni.
- pH: 2.0 to 4.5.

In a Watts bath, $NiSO_4$ is the main source of Ni^{2+} ions in the plating bath [11]. The main purpose of adding $NiCl_2$ to a Watts bath is to improve the Ni anode dissolution [11]. In addition, $NiCl_2$ also acts as a secondary source of Ni^{2+} ions to the solution, it increases the conductivity of the solution and the throwing power of the plating process, and its presence yields a more uniform distribution of the thickness of the deposit, increasing its internal stress and refining its grain size [7]. H_3BO_3 is used as a buffering agent to maintain the pH at a constant value [11], also affecting the surface finish of the deposits (cracking and burning

may be observed at low concentrations of H_3BO_3) [7]. The pH of the plating solution is therefore an important parameter in commercial Ni Watts baths, as it significantly affects the plating process. Plating under strongly acidic conditions could lead to the appearance of pitting [7], as H_2 evolution would occur on the cathode.

2.3.2.3. REACTIONS AT THE CATHODE

The electrodeposition of Ni over a cathode in a Ni Watts bath occurs through the electrochemical reduction of Ni^{+2} present in the solution. It is well accepted that this process generally follows the next mechanism [18]:

C.1.1. $Ni^{2+} + X^{-} \rightarrow NiX^{+}$

C.1.2. $NiX^{+} + e^{-} \rightarrow NiX_{ads}$

C.1.3. $NiX_{ads} + e^{-} \rightarrow Ni + X^{-}$

where X^- would be OH^-, SO_4^{2-} or Cl^- [19,20]. Saraby-Reintjes and Fleischmann [19] deduced that, in the case of a Watts bath, X^- would be Cl^- and reaction C.1.2 would be the rate-determining step of the overall electrochemical reduction process after comparing the different kinetic parameters they experimentally estimated with those calculated by different models. It must be noted though that the mechanism described above may become more complex depending on the specific operational parameters of the Ni bath used (e.g. electrolyte, cathode current efficiency, temperature, additives, etc.) [18].

It was stated in the previous sub-section that cathode current efficiency for general Ni Watts bath formulations usually are 90-97 % [7], being the generation of H_2 the other electrochemical process that generally occurs in the cathode [18,21]. H_2 generation would occur during the electrodeposition of Ni from aqueous solutions following the next mechanisms [22-24]:

C.2.1. $Ni + H^{+} + e^{-} \rightarrow (Ni - H)_{ads}$

C.2.2.a $2\ (\mathrm{Ni-H})_{ads} \rightarrow 2\ \mathrm{Ni} + \mathrm{H_2}$

C.2.2.b $(\mathrm{Ni-H})_{ads} + \mathrm{H^+} + \mathrm{e^-} \rightarrow \mathrm{Ni} + \mathrm{H_2}$

where the discharge (reaction C.2.1) would be followed by either Tafel recombination (reaction C.2.2.a) or electrochemical desorption (reaction C.2.2.b). A small fraction of the adsorbed hydrogen might also be absorbed into the Ni lattice [25]:

C.2.2.c $(\mathrm{Ni-H})_{ads} \leftrightarrow \mathrm{Ni(H)_{ads}}$

2.3.2.2. REACTIONS AT THE ANODE

Ni anode dissolution occurs through an electrochemical oxidation process. The electrochemical oxidation of Ni in $NiSO_4$ aqueous solutions is limited due to the formation of a passive film over the surface of Ni [7], which then either thickens while the electrochemical oxidation of Ni continues or stops growing and O_2 generation is observed as the oxidation of OH^- becomes the main anodic reaction [26] after current density is increased. The overall electrochemical oxidation of Ni is likely to involve the presence of adsorbed OH^- and may occur in three steps [27]:

A.1. $\mathrm{Ni} + \mathrm{OH^-} \rightarrow \mathrm{NiOH_{ads}} + \mathrm{e^-}$

A.2. $\mathrm{NiOH_{ads}} \rightarrow \mathrm{NiOH^+} + \mathrm{e^-}$

A.3. $\mathrm{NiOH^+} \rightarrow \mathrm{Ni^{2+}} + \mathrm{OH^-}$

where passivation would take place as follows [7,27]:

A.2.1. $\mathrm{NiOH_{ads}} + \mathrm{OH^-} \rightarrow \mathrm{Ni(OH)_2} \downarrow + \mathrm{e^-}$

A.2.2 $\mathrm{Ni(OH)_2} \downarrow \rightarrow \mathrm{NiO} \downarrow + \mathrm{H_2O}$

When Cl^- is added (e.g. in the form of $NiCl_2$) to a $NiSO_4$ aqueous solution, although passivation still occurs [28,29], a small increase in the applied potential (+0.2 V vs. standard calomel electrode) at the anode results in a quick rise in the anode current density with no generation of O_2 [30]. In this case, species like $NiCl_{ads}$ and $NiCl^+$ interfere with the

electrochemical oxidation process described above [7], resulting in an increase of anode current efficiency up to 100%. However, chloride-assisted Ni anode dissolution is localised, taking place beneath or through the NiO film formed over the surface of the Ni anode, and hence its tendency to dissolve through pits on the surface [7].

2.3.3. ELECTRODEPOSITION OF NI-BASED COMPOSITE COATINGS

Since Fink and Prince first studied the co-deposition of Cu and graphite [31], the electrodeposition of metal-based composites with inert particles has received wide attention from the scientific community. Particles, when properly dispersed, may substantially improve certain operational properties of the coating such as hardness, wear or the resistance to corrosion, and impart them new properties (antifriction, magnetic, catalytic, etc.) [32]. Among the different metals used to produce such composite coatings, we may find Ni, Cu, Cr, Zn, noble metals and their alloys, and as the dispersed solid phase, we may find oxides, carbides, nitrides, carbon powders or polymer particles [32,33]. Ni-based composite coatings constitute the majority of the composites studied in the literature. Most of these coatings are electrodeposited from Watts and Sulphamate baths containing different surfactants, mainly sodium dodecyl sulphate (SDS), which has been widely used in recent years. Hard particles such as oxides (Al_2O_3, TiO_2, CeO_2, etc.) and carbides (SiC, WC, etc.) are more often incorporated to electrodeposited coatings, although inherently soft, lubricant particles such as graphite and PTFE are also being used to improve the performance of the coatings. Table 2.1 includes different examples on the particles, electrolytes and additives, and the effect that the particles and/or plating parameters may have on the final characteristics of the resulting Ni-based composite coatings. Although the majority of the work on electrodeposited composite coatings is conducted with continuous current processes, pulsed-plating methods are progressively gaining more attention, as they are a way to improve particle incorporation into the coatings [34]. Other electrodeposition

methods such as brush plating [35] have been also employed to produced composite coatings, although their use is uncommon.

Table 2.1. Examples of particles, electrolytes and additives used for the electrodeposition of Ni-based composites coatings.

Particle	Ni electrolyte	Effect of particles/plating parameters on final properties of coatings	Ref
Al_2O_3	- Sulphamate bath - Pyrophosphate bath	- Sulphamate bath: Incorporation of particles modified the microstructure. Hardness was proportional to particle content. - Pyrophosphate bath: Incorporation of particles modified the microstructure.	[36]
Al_2O_3	Watts bath	- Incorporation of particles promoted (111) instead of (200) crystal planes. - Higher concentration of particles in electrolyte increased both hardness and roughness and decreased both wear rate and coefficient in friction.	[37]
Al_2O_3	Watts bath with SDS (surfactant) and hexadecyl pyridinium bromide (HPB, surfactant)	- Particle content in composite reliant on both HPB and particle concentration in electrolyte. Increase in either HPB or particle concentration and current density yielded higher hardness and lower wear rates.	[38]
CeO_2	Sulphamate bath with SDS (surfactant)	- Particle incorporation dependent on current density. - Hardness increased with particle content in coating. - Composites presented improved corrosion resistance.	[39]
La_2O_3	Sulphamate bath with SDS (surfactant)	- Particle content in coating influenced by particle concentration in electrolyte, current density, temperature and stirring speed. - Enhancement of hardness by increasing particle content in composites.	[40]
TiO_2	Watts bath with SDS (surfactant)	- Pulse plating parameters influenced particle content in composites, which directly affect the hardness of the deposits.	[41]
Titanates	Watts bath with SDS (surfactant) and wetting and hardener additives	- Composites containing nanotubular titanates showed lower hardness values and no significant improvement in wear rate, coefficient of friction and elastic modulus compared to pure Ni deposits.	[42]
Y_2O_3	Sulphate bath with SDS (surfactant)	- Higher particle incorporation by increasing particle concentration in electrolyte, Higher particle content in coating reduced both wear weight loss and coefficient of friction while enhancing hardness. - Particles promoted (200) and (220) crystal planes.	[43]

Particle	Ni electrolyte	Effect of particles/plating parameters on final properties of coatings	Ref
ZrO_2	Watts bath with surfactant	Properties of coatings affected by plating methods (continuous, pulsed, and pulsed reversed electrodeposition). In all cases, composites showed higher hardness values and lower wear weight losses than pure Ni deposits.	[44]
SiC	Watts bath with SDS (surfactant)	The incorporation of particles significantly enhanced hardness, wear and corrosion resistance of Ni deposits. Composites presented a generally improved tribological performance.	[45]
SiC	Watts bath with SDS (surfactant)	Composites showed a refined grain size, improved corrosion resistance and higher hardness than pure Ni deposits. Final application for train axles was presented.	[46]
WC	Watts bath	Particle agglomeration at temperatures above 50 °C. Composite coatings showed worse corrosion performance than pure Ni deposits.	[47]
hBN	Sulphamate bath with benzalkonium saccharinate (surfactant) and saccharin (carrier)	Composites presented higher hardness and wear resistance than pure Ni coatings. Particle concentration in electrolyte affected particle content in composites, resulting in a proportional improvement in wear resistance.	[48]
Fullerenes	Bath consisting of nickel sulphate, nickel chloride and potassium acetate	Composites presented a slightly improved corrosion resistance compared with pure Ni deposits.	[49]
Mica	Sulphate bath with SDS (surfactant)	Particle content in composites increased with particle concentration in electrolyte, pH, current density and temperature of bath. Hardness of coatings increased with particle content. Composites presented improved corrosion resistance than pure Ni deposits.	[50]
PTFE	Sulphamate bath with non-ionic wetting agent	Particle content in composites increased with particle concentration in electrolyte, although it decreased with higher current densities and stirring speed.	[51]

According to the papers previously mentioned, whereas it is quite clear that particle content in the coating increases when the particle concentration in the electrolyte is higher, some contradictory results have been obtained regarding the effect of the current density and the stirring speed. In this sense, the general effects of the working parameters on the particle content were discussed by Celis et al. [52] (Figure 2.2), and in the case of the current density and the stirring speed, electro-kinetic and flow regimes seem to have a great influence on the incorporation of particles into the electrodeposited metal.

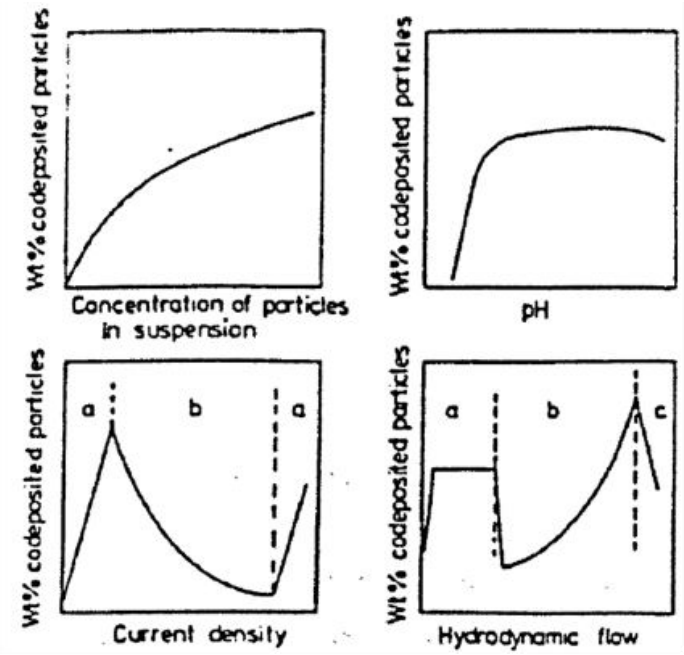

Figure 2.2. General effects of the concentration of particles in the electrolyte, pH, current density (a: charge transfer overvoltage, b: concentration overvoltage) and the hydrodynamic flow (a: laminar regime, b: transition zone, c: turbulent regime) on the electrodeposition of metal composite coatings with embedded particles. Adapted from Ref. [52].

2.3.3.1. MECHANICAL PROPERTIES

The incorporation of hard particles quite often leads to an increase in the hardness of the materials, which generally results in the improvement of wear resistance and the reduction of the coefficient of friction. The incorporation of Al_2O_3 particles constitutes a good example, as many studies have focused on the co-deposition of such particles with different metals. Ni-based composite coatings with Al_2O_3 particles produced from different baths exhibit higher hardness and wear resistance and lower coefficient of friction [36-38], with the properties usually depending on the particle content in the electrodeposited composite coatings. Regarding other oxides, the incorporation of particles such as TiO_2, CeO_2, ZrO_2, etc. also increases the hardness of electrodeposited Ni [39,41], generally resulting in the improvement of the wear resistance [44]. Co-deposition of carbides such as SiC or WC with Ni also modifies and enhances the mechanical properties of the deposits (hardness [45,46] and wear resistance [45]).

Regarding the incorporation of softer particles into Ni deposits, not many works are available in the literature. The incorporation of both hBN and mica into electrodeposited Ni has resulted in the improvement of hardness. Nevertheless, none of these composites have been produced from Watts bath formulations (whereas Ni/hBN composite coatings were prepared with a sulphamate bath [48], Ni/mica composite coatings were electrodeposited from a sulphate bath), and in both cases surfactants were employed. The lack of papers focused on the electrodeposition of Ni-based composite coatings with soft/lubricant particles from an additive-free Watts bath obviously reflects the challenging task of producing Ni composites with such particles from these baths.

2.4. Ultrasound-assisted electrodeposition of Ni and Ni-based composite coatings

2.4.1. Introduction

2.4.1.1 Sonochemistry

Sonochemistry [53] is the area of high-energy Chemistry which studies chemical reactions and processes involving the application of an ultrasonic field in a frequency range which commonly varies between 20 kHz and 10 MHz. It allows chemists to increase the conversion, improve the yield, initiate and change the reaction pathways in all sorts of biological, chemical or electrochemical processes [54], and is becoming a prominently used technique in a wide variety of research areas [55]. Overall, there is a wide range of both chemical and physical effects that are observed when high-intensity ultrasound is used in Chemistry, as shown in Figure 2.3 [56].

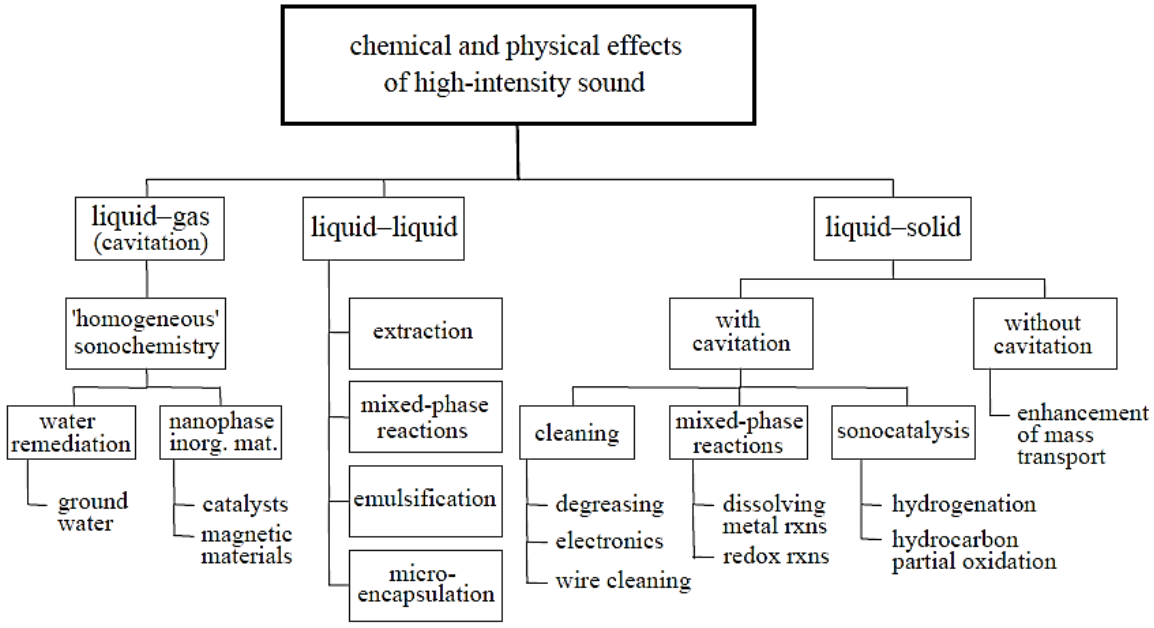

Figure 2.3. Classification of the chemical and physical effects of ultrasound. Adapted from Ref. [56].

The formation of acoustic cavitation [57] is inherent to Sonochemistry, as almost all of the applications of ultrasound in chemical processing depend on this phenomenon [58]. As a mechanical wave, ultrasound is propagated through a liquid by a series of compression (positive pressure) and rarefaction (negative pressure) cycles induced in the molecules of the medium through which it passes. A cavity or 'bubble' may form in the liquid during the cycles of negative pressure, when the power is high enough, as the 'expanding' forces during the rarefaction cycle exceed the 'attraction' forces of the molecules of the liquid. When the bubble grows to a critical size, it becomes unstable and violently collapses, as shown in Figure 2.4 [59,60]. It is at this point (named 'hot spot') when remarkably high temperatures and pressures (around 5000 K and 1000 atm., respectively) are achieved, involving heating and cooling rates of an order of magnitude above 10^{10} K/s [61-63].

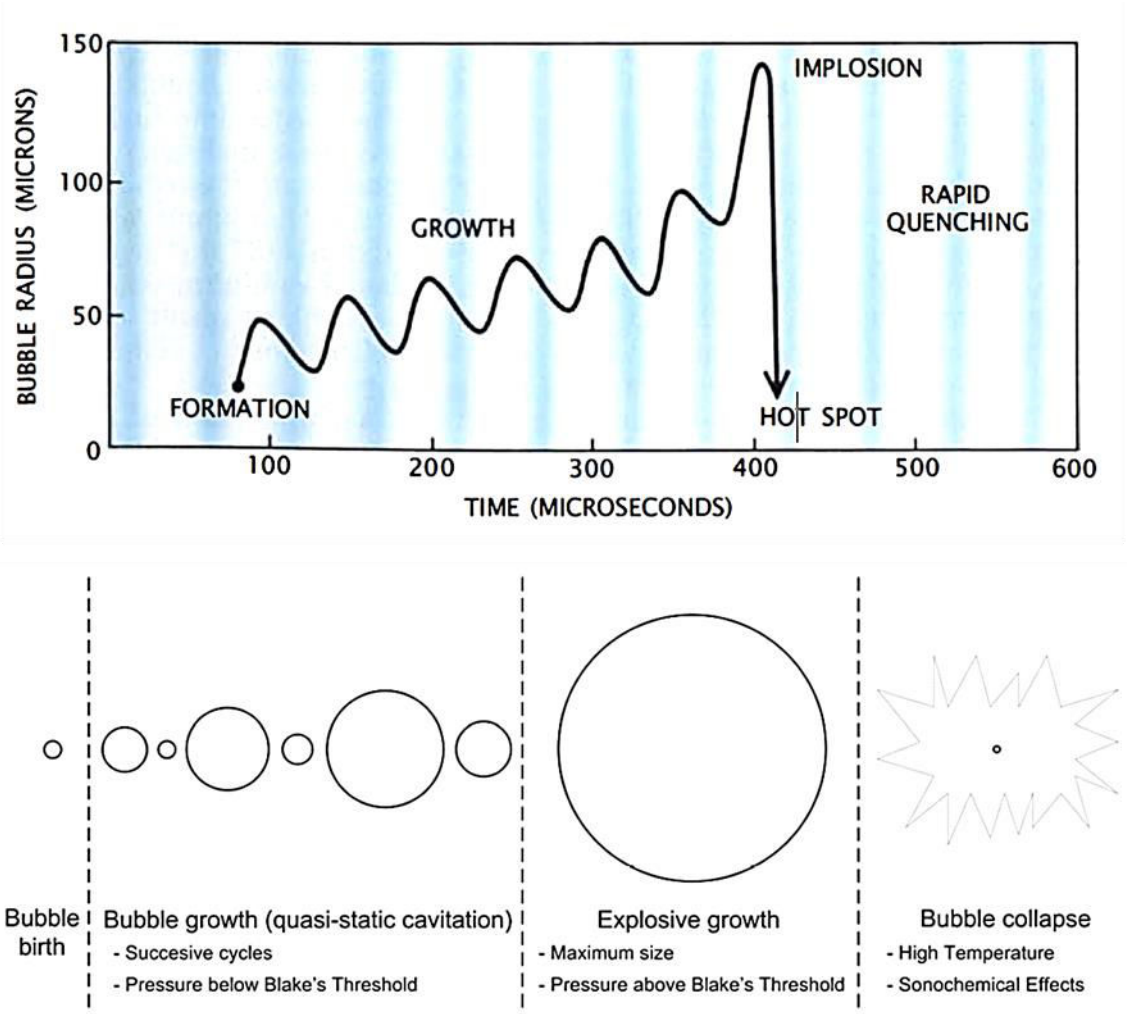

Figure 2.4. Bubble growth and implosion in a liquid irradiated with ultrasound. Large alternating stresses within the irradiated liquid form by setting an ultrasonic field which generates positive (blue colour in upper image) and negative (white colour in upper image) pressure areas. Adapted from Refs. [59] and [60].

The implosion of the bubble takes place with a collision density of 1.5 kg/cm^2 and pressure gradients of 2 TPa/cm, and the enormous pressures inside the bubble are released into the liquid as shock waves [55]. The events which result as a consequence of the existence of these cavitating bubbles (Figure 2.5 [64]) are the basis for the application of Sonochemistry in several areas such as material science [65,66], synthetic chemistry [67,68], water remediation [69], biotechnology [70], food technology [71] and Electrochemistry [72].

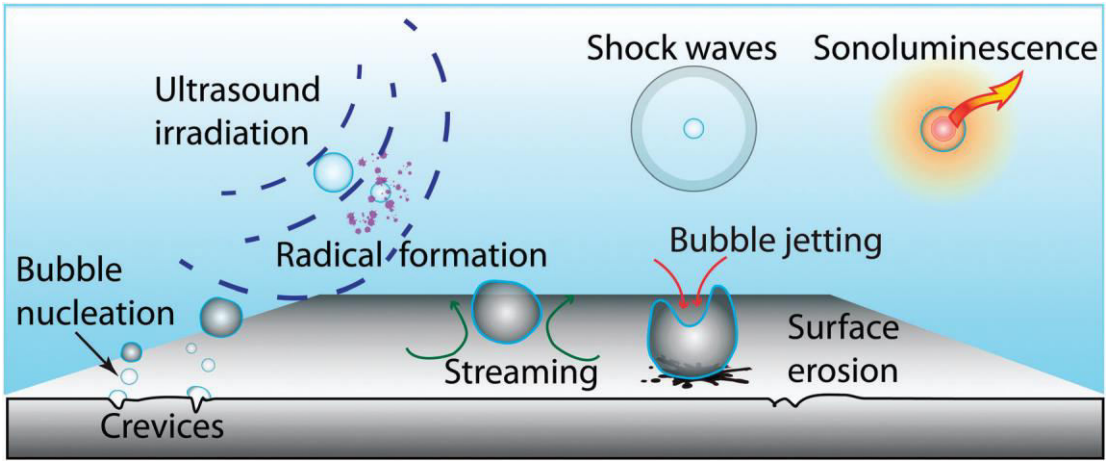

Figure 2.5. Schematic representation of the main effects of cavitation induced by ultrasound irradiation. Adapted from Ref. [64].

2.4.1.2. SONOELECTROCHEMISTRY

Among the applications of ultrasound in Chemistry we find Sonoelectrochemistry [73], which has experienced a continuous growth since Morigushi first investigated the effect of acoustic waves on the water decomposition voltage of a Pt electrode in the 1930s [74]. In recent years, Sonoelectrochemistry has become an active research area due to its potential use in many different applications, generating close to a thousand scientific papers [72].

Sonoelectrochemistry has been defined by González-García et al. [72] as *'the combination of ultrasound and electrode processes'* where the propagation of ultrasound and the inherent ultrasonic cavitation observed in any sonochemical process bring both mechanical and chemical effects which obviously make an impact in *'any heterogeneous process, such as the electron transfer at the electrode surface in a sonoelectrochemical process'* [75]. Diverse cavitation phenomena such as acoustic streaming and micro-jetting [76], shock waves [77,78], promotion of mass transport from/to the electrode [79-81] and electrode surface cleaning [82] are found among the mechanical effects reported, while the chemical effects include the enhancement of electrochemiluminescence [83], low-temperature processes [84] and high pressure Sonoelectrochemistry [85].

Acoustic streaming and micro-jetting present great benefits for Electrochemistry. The acoustic streaming is proportional to the sonication intensity [86], and it occurs in different regions of the system: i) bulk solution, ii) surface of solids and iii) boundary layer [58]. Figure 2.6 [87] displays how the flow regime develops in those regions. Regarding micro-jetting, it was theoretically predicted by Plesset and Chapman [88] and then experimentally confirmed by Lauterborn and Bolle [89], who observed that bubbles near a solid surface collapsed asymmetrically, with a micro-jet forming towards the solid and striking the surface. Figure 2.7 displays the asymmetric collapse of a bubble near a solid surface and the formation of a micro-jet [90].

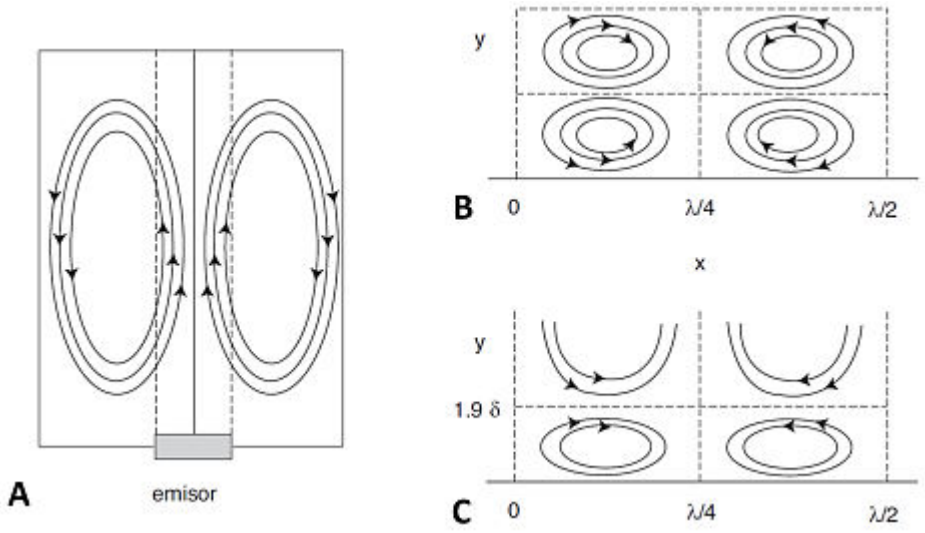

Figure 2.6. Acoustic streaming flow patterns in different areas: (A) bulk solution, (B) solid surface, and (C) diffusion boundary layer. Adapted from Ref. [87].

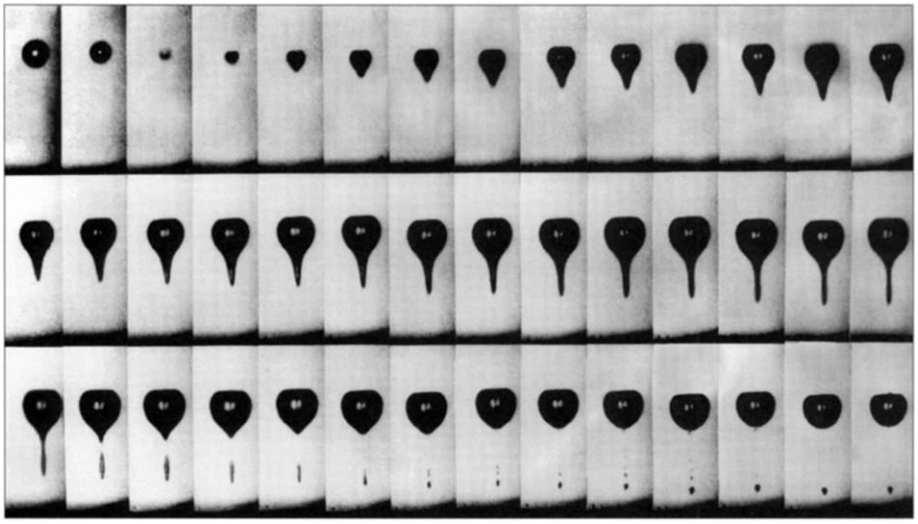

Figure 2.7. Example of a bubble collapsing near a solid surface and the formation of a micro-jet. Adapted from Ref. [90].

The combination of all these ultrasonic effects enhances the mass transport of electroactive species to the surface of the electrodes, reducing the diffusion boundary layer. Nevertheless, it must be kept in mind that, as González-García et al. [72] also noted in their review, although both mechanical and chemical effects are observed at both low and high frequencies [91], the governing effects may be different depending on the working frequency [92]. For general applications of ultrasound in Chemistry, it has been found that mechanical effects are more remarkable at lower frequencies, while pure chemical effects (i.e. generation of radical species) are more evident at higher frequencies [93]. Overall, mechanical and chemical phenomena enhance the mass transfer near the surface of the electrode and the kinetics of the electrodic reaction itself, respectively, in many different electrochemical processes.

2.4.2. Ultrasound-assisted electrodeposition of Ni

Among the different applications of Sonoelectrochemistry, the ultrasound-assisted electrodeposition of metals has received wide attention for a long time, as it was one of the first sonoelectrochemical processes studied by the research community [94,95]. Few works are available in the literature regarding the electrodeposition of Ni under ultrasound. Most

of these works are focused on the effect of ultrasound on the characteristics of the resulting Ni deposit, although a few authors have tried to evaluate the effect of ultrasound on the electrokinetic parameters of the process. A good example of the latter is the work by Kobayasi et al. [96], who studied the effect of sonication on the electrodeposition of Ni from a Watts bath at various frequencies (28, 45 and 100 kHz). In this work, the authors observed that the use of ultrasound reduced the cathodic overpotential necessary to electrodeposit Ni from the plating solution, promoting the charge transfer reaction in the following order: silent conditions $\leq$100 kHz <28 kHz <45 kHz.

Regarding the effect of ultrasound on the characteristics of electrodeposited Ni, Lampke et al. recently reported how ultrasound can refine the grain size of Ni deposits [97]. This beneficial effect of ultrasound on refining the grain size of electrodeposited coatings was already pointed out forty years ago by Walker and Walker [98], who were among the first researchers that observed that the effect of ultrasound on the grain size was the controlling factor in increasing the hardness and decreasing the porosity of electroplated coatings. Such effect of the refinement of the grain size by ultrasound would be responsible for the increase in hardness observed for different electrodeposited metals, including Ni [99-101] and its alloys [102,103]. Regarding other properties of Ni coatings, different authors have reported that the use of ultrasound may enhance the residual stress [104], wear resistance [105], fatigue strength [106], and corrosion resistance [107].

2.4.3. ULTRASOUND-ASSISTED ELECTRODEPOSITION OF NI-BASED COMPOSITE COATINGS

In the case of the electrodeposition of composite coatings, the implementation of ultrasound may assist in a further enhancement of the characteristics of electrodeposited composite coatings, as discussed in the next sub-sections. Table 2.2 includes some examples of the use of ultrasound in the electrodeposition of composite coatings and how the deposits are affected. Again, Ni and its alloys constitute the majority of the works found in the literature,

although in this case the use of surfactants is not as required as in the electrodeposition of composite coatings in silent conditions due to the benefits that ultrasound presents in the dispersion of particles.

Table 2.2. Examples of particles, electrolytes, and ultrasonic parameters used for the ultrasound-assisted electrodeposition of Ni-based composites coatings.

Particles	Ni electrolyte	Ultrasonic parameters	Effect of ultrasound/particles/plating parameters on final properties of coatings	Ref
Al_2O_3	Sulphamate bath	- System: horn - Frequency: 22.5 kHz - Power: 0.005 W/cm^3	- Ultrasonic irradiation of the electrolyte prior to electrodeposition significantly reduced particle agglomeration. - Both ultrasonic and chemical dispersion with CTAB (cetyl trimethyl ammonium bromide) presented similar results, although particle content was slightly higher for the latter. - Decrease in Ni^{2+} concentration in electrolyte generally lead to higher particle de-agglomeration and particle content in composites.	[108]
Al_2O_3	Watts bath	- System: horn - Frequency: unknown - Power: unknown	- Ultrasound during deposition improved the incorporation of particles in both continuous and pulse-plating. - No significant difference in corrosion resistance between composites and pure Ni deposits was reported as particle agglomeration was not completely avoided by ultrasound.	[107]
Al_2O_3	Watts bath	- System: horn - Frequency: 24 kHz - Power: 38 W/cm^2	- Ultrasonic irradiation of the electrolyte prior to electrodeposition minimized particle agglomeration, shifting the peaks observed in particle size distribution curves towards smaller diameters. Ultrasound enhanced particle dispersion in coatings. - Increasing particle concentration in bath increased particle incorporation into the metal matrix, resulting in higher hardness and wear resistance. - Composites electrodeposited under ultrasound always presented higher particle content and improved hardness and wear resistance. - Composites presented finer grains than pure Ni deposits. For both pure Ni and composite coatings, ultrasound during plating further enhanced grain refinement.	[101]

Particles	Ni electrolyte	Ultrasonic parameters	Effect of ultrasound/particles/plating parameters on final properties of coatings	Ref
Al_2O_3 whiskers	Sulphamate bath	Unknown	- Ultrasound used to prevent particle agglomeration prior to deposition. - Particle incorporation with/without ultrasound increased when decreasing pulse-plating frequency. - Composite coatings produced with ultrasound seemed to present lower particle content than those without ultrasound, although in the latter larger aggregates were incorporated.	[109]
CeO_2	Watts bath with SDS (surfactant)	- System: unknown - Frequency: 28 kHz - Power: 300 W	- Incorporation of particles remarkably increased hardness and wear rate of coatings. Further improvement in both properties was observed when ultrasound was used during the electrodeposition. - The orientation of Ni crystals in composite coatings was strongly affected by ultrasound.	[110]
MoO_3	Watts bath	- System: unknown - Frequency: 22 kHz - Power: 60 W	- Ultrasound to prevent particle agglomeration prior to deposition.	[111]
TiO_2	Watts bath with SDS (surfactant)	- System: bath - Frequency: 28 kHz - Power: unknown	- Ultrasound reduced the incorporation of agglomerated particles into the coatings. - Particle content in coating increased by increasing particle concentration in electrolyte. Hardness related to particle content in composites.	[112]
TiO_2	Watts bath with SDS (surfactant)	- System: bath - Frequency: 35 kHz - Power: unknown	- Nano-size particles well dispersed in the coating when ultrasound was used during the electrodeposition. - The incorporation of particles into the coating resulted in further refinement of the grain size. - Particle size affected final properties of the composite: for same particle content, composites with nano-size particles presented significantly higher hardness than composites with submicron-size particles.	[97]
SiC	Watts bath with sodium dodecyl-glycol (surfactant), 1,4-butynediol (brightener) and p-toluene sulphonamide (carrier)	Unknown	- Ultrasound employed to obtain a better dispersion of particles in the electrolyte. - Composites deposited under ultrasound presented finer grain size than those produced without ultrasound. - Incorporation of particles into Ni deposits changed the orientation of crystals. - Composites presented better corrosion resistance than pure Ni deposits.	[113]

Particles	Ni electrolyte	Ultrasonic parameters	Effect of ultrasound/particles/plating parameters on final properties of coatings	Ref
SiC	Watts bath	- System: bath - Frequency: unknown - Power: unknown	- Ultrasound drastically reduced particle agglomeration, especially at lower pH. - Ultrasound did not affect particle content for continuous plating, but it really increased particle incorporation into pulse-plated coatings. - Composites plated in all conditions presented enhanced hardness compare to pure Ni deposits. Pure Ni and composite coatings deposited under ultrasound had an improved corrosion resistance (by reducing the porosity of the deposits).	[100]
SiC	Watts bath	- System: horn - Frequency: unknown - Power: unknown	- Ultrasound to prevent particle agglomeration prior to deposition. - Ultrasound during deposition improved the incorporation of particles in both continuous and pulse-plating. - Composites presented improved corrosion resistance than pure Ni deposits.	[107]
SiC	Sulphamate bath with CTAB and SDS (surfactants)	- System: bath - Frequency: 38 kHz - Power: 200 W	- Ultrasound improved the incorporation of finely de-agglomerated particles into the coating, resulting in composite coatings with a homogeneous distribution of particles. - Corrosion resistance was improved, especially in those composites produced under ultrasound. - Synergic effect of ultrasound and particles on the mechanical properties of the coatings.	[114]
WC	Watts bath with SDS and CTAB (surfactants)	- System: unknown - Frequency: 40 kHz - Power: 350 W	- Ultrasound used to disperse particles in baths where no surfactant was used. - Composites presented higher hardness, elastic module and corrosion resistance. - Incorporation of particles strongly affected surface morphology of deposits.	[115]
TiN	Watts bath	- System: unknown - Frequency: unknown - Power: 0-300 W	- Composite coatings with dispersed particles were obtained with ultrasound during deposition. - The incorporation of particles and ultrasound refined the grain size of the coatings.	[116]

Particles	Ni electrolyte	Ultrasonic parameters	Effect of ultrasound/particles/plating parameters on final properties of coatings	Ref
WS_2	Watts bath with CTAB (surfactant)	- System: horn - Frequency: 24 kHz - Power: 20, 30 and 40 W/cm^2	- Ultrasonic irradiation (20 W/cm^2) of the electrolyte during 10 minutes prior to electrodeposition to avoid particle agglomeration. - Particle content in the coating increased with ultrasonic power up to 30 W cm^{-2}, slightly decreases at higher intensity values. - More compact deposits with uniform thickness produced under the presence of ultrasound. - Composite coatings, especially those produced under ultrasound, presented better mechanical properties (i.e. hardness, reduced Young's modulus, elastic strain to failure and elastic recovery). - Composite coatings, especially those produced under ultrasound, presented better tribological performance (i.e. lower coefficient of friction).	[117]

2.4.3.1. EFFECT OF ULTRASOUND ON THE DISPERSION OF PARTICLES

The use of ultrasound in the dispersion of particles is widely extended due to the unique features that ultrasonic cavitation presents in order to de-agglomerate aggregated particles in aqueous and non-aqueous suspensions. In the electrodeposition of Ni-based composite coatings, ultrasonic irradiation of the electrolyte is in many cases an essential step prior to the electrodeposition process itself in order to finely disperse the particles and reduce their agglomeration [107,108,111], combined in some cases with the addition of a surfactant to enhance the dispersion of the particles [112,113] or to allow the successful deposition of the Ni composite coatings [117]. The potential of ultrasound in terms of particle de-agglomeration can be estimated by taking a look at the study conducted by García-Lecina et al. [101] focused on the electrodeposition of Ni-based composite coatings with embedded Al_2O_3 particles. The authors noticed that ten minutes of ultrasonic irradiation was enough to achieve a better particle size distribution with less and smaller agglomerates in the Watts bath they used.

The use of ultrasound during the electrodeposition process also improves the dispersion and de-agglomeration of particles in the electroplated coatings [112]. A better distribution of particles in Ni deposits was observed by Lampke et al. [97] when incorporating nano-size TiO_2 particles into Ni coatings under ultrasound, as shown in Figure 2.8.

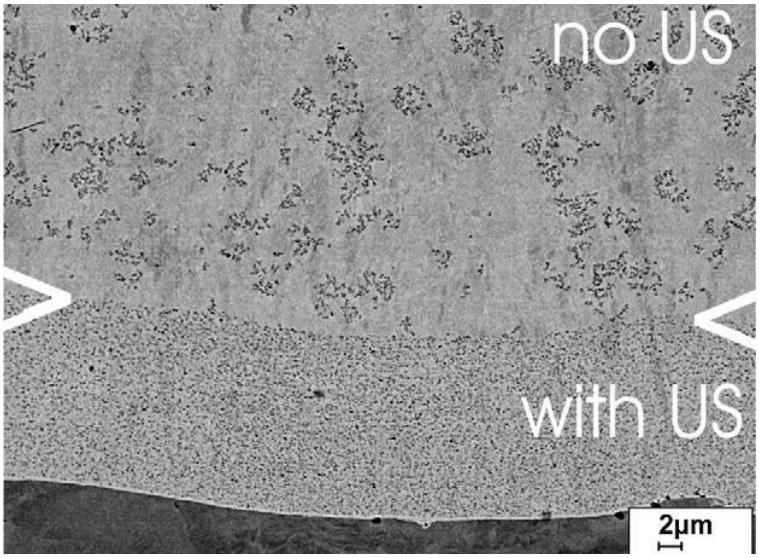

Figure 2.8. Well-dispersed particles under ultrasound conditions (lower part from substrate up to the markers ><) and nano-particle agglomeration under silent conditions (upper part). Adapted from Ref. [97].

Ultrasound has also been successful in increasing the incorporation of particles into electrodeposited coatings [101,107]. Zanella et al. observed that, although ultrasound did not have a significant effect in particle content in Ni/SiC composites produced by continuous-current plating, it increased particle incorporation into the coatings deposited by pulsed-plating methods [100]. It must be noted though that, in some cases reported in the latter paper, a reduction in particle content in composite coatings electrodeposited with ultrasound is due to the fact that large agglomerates are not incorporated into the coating.

2.4.3.2. MECHANICAL PROPERTIES

As previously mentioned in Section 2.2.3.1, the incorporation of hard particles into electrodeposited coatings generally results in an increase in hardness and the improvement of other mechanical properties such as wear resistance or and coefficient of friction. The use of ultrasound during the electroplating of composite coatings seems to enhance this

hardening effect, as observed by Xue et al. on their Ni/CeO_2 composites [110]. The authors did not only observe an increase on the microhardness of the deposits by adding the particles, but also observed an increase in hardness and enhancement of wear resistance in those composite coatings plated under ultrasound. Similar results were obtained by García-Lecina et al. [101] on Ni/Al_2O_3 composite coatings, as they observed that both ultrasound and concentration of particles in the electrolyte had an effect on the hardness of the coatings (Figure 2.9). They deduced the combination of two phenomena, as suggested by Lampke et al. [97], to explain the increase in hardness of composite coatings plated under ultrasound: i) the presence of fine, well-dispersed Al_2O_3 nanoparticles in the Ni matrix that would act as strong obstacles for dislocation movement, and ii) a finer grain size of the Ni crystals due to the presence of ultrasound. In this work, wear resistance was also enhanced when increasing the particle concentration in the electrolyte, and the presence of ultrasound further improved the performance of the coatings.

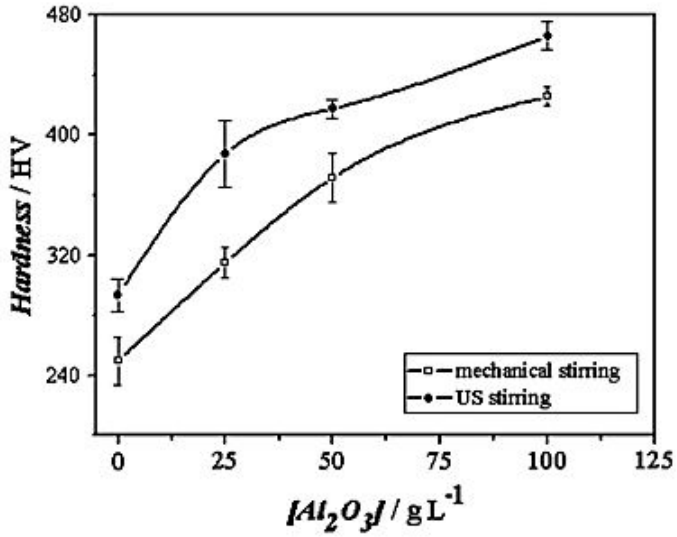

Figure 2.9. Effect of Al_2O_3 concentration in the electrolyte on the hardness of Ni/Al_2O_3 composite coating obtained under mechanical stirring and ultrasonic (US) stirring. Adapted from Ref. [101].

2.4.3.3. INFLUENCE OF ULTRASONIC PARAMETERS

Most of the previous studies have mainly focused on the general effect of ultrasound on the plating process and the properties of the coatings. However, as previously discussed in this

chapter, the frequency and the power employed may yield quite different results. In this sense, this final section deals with the few works by different authors that report the effect of frequency and power on the characteristics of electrodeposited composite coatings. Nevertheless, it must be pointed out that these works do not only refer to Ni coatings, but also to Ni-based and Zn-based alloys, due to the lack of papers available in the literature dealing with this topic.

Effect of ultrasonic frequency

Only a couple of works have been found in the literature regarding the study of the effect of the ultrasonic frequency on the electrodeposition of composite coatings with particles. These works, both from the same research group, are focused on the electrodeposition of Ni-W alloys with Al_2O_3 particles [118,119]. In these papers, the authors investigated the effect of low-frequency (35 kHz) and high-frequency (130 kHz) ultrasound on the characteristics of the composites. The results not only pointed that the presence of ultrasound during plating significantly reduced particle agglomeration, resulting in a more uniform dispersion of particles in composites, but also that composites produced at 130 kHz presented a lower and less uniform particle content than those electrodeposited at 35 kHz, as shown in Figure 2.10 for Ni-W/Al_2O_3 composite coatings produced from baths with different particle concentrations. The reason for this is that the formation and intensity of cavitation phenomena progressively decrease as the ultrasonic frequency is increased as rarefaction and compression cycles are shorter, resulting in bubbles with a smaller resonant size [55]. Larger bubbles undergo a more violent collapse, and therefore, mechanical effects caused by the presence of cavitation phenomena are predominant at lower frequencies, whereas chemical effects are more significant at higher frequencies [93,120,121]. The mechanical effects would be the ones of interest for the electrodeposition of composite coatings with embedded particles, as mechanical events such as acoustic streaming, formation of micro-jetting and shockwaves would be the ones enhancing the dispersion and

de-agglomeration of particles in the electrolyte and the incorporation of well-dispersed and uniformly distributed particles into the electrodeposited coating.

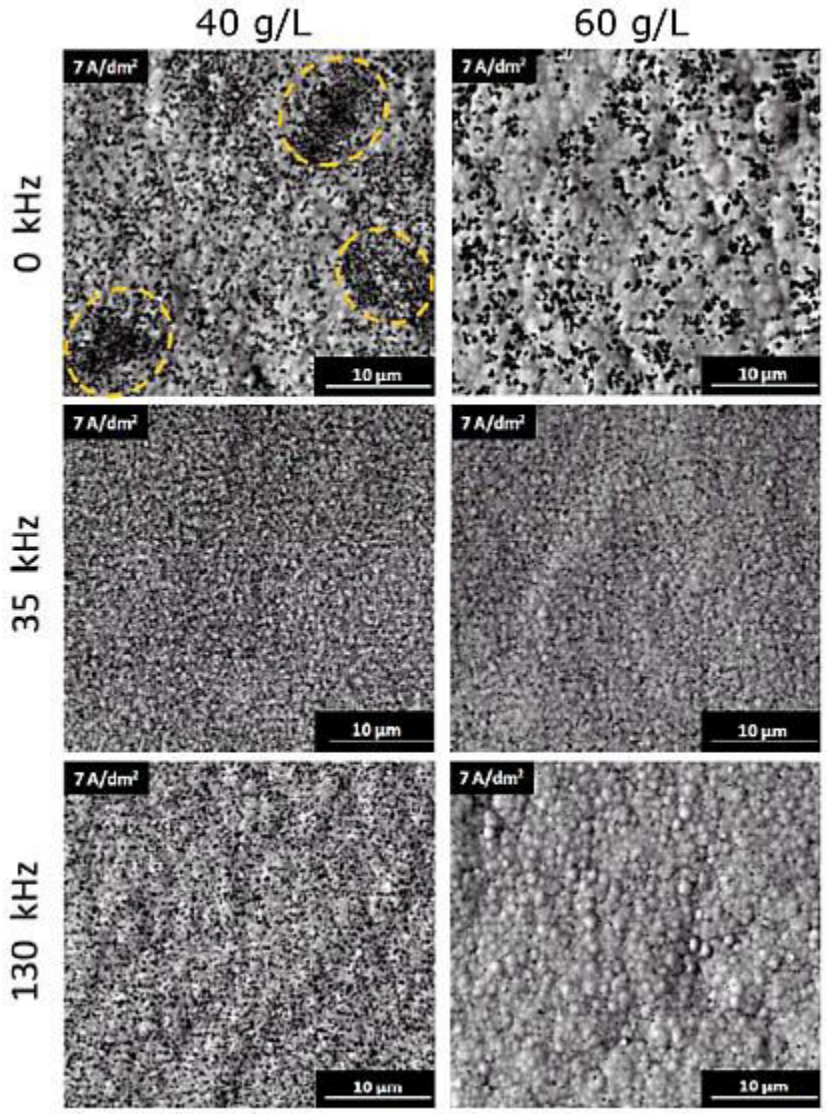

Figure 2.10. SEM images of surface morphology of Ni-W/Al_2O_3 composites electrodeposited under different ultrasonic frequency from baths with different particle concentration. Adapted from Ref. [119].

Effect of ultrasonic power

As in the case of ultrasonic frequency, not many works focused on the effect of ultrasonic power are available in the literature. Among these, the study of the effect of ultrasound on the electrodeposition of Zn-Ni/Al_2O_3 composites by Zheng et al. [122] constitutes the best example of how ultrasonic power may affect particle incorporation. In this paper, the authors observed that higher ultrasonic powers (they used a 20 kHz ultrasonic horn in their

study) yielded an increase in the content of the particles in the coating. However, they also observed that there was a maximum value for the particle content versus ultrasonic power, and then, a further increase in the power would lead to a decrease in the particle content in the coating (Figure 2.11). According to the authors, a possible explanation for this could be that the Al_2O_3 particles collide with the cathode under strong sonication (which occurs at the highest powers) and then break away from there, which would result in a decrease in the particle content in the coating. García-Lecina et al. [117] recently observed the same trends in their Ni-based composite coatings containing inorganic fullerene-like WS_2 particles (IF-WS_2): particle incorporation into the Ni matrix increased with ultrasonic powers† up to 30 W cm^{-2}, and slightly decreased at higher powers (40 W cm^{-2}) due to excessive forced convection in the latter.

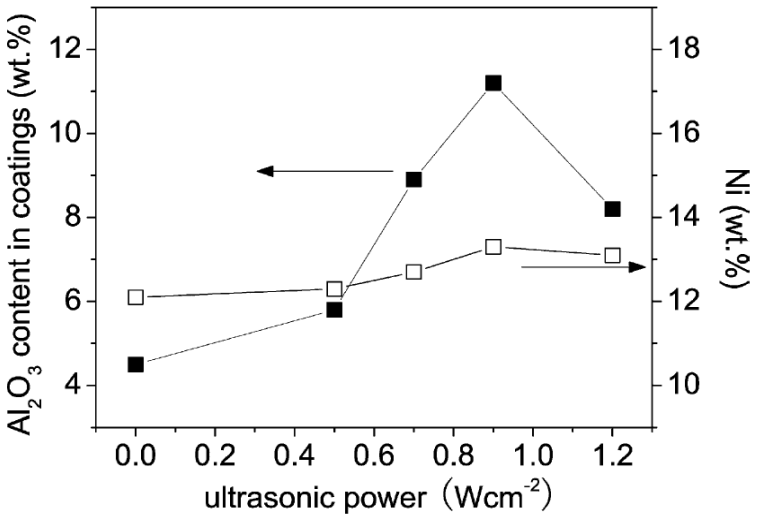

Figure 2.11. Influence of ultrasonic power on the nano-alumina contents in Zn-Ni/Al_2O_3 nanocomposite coatings and Ni contents in the Zn-Ni matrix of composite coatings. Adapted from Ref. [122].

For the Zn-Ni/Al_2O_3 composites [122], the same trend was observed in the mechanical properties such as the hardness of the material which allowed them to correlate the hardness of the coating strictly to the particle content (Figure 2.12), with no other effect of

† Ultrasonic power values included in Garcia-Lecina's work were not estimated according to the classical calibration method described in Appendix A and therefore should be cautiously considered, as it seems that the authors just divided the transducer output power by the emitter area.

the ultrasonic power. Similar observation was observed for the Ni/IF-WS_2 composite coatings produced by García-Lecina et al. [117], as hardness, reduced Young's modulus and elastic recovery seemed to be more related to the particle content in the coating than the ultrasonic power itself, whereas the elastic strain to failure, although significantly enhanced by the presence of particles, also was progressively improved by further increase in the ultrasonic power.

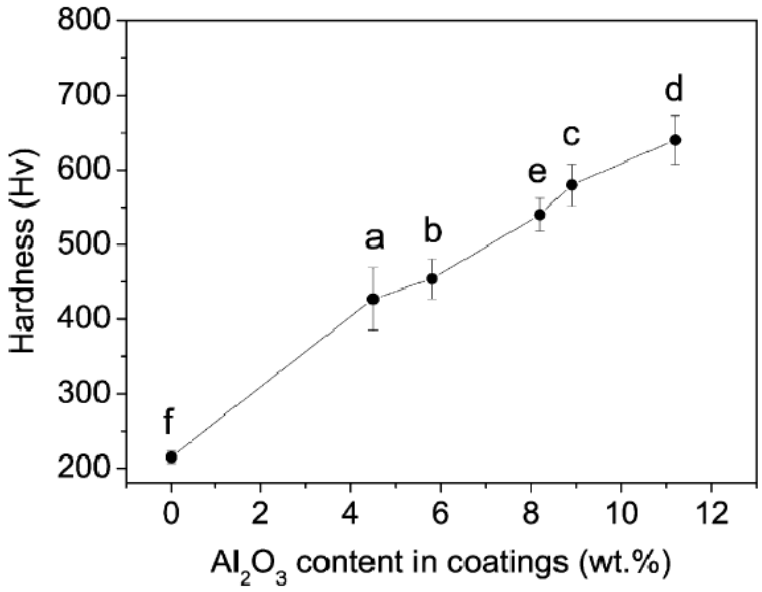

Figure 2.12. Hardness of Zn-Ni alloy (f) and Zn-Ni/Al_2O_3 composite coatings fabricated under different powers: (a) 0 W cm^{-2}; (b) 0.5 W cm^{-2}; (c) 0.7 W cm^{-2}; (d) 0.9 W cm^{-2}; (e) 1.2 W cm^{-2}. Adapted from Ref. [122].

2.5. SUMMARY OF LITERATURE REVIEW AND NOVELTY OF THE RESEARCH PROJECT

The first part of this chapter (Section 2.1) briefly reviews recent developments in the use of Ni composite coatings as diffusion barrier layers in overlay systems for bearing applications. These are based on electroless Ni plating processes with no advanced dispersing method, which present a series of drawbacks related to the plating process itself (e.g. complexity, operational temperature, lifespan of chemicals, low deposition rate, expensive effluent treatment) and the lack of a proper dispersing method to prevent particle agglomeration in

the plating bath. These facts, combined with the lack of published literature focused on the study of diffusion issues in Pb-free overlay systems with Ni diffusion barrier layers in overlay systems, highlight the novelty of the main goal of the research here presented:

Electrodeposition of Ni composite coatings with enhanced tribological performance acting as diffusion barrier layers in bearing overlay systems

The second part of this chapter (Section 2.3) briefly reviews the electrodeposition of Ni from the so-called Watts bath and how Ni composite coatings with embedded particles can be electrodeposited from different electrolytes, whereas the third part of the chapter (Section 2.4) is dedicated to the use of ultrasound in the electrodeposition of Ni and Ni-based composite coatings. The use of ultrasound during the electrodeposition of metals refine the grain size of the deposit, resulting in a general improvement of the mechanical and corrosion resistance properties of Ni, which suggests that the use of ultrasound on its own could already improve the overall performance of Ni coatings when acting as diffusion barrier layers. Regarding the electrodeposition of Ni composites with particles, a general improvement in the de-agglomeration and dispersion of particles in Watts and sulphamate electrolytes, with and without further addition of additives and surfactants, is usually achieved when the electroplating bath is sonicated. The use of ultrasound facilitates the dispersion of particles to the point that more studies are found with the absence of additives or surfactants in the electrolyte. Further improvement in the distribution of fine, well-dispersed particles in Ni coatings is generally achieved when ultrasound is also used during the electrodeposition process, resulting in enhanced hardness and wear resistance.

It is interesting to point out that the addition of surfactants to the electrolyte is nearly a must in order to produce Ni composites coatings in absence of ultrasound. Related to this, the use of ultrasound has already been proved quite successful in the electrodeposition of Ni composite coatings with hard particles (i.e. Al_2O_3, SiC, TiN) from additive-free Watts bath formulations. However, very little research has been carried out so far related to the

ultrasound-assisted electrodeposition of Ni composite coatings with soft particles from a Watts bath. Only one work, contemporary to the present PhD research project, is available in the literature regarding the ultrasound-assisted electrodeposition of Ni composite coatings with lubricant articles (IF-WS_2 particles) from a Watts bath [117]. Nevertheless, the addition of a surfactant was also necessary in this latter case, and this fact itself highlights another aspect of novelty of the research here presented:

> ***Electrodeposition of Ni composite coatings with soft particles from an additive-free Watts bath with the aid of ultrasound***

In this sense, the work included in this thesis addresses the knowledge gap of understanding how ultrasonic cavitation may interact with the stirring of the solution, and the effect that this has on the dispersion of particles and their incorporation into the Ni coatings during the electrodeposition process. By understanding this interaction and selecting the best conditions for the dispersion and the electrodeposition stages separately, it has been possible to electrodeposit Ni composite coatings with enhanced tribological performance (i.e. Ni/WS_2 composite) from an additive-free bath with no further addition of a surfactant.

Regarding the electrodeposition of thin Ni coatings under ultrasound, although a few works are found in the literature regarding the benefits in terms of the mechanical performance of such coatings, no detailed studies are found on the effect that low-frequency ultrasound, more specifically the ultrasonic power, could have on the characteristics of electrodeposited Ni coatings. In this sense, the ***study of the effect of low-frequency ultrasound on the characteristics of Ni coatings electrodeposited from a Watts bath*** is a secondary aspect of novelty of the present thesis.

2.6. REFERENCES

[1] R. Reinicke, M. Seremeti, DE patent 102010011083, 2011.

[2] R. Reinicke, M. Seremeti, K. Pucher, DE patent 102011013881, 2011.

[3] A. D. McNaught, A. Wilkinson, IUPAC. Compendium of Chemical Terminology, 2nd ed. (the 'Gold Book'), Blackwell Scientific Publications, Oxford, 1997. XML on-line corrected version: M. Nic, J. Jirat, B. Kosata, A. Jenkins, http://goldbook.iupac.org

[4] M. Schlesinger, Electroplating, in: Zoltan Nagy (Ed.), Electrochemistry Enciclopedia, http://electrochem.cwru.edu/encycl/index.html

[5] Y.D. Gamburg, G. Zangari, Theory and practice of Metal Electrodeposition, Springer, New York-Dordrecht-Heidelberg-London, 2011.

[6] G. Bird, Phil. Trans. R. Soc. Lond. 127 (1837) 37.

[7] G.A. Di Bari, Electrodeposition of Nickel, in: M. Schlesinger, M. Paunovic (Eds.), Modern Electroplating, 5th ed., John Wiley & Sons, Hoboken, 2010.

[8] The socio-economic impact of the nickel industry in the EU: United Kingdom country report (prepared for The Nickel Institute), The Weinberg Group LLC, Brussels, 2008.

[9] F.B. Howard-White, Nickel, an historical review, Methuen and Co, London, 1963.

[10] R. Boettger, J. Prakt. Chem. 30 (1843) 257.

[11] J.K. Dennis, T.E. Such, Nickel and Chromium plating, 3rd ed., Woodhead Publishing, Cambridge, 1993.

[12] G. Gore, The art of electro-metallurgy including all known processes of electro-deposition (2nd ed.), D. Appleton and Co, New York, 1884.

[13] I. Adams, US patent 93157, 1869.

[14] I. Adams, US patent 136634, 1873.

[15] W.H. Remington, US patent 82877, 1868.

[16] E. Weston, US patent 211071, 1878.

[17] O.P Watts, Trans. Am. Electrochem. Soc. 29 (1916) 395.

[18] R. Oriňáková, A. Turoňová, D. Kladeková, M. Gálová, R.M. Smith, J. Appl. Electrochem. 36 (2006) 957.

[19] A. Saraby-Reintjes, M. Fleischmann, Electrochim. Acta 29 (1984) 557.

[20] P. Allongue, L. Cagnon, C. Gomes, A. Gu¨ ndel and V. Costa, Surf. Sci. 557 (2004) 41.

[21] K.D. Song, K.B. Kim, S.H. Han, H.K. Lee, Electrochem. Commun. 5 (2003) 460.

[22] M. Enyo, in: J.O'M. Bockris, B.E. Conway (Eds.), Modern Aspects of Electrochemistry, vol. 11, Plenum Press, New York,1975, p. 251.

[23] J.O'M. Bockris, S.U.M. Khan, in: Surface Electrochemistry, Plenum Press, New York, 1993, p. 833.

[24] K.J. Vetter, in: Electrochemical Kinetics, Academic Press, New York, 1967, pp. 525–535.

[25] M.H. Abd Elhamid, B.G. Ateya, H.W. Pickering, J. Electrochem. Soc. 144 (1997) L58.

[26] G.A. DiBari, J.V. Petrocelli, J. Electrochem. Soc. 112 (1965) 99.

[27] G. Okamoto, N. Sato, J. Electrochem. Soc. 110 (1963) 605.

[28] A.C. Hart, S.A. Watson, Met. Finish. 19 (1973) 332.

[29] A.C. Hart, W.R. Wearmouth, A.C. Warner, Trans. Inst. Met. Finish. 54 (1976) 56.

[30] G. Okamoto, N. Sato, J. Electrochem. Soc. 110 (1963) 605.

[31] C.G. Fink, J.D. Prince, Trans. Am. Electrochem. Soc. 54 (1928) 315.

[32] V.N. Tselulkin, Prot. Met. Phys. Chem. Surf. 45 (2009) 312.

[33] C.T.J. Low, R.G.A. Wills, F.C. Walsh, Surf. Coat. Technol. 201 (2006) 371.

[34] D. Thiemig, R. Lange, A. Bund, Electrochim. Acta 52 (2007) 7362.

[35] J. Tan, T. Yu, B. Xu, Q. Yao, Tribol. Lett. 21 (2006) 107.

[36] A. Bund, D. Thiemig, Surf.Coat. Technol. 201 (2007) 7092.

[37] Q. Feng, T. Li, H. Yue, K. Qi, F. Bai, J. Jin, Appl. Surf. Sci. 254 (2008) 2262.

[38] H. Gül, F. Kılıc¸ , S. Aslan, A. Alp, H. Akbulut, Wear 267 (2009) 976.

[39] S.T. Aruna, C.N. Bindu, V.E. Selvi, V.K.W. Grips, K.S. Rajam, Surf. Coat. Technol. 200 (2006) 6871.

[40] Y.-J. Xue, D. Zhu, F. Zhao, J. Mater. Sci. 39 (2004) 4063.

[41] S.A. Lajevardi, T. Shahrabi, Appl. Surf. Sci. 256 (2010) 6775.

[42] C.T.J. Low, J.O. Bello, J.A. Wharton, R.J.K. Wood, K.R. Stokes, F.C. Walsh, Surf. Coat. Technol. 205 (2010) 1856.

[43] L. Tian, J. Xu, Appl. Surf. Sci. 257 (2011) 7615.

[44] W. Wang, F.-Y.Hou, H. Wang, H.-T.Guo, Scripta Mater. 53 (2005) 613.

[45] M. Lekka, N. Koulombi, M. Gajo, P.L. Bonora, Electrochim. Acta 50 (2005) 4551.

[46] M. Lekka, C. Zanella, A. Klorikowska, P.L. Bonora, Electrochim. Acta 55 (2010) 7876.

[47] M. Surender, R. Balasubramaniam, B. Basu, Surf. Coat. Technol. 187 (2004) 93.

[48] E. Pompei, L. Magagnin, N. Lecis, P.L. Cavallotti, Electrochim. Acta 54 (2009) 2571.

[49] V. N. Tseluikin, N. D. Solov'eva, and I. F. Gun'kin, Prot. Met. 43 (2007) 388.

[50] A.J. Rethinam, G.N.K.R. Bapu, R.M. Krishnan, Mater. Chem. Phys. 85 (2004) 251.

[51] P. Bercot, E. Peña-Muñoz, J. Pagetti, Surf. Coat. Technol. 157 (2002) 282.

[52] J.P. Celis, J.R. Roos, C. Buelens, J. Fransaer, Trans. Inst. Met. Finish. 69 (1991) 133.

[53] K.S. Suslick, Science 247 (1990) 1439.

[54] L.H. Tohmpson, L.K. Doraiswamy, Ind. Eng. Chem. Res. 38 (1999),1215.

[55] T.J. Mason, J.P. Lorimer, Applied Sonochemistry: The use of power ultrasound in chemistry and processing, Wiley-VCH, Weinheim, 2002.

[56] K.S. Suslick, Y. Didenko, M.M. Fang, T. Hyeon, K.J. Kolbeck, W.B. McNamara III, M.M. Mdleleni, M. Wong, Phil. Trans. R. Soc. Lond. A 357 (1999) 335.

[57] O. Louisnard, J. González-García, Acoustic cavitation, in: H. Feng, G. Barbosa-Canovas, J. Weiss (Eds.), Ultrasound technologies for food and bioprocessing, Springer, New York-Dordrecht-Heidelberg-London, 2011.

[58] T.J. Mason, V. Sáez, An introduction to Sonoelectrochemistry, in: B.G. Pollet (Ed.), Power ultrasound in Electrochemistry: From versatile laboratory tool to engineering solution, John Wiley & Sons, Chichester (UK), 2012.

[59] K.S. Suslick, Sci. Am. 260 (1989), 80.

[60] J. González-García, V. Sáez, I. Tudela, M.I. Díez-García, M.D. Esclapez, O. Louisnard, Water 2 (2010) 28.

[61] K.S. Suslick, D.A. Hammerton, R.E. Cline, J. Am. Chem. Soc. 108 (1986) 5641.

[62] E.B. Flint, K.S. Suslick, Science 253 (1991) 1397.

[63] K.S. Suslick, Sonochemistry, in: Kirk-Othmer Encyclopedia of Chemical Technology, 4th edition, John Wiley & Sons, New York, 1998.

[64] D. Fernandez Rivas, P. Cintas, H.J.G.E. Gardeniers, Chem. Commun. 48 (2012) 10935.

[65] K.S. Suslick, G.J. Price, Annu. Rev. Mater. Sci. 29 (1999) 295.

[66] A. Cobley, T.J. Mason, L. Paniwnyk, V. Sáez, Aspects of ultrasound and materials science, in: D. Chen, S.K. Sharma, A. Mudhoo, Handbook of applications of ultrasound: Sonochemistry for sustainability, CRC Press, Boca Raton FL, 2012.

[67] G. Cravotto, P. Cintas, Chem. Soc. Rev. 35 (2006) 180.

[68] P. Cintas, G. Palmisano, G. Cravotto, Ultrason. Sonochem. 18 (2011) 836.

[69] N.H. Ince, G. Tezcanli, R.K. Belen, I.G. Apikyan, Appl. Catal. B 29 (2001) 167.

[70] E.V. Rokhina, P. Lens, J. Virkutyte, Trends Biotechnol. 27 (2009) 298.

[71] F. Chemat, Zill-e-Huma, M. K. Khan, Ultrason. Sonochem. 18 (2011) 813.

[72] J. González-García, M.D. Esclapez, P. Bonete, Y. Vargas Hernández, L. Gaete-Garretón, V. Sáez, Ultrasonics 50 (2010) 318.

[73] T.J. Mason, J.P. Lorimer, D.J. Walton, Ultrasonics 28 (1990) 333.

[74] N. Morigushi, J. Chem. Soc. Jpn. 55 (1934) 749.

[75] J. Klima, C. Bernard, Ch. Degrand, J. Electroanal. Chem. 367 (1994) 297.

[76] J. Klima, C. Bernard, J. Electroanal. Chem. 462 (1999) 181.

[77] P.R. Birkin, D.G. Offin, P.F. Joseph, T.G. Leighton, J. Phys. Chem. B 109 (2005) 16997.

[78] J.L. Hardcastle, J.C. Ball, Q. Hong, F. Marken, R.G. Compton, S.D. Bull, S.G. Davis, Ultrason. Sonochem. 7 (2000) 7.

[79] D.J. Walton, S.S. Phull, A. Chyla, J.P. Lorimer, T.J. Mason, L. Burke, M. Murphy, R.G. Compton, J.C. Eklund, S.D. Page, J. Appl. Electrochem. 25 (1995) 1083.

[80] E.L. Cooper, L.A. Coury Jr., J. Electrochem. Soc. 145 (1998) 1994.

[81] K.B. Holt, J. Del Campo, J.S. Foord, R.G. Compton, F. Marken, J. Electroanal. Chem. 513 (2001) 94.

[82] F. Marken, R.G. Compton, Electrochim. Acta 43 (1998) 2157.

[83] D.J. Walton, S.S. Phull, D.M. Bates, J.P. Lorimer, T.J. Mason, Ultrasonics 30 (1992) 186.

[84] F.J. del Campo, A. Neudeck, R.G. Compton, F. Marken, J. Electroanal. Chem. 477 (1999) 71.

[85] D.L. Goldfarb, H.R. Corti, F. Marken, R.G. Compton, J. Phys. Chem. A 102 (1997) 2055.

[86] V. Frenkel, R. Gurka, A. Liberzon, U. Shavit, E. Kimmel, Ultrasonics 39 (2001) 153.

[87] J. Lighthill, J. Sound Vib. 61 (1978) 391.

[88] M.S. Plesset, R.B. Chapman, J. Fluid Mech. 47 (1971) 283.

[89] W. Lauterborn, H. Bolle, J. Fluid Mech. 72 (1975) 391.

[90] C.-D. Ohl, T. Kurz, R. Geisler, O. Lindau, W. Lauterborn, Phil Trans. R. Soc. Lond. A 357 (1999) 269.

[91] F.J. del Campo, B.A. Coles, F. Marken, R.G. Compton, E. Cordemans, Ultrason. Sonochem. 6 (1999) 189.

[92] R.G. Compton, J.L. Hardcastle, J. del Campo, Sonoelectrochemistry, Physical Aspects, in: Bard-Stratmann (Ed.), Encyclopedia of Electrochemistry, in: Pat Unwin (Ed.), Instrumentation and Electrochemical Chemistry, vol. 3, 2003, pp. 312-327.

[93] T.J. Mason, A.J. Cobley, J.E. Graves, D. Morgan, Ultrason. Sonochem. 18 (2011) 226.

[94] S.R. Rich, Plat. 42 (1955) 1407.

[95] J. Dereska, E. Yeager, F. Kovorka, J. Acoust. Soc. Am. 29 (1957) 769.

[96] K. Kobayasi, A. Chiba, N. Minami, Ultrasonics 38 (2000) 676.

[97] T. Lampke, D. Dietrich, A. Leopold, G. Alisch, B. Wielage, Surf. Coat. Technol. 202 (2008) 3967.

[98] C.T. Walker, R. Walker, Electrodepos. Surf. Treat. 1 (1973) 457.

[99] P.B.S.N.V. Prasad, R. Vasudevan, S.K. Seshadri, S. Ahila, Mater. Lett. 17 (1993) 357.

[100] C. Zanella, M. Lekka, P.L. Bonora, Surf. Eng. 26 (2010) 511.

[101] E. García-Lecina, I. García-Urrutia, J.A. Díez, J. Morgiel, P. Indyka, Surf. Coat. Technol. 206 (2012) 2998.

[102] T.R. Mahmood, J.K. Dennis, P.L. Barrett, Surf. Technol. 22 (1984) 219.

[103] R. Walker, S.A. Halagan, Plat. Surf. Finish. 72 (1985) 68.

[104] P.B.S.N.V. Prasad, R. Vasudevan, S.K. Seshadri, J. Mater. Sci. Lett. 11 (1992) 1424.

[105] P.B.S.N.V. Prasad, R. Vasudevan, S.K. Seshadri, J. Mater. Sci. Lett. 12 (1993) 902.

[106] P.B.S.N.V. Prasad, S. Ahila, R. Vasudevan, S.K. Seshadri, J. Mater. Sci. Lett. 13 (1994) 15.

[107] C. Zanella, M. Lekka, S. Rossi, F. Deflorian, Corros. Rev. 29 (2011) 253.

[108] S.-L. Kuo, Y.-C.Chen, M.-D.Ger, W.-H.Hwu, Mater. Chem. Phys. 86 (2004) 5.

[109] N.S. Qu, K.C. Chan, D. Zhu, Scripta Mater. 50 (2004) 1131.

[110] Y.-J. Xue, J.-S. Li, W. Ma, M.-D. Duan, M.-M. Lan, Fabrication and wear resistance of Ni-CeO_2 nanocomposite coatings by electrodeposition under ultrasound condition, in: J. Luo, Y. Meng, T. Shao, Q. Zhao (Eds.), Advanced Tribology - Proceedings of CIST2008 & ITS-IFToMM2008, Tsinghua University Press (Beijing) and Springer (Dordrecht, Heidelberg, London, New York), 2010, pp. 695-696.

[111] T.V. Sviridova, L.I. Stepanova, D.V. Sviridov, J. Solid State Electrochem. 16 (2012) 3799.

[112] S.A. Lajevardi, T. Shahrabi, V. Hasannaeimi, Mater. Corros. 62 (2011) 29.

[113] C. Cai, X.B. Zhu, G.Q. Zheng, Y.N. Yuan, X.Q. Huang, F.H. Cao, J.F. Yang, Z. Zhang, Surf. Coat. Technol. 205 (2011) 3448.

[114] G. Gyawali, S.H. Cho, D.J. Woo, S.W. Lee, Trans. Inst. Met. Finish. 90 (2012) 274.

[115] S. Mohajeri, A. Dolati, S. Rezagholibeiki, Mater. Chem. Phys. 129 (2011) 746.

[116] F.-f. Xia, M.-h.Wu, F. Wang, Z.-y. Jia, A.-l. Wang, Curr. Appl. Phys. 9 (2009) 44.

[117] E. García-Lecina, I. García-Urrutia, J.A. Díez, J. Fornell, E. Pellicer, J. Sort, Electrochim. Acta 114 (2013) 859.

[118] P. Indyka, E. Beltowska-Lehman, M. Bieda, J. Morgiel, L. Tarkowski, Surf. Coat. Technol. 211 (2012) 62.

[119] E. Beltowska-Lehman, P. Indyka, A. Bigos, M. Kot, L. Tarkowski, Sol. St. Phen. 186 (2012) 234.

[120] G. Portenlänger, H. Heusinger, Ultrason. Sonochem. 4 (1997) 127.

[121] K.V.B. Tran, T. Kimura, T. Kondo, S. Koda, Ultrason. Sonochem. 21 (2014) 716.

[122] H.-Y. Zheng, M.-Z. An, J. Alloy. Compd. 459 (2008) 548.

3. EXPERIMENTAL METHODS

3.1. OVERVIEW

This chapter summarizes all the information regarding the experimental work carried out during the present project. The different experimental procedures and methods have been divided into four major sections:

1. 'Wet chemistry' experiments, which includes all the information and details regarding the ultrasonic equipment used, the Watts bath employed, the plating set-up and the electroplating experiments carried out for each study.
2. Characterization of coatings, which refers to all the different methods and techniques employed to characterize the Ni deposits and Ni-based composite coatings produced during the electroplating experiments.
3. Performance of coatings acting as tribologically active layers, regarding the tribological analysis (i.e. 'scratch' tests under lubricated and non-lubricated conditions) performed on selected Ni-based coatings electrodeposited on real Pb-bronze substrates.
4. Performance of coatings acting as diffusion barrier layers, which refers to the different tests performed on samples were selected Ni-based coatings were used as interlayers between Cu substrates and Sn-Cu overlays electrodeposited on top of the Ni-based coatings.

3.2. 'WET CHEMISTRY' EXPERIMENTS

3.2.1. ULTRASONIC EQUIPMENT

As previously explained in Section 2.3.1.2, despite the fact that both mechanical and chemical effects of the introduction of ultrasound and the presence of acoustic cavitation in a liquid are observed at both low and high frequencies, mechanical effects (e.g. acoustic streaming, micro-jetting, release of shockwaves) are predominant at lower frequencies, whereas chemical effects (e.g. radical formation, sonoluminescence) are more significant at higher frequencies. Mechanical effects are of special interest in electroplating not only due to the improvement of mass transport to/from the electrode, but also due to grain size refinement and structure modification, which may result in the enhancement of the mechanical properties of electrodeposited Ni coatings in this particular case. These mechanical effects of acoustic cavitation are also helpful to disperse particles in the working

solution and de-agglomerate large agglomerates and aggregates that otherwise would form and grow in the electrolyte and therefore be incorporated into the electrodeposited coatings. Due to the nature of the project and the availability of ultrasonic equipment from industrial suppliers, it was decided to study the effect that low-frequency ultrasound, which commonly ranges from 20 to 100 kHz, has on the electrodeposition of Ni on Cu substrates and on the dispersion of lubricant particles in both the plating solutions and the electrodeposited coatings.

An ultrasonic bath was used in the present research project in order to establish an ultrasonic field in the electrolyte. The different reasons for using this type of system instead of an ultrasonic horn were:

1. *Cavitation erosion.* High-power ultrasonic horns, although very effective in order to disperse particles in short periods of time, produce very violent cavitation phenomena that may erode the surface of the deposits if they are placed near the transducer. Violent cavitation near the electrode can also have a negative effect in particle content in electrodeposited composite coatings, as particles may collide with the surface of the electrode under strong cavitation and then break away from there [1] or might be removed from the surface of the cathode by the 'scrubbing action' of cavitating bubbles.
2. *Ultrasonic power.* Very high acoustic pressures can be achieved in a liquid when using a horn-type transducer in a small laboratory beaker. Nevertheless, these high ultrasonic powers are unlikely to be achieved in a large tank for electroplating bearings, whereas the pressure amplitude and acoustic field in an ultrasonic bath would be very much alike. In fact, due to the special nature of how bearings are electroplated (bearings are mounted in a jig inside a box with a narrow gap facing the anode to ensure an electric field as uniform as possible on the inner surface of the bearings), the only feasible option to set an effective ultrasonic field in plating tanks for electroplating bearings would be the use of submersible units that would

consist of different transducers with the same basic design as those used in ultrasonic baths.

3. *Ultrasonic attenuation.* Very high ultrasonic pressures can be achieved with a horn, which would obviously result in violent cavitation phenomena in the fluid. Nevertheless, most of the cavitation actually occurs near the emitter surface of the horn, as the highest pressures are achieved in this region. The formation of these cavitating bubbles has a negative effect when considering the application of ultrasound in bearing plating: a strong attenuation of the ultrasonic field in the region near the emitter surface due to the presence of the bubbles themselves [2,3]. This effect is much less significant in an ultrasonic bath, where a more homogeneous ultrasonic field can be set, resulting in the observation of cavitation phenomena not only near the emitter surface of the transducers, but also further away from this point.

The ultrasonic bath employed was a QS12 cleaning bath (ultrasonic frequency: ≈35 kHz, ultrasonic transducer power: 200 W, heating power: 300 W, working capacity: 12.5 L) provided by Ultrawave Ltd. This ultrasonic bath was equipped with a generator system which allowed its operation at different ultrasonic output powers (from 50% to 100%). For ultrasonic output powers of 60%, 80% and 100%, the estimated ultrasonic power† by calorimetry [4] was 0.011, 0.124 and 180 W/cm^3, respectively. More details on the calibration experiments by calorimetry are included in Appendix A.

3.2.2. Ni Watts bath

The Ni-based plating method employed in the present research was based on a standard Ni Watts bath process currently employed by DIBE [5,6]. Such Ni Watts bath process is free of additives.

† Ultrasonic power estimated by calorimetry is expressed in W/cm^3 as these are the units generally used in Sonochemistry and Sonoelectrochemistry.

The chemical and operational parameters of the Watts bath in the production line are:

- $NiSO_4.6H_2O$: ≈290.0 ± 20.0 g/L
- $NiCl_2.6H_2O$: ≈52.5 ± 7.5 g/L
- H_3BO_3: ≈32.5 ± 7.5 g/L
- pH: 3.2 (2.5 to 3.5)
- Temperature: 50 ± 5 °C
- Current density‡: 4.0 A/dm²

3.2.2.1. PREPARATION OF THE BATH

The Ni plating solutions were prepared according to DIBE's procedure [5] with aqueous solutions of 550 g/L $NiSO_4.6H_2O$ and 720 g/L $NiCl_2.6H_2O$ supplied by Schloetter Co. Ltd. and H_3BO_3 (>99.5%) provided by Fisher Scientific UK Ltd. As both $NiSO_4.6H_2O$ and $NiCl_2.6H_2O$ were provided as concentrated aqueous solutions, the volume necessary to make 1 L of solution was:

- Deionised water: 0.398 L.
- $NiSO_4.6H_2O$: 0.529 L.
- $NiCl_2.6H_2O$: 0.073 L.

The steps necessary to prepare 1 L of solution were:

1. Filling of the vessel up to one third (0.333 L) with deionised water.
2. Addition of 0.529 L of $NiSO_4.6H_2O$ and 0.073 L of $NiCl_2.6H_2O$ while stirring. Add the rest of the deionised water and heat the resulting solution to 50 °C.
3. Addition of 32.5 g of H_3BO_3 and thoroughly stir the solution

‡ Current density is expressed in A/dm² as these are the units generally used in the Surface Finishing industry.

3.2.3. EXPERIMENTAL SET-UP

3.2.3.1. ELECTRODEPOSITION OF NI AND NI-BASED COMPOSITE COATINGS UNDER ULTRASOUND

All the electrodeposition experiments were conducted in a 0.6 L beaker containing 0.5 L of the plating solution immersed in an Ultrawave QS12 ultrasonic bath as shown in Figure 3.1. The beaker was always placed in the centre of the bath at a certain depth (11 cm between the bottom of the beaker and the surface of the water) with a certain water level (2 cm between the edge of the ultrasonic bath and the surface of the water) in the ultrasonic bath to ensure the reproducibility of the experiments. An IPS2010 power supply unit (0 to 20 V, 1 to 10 A) from ISO-TECH was used as the rectifier. A CAT R18 85W overhead stirrer (110 to 2000 rpm) equipped with a 3-point propeller shaft (5 cm wide) was used in those experiments conducted under mechanical agitation, once it was confirmed that the presence of the propeller had no effect on the characteristics of the Ni deposits produced.

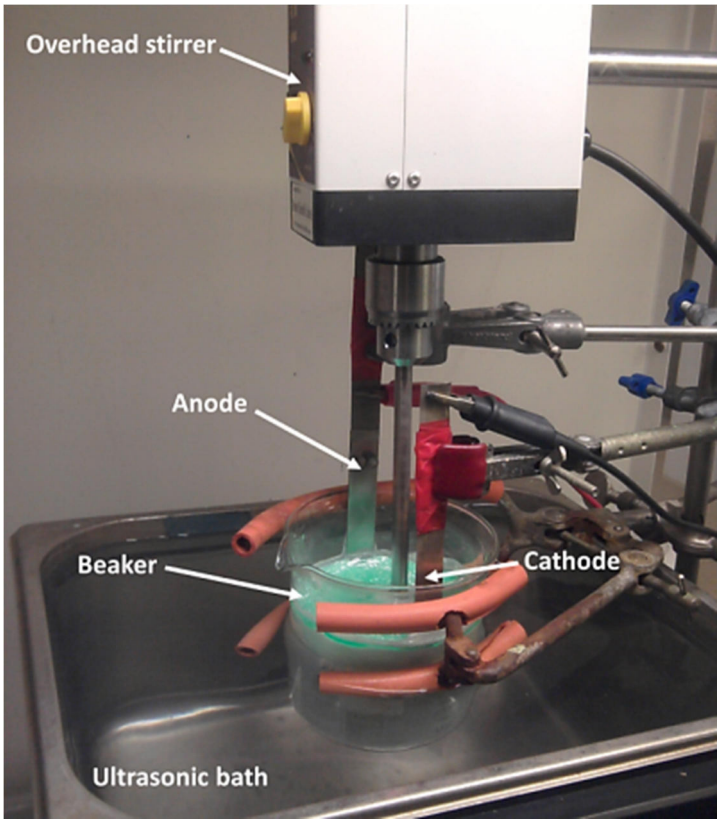

Figure 3.1. Experimental set-up for small scale electroplating experiments.

Cu substrates (5×2×0.12 cm) supplied by Metal Sheets Ltd. were used as cathodes in most of the electrodeposition experiments. As the back side of the Cu substrate was masked in order to have a better control of the thickness of the coatings (Figure 3.2), the active area of the Cu cathodes directly facing the anode (2×2 cm), which was 4 cm^2, was the area considered for the calculation of the current density applied during the electrodeposition experiments. In order to achieve a good adhesion of the Ni-based coatings on the Cu substrates, the samples to be plated were vapour-degreased for 15 minutes in a Dürr Ecoclean degreaser and the cathode surface was activated with an anodic acid etching process (Cu substrate acting as an anode in a HCl 25% solution at 3 A/dm^2 for 1.5 minutes). In all the experiments, Ni anodes (7×14×0.05 cm) with an approximate active area of 20 cm^2 were produced from Ni 201 sheets (99.0% of Ni) supplied by William Gregor Ltd.

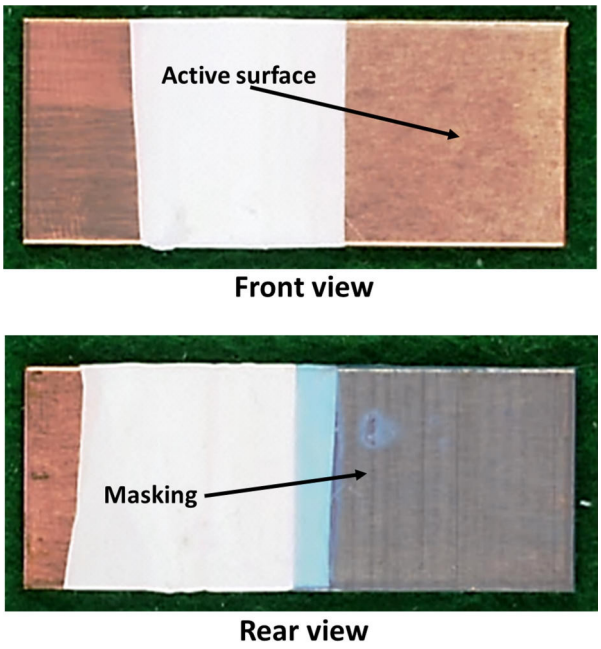

Figure 3.2. Cu substrates with masked back side employed in the electrodeposition experiments.

3.2.4. EXPERIMENTAL PROCEDURES

3.2.4.1. ULTRASOUND-ASSISTED ELECTRODEPOSITION OF NI COATINGS

Electrodeposition of Ni coatings on Cu substrates under ultrasound

The objective of this stage of the study was to observe the effect that ultrasound (i.e. ultrasonic power) has on the characteristics of Ni coatings electrodeposited from the Watts bath. Ni deposits were electrodeposited on the Cu substrates under five different agitation conditions (silent/still, ultrasonic agitation at 0.011, 0.124 and 0.180 W/cm^3, and mechanical agitation at 300 rpm) at 4 A/dm^2 to be later examined by different methods: XRD, FIB-SEM, etc. Plating time was 14 minutes in order to achieve a Ni coating with a thickness around 6 μm in the central area of the Cu substrate after considering that, due to the substrate geometry used (2×2 cm^2 active area) and the absence of a levelling agent, 'edge build-up'§ was quite significant towards the edges of the surface of the cathode. The reason for producing such thin deposits is that most of the Ni coatings used as interlayers in bearing applications are not usually thicker than 6 μm.

Effect of ultrasound on the stability of the Watts bath

The purpose of this part of the study was to observe any signs that might suggest the modification of the chemical parameters of the Watts bath due to the chemical effects of ultrasound (e.g. radical formation) after being irradiated for a certain time. For this reason, electroplating experiments in freshly prepared solutions were performed during 360 minutes (i.e. 6 hours) to observe any change in the pH and the concentration of $NiSO_4.6H_2O$, $NiCl_2.6H_2O$ and H_3BO_3.

To have an initial idea of the stability of the Watts Ni bath under continuous sonication during longer electrodeposition experiments, the following experimental process was performed at four different ultrasonic conditions (0 - still, 0.011, 0.124 and 0.180 W/cm^3):

§ Edge build-up: phenomenon where, as one moves from the centre of the active surface towards the edges of the deposit, the coating gets thicker, ending up with a greater thickness near the edges compared to the thickness observed in the central area.

1. Preparation of 0.5 L of the Ni Watts bath.
2. Initial evaluation of the bath parameters: $NiSO_4.6H_2O$, $NiCl_2.6H_2O$, H_3BO_3 and pH.
3. Plating of four Cu substrates for 14 minutes each at 4 A/dm^2.
4. Top-up with deionised water to compensate evaporation after 120 minutes. Evaluation of the bath parameters ($NiSO_4.6H_2O$, $NiCl_2.6H_2O$, H_3BO_3 and pH) after 120 minutes from the beginning of the experiment.
5. Plating of four thin Cu substrates for 14 minutes each at 4 A/dm^2.
6. Top-up with deionised water to compensate evaporation after 120 minutes. Evaluation of the bath parameters ($NiSO_4.6H_2O$, $NiCl_2.6H_2O$, H_3BO_3 and pH) after 240 minutes from the beginning of the experiment.
7. Plating of four thin Cu substrates for 14 minutes each at 4 A/dm^2.
8. Top-up with deionised water to compensate evaporation after 120 minutes. Final evaluation of the bath parameters ($NiSO_4.6H_2O$, $NiCl_2.6H_2O$, H_3BO_3 and pH) after 360 minutes from the beginning of the experiment.

Different analytical procedures were followed to evaluate the chemical parameters of the bath. More details on such analytical procedures may be found in Appendix B.

3.2.4.2. ULTRASOUND-ASSISTED ELECTRODEPOSITION OF NI-BASED COMPOSITE COATINGS WITH LUBRICANT PARTICLES

Freshly-made plating solutions were again prepared for this study. Four different lubricant particles were employed due to their lubricant properties, their commercial availability and the cost for its future use in production: i) WS_2 (D50[**] ≈ 0.6 μm, D90[††] ≈ 5 μm) supplied by M K Impex Corp, ii) hexagonal BN or hBN (D50 ≈ 0.5 μm, D90 ≈ 1.1 μm) also supplied by M K Impex Corp, iii) MoS_2 (D50 ≈ 1.2 μm) from Asbury, and iv) ZONYL MP1100 - PTFE

[**] D50 is the median particle size, meaning that 50% of the particles are smaller than the D50 size. This implies that 50% of the particles have a larger size than the D50 size.

[††] D90 is the 90th percentile of the particle size, meaning that 90% of the particles are smaller than the D90 size. This implies that 10% of the particles have a larger size than the D90 size.

agglomerates (1.8 to 4 μm) of submicron-sized particles supplied by Du Pont. Figure 3.3 displays the structure and size of the different particles used in the present research project.

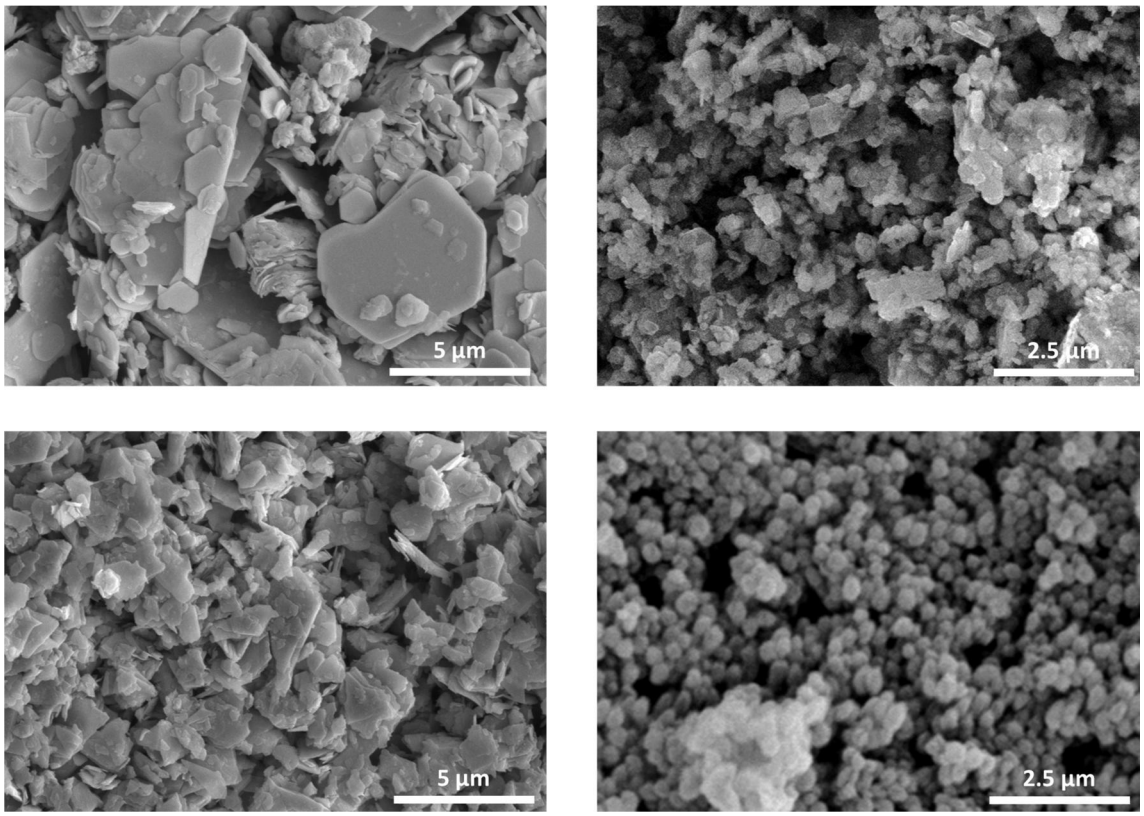

Figure 3.3. SEM images of the different lubricant particles used in the present research project: A) WS_2, B) hBN, C) MoS_2 and D) PTFE.

Although the concentration range of both lubricant and hard particles commonly found in the bibliography is 5 to 50 g/L, a concentration in the lower range, 15 g/L, was chosen for the present research project due to production cost in an eventual scaling up of the process: The maximum cost of the Watts bath with any dispersed particles was set at a 120% of a regular Watts bath by DIBE, which is roughly estimated around £8000 for a 850 L tank as those currently used in the production lines. This meant that the amount of particles added to 850 L of Watts bath could not cost more than £1600. Considering the unitary prices of the different commercially available particles (£51.10 per kg of WS_2, £115.21 per kg of hBN, £23.85 per kg of MoS_2 and £44.00 per kg of PTFE), a concentration of 15 g/L of the most

expensive particle (hBN) in 850 L of Watts bath would be £1468.92, under the limit of £1600.

Effect of ultrasound on the dispersion of particles in the Ni Watts bath

Visual appearance of dispersions

Different dispersions were produced with the four particles studied using the same experimental set-up previously described in Section 3.2.3.2. Particles were dispersed for 30 minutes under different conditions, and then, the dispersion was observed by the naked eye in order to check the change in visual appearance with time once the dispersing method was stopped. The three dispersing conditions employed were: i) mechanical agitation at 300 rpm in absence of ultrasound, ii) ultrasound at 0.180 W/cm^3, and iii) combined ultrasound/mechanical agitation at 0.180 W/cm^3 - 300 rpm. The reason for using ultrasound at 180 W/cm^3 was that, in order to maximize the incidence of physical effects induced by ultrasound, a high degree of cavitation activity in the overall system is necessary, and the highest cavitation activity is obviously achieved at the highest ultrasonic power available [7].

Particle size distribution experiments

Dispersions were again produced with the different particles for the particle size distribution studies, although in this case diluted Ni Watts bath solutions containing a low concentration of particles were used due to the analytical method (laser diffraction) employed for the estimation of the particle size distribution in the dispersions, which requires the use of clear solutions with low particle content. Laser diffraction methods are based on the measurement of the intensity of light scattered as a laser beam passes through a dispersed particulate sample by different detectors. Said intensity of light is analysed by different algorithms, mainly based on the Mie theory [8,9], in order to estimate the size of the particles that created the scattering pattern [10].

In the present project, a Mastersizer 2000 system provided by Malvern Instruments Ltd was employed. This system was equipped with red light (max. 4 mW He-Ne, 632.8 nm) and blue light (max. 0.3 mW LED, 470 nm) sources and a reverse Fourier lens arrangement (convergent beam), allowing the detection of particles with sizes ranging from 0.02 to 2000 μm. As in the visual appearance experiments, 0.5 L dispersions consisting of very diluted Ni Watts electrolyte (1 to 100 dilution) containing a low concentration of particles (0.1 g/L) were prepared by applying three different dispersing methods: mechanical agitation at 300 rpm in absence of ultrasound, ultrasound at 0.180 W/cm^3, and combined ultrasound/mechanical agitation at 0.180 W/cm^3 - 300 rpm) for 30 minutes. Once the dispersion process was completed, particle size distribution measurements were carried out by circulating the dispersions through the Mastersizer 2000 system under 1000 rpm agitation for 30 seconds to ensure a proper circulation.

Electrodeposition of Ni-based composite coatings on Cu substrates under ultrasound

This stage of the study had two main objectives: i) to evaluate the feasibility of the production of Ni-based composite coatings with embedded lubricant particles under different conditions, and ii) to characterize those selected composite coatings which presented a more uniform distribution of particles in the deposit. According to the results obtained during the first stage of the study, it was decided that Ni-based composite coatings containing WS_2, hBN and MoS_2 particles would be produced under different plating conditions.

A common dispersing method was employed in all the experiments in order to make proper comparisons between the different plating conditions used and the different composite coatings produced. It was decided that, in all cases, the particles would be previously dispersed in the Ni Watts bath for 30 minutes under the combined ultrasound/mechanical agitation dispersion method, as it was found out during the experiments that such

dispersing method produced the best dispersions. Ni-based composite coatings containing lubricant particles were plated under three different conditions: i) mechanical agitation at 300 rpm in absence of ultrasound, ii) ultrasound at 0.180 W/cm^3 and iii) combined ultrasound/mechanical agitation at 0.180 W/cm^3 - 300 rpm. The same experimental set-up and electroplating parameters used in the electrodeposition of pure Ni coatings (current density: 4 A/dm^2, plating time: 14 minutes) were used for the electrodeposition of the Ni-based composite coatings.

3.2.4.3. EVALUATION OF NI-BASED COATINGS ACTING AS TRIBOLOGICALLY ACTIVE LAYERS

Selected Ni-based coatings, namely Ni coatings electroplated under either mechanical agitation at 300 rpm and ultrasound at 0.180 W/cm^3 and Ni/WS_2 and Ni/hBN composite coatings, both electroplated under ultrasound at 0.180 W/cm^3, were again electrodeposited using the same experimental set-up and electroplating parameters (current density: 4 A/dm^2, plating time: 14 minutes) described in previous sections of this chapter. In this case though, larger substrates with a greater surface (5×5 cm^2 active area) were employed to ensure that the region of the deposits where the tribological analysis (i.e. friction tests) was going to be performed had a uniform thickness with lesser effect of edge build-up. For these experiments, a Pb-bronze alloy (≈0.15 cm thick) sintered on top of a steel plate (≈0.1 cm thick) equivalent to real bronze-based bearing systems (where Ni coatings are electrodeposited over the Pb-bronze surface) was used as the substrate material instead of pure Cu due to the low coefficient of friction this Pb-bronze alloy presents.

3.2.4.4. EVALUATION OF NI-BASED COATINGS ACTING AS INTERLAYERS

As in Section 3.2.4.3, a few selected coatings, namely Ni coatings electroplated under either mechanical agitation at 300 rpm and ultrasound at 0.180 W/cm^3 and Ni/WS_2 and Ni/hBN composite coatings, both electroplated under ultrasound at 0.180 W/cm^3, were again electrodeposited on Cu substrates (2×2 cm^2 active area) according to the previously

mentioned procedures (same experimental set-up, current density: 4 A/dm^2) in order to evaluate the performance of these Ni-based deposits as interlayer coatings. In this case though, the plating time was 12 minutes to achieve a thickness around 5-5.5 μm in the central area of the Cu substrate. Once the Ni-based coatings were electrodeposited over the Cu substrates, a Sn-Cu overlay [11] with a thickness around 20-25 μm was electrodeposited on top of the Ni-based coatings in order to simulate a bearing overlay system as those commonly found in medium-speed diesel engines [12].

3.3. CHARACTERISATION OF COATINGS

A thorough analysis of the characteristics of the Ni-based coatings electrodeposited on the Cu substrates was performed in order to evaluate the effect of ultrasound and the incorporation of particles in the properties of the material. All the different analytical techniques were applied in the central area of the deposits, where the electric current was expected to be more uniform and perpendicular to the substrate, as it occurs in the production electroplating lines used for the manufacturing of bearings. The purpose of this was to minimize the effect of edge build-up on the microhardness, XRD spectra and SEM images.

3.3.1. OPTICAL MICROSCOPE IMAGING

Images of the cross-section of the different deposits produced during the present research project were obtained with an optical microscope in order to check the thickness and the distribution of particles in the Ni-based composite coatings. For this purpose, the Cu substrates were horizontally cut through the horizontal symmetry axis of the deposit, mounted on DuroFast (Struers) epoxy resin and thoroughly polished until a fine surface finish was achieved (more information on the polishing procedure is found in Appendix C). The cross-section was then examined under a Nikon microscope equipped with a Lumenera Infinity 2 camera.

3.3.2. GD-OES ANALYSIS

To analyse the particle content in selected composite coatings, Glow Discharge-Optical Emission Spectroscopy (GD-OES) analysis was performed in the central area of the some of the samples. In this analytical technique, material is uniformly sputtered from the surface of the sample being analysed by a stream of Ar ions and then atomised and excited in a low-pressure plasma discharge away from the sample surface [13]. The different atoms present in the sample are quantified by analysing the composition and intensity of the light emitted by the plasma discharge with an optical emission spectrometer. As the material of the surface is removed layer by layer, GD-OES is widely employed for rapid depth profile analysis of surfaces, thin films and coatings [14]. The data obtained is generally very consistent with other techniques such as Secondary Ion Mass Spectrometry (SIMS) and X-ray Photoelectron Spectroscopy (XPS), with the advantage that GD-OES analysis requires simple sample preparation [15].

The GD-OES analysis was performed on selected composite coatings (around 6 μm thick) with a SPECTRUMA GDA 750 spectrometer equipped with a Grimm-type glow discharge source of 2.5 mm in diameter. Depth profiles were measured in the DC excitation mode at a constant voltage of 1000 V and current of 13 mA in order to achieve a good depth resolution following a similar methodology to that of Wilke et al. [16,17]. The wavelengths of interest for the different materials were 225.3 nm for Ni2, 219.2 nm for Cu2, 208.9 nm for B, 149.2 nm for N, 400.8 nm for W and 180.7 nm for S. Quantitative depth profiles were obtained with a proprietary algorithm software based on the concept of emission yield [18,19].

3.3.3. XRD ANALYSIS

X-Ray Diffraction (XRD) analysis allows the determination of the crystal structure of a thin film by irradiating the sample with a beam of X-rays over a variable incident angle range. These X-rays interact with the atoms of the sample to be examined, resulting in a diffracted X-ray spectrum which is characteristic of the elements and the phase present in the sample.

Therefore, this method enables the identification of the different crystal planes in the sample. The diffractograms included in the present work were recorded with a step size of 0.1° for 2θ ranging from 40 to 100° and measuring time of 1 second per step with a Bruker D8 Advance XRD system operating with Cu-Kα radiation.

3.3.4. SEM/FIB-SEM/FEG-SEM IMAGING

A Scanning Electron Microscope (SEM) is a type of electron microscope that provides information of the surface topography of a sample by scanning it with a beam of electrons in a raster pattern. The interaction of the emitted electrons with the atoms of the sample produce a range of different signals which contain diverse information about the sample such as the structure of the surface or its composition, among others. The range of signals includes secondary electrons (SE), which provide high-resolution images detailing the surface of the sample; back-scattered electrons (BSE), which provide information about the presence and distribution of different elements in the sample (the intensity of BSE is related to the atomic number of the elements); and X-rays, which are used to estimate the composition of the sample [20].

Besides classic SEM analysis, other advanced SEM techniques were used to characterise the coatings produced in the present project: Focused Ion Beam - Scanning Electron Microscope (FIB-SEM) and Field-Emission Gun - Scanning Electron Microscope (FEG-SEM). A FIB-SEM system is similar to that of a SEM, but with a gallium ion (Ga^+) beam instead of the electron beam. A fine ion beam can be used for high-resolution imaging, while a heavy beam is employed for fast and rough milling [21]. This enables the machining of the sample inside the FIB-SEM, allowing the examination of the cross-section and grain structure (by ion channelling contrast [22]) of the coatings without cutting and mounting the sample in epoxy or bakelite resin. In a FEG-SEM equipment, electrons are emitted through the so-called 'tunnelling effect' from a sharp tip of a tungsten wire which sucks the electrons out of the

cathode by tunnelling them below the potential barrier [23]. A FEG-SEM system not only provides a higher resolution than a regular SEM, but also a higher performance.

In the present research project, SEM analysis with a HITACHI S3200N system was conducted to observe the cross-section of some of the coatings produced, FIB-SEM analysis was carried out with a FEI Nova 600 Nanolab Dualbeam system to visualize the surface morphology and microstructure of the coatings, while FEG-SEM analysis was performed with a JEOL 6610 LVSEM system to analyse the cross-section of the samples produced during the diffusion tests. In selected coatings, FEG-SEM analysis was coupled with an energy-dispersive X-ray spectroscopy (EDS) detector (AzTEC EDS) for elemental analysis.

3.3.5. MICROHARDNESS TESTS

Vickers microhardness tests [24] were carried out to observe any effect of the presence of particles and refinement of grain size by ultrasound on the hardness of the coatings. In a Vickers microhardness test, a Vickers diamond indenter (squared pyramid with an angle of 136° between faces) is forced into the cross-section of the coating, and the resulting indentation is then measured in order to calculate the hardness.

Microhardness tests were performed on the cross-section of deposits with a thickness around 6 μm. The samples to be tested were prepared in the same way as the samples previously prepared for optical microscope imaging: coatings deposited on Cu substrates were horizontally cut near the horizontal symmetry axis of the deposit, mounted on DuroFast (Struers) epoxy resin and thoroughly polished as described in Appendix C. Microhardness was then evaluated in five random locations around the central area of the cross-section of at least 5 samples (Figure 3.3).

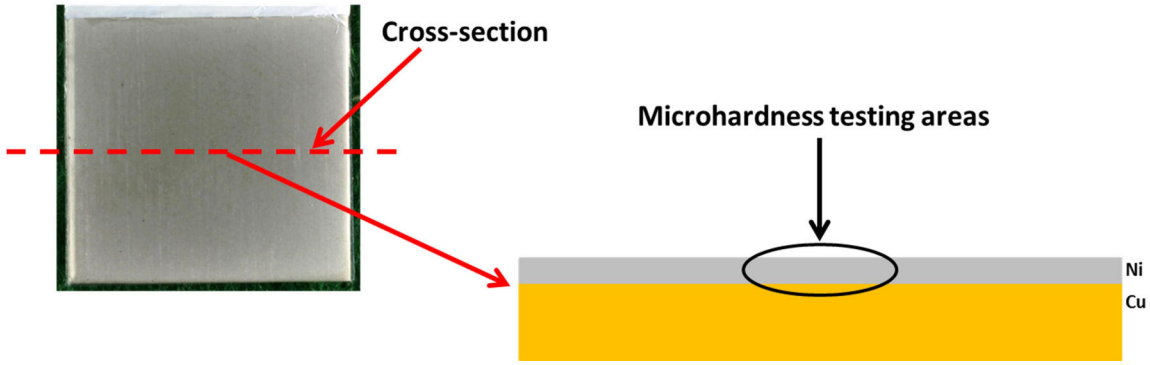

Figure 3.3. Area of the electroplated Ni-based coatings deposited on thick Cu substrates where microhardness was measured.

Microhardness tests were carried out with a Mitutoyo MicroWiZhard HM-221 hardness testing machine. A load of 2 g-force was applied during 10 seconds in all measurements. This load was selected as it was in the range (1-1000 g-force) recommended by the American Society for Testing and Materials (ASTM) for Vickers microhardness testing [24] and it was low enough to obtain indentations with regular diamond shapes, as illustrated in Figure 3.4. The diagonals d_1 and d_2 of the resulting diamond indentation (Figure 3.4) were then measured and the final Vickers microhardness was estimated with the next equation:

$$HV = \frac{2\,F\,\sin\frac{136°}{2}}{d^2} \qquad (4.1)$$

where F is the applied load and d is the mean value of d_1 and d_2.

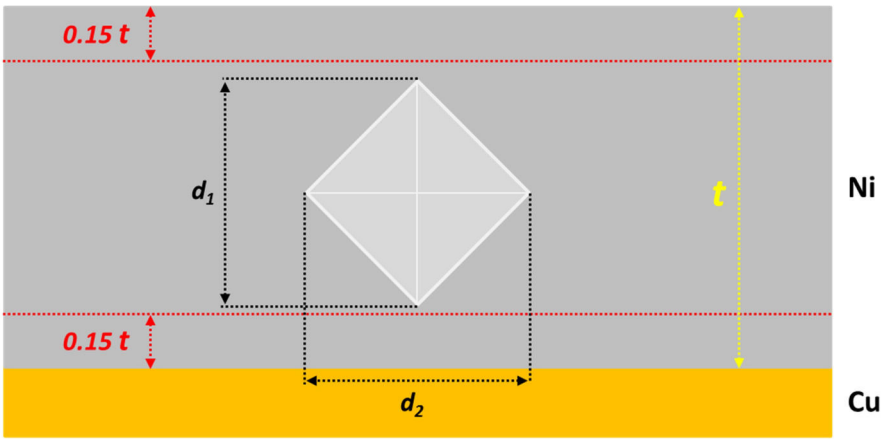

Figure 3.4. Diagram showing the diamond shape and the location of indentations within the coating in the Vickers microhardness tests performed on all the coatings selected for hardness tests. Thickness t was 6-7 µm for all the samples tested during this research.

Microhardness measurements were carefully carried out in order to obtain uniform and nicely-shaped diamond indentations and hence reproducible microhardness measurements. Special care was taken to produce the indentations in the centre of the coating, always leaving a distance of at least 15% of the thickness of the coating (t in Figure 3.4) between the top and bottom limits of the indentation and the resin/coating and coating/substrates interfaces, respectively. The main goal was to minimise the influence of both resin mount and substrate on the hardness values while producing indentations that would cover the largest possible area of the cross-section of the coating in order to account for the influence of both large columnar crystals, small refined grains and even the presence of the inherently soft lubricant particles in the different coatings produced during the research.

The methodology followed to measure the Vickers microhardness in the coatings electrodeposited during this PhD project may present some limitations, as one could consider that the distance between the limits of the indentations and the resin/coatings and coating/substrates interfaces might not be enough. One option was to perform the measurements on the surface, but in this case the measured values would also be affected by the roughness of the coatings and the potential presence of particles attached to the surface. In addition, not knowing the exact depth of the indentation (roughly about 1/7 of the diagonal) would have made it more difficult to decide which loads would allow the evaluation of the hardness from the surface accounting for all the different features observed in the coatings (large columnar crystals, small refined grains, presence of particles) without the influence of the substrate under the tested coating. Another option could have been nano-indentation measurements. Nevertheless, this technique would have required many more measurements in order to account for all the variation in size and shape of the crystals, as well as the presence of particles (Ni/WS_2 composite coatings reported in Chapter 5 would have exhibited a significantly larger dispersion of results considering their small grain size and the relatively large particle size). Koops microhardness [25] would have probably been the best option for measuring the hardness

of the coatings produced during this PhD project. Unfortunately, such technique was not accessible, and hence the methodology followed in this project which, to the student's best knowledge, presented the best compromise in order to obtain meaningful and reproducible microhardness values.

3.4. PERFORMANCE OF COATINGS ACTING AS TRIBOLOGICALLY ACTIVE LAYERS

In order to have an initial idea of how the different Ni-based coatings would behave on a real bearing in those cases where they became tribologically active, tribological analysis was performed on selected coatings: both Ni coatings electroplated under either mechanical agitation at 300 rpm and ultrasound at 0.180 W/cm^3, and Ni/WS_2 and Ni/hBN composite coatings, both electroplated under ultrasound at 0.180 W/cm^3. A scratch tester was used for this analysis, as it is a reliable tool for friction measurements at low sliding speeds [26].

3.4.1. SCRATCH TESTS

In a scratch test, a ball supported on a holder is used to literally scratch the surface of the tested sample under a control normal load (F_N) while the sample moves at a constant sliding pace, as shown in Figure 3.5. The force 'pulling' the ball in the same direction of the sample motion, noted as 'tangential force' (F_T) in Figure 3.5, is measured during the test, enabling to estimate the coefficient of friction of the coatings as the relation between the tangential force and the normal load (F_T/F_N). Acoustic emission is also recorded during the test in order to observe any critical failure of the coating (higher peaks in acoustic 'noise' emitted during the test are observed when there is significant wear damage in the coating damage, resulting in critical coating failure). The test ball is analysed before and after the test in order to determine any transference of material from the coating to the ball (or vice versa), while the trace left by the ball on the surface of the coating is also evaluated to have

an idea of wear and to see whether any debris was produced and accumulated during the tests.

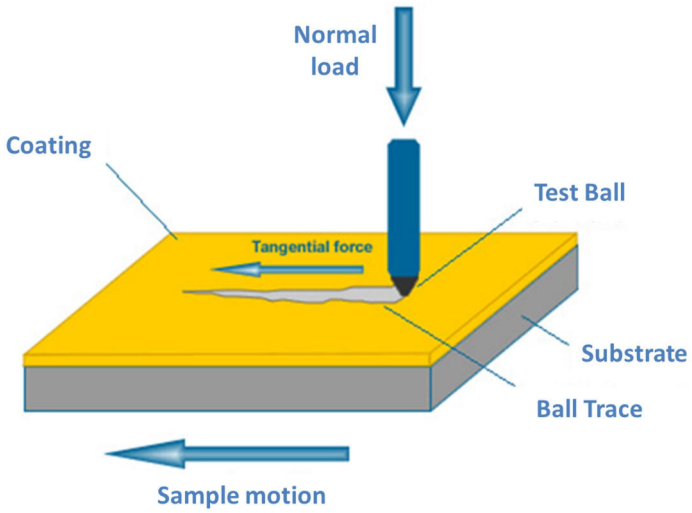

Figure 3.5. Schematic diagram of a 'scratch' test.

During the PhD research project here presented, a UMT Scratch Tester from Bruker was used to conduct the scratch tests under two different conditions: lubricated or 'wet' and non-lubricated or 'dry' conditions, being the main difference between both the lubrication of the surface of the coating via one single drop of SAE 10 oil immediately before the wet tests started. Under both wet and dry conditions, the parameters of the scratch tests were:

- Sliding distance: 1 cm
- Sliding speed: 1 cm/min
- Load: 60 N
- Ball diameter: 0.63 cm
- Ball material: JIS SUJ2 - ISO 100Cr6
- Temperature: 20 °C
- Number of scratches: 10[‡‡]

[‡‡] 10 scratches, starting and ending on the same respective start/end points, were performed in each single test in order to better show the evolution of the coefficient of friction when the Ni-based coatings were continuously acting as the tribologically active layer, as this situation is much closer to what would really take place in a real bearing, instead of tests consisting of just one single scratch.

High-resolution images of the ball (before and after the test) and the trace left on the coatings after the tests were obtained for a better interpretation discussion of the 'coefficient of friction' data obtained during the scratch tests. Detailed 3D images of the middle point of the traces left on the coatings after the tests were also obtained with a white light interferometer (MicroXAM2 from KLA Tencor) to estimate the depth of the resulting wear track.

3.5. PERFORMANCE OF COATINGS ACTING AS DIFFUSION BARRIER LAYERS

In order to evaluate how the novel Ni-based materials could perform as diffusion barrier layers in bronze-based bearing applications, adhesion and diffusion studies were carried out in samples consisting of i) a Cu substrate as those previously described in Section 3.2.3.1, ii) a Ni-based coating electrodeposited on the Cu substrate for 12 minutes in order to achieve a deposit thickness around 5 μm in the central area of the substrate, and iii) a Sn-Cu overlay (2.5-4.5% of Cu) with a thickness around 25-30 μm electrodeposited on top of the Ni-based coating. As previously commented in Section 3.4, samples with four different Ni-based diffusion barrier layers (both Ni coatings electroplated under either mechanical agitation at 300 rpm and ultrasound at 0.180 W/cm^3, and Ni/WS_2 and Ni/hBN composite coatings, both electroplated under ultrasound at 0.180 W/cm^3) were evaluated.

3.5.1. ADHESION STUDIES

Adhesion or 'bonding' tests provide an estimation of the adhesion or 'bond' strength of the substrate-coating systems, giving an idea of how 'strongly' an electrodeposited coating is attached to the substrate. In a bonding test, the surface of the sample plated with the coating to be tested is glued to a test dolly with a defined area. The sample is then mounted in a special housing fixed to the base of a tensile test machine and the dolly is attached to the moving end of the tensile tester. A constant pulling displacement is set at the moving end of

the tester, which stops pulling away from the housing when the dolly is snapped away from the sample by failure of either the glue or the coating at a certain applied load. The failure stress is then calculated as the applied load divided by the area of the dolly. Bonding tests were performed with a Hounsfield-5000 tensile test machine equipped with a special jig designed for bonding tests according to Daido Metal's procedure [27] included in Appendix D. The tests were carried out in samples as plated and after being heat-treat for 500 h at 130 °C. After each bonding test, pictures of both the dolly and the tested coating were taken in order to analyse the bonding failure.

3.4.2. DIFFUSION TESTS

For the diffusion study, the cross section of the central area of the samples was examined as plated and after being annealed for 1000 and 3000 hours at 130 °C with an optical microscope and a FEG-SEM system in order to observe any change in terms of thickness and structure of the whole overlay system (Sn-Cu overlay + Ni-based diffusion barrier + Cu substrate). The samples to be analysed were again horizontally cut near the horizontal symmetry axis of the deposit, mounted on ConduFast (Struers) conductive acrylic resin and thoroughly polished as described in Appendix C.

3.5. REFERENCES

[1] H.-Y. Zheng, M.-Z. An, J. Alloy. Compd. 459 (2008) 548.

[2] O. Louisnard, Ultrason. Sonochem. 19 (2013) 56-65.

[3] O. Louisnard, Ultrason. Sonochem. 19 (2012) 66-76.

[4] T.J. Mason, Practical sonochemistry: User's guide to applications in chemistry and chemical engineering, Ellis Horword Ltd., Chichester, 1991.

[5] C. McAleese, Process Instruction 7526-41, Daido Industrial Bearings Europe, 2009.

[6] G. Coles, Process Instruction 7530-12, Daido Industrial Bearings Europe, 2009.

[7] B. Misek, D.N. Skauen, J. Am. Pharm. Assoc. 47 (1958) 32.

[8] G. Mie, Ann. Phys. (Berlin) 330 (1908) 377.

[9] T. Wriedt, Mie theory: A review, in: W. Hergert, T. Wriedt (Eds.), The Mie Theory, Springer Series in Optical Sciences 169, Springer-Verlag, Berlin-Heidelberg, 2012.

[10] Malvern Instruments Ltd, Mastersizer 2000.

http://www.malvern.com/labeng/products/mastersizer/ms2000/mastersizer2000.htm

[11] H. Tsuji, H. Ishikawa, T. Shibayama, GB patent 2375801, 2002.

[12] I. Kerr, Plain bearing condition – A barometer of engine health, Bearing service experience & material development (The first 100 years), Seminar at the Royal Institution of Naval Architects, February 2012.

[13] P. Hunault, C. Maul, MilleniumSteel 2k1 (2001) 357.
http://www.leco.com/support/application-support-spectroscopy/articles-references?task=document.viewdoc&id=906

[14] T. Nelis, J. Pallosi, Appl. Spectrosc. Rev. 41 (2006) 227.

[15] S. Suzuki, K. Kakita, J. Surf. Anal. 12 (2005) 174.

[16] M. Wilke, M. Analytis, V. Breternitz, Ch. Knedlik, G. Teichert, Recalibration-free measurement of the compound layer thickness of nitrocarburized samples by glow discharge optical emission spectrometry (GD-OES), 51st Internationales Wissenschaftliches Kolloquium, Technische Universität Ilmenau, Germany, September 2006.

[17] M. Wilke, G. Teichert, R. Gemma, A. Pundt, R. Kirchheim, H. Romanus, P. Schaaf, Thin Solid Films 520 (2011) 1660.

[18] A. Bengston, T. Nelis, Anal. Bioanal. Chem. 385(2006) 568.

[19] A. Bogaerts, J. Anal. At. Spectrom. 22 (2007) 13.

[20] J.H. Wittke, GLG 510 - Electron Microprobe Techniques (class notes), Northern Arizona University, 2008.

http://www4.nau.edu/microanalysis/Microprobe/NewOverview.html

[21] S. Reyntjens, R. Puers, J. Micromech. Microeng. 11 (2001) 287.

[22] FEI Company, Focused ion beam technology, capabilities and applications, 2008.

http://www.fei.com/uploadedfiles/documents/content/2006_06_fib_overview_pb.pdf

[23] J.L. Lábár, Introduction to electron microscopes: electron optics, interactions and signals, Introduction to electron microscopes: electron optics, interaction and signals, Proceedings of the 5th regional workshop - EMAS 2002, Electron probe microanalysis today - Practical aspects, Szczyrk, May 2002.

[24] ASTM E384-11e1, Standard test method for Knoop and Vickers hardness of materials, ASTM International, West Conshohocken, 2011.

[25] ASTM B578-87, Standard test method for microhardness of electroplated coatings, ASTM International, West Conshohocken, 2009.

[26] I. Nieminen, P. Andersson, K. Holmberg, Wear 130 (1989) 167.

[27] M. Pal, Laboratory Instruction EIS-016, Daido Metal EHQ R&D, 2012.

4. ULTRASOUND-ASSISTED ELECTRODEPOSITION OF NI COATINGS

4.1. OVERVIEW

Ni diffusion barrier layers are a key element in electroplated bronze-based bearings due to the resistance they provide to the diffusion of Sn and Cu from the overlay to the lining (and vice versa) which could lead to the uncontrolled formation and growth of undesired intermetallic compounds such as Cu_3Sn. However, in order to achieve a good 'diffusion resistance', the Ni diffusion barrier layers must be relatively thick (i.e. > 5 μm), which increases manufacturing costs and results in a more expensive material. Such an increase in manufacturing costs due to thick Ni diffusion barrier layers has become a major concern due to the fact that Ni prices have generally increased in the last two decades and become quite unstable in the last 5-10 years [1]. Since electroplated Ni presents a classical columnar

structure [2,3], a modification of said columnar structure and refinement of the grain size, assuming that lattice-controlled diffusion was predominant over boundary-controlled diffusion, could enable the electrodeposition of thinner Ni layers with improved tribological and 'anti-diffusion' properties. As mentioned in Section 2.3 of the literature review, the use of ultrasound during the electrodeposition of metals is an effective way to modify the microstructure and refine the grain size of electrodeposited coatings, and therefore, a great option to produce thinner Ni diffusion barrier layers. In such context, the aim of the study presented in this chapter was to evaluate the effect that ultrasound could have on the characteristics of Ni deposits produced from the Ni Watts bath currently employed by DIBE in its production line and on the stability of the bath itself after being irradiated with ultrasound. This study was structured in two parts:

1. A first stage focused on the electrodeposition of Ni on Cu substrates under ultrasound at different ultrasonic powers to study the effect that the ultrasonic power may have on the characteristics of the Ni deposits.
2. A second stage where a simple study of the stability of the chemical parameters of the Watts bath with longer ultrasonic irradiation was applied with the objective of observing any effect that ultrasound might have on those parameters and how ultrasound could affect the long term stability of the Watts bath.

4.2. Electrodeposition of Ni coatings under ultrasound

Ni coatings (around 6 μm thick) were electrodeposited under five different agitation conditions (silent/still, mechanical agitation at 300 rpm and ultrasonic agitation at 0.011, 0.124 and 0.180 W/cm^3) at 4 A/dm^2 for 14 minutes in order to evaluate how ultrasound could affect the characteristics of pure Ni deposits in terms of their visual

appearance/surface finish, orientation of Ni crystals, surface morphology and crystal structure and hardness of the deposits.

4.2.1. SURFACE FINISH

Figure 4.1 displays some examples of Ni coatings deposited on Cu substrates under the different agitation conditions studied: silent/still, mechanical agitation at 300 rpm and ultrasonic agitation at 0.011, 0.124 and 0.180 W/cm^3. Under silent/still conditions and mechanical agitation, deposits with good visual appearance were obtained with a slightly clearer grey colour near the edges and corners of the coated Cu substrate due to edge build-up (edge build-up occurs in these areas due to locally higher current densities). Some evidence of edge build-up was also observed in the Ni coatings electrodeposited under ultrasound, although the visual appearance of the these deposits was not as good as that of Ni coatings produced in the absence of ultrasound, as erosion marks due to the presence of cavitating bubbles were clearly observed in some areas of the Ni deposits produced under ultrasound. Nevertheless, whilst in Ni coatings electrodeposited at either 0.011 or 0.180 W/cm^3 the erosion marks were very small compared to the coated area of the Cu substrate, they were far more prominent in Ni deposits produced at 0.124 W/cm^3, indicating the presence of much more aggressive cavitation phenomena near the surface of the Cu substrates at that particular ultrasonic power. In all cases though, the appearance of the marks was quite random, as no patterns regarding when the marks appeared in the deposits was observed.

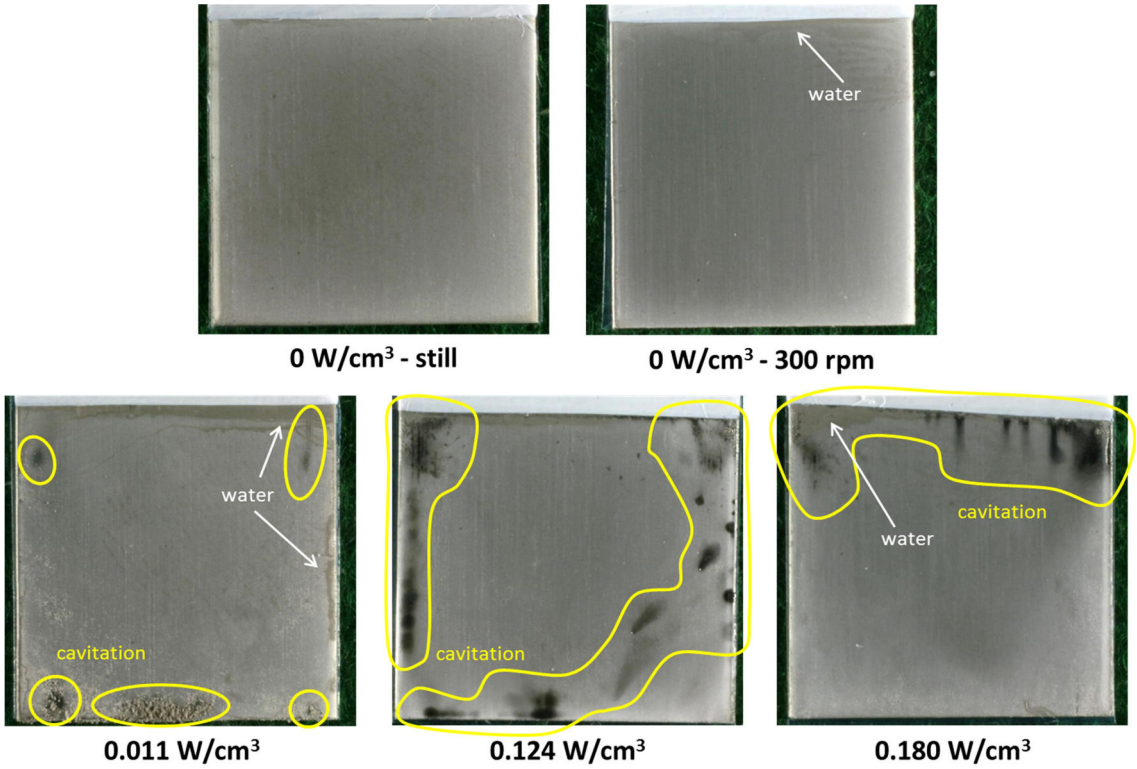

Figure 4.1. Examples of Ni coatings electrodeposited on Cu substrates under different conditions: silent/still, mechanical agitation at 300 rpm and ultrasonic agitation at 0.011, 0.124 and 0.180 W/cm^3. Moisture (water) stains can also be seen near the edges in some of the samples. Electrodeposition time: 14 minutes. Current density: 4 A/dm^2.

Sonication not only affected the surface finish of the electroplated samples; it was also observed that ultrasound had an effect on the appearance of the anodes after being used for 360 minutes (Figure 4.2). When no ultrasound was applied during plating, uniformly distributed pitting was observed. However, the pitting distribution slightly changed when ultrasonic irradiation at 0.011 W/cm^3 was introduced in the plating process, as some discontinuities in the corrosion marks were observed, especially in the lower half of the surface of the Ni anodes. This discontinuity became even more evident at higher ultrasonic powers, reaching a point where three pressure antinodes are clearly seen on the surface of the anode. In fact, the cavitation activity with the ultrasonic power can approximately be estimated by just looking at the erosion of anodes continuously used in the stability tests further commented in Section 4.3 in this chapter: at 0.011 W/cm^3, the ultrasonic power was so low that only two pressure antinodes (antinode 1 at the bottom and antinode 2 on central

area of the anode) were noticed in the erosion marks observed in the anode. The antinodes became more evident at 0.124 W/cm^3, where signs of localised, randomly aggressive streamers were observed around them. A third pressure antinode (antinode 3) forming near the liquid level at this power was also noticed, although it was not as evident as the other antinodes. Some marks with unpredictable patterns were also observed between antinodes 2 and 3 in anodes used at 0.124 W/cm^3. The third antinode is clearly seen at 0.180 W/cm^3, with well-defined limits within the three pressure antinodes. It is interesting to note that, while erosion marks for antinodes 1, 2 and 3 were broader and more uniform in the anodes used at 0.180 W/cm^3 compared to the anodes used at 0.124 W/cm^3 (as it would be expected considering that the ultrasonic power is higher), localised areas corresponding to antinodes 1 and 2 showed significantly higher erosion in the anodes used at 0.124 W/cm^3 than the anodes used at 0.180 W/cm^3.

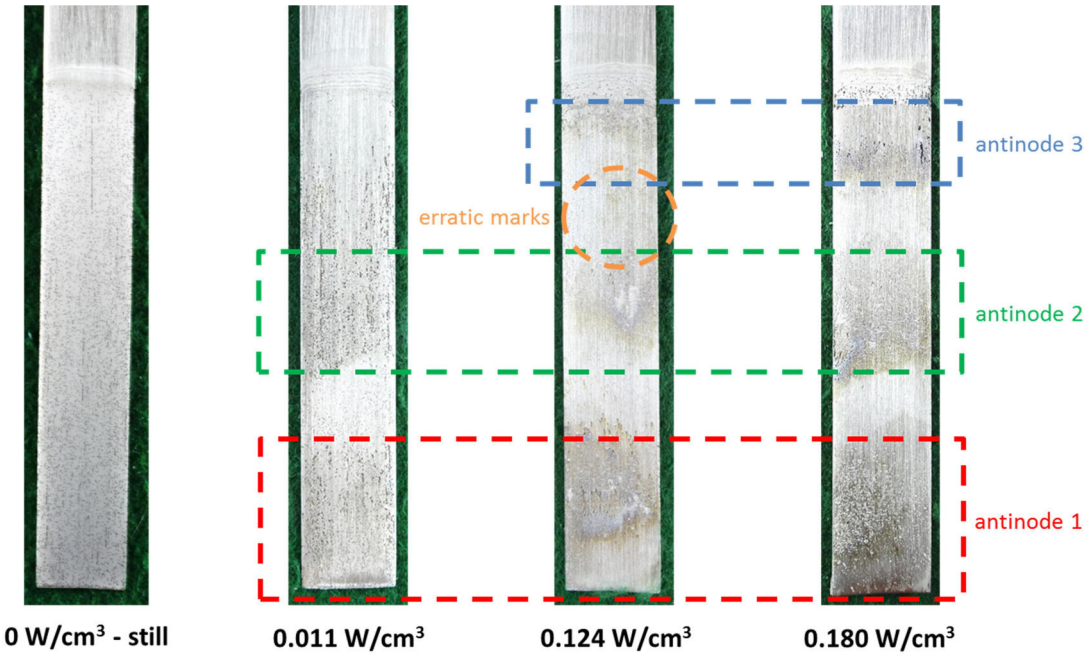

Figure 4.2. Final appearance of the Ni anodes for plating experiments (around 360 minutes) at different ultrasonic powers.

In summary, the presence of ultrasound affected the surface finish of the electroplated coatings. Non-uniform deposits were produced with ultrasonically-assisted plating, especially at 0.124 W/cm^3. This undesired effect was not easy to predict, as its appearance

and distribution was quite random and chaotic. The patterns of the non-uniform surface seemed quite similar to the bubble streamers commonly observed in ultrasonic systems. Surprisingly, the marks were less significant at the highest power employed, where a higher cavitation activity would be expected. Larger and more prominent clusters of bubbles were observed in the symmetry axis of the beaker at 0.180 W/cm^3, while other minor bubble structures could also be noticed near the surface of the electrodes, especially at lower ultrasonic powers where the clusters in the symmetry axis seemed less obvious. Some evidence for this was the appearance of the anodes: erratic, randomly aggressive marks were observed at 0.124 W/cm^3, while pressure antinodes were not as well defined as on the anode employed at 0.180 W/cm^3. The reason for these erratic and random marks forming on both cathode and anode at lower-medium powers, especially at 0.124 W/cm^3, could be the formation of random local bubble structures attached to the surface of both cathode and anode similar to those observed by Krefting et al. in a large ultrasonic system operated at 40 kHz [4]. In their work, the authors found that these bubble structures and their effect on the surface of solids was quite random compared to freely existing structures such as jellyfish structures (layered cavitation bubble structures with bubble streamers) which were highly reproducible. In the present case, a higher ultrasonic power (0.180 W/cm^3) yielded higher pressures at the antinodes, especially in the symmetry axis of the beaker, which lead to the formation of larger clusters of bubbles that would 'attract' and remove those bubbles that would form random structures in solid surfaces and otherwise erode the surface of the deposit, as in the samples plated at 0.124 and 0.011 W/cm^3 to a lesser extent.

4.2.2. CRYSTAL ORIENTATION

In order to have a deeper understanding of the effects of ultrasound on the electrodeposition of Ni at 4 A/dm^2, XRD analysis was conducted on samples plated under different agitation conditions (Figure 4.3). The 2θ scans showed that, under silent still/conditions, about the same height of (111) and (200) crystal planes were obtained,

with small peaks related to (220), (311) and (222) planes. Relatively higher peaks were observed for the (111) and (311) planes in coatings electrodeposited under mechanical agitation, along with a relative decrease in the intensity of the (200) planes. Although Ni coatings electrodeposited under ultrasound at 0.011 W/cm^3 also presented high intensities for (111) crystal planes, those were relatively lower in Ni deposits produced at 0.124 W/cm^3 and 0.180 W/cm^3, which presented remarkably high peaks for (200) crystals.

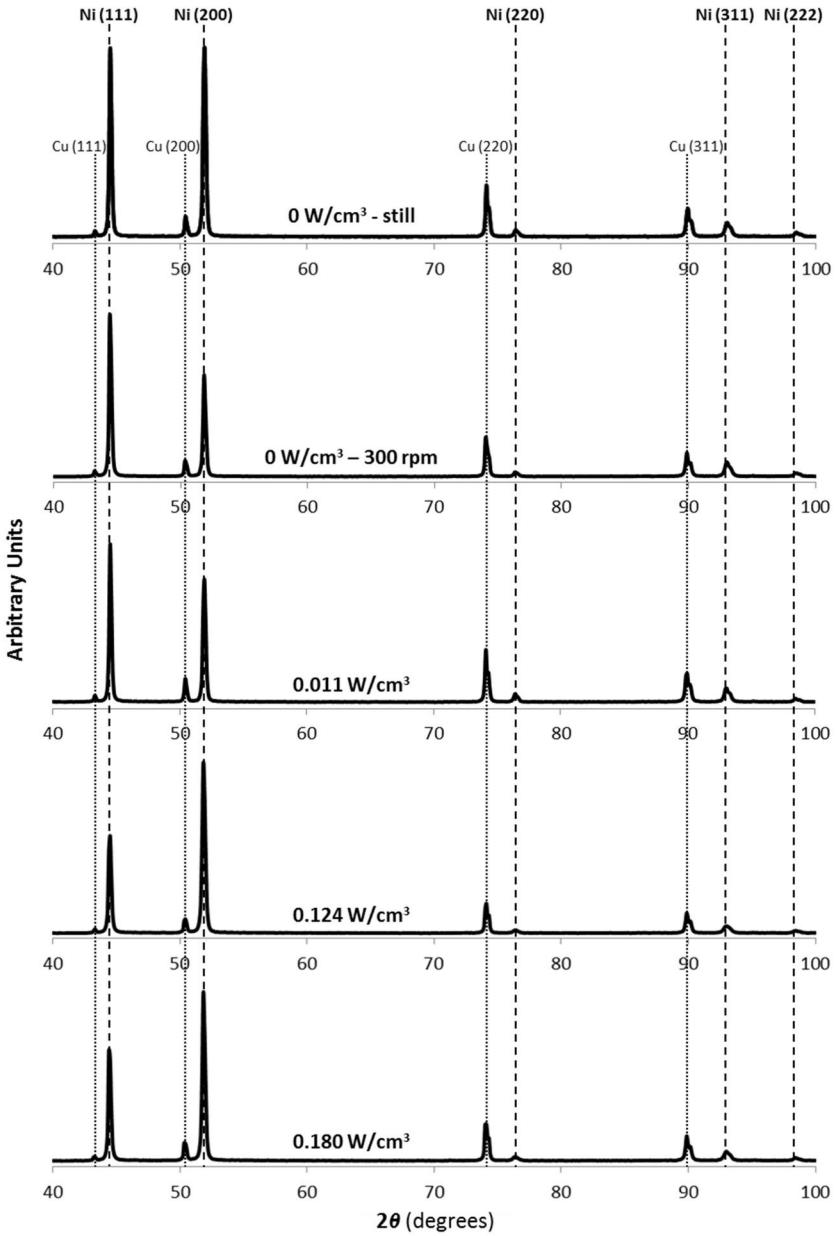

Figure 4.3. XRD spectra of Ni coatings electrodeposited on Cu substrates under different conditions: silent/still, mechanical agitation at 300 rpm and ultrasonic agitation at 0.011, 0.124 and 0.180 W/cm^3. Peaks related to the Cu substrate are also highlighted. Electrodeposition time: 14 minutes. Current density: 4 A/dm^2.

In order to quantify the different crystal planes observed in the XRD spectra previously shown, the 'Relative Texture Coefficient' (RTC) method developed by Bérubé and L'Espérance [5] was used. This method, which is commonly used to quantify crystal planes in electrodeposited metal-based coatings [6-10], not only yields normalized and quantitative data of the different crystals planes observed in a sample, but also eliminates the roughness effect of the deposits analysed. The Relative Texture Coefficient or $RTC_{(hkl)}$ for a (hkl) crystal plane is defined as:

$$RTC_{(hkl)} = 100 \times \frac{I_{(hkl)}/I_{(hkl),P}}{\sum_1^5 I_{(hkl)}/I_{(hkl),P}} \quad (4.1)$$

where $I_{(hkl)}$ is the intensity of the reflection for the (hkl) crystal plane in the analysed sample and $I_{(hk\ ).P}$ is the intensity of the reflection for the same crystal plane in a standard Ni powder sample with random orientation. The denominator in Equation 4.1 is the sum of the relation between $I_{(hkl)}$ and $I_{(hkl).P}$ for all the different crystal planes observed in the XRD scans, which for the case of Ni are (111) for $2\theta \approx 44.50°$, (200) for $2\theta \approx 51.85°$, (220) for $2\theta \approx 76.38°$, (311) for $2\theta \approx 92.94°$ and (222) for $2\theta \approx 98.45°$ [11]. The relative intensities for the crystal planes in the standard Ni powder sample with random orientation are $I_{(111).P}$ = 999, $I_{(200).P}$ = 420, $I_{(220).P}$ = 161, $I_{(311).P}$ = 144 and $I_{(222).P}$ = 39 [11].

In all the deposits, $RTC_{(200)}$ always reached the highest value, although its presence would vary from 30% in Ni electrodeposits produced under mechanical agitation to 50% in Ni coatings electrodeposited under ultrasound at 0.124 W/cm^3. Regarding (220) planes, $RTC_{(220)}$ values always remained lower than 10% in all cases, whereas the (111), (311) and (222) crystal planes seemed to be linked to each other: taking the $RTC_{(111)}$, $RTC_{(311)}$ and $RTC_{(222)}$ values of the Ni coating electrodeposited under silent/still conditions as a reference, it was observed that, in all the Ni deposits where $RTC_{(111)}$ was higher (Ni coatings under either mechanical agitation or ultrasound at 0.011 W/cm^3), $RTC_{(311)}$ and $RTC_{(222)}$ would also proportionally increase, while for all those deposits where $RTC_{(111)}$ was lower (Ni deposits

under ultrasound at either 0.124 W/cm^3 or 0.180 W/cm^3), a proportional decrease was observed for $RTC_{(311)}$ and $RTC_{(222)}$. This increase/decrease would inversely be connected to the $RTC_{(200)}$ values. It is worth noting the relative large RTC values estimated for (222) and, to a less extent, (311) and (220) crystal planes when compared to the RTC values estimated for the (111) and (200) crystal planes. This is caused by the own nature of the RTC method: as the intensity of the reflection for a (hkl) crystal plane in the analysed deposit ($I_{(hkl)}$) is divided by the relative intensity of the reflection of that same crystal in the randomly oriented powder ($I_{(hkl).P}$), in those cases where $I_{(hkl).P}$ may be very small, as in the case of (220), (311) and (222) crystal planes.

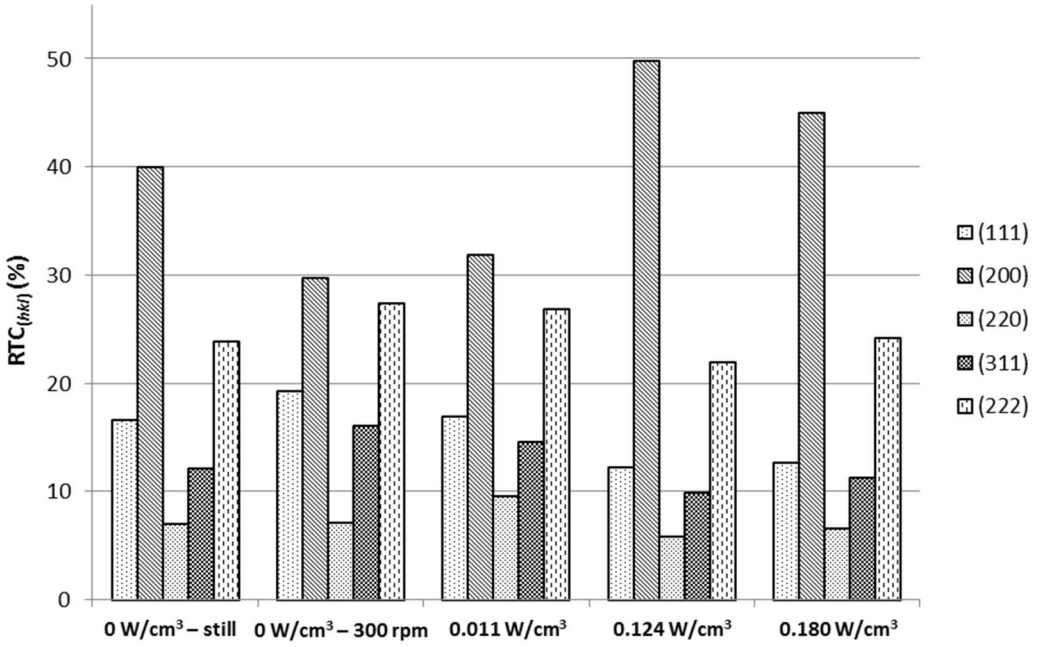

Figure 4.4. $RTC_{(hkl)}$ estimated for the different crystal planes observed in Ni coatings electrodeposited under different conditions: silent/still, mechanical agitation at 300 rpm and ultrasonic agitation at 0.011, 0.124 and 0.180 W/cm^3.

Electrocrystallization on [111] and [311] directions can be associated to a dispersed [211] preferred orientation [12-14], implying that (111), (311) and (222) crystal planes may be attributed to Ni grains with a [211] orientation. On the other hand, (200) and (220) crystal planes obviously depict Ni crystals growing with [100] and [110] orientations [6], respectively. Therefore, $RTC_{[hkl]}$ values analogous to $RTC_{(hkl)}$ were obtained by defining:

$$RTC_{[100]} = RTC_{(100)} \quad (4.2)$$

$$RTC_{[110]} = RTC_{(220)} \quad (4.3)$$

$$RTC_{[211]} = RTC_{(111)} + RTC_{(311)} + RTC_{(222)} \quad (4.4)$$

As expected from the $RTC_{(hkl)}$ coefficients previously included in Figure 4.4, there was an inverse relationship between the [100] and [211] orientations (Figure 4.5): the higher $RTC_{[100]}$ is, the lower $RTC_{[211]}$ gets, and vice versa.

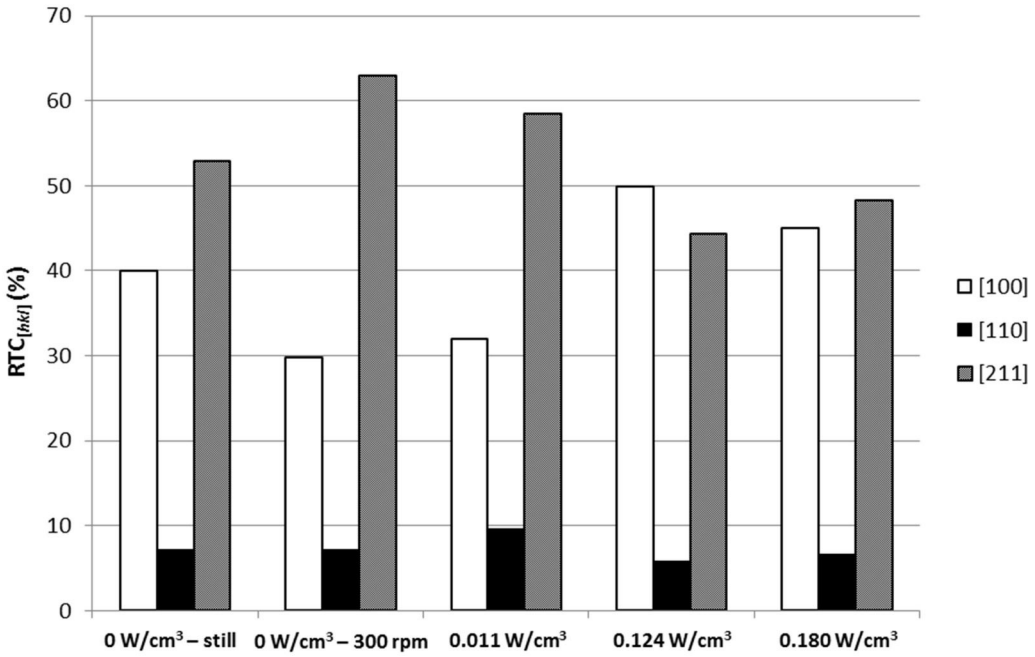

Figure 4.5. $RTC_{[hkl]}$ estimated for [100], [110] and [211] orientations in Ni coatings electrodeposited under different conditions: silent/still, mechanical agitation at 300 rpm and ultrasonic agitation at 0.011, 0.124 and 0.180 W/cm^3.

The preferential orientation of Ni crystals in the electroplated coating is under the influence of the so-called 'inhibition effect' [15-17]. Electrodeposition of Ni with no inhibition of crystal growth yields deposits with a [100] preferred orientation, commonly known as the 'free' growth mode. Amblard and co-workers related the inhibition of the electrocrystallization of Ni, particularly the [100] growth mode, by the presence of different species in the electrolyte-cathode interface for additive-free Watts plating solutions [18-21]:

- Crystal growth in the [110] direction is observed when the electrocrystallization in the [100] orientation is inhibited by the presence of adsorbed atomic hydrogen (H_{ads}) covering the surface of the cathode.
- [211] orientation is the least inhibited by the presence of colloidal and/or precipitated $Ni(OH)_2$ near the electrolyte-cathode interface.
- Electrocrystallization in the [210] orientation is caused by massive presence of gaseous hydrogen (H_2) due to massive hydrogen evolution at the cathode.

These inhibiting species would however not be incorporated to the final deposit, as they would be '*sufficiently stable on certain crystal faces to modify growth while at the same time being sufficiently unstable so as to allow decomposition and/or release so as not to be co-deposited*' [22].

Ni coatings produced under silent/still conditions in the present study had a combined [100] and [211] preferred orientation, with a slightly higher predominance of the latter. Significantly higher $RTC_{[211]}$ and lower $RTC_{[100]}$ values were observed for the Ni deposits electrodeposited under mechanical agitation, suggesting that the agitation of the solution 'promoted' the formation of [211] textures instead of the 'free' [100] growth mode. Such inhibition effect on the free growth mode, as suggested by Amblard et al. [20], is due to the presence of colloidal and precipitated $Ni(OH)_2$ near the electrolyte-cathode interface, which can be related to a localised increase of the pH near the interface [23]. The cause for this alkalization near the electrode surface would be the local discharge and adsorption of hydrogen [20]. An enhancement in the discharge of hydrogen due to a lower cathode current efficiency could explain the increase in pH and the presence of $Ni(OH)_2$ near the surface. In this sense, different authors have recently reported a decrease in the cathode current efficiency and an increase in hydrogen evolution with mechanical agitation for the electrodeposition of Ni [24,25]. This decrease in efficiency with agitation, although it can be quite small depending on the working conditions, may have a significant effect on the crystal structure. Nevertheless, taking into account the uniformity in terms of thickness of the Ni

deposits (5.5-6 μm in the central area of the Ni coatings independently of the agitation conditions) and the lack of hydrogen bubbles being produced at the cathode, no experimental evidence was observed that could suggest a significant decrease in cathode current efficiency with agitation for the Ni Watts bath formulation and the plating conditions employed in the present study. The other possible explanation for the increase in pH would therefore be the adsorption of hydrogen in the cathode surface [20], a phenomenon that could be enhanced by an increase in agitation, as recently suggested in different studies [26,27].

Ni deposits produced under ultrasound at 0.011 W/cm^3 presented similar results as those observed for coatings produced under mechanical agitation, although $RTC_{[100]}$ and $RTC_{[211]}$ were not as low and high, respectively. The key for this similarity between Ni coatings produced under either mechanical agitation or ultrasound at 0.011 W/cm^3 is 'agitation' itself: while in the first case the electrolyte is agitated by the mechanical stirring action of the overhead stirrer, in the second case the electrolyte is agitated by the 'acoustic streaming' effect induced by the ultrasonic field set in the bath. One would assume that, at a higher ultrasonic power (0.124 W/cm^3), an even more evident increase in the $RTC_{[211]}$ coefficient would be obtained, as stronger acoustic streaming is expected. But according to the results obtained during the present research, the intensity of the cavitation activity near the surface also took a key role, as the presence of Ni crystals with preferred [100] was increased to a point where the [211] orientation was no longer predominant ($RTC_{[100]} > RTC_{[211]}$ under ultrasound at 0.124 W/cm^3). These were the deposits that presented the highest rate of erosion marks due to the presence of cavitation in the form of randomly-attached bubble structures near the surface. A further increase in the ultrasonic field (0.180 W/cm^3) reduced the formation of such bubble structures near the surface of the cathode, but the overall increase in the cavitation activity in the plating solution still kept a significantly higher presence of crystals with [100] orientation and lower presence of crystals with [211] orientation compared with Ni coatings produced under mechanical agitation. In addition, as

in the Ni deposits produced under silent conditions, ultrasound did not have much effect on the electrocrystallization of Ni in the [110] direction, as $RTC_{[110]}$ values again remained around 6-9%. These results agree to some extent with the observations made by Kobayasi et al. [28], as they also noticed a similar trend regarding the crystal orientation with different ultrasonic frequencies: i) increase in the proportion of Ni crystals with a [100] orientation, ii) decrease in the proportion of Ni crystals with a [211] orientation, and iii) a low, fairly constant proportion of Ni crystals with a [110] orientation. In their case though, they suggested that this finding was due to the hypothetical effect that ultrasound could have on the activation energies of the surface diffusion of Ni adions to the different crystal faces, ignoring the 'inhibition effect' caused by the presence of inhibiting species in the cathode-electrolyte interface.

Overall, all these results suggest that the presence of cavitating bubbles near the cathode surface counteract the effect of agitating the plating solution, as the action of the bubbles apparently reduced the adsorption of hydrogen on the surface of the cathode. This implies that local alkalization of the electrolyte near the cathode-electrolyte interface would be reduced to some extent when using ultrasound, resulting in reduced formation of $Ni(OH)_2$ near the surface and, therefore, a less inhibited electrocrystallization of Ni with higher presence of Ni crystals with [100] orientation. Nevertheless, other effects of the presence of cavitation phenomena near the electrode on the double layer must not be discarded in order to explain the electrodeposition of Ni coatings with higher proportion of crystals growing on the [100] direction. For example, the presence of cavitating bubbles could disturb the formation of a double layer structure on the electrode surface, resulting in either a decrease in the formation of precipitated and colloidal $Ni(OH)_2$ or its removal from the cathode-electrolyte interface.

4.2.3. SURFACE MORPHOLOGY AND GRAIN STRUCTURE

FIB-SEM analysis was performed to observe any significant effect of ultrasound on the surface morphology and structure of thin electrodeposited Ni coatings at 4 A/dm^2. Tilted FIB-SEM images of the surface of the coatings produced under different conditions are shown in Figures 4.6 to 4.10. Irregular grooves and nodule-shaped structures with a cauliflower-like appearance were noticed in all the deposits. This latter morphology is quite common in Ni electroplating, as it has previously been reported in many previous different studies [29,30]. Nevertheless, some differences were observed in the coatings plated under the different conditions used. For the coatings plated in absence of ultrasound, irregular grooves were clearly observed all over the surface, more prominently in those coatings plated under mechanical agitation, while the presence of nodule-shaped structures was minimal. On the other hand, the presence of such nodule-shaped structures was far more evident in the coatings electroplated under ultrasound at 0.011 and 0.180 W/cm^3, where irregular grooves where harder to locate. For the coatings electroplated under ultrasound at 0.180 W/cm^3 though, the nodule-shaped structures were not as predominant as in the Ni deposits produced at 0.011 and 0.180 W/cm^3.

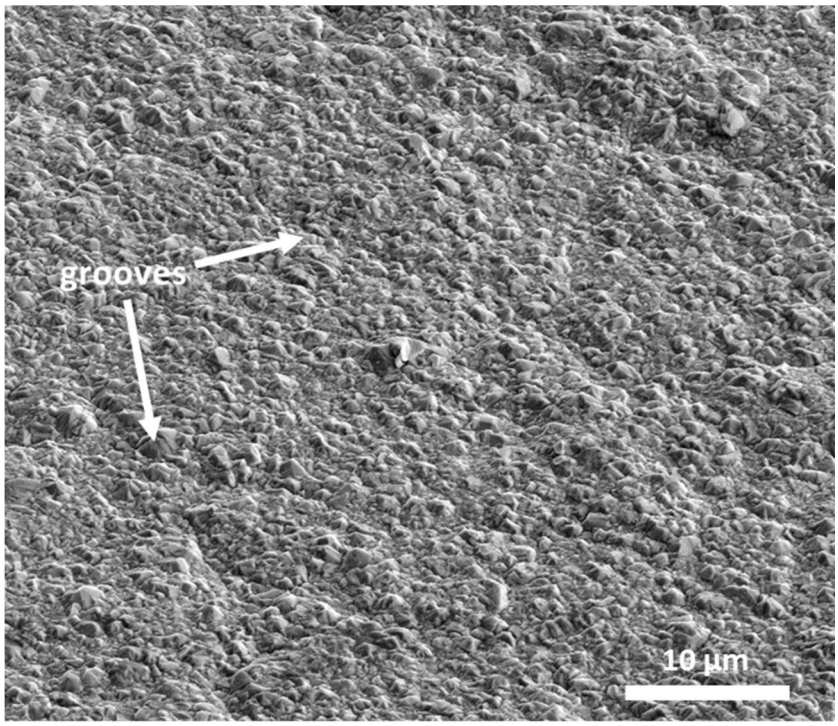

Figure 4.6. Tilted FIB-SEM image of the surface of Ni electrodeposited under silent/still conditions. Electrodeposition time: 14 minutes. Current density: 4 A/dm^2.

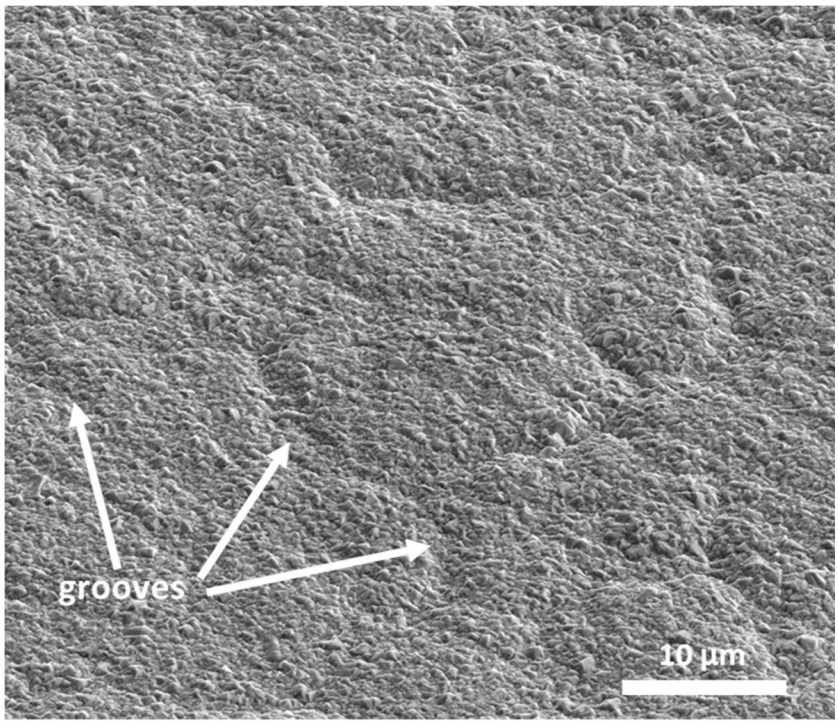

Figure 4.7. Tilted FIB-SEM image of the surface of Ni electrodeposited under mechanical agitation at 300 rpm. Electrodeposition time: 14 minutes. Current density: 4 A/dm^2.

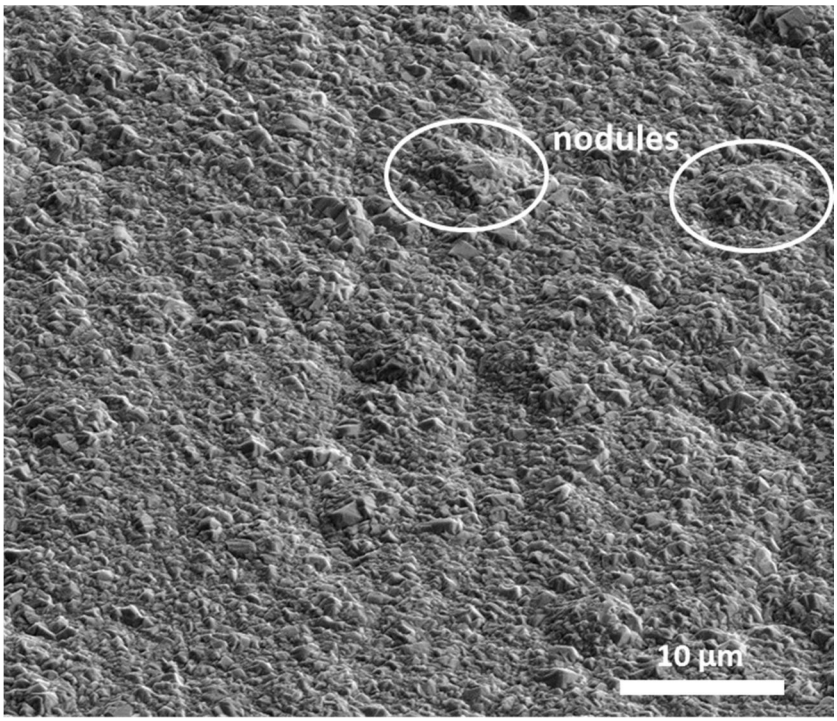

Figure 4.8. Tilted FIB-SEM image of the surface of Ni electrodeposited under ultrasound at 0.011 W/cm^3. Electrodeposition time: 14 minutes. Current density: 4 A/dm^2.

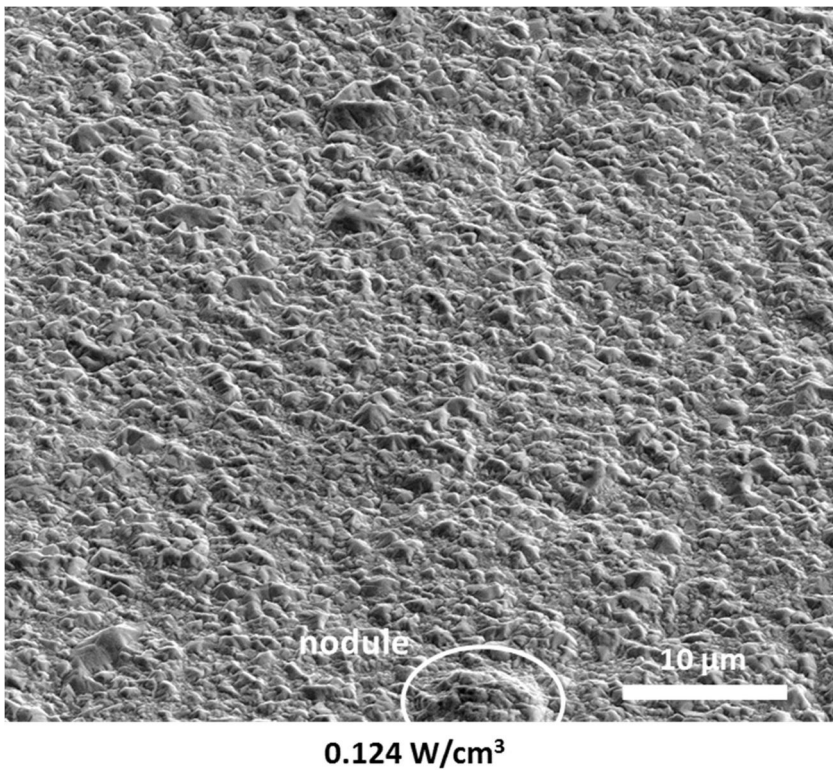

Figure 4.9. Tilted FIB-SEM image of the surface of Ni electrodeposited under ultrasound at 0.124 W/cm^3. Electrodeposition time: 14 minutes. Current density: 4 A/dm^2.

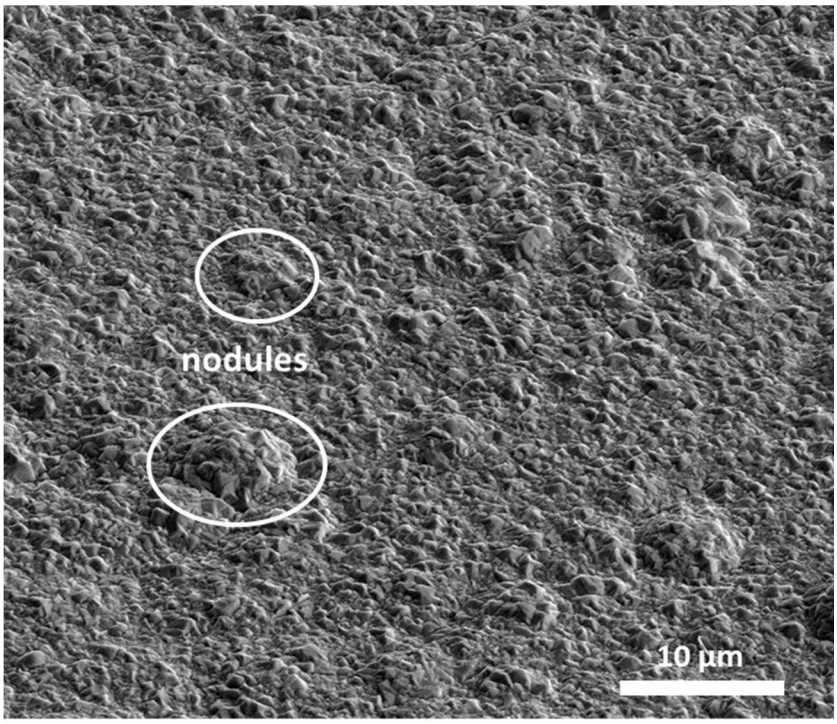

Figure 4.10. Tilted FIB-SEM image of the surface of Ni electrodeposited under ultrasound at 0.180 W/cm^3. Electrodeposition time: 14 minutes. Current density: 4 A/dm^2.

Although the association of the grain orientation to the surface morphology may sound rather subjective, different researchers have employed high magnification SEM analysis in the past to identify different crystal orientations according to structural differences noticed in the surface of electrodeposited Ni coatings [7,8,14,31], as shown in Figure 4.11 [8]. For this reason, high magnification FIB-SEM images of the coatings plated under the different agitation conditions at 4 A/dm^2 were obtained to check whether the structure of the crystals observed on the surface agreed to some extent with the results observed in the XRD analysis.

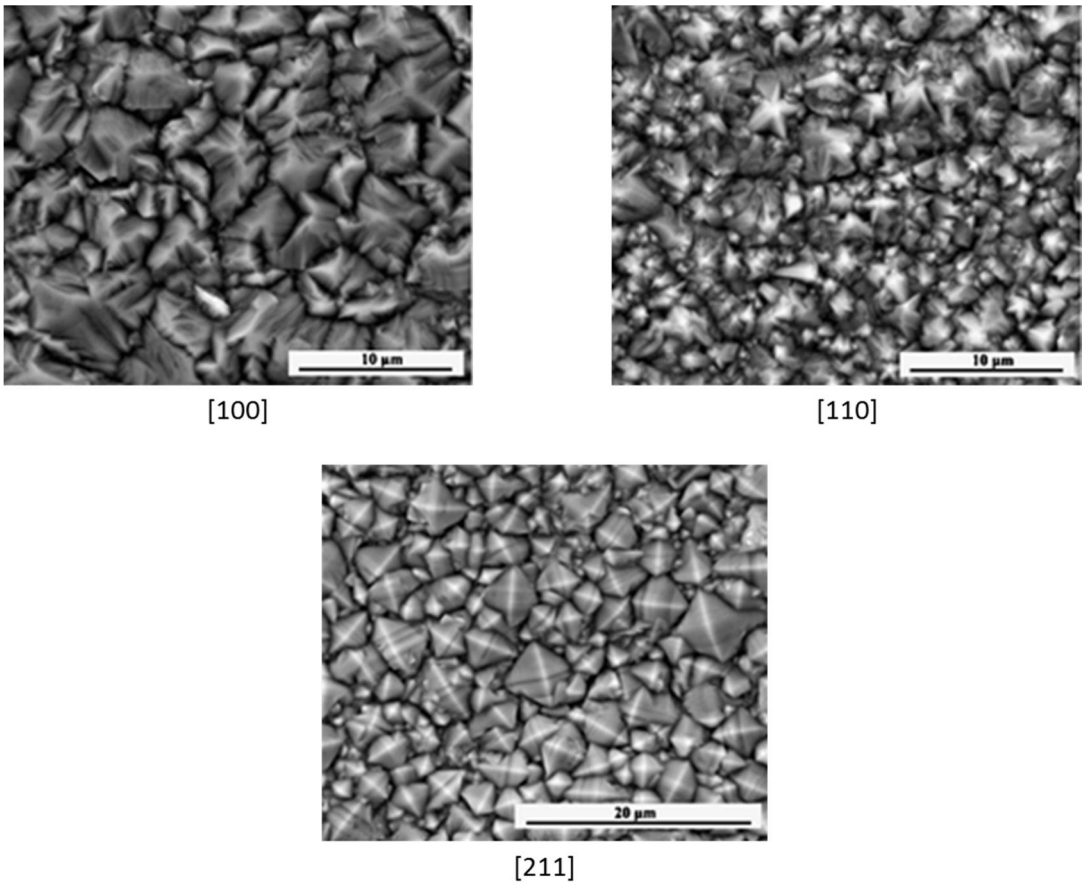

Figure 4.11. SEM surface micrographs presenting the typical morphology of pure Ni crystallites with [100], [110], and [210] preferred orientations. Adapted from Ref. [8].

Figures 4.12 to 4.16 display high-magnification FIB-SEM images of the coatings, which apparently seem to reflect to a certain degree the results obtained in the XRD analysis. Large Ni crystals with an irregular structure similar to that of crystals with a [100] orientation reported by other authors [7,8,14,31] were routinely observed seen in Ni coatings produced under silent/still conditions (Figure 4.12), along with some smaller crystals with what seemed a regular pyramidal structure and binary symmetry similar to that of crystals growing in the [211] direction reported elsewhere [7,8,14]. Although the assumed [211] textures seemed rather small, the assumed [100] structures showed a wide range of sizes, as previously reported by Vicenzo and Cavalloti [31]. The surface structure appeared to change for the deposits plated under mechanical agitation, as the presence of crystals with the assumed [211] orientation became more evident (Figure 4.13), while crystals with apparent [100] and [211] were observed in the coatings plated under ultrasound at 0.011 W/cm^3

(Figure 4.14). However, fewer Ni grains apparently resembling crystals with a [211] orientation were noticed in the surface of the deposits plated under ultrasound at 0.124 and 0.180 W/cm^3 (Figures 4.15 and 4.16, respectively). In these last two cases, the largest Ni grains with a structure similar to that of Ni crystals with a [100] orientation reported by other authors [7,8,14,31] were smaller than the largest ones of the same type noticed under silent/still conditions, and the proportion of very small crystals seemed to be greater, especially in the deposits plated at 0.124 W/cm^3 (Figure 4.15). These two features roughly suggested that the deposits plated under ultrasound at higher powers (0.124 and 0.180 W/cm^3) could present a random mixture of relatively large and very small crystals, indicating the modification of the microstructure of the deposit and the refinement of the grain size to a certain extent by ultrasound. It is worth noting that very few grains with what seemed a pseudo-pentagonal crystal symmetry similar to that of Ni crystals with a [110] orientation such as those reported by other authors [7,8,14] were observed in all the samples evaluated, agreeing to some extent with the low $RTC_{[110]}$ values previously estimated and included in Figure 4.5.

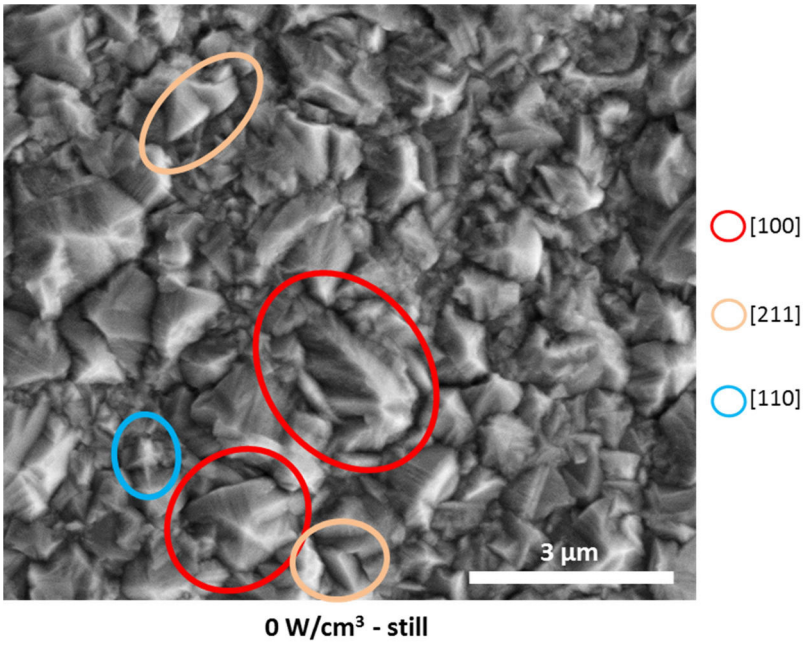

Figure 4.12. High magnification FIB-SEM images of the surface of Ni electrodeposited under silent/still conditions. Electrodeposition time: 14 minutes. Current density: 4 A/dm^2. Some of the crystals with a surface

morphology similar to that of Ni crystals with different orientations reported by other authors [7,8,14,31] are highlighted with different colours.

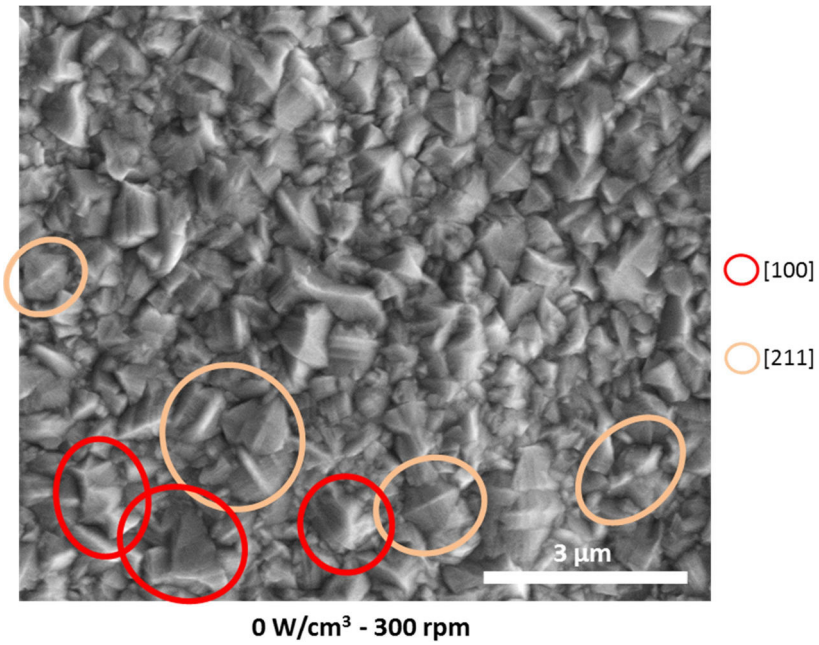

Figure 4.13. High magnification FIB-SEM images of the surface of Ni electrodeposited under mechanical agitation. Electrodeposition time: 14 minutes. Current density: 4 A/dm^2. Some of the crystals with a surface morphology similar to that of Ni crystals with different orientations reported by other authors [7,8,14,31] are highlighted with different colours.

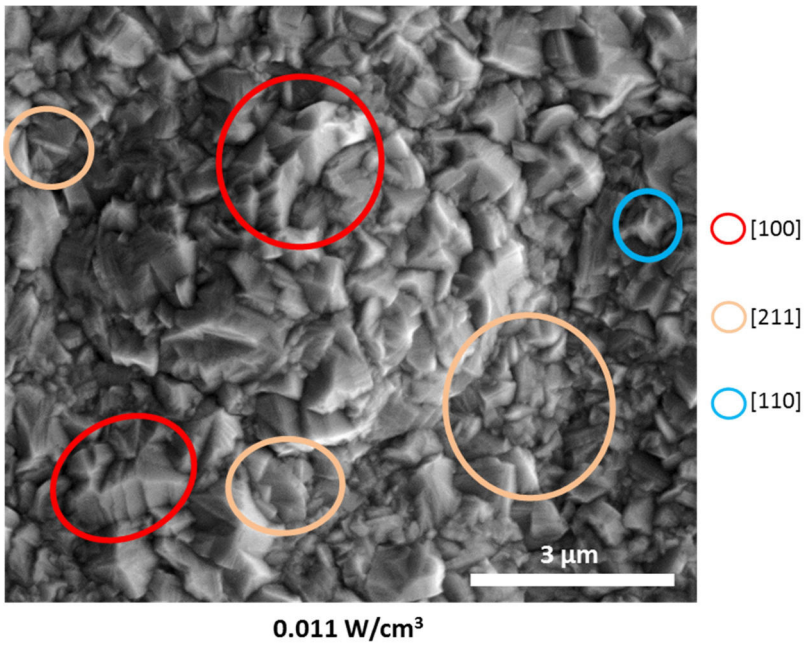

Figure 4.14. High magnification FIB-SEM images of the surface of Ni electrodeposited under ultrasound at 0.011 W/cm^3. Electrodeposition time: 14 minutes. Current density: 4 A/dm^2. Some of the crystals with a surface

morphology similar to that of Ni crystals with different orientations reported by other authors [7,8,14,31] are highlighted with different colours.

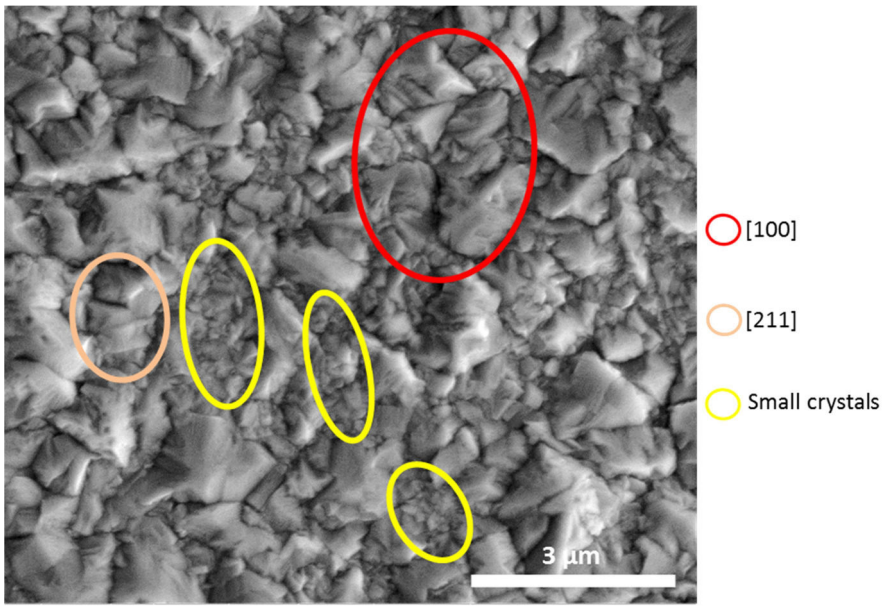

Figure 4.15. High magnification FIB-SEM images of the surface of Ni electrodeposited under ultrasound at 0.124 W/cm^3. Electrodeposition time: 14 minutes. Current density: 4 A/dm^2. Some of the crystals with a surface morphology similar to that of Ni crystals with different orientations reported by other authors [7,8,14,31] are highlighted with different colours.

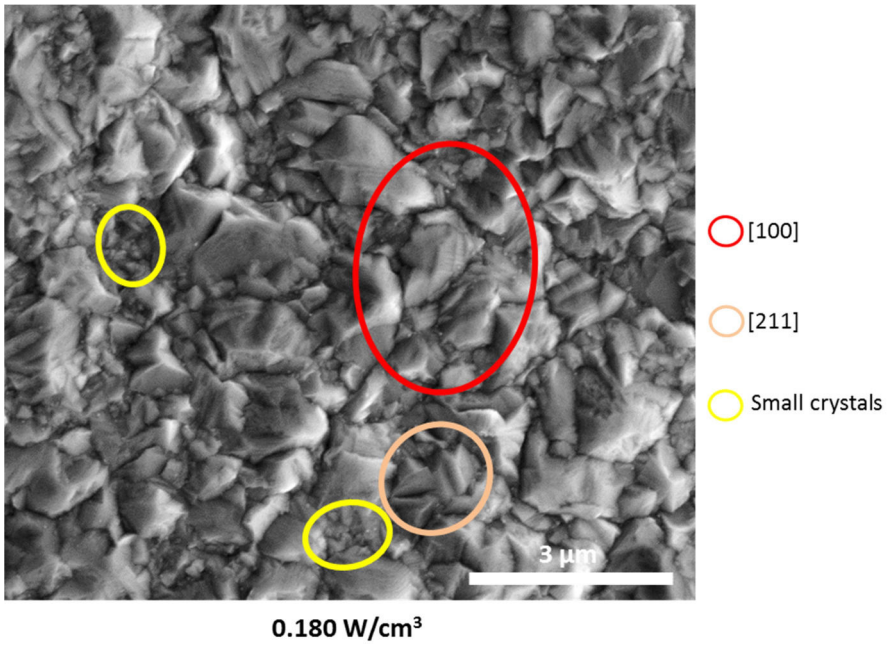

Figure 4.16. High magnification FIB-SEM images of the surface of Ni electrodeposited under ultrasound at 0.180 W/cm^3. Electrodeposition time: 14 minutes. Current density: 4 A/dm^2. Some of the crystals with a surface

morphology similar to that of Ni crystals with different orientations reported by other authors [7,8,14,31] are highlighted with different colours.

Further evaluation of the cross-section of the Ni deposits was performed to check the effect of ultrasonic irradiation on the microstructure of Ni coatings and confirm whether the presence of ultrasound would refine the grain size to a certain extent. A FIB-SEM system was again used for this purpose, allowing the examination of in-situ cross-sections in all the different Ni deposits produced. Figure 4.17 displays the cross-section of Ni deposits produced under either silent/still conditions or mechanical agitation at 300 rpm. Whereas the Ni coatings electrodeposited under silent/still conditions exhibited a characteristic columnar structure mainly consisting of large crystals, the Ni deposits produced under mechanical agitation consisted of a combination of columnar crystals and smaller grains. Related to the latter, both columnar crystals and smaller grains in the Ni coatings electrodeposited under mechanical agitation seemed to exhibit a higher aspect ratio than the large columnar crystals observed in the deposits produced under silent/still conditions.

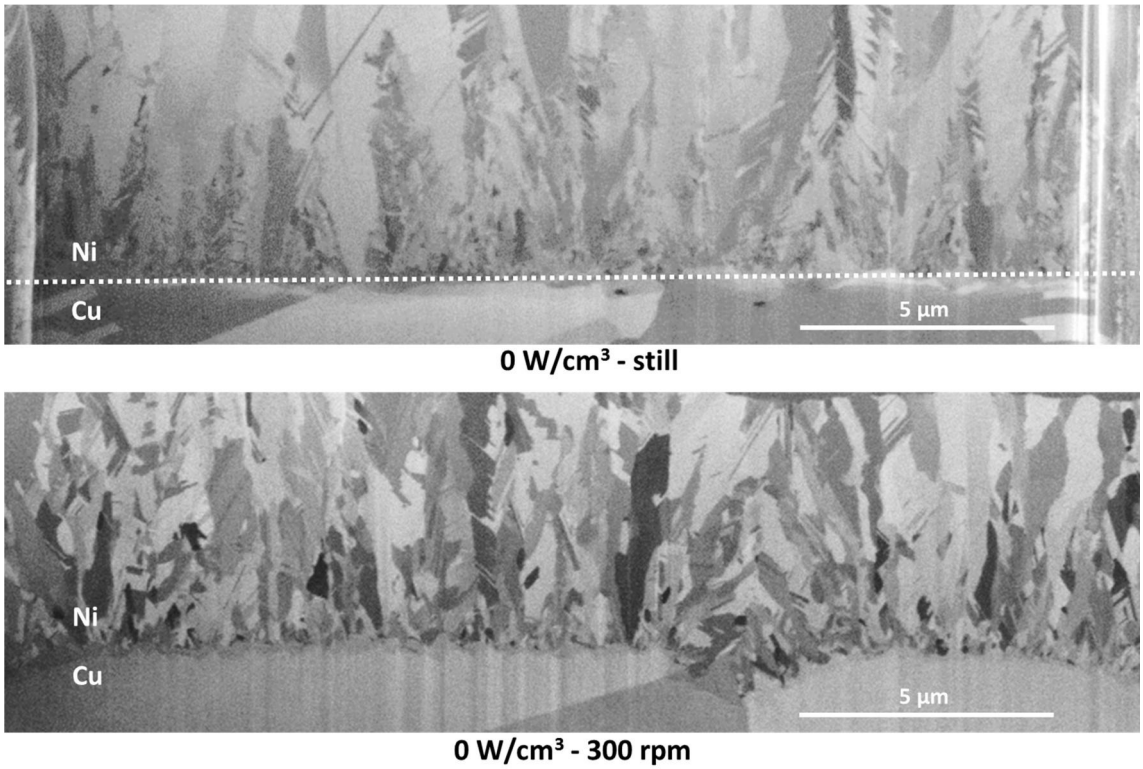

Figure 4.17. FIB-SEM images of the cross-section of Ni coatings deposited under silent/still conditions and mechanical agitation at 300 rpm. Electrodeposition time: 14 minutes. Current density: 4 A/dm^2.

Figure 4.18 displays the cross-section of Ni deposits produced under ultrasound at different powers. Ni coatings electrodeposited at 0.011 W/cm^3 exhibited a columnar structure quite similar to that of Ni deposits produced under silent/still conditions, although quite a few small grains could be noticed in the coatings produced with the presence of ultrasound. The presence of small grains was far more noticeable in the Ni coatings electrodeposited under ultrasound at either 0.124 W/cm^3 or 0.180 W/cm^3, as a very significant proportion of very small grains (some of them down to the nano-scale) were present along with some large columnar crystals.

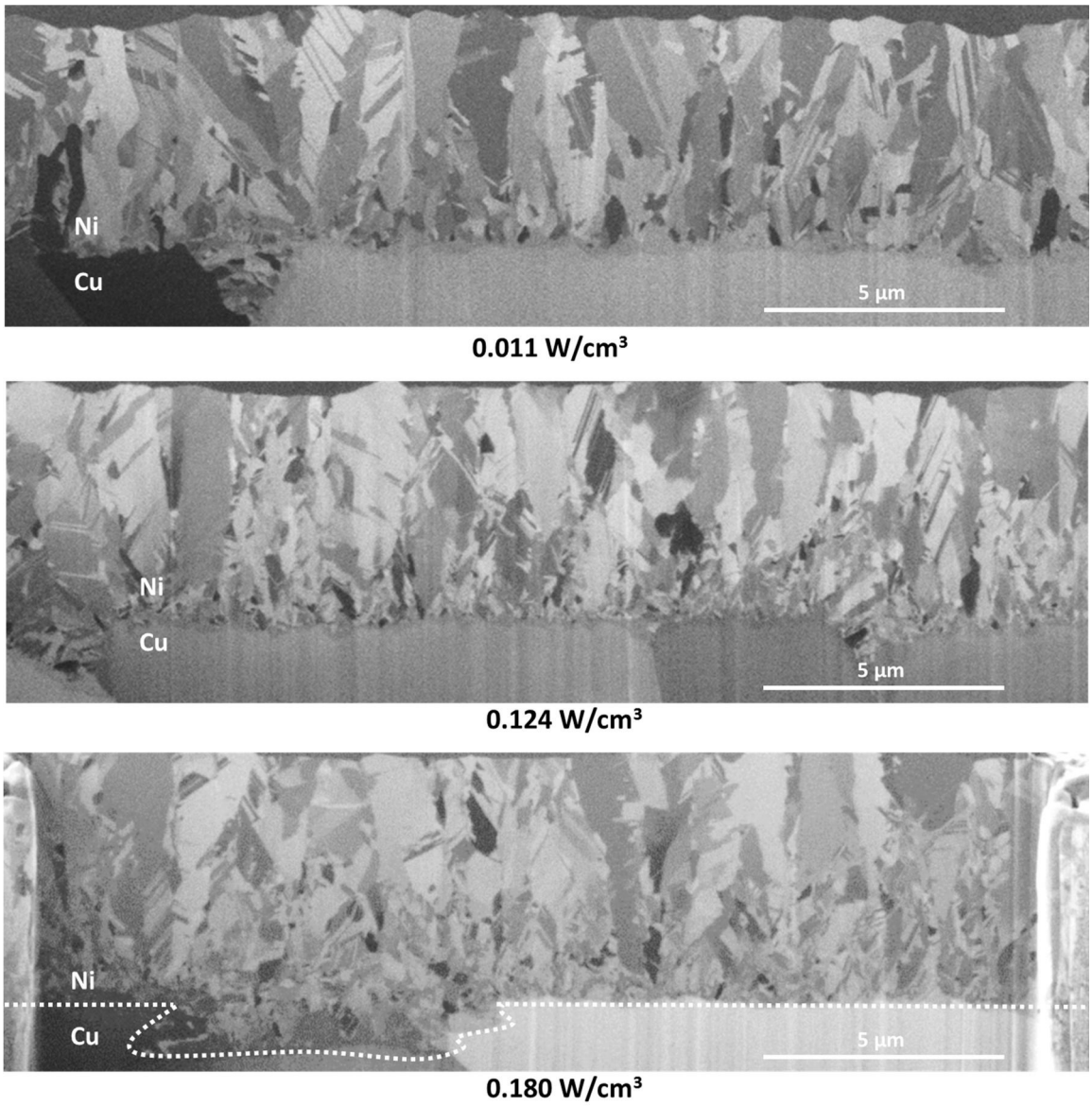

Figure 4.18. FIB-SEM images of the cross-section of Ni coatings deposited under ultrasound at 0.011, 0.124 and 0.180 W/cm^3. Electrodeposition time: 14 minutes. Current density: 4 A/dm^2.

In summary, FIB-SEM analysis of both surface morphology and grain structure suggest that both mechanical agitation and ultrasound modify to some extent the appearance and structure of Ni deposits compared to silent/still conditions. Nevertheless, two different trends were observed:

1. In terms of surface morphology, whereas mechanical agitation seemed to promote the appearance of grooves on the surface of the deposit, ultrasound promoted the formation of nodular structures in the surface. Nevertheless, the formation of nodules in Ni coatings electrodeposited under ultrasound at 0.124 W/cm^3 was not as significant as in those produced under ultrasound at other ultrasonic powers. This would be related to the nature of cavitation phenomena (randomly-attached bubble structures near the surface) occurring near the surface of the coatings electrodeposited at 0.124 W/cm^3.
2. In terms of grain structure, both mechanical agitation and ultrasound had a grain refinement effect, although in both cases columnar crystals were still clearly noticeable in the metal matrix. Nevertheless, whereas mechanical agitation seemed to have a 'thinning' effect resulting in Ni grains with higher aspect ratio, the coatings electrodeposited under ultrasound, especially at 0.124 W/cm^3 and 0.180 W/cm^3, exhibited a more fragmented structure alternating large columnar crystals with areas with very small Ni grains.

Grain refinement and structure modification by ultrasound has already been widely suggested in the past [32,33], although most of the works available in the literature related to electrodeposited Ni coatings only showed some evidence of the grain refinement effect by ultrasound on the surface of the coatings [34,35]. Regarding this, Lampke et al's electron back-scattered diffraction (EBSD) results showed that, whereas large Ni crystals were still noticeable in Ni deposits produced under ultrasound, many small crystals could be observed, resulting in an overall grain refinement when compared with Ni coatings electrodeposited in absence of ultrasound [36]. A similar effect in the microstructure was

observed in the present study, as the use of ultrasound during the electrodeposition, particularly at high powers, resulted in a more fragmented structure where columnar crystals were observed alternating with very small grains.

4.2.4. HARDNESS

Microhardness tests were performed on the different Ni deposits (Figure 4.19) in order to initially observe any effect that the previously suggested modification of the structure of the deposit by ultrasound may have on the mechanical properties of the material. The coatings plated under silent/still conditions showed the lowest microhardness values, around 282 HV, quite similar to the values measured for the deposits plated under mechanical agitation (288 HV), while the coatings produced under ultrasound had higher microhardness values. Ni deposits plated at 0.124 W/cm^3 presented the highest microhardness (slightly lower than 360 HV, 27% more than electrodeposited Ni under silent/still conditions), followed by those plated at 0.180 W/cm^3 (311 HV, 10% more than electrodeposited Ni under silent/still conditions) and 0.011 W/cm^3 (296 HV, around 5% more than electrodeposited Ni under silent/still conditions).

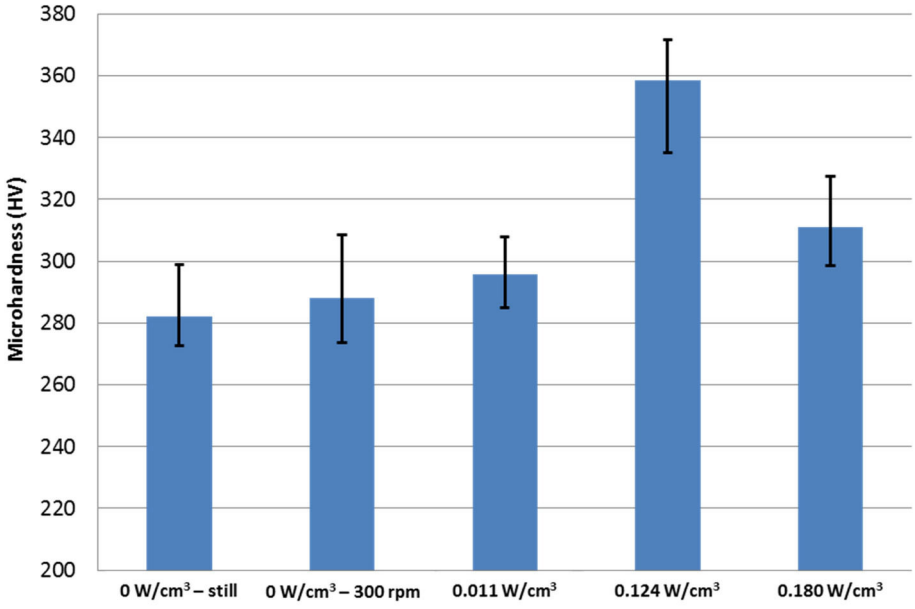

Figure 4.19. Microhardness values measured in the central area of the cross-section of Ni coatings (≈6 μm) electroplated onto Cu substrates under different agitation conditions. Electrodeposition parameters:

electrodeposition time: = 14 minutes, current density: 4 A/dm^2. Microhardness measurement parameters: load = 2 g-force, load time = 10 seconds.

Ni crystals with the [100] preferred orientation are commonly associated with a ductile behaviour [37,38] with less brittleness [39] and lower values of internal stress and hardness [40], while the [211] growth mode is generally related to higher values of hardness [41]. However, in the present study, no significant increase was observed for the deposits plated under mechanical agitation, with a high proportion of [211] textures, compared to the coatings produced under silent/still conditions, which had a similar proportion of crystals with [100] and [211] preferred orientations. On the other hand, the increase in hardness of the coatings deposited under ultrasound is concurrent with previous studies by Prasad et al. [42] (from 235 HV to 332 HV in 50-micron-thick Ni coatings deposited on mild steel cathodes in a Watts bath at 4 A dm^{-2} in a 22 kHz ultrasonic bath), Zanella et. al. [34] (from ≈300 HV to ≈320 HV in Ni coatings plated onto a low carbon steel substrate in a Watts bath at 2 A dm^{-2} under unknown ultrasonic conditions), and García-Lecina et al. [35] (from ≈250 HV to ≈300 HV in Ni coatings plated onto mild steel cathodes in a Watts bath at 5 A dm^{-2} with a 24 kHz ultrasonic horn). In this latter case, the authors pointed out that the increase in hardness could be due a change in the structure of the deposit, as previously suggested by Lampke et al. [36]. The higher presence of smaller grains on the surface of Ni coatings electrodeposited under ultrasound at 0.124 W/cm^3 and 0.180 W/cm^3 (Figures 4.15 and 4.16) and the grain size refinement and fragmentation of the microstructure of Ni deposits produced under ultrasound at those same powers (Figure 4.18) would therefore be responsible to some extent for the increase in hardness observed in the thin Ni coatings electrodeposited under ultrasound at higher power. Nevertheless, structure modification was also observed in the Ni coatings electrodeposited under mechanical agitation (Figure 4.17), although these deposits did not exhibit any significant increase in hardness. This means that the presence of ultrasound during the electrodeposition must have another effect which may result in the increase in hardness here reported. In this sense, Walker and

Walker suggested that work hardening during electrodeposition could also occur due to the presence of ultrasonic cavitation near the cathode, especially in those areas were pitting or erosion could appear due to the effect of cavitation [43]. Work hardening by cavitation near the surface would also explain why the Ni coatings electrodeposited at 0.124 W/cm^3, the ones with erosion marks caused by random bubble structures attached to the surface, exhibited a significantly higher hardness than those electrodeposited at 0.180 W/cm^3.

4.3. STABILITY OF THE BATH

As previously explained in Section 3.2.4.1 in Chapter 3, the main goal of this study was to observe any signs that could point to the modification of the chemical parameters of the Watts bath after being irradiated for a certain time. The chemical parameters of the bath chemical parameters (concentration of $NiSO_4.6H_2O$, $NiCl_2.6H_2O$ and H_3BO_3 and pH) were routinely checked during electroplating experiments conducted in freshly prepared solutions at different ultrasonic powers during 360 minutes. Although 360 minutes of continuous sonication may initially seem a short time to see any particular effect of ultrasound on the chemical parameters of the bath, it is generally more than enough to induce drastic changes in pH in different sonochemical and sonoelectrochemical processes [44,45] due to the production of acids such as nitric acid from the air dissolved in the liquid [46], among other free-radical reactions that may occur in the electrolyte [47].

Tables 4.1 to 4.4 show the chemical parameters (concentration of $NiSO_4.6H_2O$, $NiCl_2.6H_2O$, and H_3BO_3, and pH) of the Watts bath that were followed during the stability experiments performed in the present study. In all cases, no significant changes were observed during the experiments performed under ultrasound when compared with the Ni Watts bath that was not irradiated with ultrasound, as the values of all the chemical parameters remained fairly constant during all the experiments. Related to this, the small fluctuations observed in the measured values would be mainly caused by the small additions of deionised water

carried out every 120 minutes to compensate water evaporation at 50 °C which occurred in all the experiments.

Table 4.1. Concentration of $NiSO_4.6H_2O$ during plating experiments carried out at different ultrasonic powers.

	Ultrasonic power (W/cm^3)			
	0 - still	0.011	0.124	0.180
$NiSO_4.6H_2O$ start (g/l)	292.4	293.3	286.9	283.9
$NiSO_4.6H_2O$ after 2 hours (g/l)	295.1	288.9	289.7	286.5
$NiSO_4.6H_2O$ after 4 hours (g/l)	296.4	290.3	289.6	284.7
$NiSO_4.6H_2O$ after 6 hours (g/l)	291.9	291.5	290.9	287.5

Table 4.2. Concentration of $NiCl_2.6H2O$ during plating experiments carried out at different ultrasonic powers.

	Ultrasonic power (W/cm^3)			
	0 - still	0.011	0.124	0.180
$NiCl_2.6H_2O$ start (g/L)	49.2	55.0	49.4	53.6
$NiCl_2.6H_2O$ after 2 hours (g/l)	51.0	53.6	53.5	51.3
$NiCl_2.6H_2O$ after 4 hours (g/l)	50.6	53.7	51.0	51.0
$NiCl_2.6H_2O$ after 6 hours (g/l)	50.1	53.1	53.4	52.0

Table 4.3. Concentration of H_3BO_3 during plating experiments carried out at different ultrasonic powers.

	Ultrasonic power (W/cm^3)			
	0 – still	0.011	0.124	0.180
H_3BO_3 start (g/L)	32.3	33.1	33.5	35.7
H_3BO_3 after 2 hours (g/l)	32.4	32.8	37.5	32.8
H_3BO_3 after 4 hours (g/l)	31.9	31.6	35.1	34.6
H_3BO_3 after 6 hours (g/l)	32.1	32.3	35.8	33.9

Table 4.4. pH during plating experiments carried out at different ultrasonic powers.

	Ultrasonic power (W/cm^3)			
	0 - still	0.011	0.124	0.180
pH start	3.20	3.13	3.23	3.31
pH after 2 hours	3.23	3.16	3.22	3.30
pH after 4 hours	3.20	3.10	3.23	3.31
pH after 6 hours	3.27	3.08	3.24	3.29

In summary, no significant effect of ultrasound on the composition and pH of the bath was observed compared to the solution employed in the experiment under silent/still conditions. This observation is fairly important, as cavitation phenomena that occur in ultrasonically-assisted chemistry processes involve the achievement of extremely high pressures (≈1000 atm) and temperatures (≈5000 K) which yields the formation of radicals from the solvent [47] that could result in the formation of undesired products that might provoke a significant modification of the chemical parameters of the bath.

4.4. CONCLUSIONS

The appearance of the electrodeposited Ni coatings shows that ultrasonic cavitation significantly affects the surface finish of the coatings, especially at 0.124 W/cm^3, where random bubble structures attached to the electrode surface strongly erode the surface of the deposits, provoking the appearance of local marks where bubble spots can easily be seen. Nevertheless, these marks are reduced at higher ultrasonic powers (0.180 W/cm^3), where higher pressure antinodes form in the beaker, removing/attracting the cavitating bubble structures from the surface. The presence of ultrasound also modified the orientation of the deposit, counteracting the effect that the agitation of the solution may have on the preferred growth mode. XRD analysis showed that, while the agitation of the solution favoured the presence of [211] textures, the presence of ultrasonic cavitation promote the electrocrystallization of Ni in the [100] preferred orientation. This trend was also observed

in FIB-SEM images of the surface different deposits. FIB-SEM images of the cross-section of certain coatings also confirmed the effect of ultrasound on the microstructure of the Ni deposits. Microhardness tests showed that ultrasound increased the hardness of electrodeposited Ni, with the hardest Ni coatings being plated under ultrasound at 0.124 W/cm^3 (27% more than under silent/still conditions). Both the apparent grain size refinement and fragmentation of the columnar crystal microstructure of the Ni deposits produced under ultrasound are determinant for the increase in the microhardness.

XRD, FIB-SEM and microhardness results are strongly related to the surface finish of the deposits, as the most significant change in crystal orientation, formation of very small crystals on the surface of the deposit and increase in microhardness, was observed in Ni deposits showing more erosion marks due to the formation of random structures attached to the surface of cathodes. These results strongly indicate that cavitation phenomena occurring near the surface is the key factor in enhancing the hardness of Ni coatings electrodeposited under ultrasound. Therefore, as cavitation activity near the surface of the cathode is lower at 0.180 W/cm^3 due to the removal of the random bubble structures that are noticed at 0.124 W/cm^3, the deposits produced at 0.180 W/cm^3 showed lower values of microhardness that those electrodeposited at 0.124 W/cm^3.

The combination of an increased hardness of the Ni deposits plated under ultrasound with the higher presence of [100] textures that are associated to a ductile behaviour with less brittleness could be of an interest for industrial applications of pure Ni coatings. Regarding the use of Ni coatings produced under ultrasound as diffusion barrier layers, the modification of the microstructure shown in Figure 4.18 could improve the tribological performance and the diffusion resistance of current Ni diffusion barrier layers in absence of ultrasound by increasing the presence of grain boundaries (i.e. very small crystals) in the coating, assuming lattice-controlled diffusion is predominant in bearing overlay systems. Nevertheless, the formation of erosion marks on the surface of the coatings should be kept

to a minimum, as these marks not only result in an undesired increase in the roughness of the deposit, but also could induce poor adhesion between the diffusion layer and the overlay, making the overlay system prone to seizure. Keeping this in mind, electrodeposited Ni under ultrasound at 0.180 W/cm^3 was selected as a suitable coating material to replace current Ni diffusion barrier layers deposited in absence of ultrasound.

4.5. REFERENCES

[1] J. Petersen, 'Electric vehicles and the natural resource cliff', published on-line in NASDAQ News (2011). http://community.nasdaq.com/News/2011-02/electric-vehicles-and-the-natural-resource-cliff.aspx?storyid=56478

[2] J.K. Dennis, T.E. Such, Nickel and Chromium plating, 3rd ed., Woodhead Publishing, Cambridge, 1993.

[3] C.S. Lin, C.Y. Lee, F.J. Chen, W.C. Li, J. Electrochem. Soc. 152 (2005) C370.

[4] D. Krefting, R. Mettin, W. Lauterborn, Ultrason. Sonochem. 11 (2004) 119.

[5] L. Ph. Bérubé, G. L'Espérance, J. Electrochem. Soc. 136 (1989) 2314.

[6] S. Surviliene, V. Jasulaitiene, A. Lisowska-Oleksiak, V. A. Safonov, J. Appl. Electrochem. 35 (2005) 9.

[7] E.A. Pavlatou, N. Spyrellis, Russ. J. Electrochem. 44 (2008) 745.

[8] S. Spanou, E.A. Pavlatou, N. Spyrellis, Electrochim. Acta 54 (2009) 2547.

[9] C.N. Panagopoulos, E.P. Georgiou, A. Tsopani, L. Piperi, Appl. Surf. Sci. 257 (2011) 4769.

[10] M. K. Camargo, U. Schmidt, R. Grieseler, M. Wilke, A. Bund, J. Electrochem. Soc. 161 (2014) D168.

[11] Inorganic Crystal Structure Database code 64989, Fachinformationszentrum Karlsruhe (Germany) and National Institute of Standards and Technology (United States of America).

[12] J. Amblard, M. Froment, G. Maurin, Electrodepos. Surf. Treat. 2 (1974) 205.

[13] E.A. Pavlatou, M. Raptakis, N. Spyrellis, Surf. Coat. Technol. 201 (2007) 4571.

[14] S. Spanou, E.A. Pavlatou, J. Appl. Electrochem. 40 (2010) 1325.

[15] H. Fischer, Elektrolytische Abscheidung und Elektrokristalisation von Metallen, Springer, Berlin, 1954.

[16] H. Fischer, Electrodep. Surf Treat. 1 (1973) 239.

[17] H. Fischer, Electrodep. Surf Treat. 1 (1973) 319.

[18] J. Amblard, M. Froment, N. Spyrellis, Surf. Technol. 5 (1977) 205.

[19] J. Amblard, M. Froment, Faraday Symp. Chem. Soc. 12 (1977) 136.

[20] J. Amblard, I. Epelboin, M. Froment, G. Maurin, J. Appl. Electrochem. 9 (1979) 233.

[21] J. Amblard, M. Froment, G. Maurin, N. Spyrellis, E. Trevisan-Souteyrand, Electrochim. Acta 28 (1983) 909.

[22] C.B. Nielsen, A. Horsewell, M.J.L. Østergård, J. Appl. Electrochem. 27 (1997) 839.

[23] A.G. Ives, J.W. Edington, G.P. Rothwell, Electrochim. Acta 15 (1970) 1797.

[24] B. Bozzini, Mater. Chem. Phys. 66 (2000) 278.

[25] X.-l. Ren, Q.-f. Wei, Z. Liu, J. Liu, Trans. Nonferrous Met. Soc. China 22 (2012) 467.

[26] E. Moti', M.H. Shariat, M.E. Bahrololoom, J. Appl. Electrochem. 38 (2008) 605.

[27] E. Moti', M.H. Shariat, M.E. Bahrololoom, Mater. Chem. Phys. 111 (2008) 469.

[28] K. Kobayasi, A. Chiba, N. Minami, Ultrasonics 38 (2000) 676.

[29] J. Kubisztal, A. Budniok, A. Lasia, Int. J. Hydrogen Energ. 32 (2007) 1211-1218.

[30] Y.-w. Song, D.-y. Shan, R.-s. Chen, E.-h. Han, Trans. Nonferrous Met. Soc. China 18 (2008) s339.

[31] A. Vicenzo, P.L. Cavalloti, Russ. J. Electrochem. 44 (2008) 716.

[32] C.T. Walker, R. Walker, Electrodepos. Surf. Treat. 1 (1973) 457.

[33] V. Sáez, M.D. Esclapez, A.J. Frías-Ferrer, P. Bonete, I. Tudela, M.I. Díez-García, J. González-García, Ultrason. Sonochem. 18 (2011) 873.

[34] C. Zanella, M. Lekka, P.L. Bonora, Surf. Eng. 26 (2010) 511.

[35] E. García-Lecina, I. García-Urrutia, J.A. Díez, J. Morgiel, P. Indyka, Surf. Coat. Technol. 206 (2012) 2998.

[36] T. Lampke, D. Dietrich, A. Leopold, G. Alisch, B. Wielage, Surf. Coat. Technol. 202 (2008) 3967.

[37] I. Matsui, Y. Takigawa, T. Uesugi, K. Higashi, Mater. Lett. 99 (2013) 65

[38] I. Matsui, Y. Takigawa, T. Uesugi, K. Higashi, Mat. Sci. Eng. A 578 (2013) 318.

[39] F. Denise, H. Leidheiser Jr., J. Electrochem. Soc. 100 (1953) 490.

[40] D.J. Evans, Trans. Faraday Soc. 54 (1958) 1086.

[41] N.A. Badarulzaman, A.A. Mohamad, S. Puwadaria, Z.A. Ahmad, J. Coat. Technol. Res. 7 (2010) 815.

[42] P.B.S.N.V. Prasad, R. Vasudevan, S.K. Seshadri, S. Ahila, Mater. Lett. 17 (1993) 357.

[43] R. Walker, C.T. Walker, Nature 244 (1973) 141.

[44] V. Sáez, M.D. Esclapez, P. Bonete, D.J. Walton, A. Rehorek, O. Louisnard, J. González-García, Ultras. Sonochem. 18 (2011) 104.

[45] V. Sáez, I. Tudela, M.D. Esclapez, P. Bonete, O. Louisnard, J. González-García, Chem. Eng. J. 168 (2011) 649.

[46] E.L. Mead, R.G. Sutherland, R.E. Verrall, Can. J. Chem. 54 (1976) 1114.

[47] Y.G. Adewuyi, Ind. Eng. Chem. Res. 40 (2001) 4681

5. ULTRASOUND-ASSISTED ELECTRODEPOSITION OF NI COMPOSITE COATINGS WITH LUBRICANT PARTICLES

5.1. OVERVIEW

Section 4.3 showed how the presence of ultrasound during the electrodeposition of Ni may modify the structure by changing the preferred orientation and refining the grain size of the Ni deposits to some extent. Ultrasound could also assist in dispersing particles in an electroplating bath, not only reducing the agglomeration of particles in the plating solution, but also preventing the incorporation of agglomerated particles and aggregates into the coating. As a result, composite coatings with a more uniform distribution of finely-dispersed particles in a metal matrix would be produced, as previously commented in Section 2.3.3.1 of the literature review. The incorporation of particles may not only result in a further refinement of the grain size of the Ni deposits, but also in the alteration of the mechanical properties of the material. Such modification in the mechanical properties of Ni coatings as those used as a diffusion barrier in bronze-based bearings may be critical if the diffusion barrier is locally exposed due to the loss of the overlay.

In this context, the objectives of the work included in this chapter were: i) to evaluate the effect that ultrasound may have on the dispersion of particles in a Ni Watts bath, ii) to produce Ni-based composite coatings with finely-dispersed particles uniformly distributed in the Ni matrix, and iii) to evaluate the properties of those coatings. This study was structured in three main parts:

1. A first stage where different lubricant particles were dispersed in the Ni Watts bath under different dispersing conditions: i) ultrasound on its own, ii) mechanical agitation on its own, and iii) combined ultrasound/mechanical agitation.
2. A second stage focused on the production and qualitative evaluation of Ni-based composite coatings with different particles electrodeposited under different conditions: i) ultrasound on its own, ii) mechanical agitation on its own, and iii) combined ultrasound/mechanical agitation.

3. And a third stage focused on the detailed characterization of those Ni-based composite coatings produced during the second stage of the study that qualitatively presented a more uniform distribution of particles, higher particle content and less agglomerates in the cross-section.

5.2. EFFECT OF ULTRASOUND ON THE DISPERSION OF PARTICLES

In this first stage of the study, dispersions containing four different particles, namely WS_2, hBN, MoS_2 and PTFE, were prepared under three different dispersing conditions: i) ultrasound at 0.180 W/cm^3, ii) mechanical agitation at 300 rpm, and iii) combined ultrasound/mechanical agitation at 0.180 W/cm^3 – 300 rpm. The three dispersing methods were evaluated following two different approaches: a) visual appearance experiments for which 'real' Ni Watts bath solutions containing 15 g/L of particles were prepared, and b) particle size distribution experiments where diluted Ni Watts bath solutions containing 0.1 g/L of particles were used.

It must be noted that the combination of both approaches followed to evaluate the suitability of the different dispersing methods, although proved quite effective as a comparative tool to select the best of the dispersing methods studied here, presented some limitations. For the visual appearance experiments, the main drawback would be the relative subjectivity of the results, especially in those cases there the black colour of the Ni Watts electrolyte containing either WS_2 or MoS_2 particles would make it quite difficult to distinguish the difference in terms of particle sinking and clarity of the suspension in the early moments after the dispersion. For the particle size distribution analysis, the main drawbacks were inherently related to the analytical technique employed, laser diffraction-based particle sizing, due to different aspects:

- A roughly approximated refractive index (RI) was considered for the WS_2 and WS_2 particles and the electrolyte due to the lack of tabulated RI values (RI = 2.75 for the WS_2 particles based on the RI values of thin WS_2 films [1]; RI = 1.8 for the hBN particles [2]; RI = 4.00 for the WS_2 particles after considering RI values of thin MoS_2 films [3]; RI = 1.33 for the diluted Ni Watts electrolyte after assuming that it would be similar to the RI of pure water). Choosing the correct RI is important to ensure accuracy of the particle size distribution curves when the Mie theory is used as in this case, and therefore some inaccuracy in the measured particle size results is expected [4].
- Although the pH was adjusted to the pH of the 'real' Ni Watts bath (3.2), the very diluted nature of the dispersions is not realistic compared to the 'real' conditions and therefore changes in the particle size could occur due to the highly conductive nature of the Ni Watts bath and the higher concentration of WS_2 particles in the real solutions. The reason for using a diluted Ni Watts electrolyte containing a very low concentration of WS_2 particles is due to the need to have clear solutions in order to have a proper transmission of the laser through the samples. This is required to ensure relatively low laser obscuration once the solids are dispersed and is inherent to the use of laser diffraction-based particle sizing methods [5]. However, not many authors explain in detail in which conditions their experiments were carried out [6], when they should clearly state the degree of dilution of the electrolyte and the (low) concentration of particles [7].
- The analytical method itself, which may not properly account for the 'non-spherical' nature of some particles, and the proprietary numerical algorithms used in the laser diffraction equipment, which are quite complex yet not experimentally validated [8].

All of this implies that, from the quantitative point of view, although particle size and particle distribution will not be too far from the measured values, one should remain relatively sceptical to the values displayed in the graphs shown in Figure 5.4, 5.7 and 5.10.

From the comparative point of view though, and based on the laser obscuration measured in all cases, the results definitely are meaningful, as laser obscuration would be to some extent related to dispersion quality. In this sense, laser obscuration was always the highest for each particle in the diluted dispersions prepared under combined ultrasound/mechanical agitation and the lowest in the diluted dispersions prepared under mechanical agitation on its own.

5.2.1. Ni Watts bath with WS_2 particles

Figure 5.1 shows the visual appearance of three Ni Watts electrolytes containing 15 g/L of WS_2 particles (D50 ≈ 0.6 μm and D90 ≈ 5 μm according to the supplier, M K Impex Corp) that were prepared under different dispersing conditions: ultrasound at 0.180 W/cm^3, mechanical agitation at 300 rpm, and combined ultrasound/mechanical agitation at 0.180 W/cm^3 – 300 rpm. No visual difference was observed in the dispersions produced under different conditions immediately after the end of the process, as a dense, black solution was obtained for all cases.

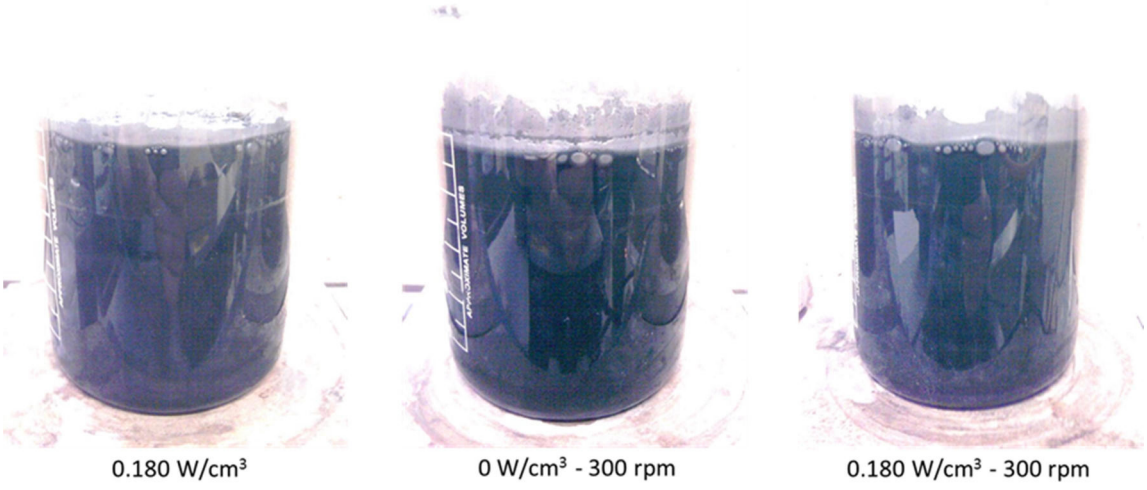

Figure 5.1. Appearance of Ni Watts bath + WS_2 dispersions (15 g/L of WS_2 particles) immediately after dispersing the particles for 30 minutes in the electrolyte under different conditions: ultrasound at 0.180 W/cm^3, mechanical agitation at 300 rpm and combined ultrasound/mechanical agitation at 0.180 W/cm^3 – 300 rpm. Images were edited (50% increase in brightness) to show the quality of the dispersion.

After 60 minutes (Figure 5.2), a clear green colour was apparent in the solution produced under mechanical agitation at 300 rpm, whereas the solutions produced with ultrasound and with the combined process presented a much darker green colour, meaning that the 'settlement rate' of the particles dispersed at 300 rpm with absence of ultrasound was higher than the particles dispersed with the other methods where ultrasound was present.

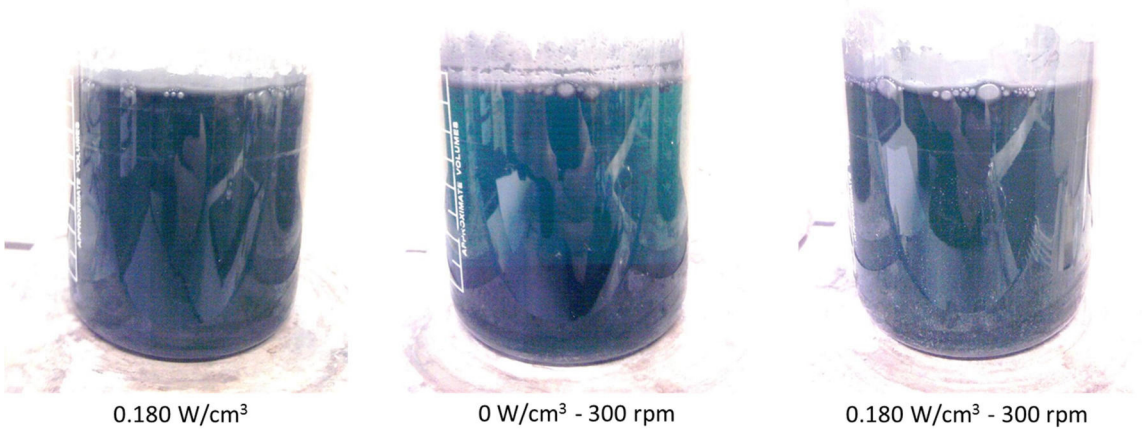

Figure 5.2. Appearance of Ni Watts bath + WS_2 dispersions (15 g/L of WS_2 particles) 60 minutes after dispersing the particles for 30 minutes in the electrolyte under different conditions: ultrasound at 0.180 W/cm³, mechanical agitation at 300 rpm and combined ultrasound/mechanical agitation at 0.180 W/cm³ – 300 rpm.. Images were edited (50% increase in brightness) to show the quality of the dispersion.

After 240 minutes (Figure 5.3), the dispersions produced with either ultrasound or combined agitation became slightly clearer, meaning that particles in both solutions were also progressively sinking after agitation had ceased. Nevertheless, the solution produced with mechanical agitation presented a much clearer green colour, and the formation of a black sludge at the bottom of the beaker was clearly noticed, confirming that a poor dispersion of WS_2 particles in the plating solution was obtained with mechanical agitation compared with the methods where ultrasound was introduced.

Figure 5.3. Appearance of Ni Watts bath + WS_2 dispersions (15 g/L of WS_2 particles) 180 minutes after dispersing the particles for 30 minutes in the electrolyte under different conditions: ultrasound at 0.180 W/cm³, mechanical agitation at 300 rpm and combined ultrasound/mechanical agitation at 0.180 W/cm³ – 300 rpm. Images were edited (50% increase in brightness) to show the quality of the dispersion.

Particle size distributions experiments were also performed on diluted Ni Watts electrolytes (1 to 100 dilution) containing a small quantity of WS_2 particles (0.1 g/L) to observe the effect that the different dispersing methods have on the particle size distribution (Figure 5.4). The combined ultrasound/mechanical agitation at 0.180 W/cm³ – 300 rpm was the best dispersing method, followed by the 'ultrasound only' method at 0.180 W/cm³, which yielded slightly higher results, whereas the dispersions with the worst quality in terms of particle size were achieved with the 'mechanical agitation only' method at 300 rpm. In all cases, single modal Gaussian-alike distribution curves were obtained.

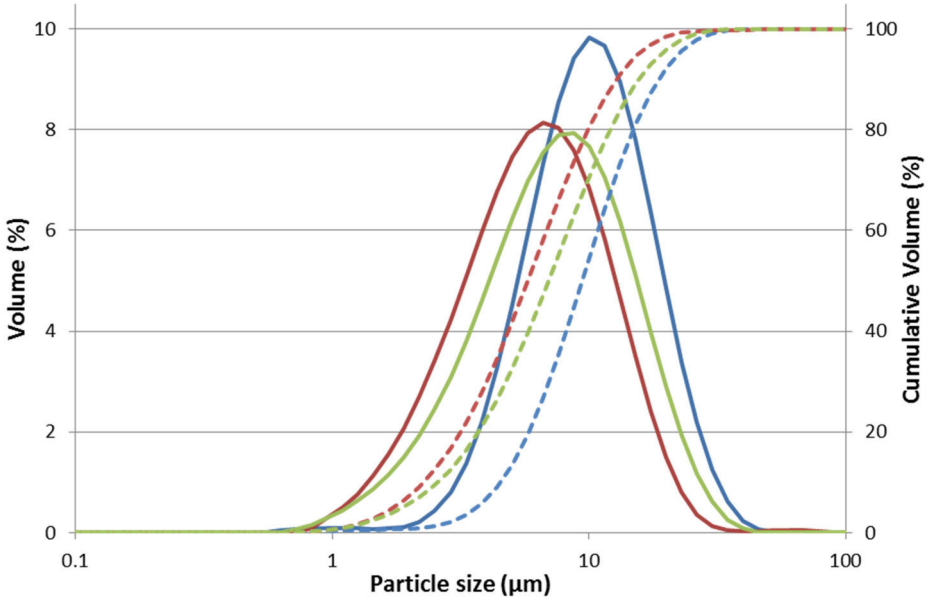

Figure 5.4. Particle size distribution curves (solid line: particle size distribution, dashed line: accumulated particle size distribution) obtained from experiments conducted in diluted Ni Watts bath + WS_2 dispersions (1 to 100 dilution, 0.1 g/L of WS_2 particles) where particles were again dispersed for 30 minutes under different conditions: ultrasound at 0.180 W/cm^3 (green lines), mechanical agitation at 300 rpm (blue lines) and combined ultrasound/mechanical agitation at 0.180 W/cm^3 – 300 rpm (red lines).

These results obtained during the particle size distribution experiments of the diluted electrolytes agree to some extent with the visual appearance of the Watts bath as prepared containing 15 g/L of WS_2 particles, suggesting that the best way of dispersing WS_2 particles was to combine mechanical agitation with ultrasound, closely followed by the use of ultrasound on its own, whereas the use of mechanical agitation on its own was clearly the worst dispersing method in both visual appearance and particle size distribution experiments.

5.2.2. Ni Watts bath with hBN particles

The visual appearance of Ni Watts baths containing 15 g/L of hBN particles (D50 ≈ 0.5 µm and D90 ≈ 1.1 µm according to the supplier, M K Impex Corp) prepared by the different dispersing methods employed (ultrasound at 0.180 W/cm^3, mechanical agitation at 300 rpm, and combined ultrasound/mechanical agitation at 0.180 W/cm^3 – 300 rpm) is displayed in Figure 5.5. The best dispersion was achieved by combining ultrasound and

mechanical agitation, as a homogeneous, white-green solution with no signs of large aggregates was produced under such conditions. The worst dispersion was obtained when mechanical agitation was used in the absence of ultrasound, as it was quite non-homogeneous with the presence of large agglomerates. In this case, particles started to sink immediately after the end of the dispersion process.

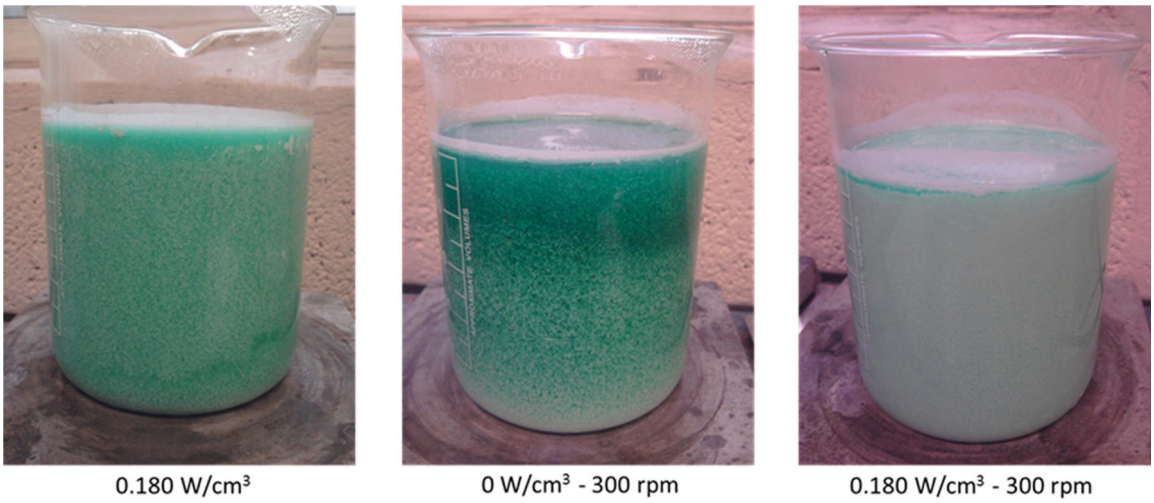

Figure 5.5. Appearance of Ni Watts bath + hBN dispersions (15 g/L of hBN particles) immediately after dispersing the particles for 30 minutes in the electrolyte under different conditions: ultrasound at 0.180 W/cm^3, mechanical agitation at 300 rpm and combined ultrasound/mechanical agitation at 0.180 W/cm^3 – 300 rpm.

After 30 minutes though (Figure 5.6), the bulk solution in the suspensions looked similar in all cases, as all the solutions presented a turbid green colour. This was due to the hBN particles agglomerating and sinking, resulting in the formation of a white sludge at the bottom of the beaker. Nevertheless, the sludge was more compact and difficult to re-disperse in the hBN dispersion produced under mechanical agitation.

Figure 5.6. Appearance of Ni Watts bath + hBN dispersions (15 g/L of hBN particles) 30 minutes after dispersing the particles for 30 minutes in the electrolyte under different conditions: ultrasound at 0.180 W/cm³, mechanical agitation at 300 rpm and combined ultrasound/mechanical agitation at 0.180 W/cm³ – 300 rpm.

As in the previous case, particle size distributions experiments were also conducted on diluted Ni Watts electrolytes (1 to 100 dilution) containing a small quantity of hBN particles (0.1 g/L) and prepared under different conditions (Figure 5.7). Again, the dispersions prepared under mechanical agitation at 300 rpm in the absence of ultrasound showed the worst quality in terms of particle size distribution, whereas both methods where ultrasound was present yielded very similar results. The difference between the presence or absence of ultrasound in the dispersion was also reflected in the single-modal Gaussian-like distribution curves obtained for the dispersions prepared with the combined and 'ultrasound only' methods, as opposed to the 'mechanical only' method, where a bi-modal curve was obtained. This bi-modal curve, where the largest peak indicates the presence of large agglomerates with particle sizes in the order of 100 μm roughly agree with the results obtained in the visual appearance experiments conducted on the dispersions prepared with the 'mechanical only' method, where particles started to form very large agglomerates that could be clearly seen by the naked eye which sink immediately after the end of the dispersion process.

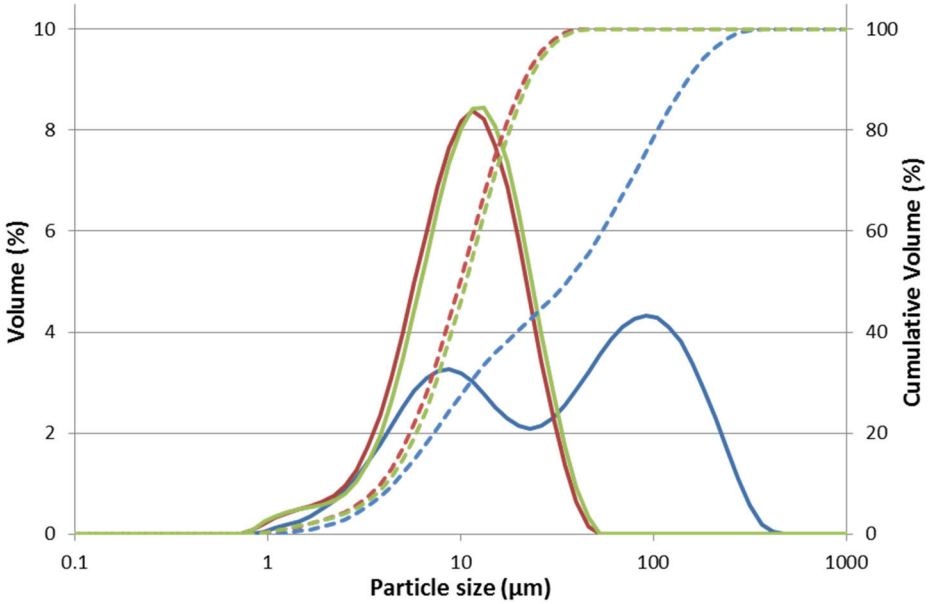

Figure 5.7. Particle size distribution curves (solid line: particle size distribution, dashed line: accumulated particle size distribution) obtained from experiments conducted in diluted Ni Watts bath + hBN dispersions (1 to 100 dilution, 0.1 g/L of hBN particles) where particles where again dispersed for 30 minutes under different conditions: ultrasound at 0.180 W/cm^3 (green lines), mechanical agitation at 300 rpm (blue lines) and combined ultrasound/mechanical agitation at 0.180 W/cm^3 – 300 rpm (red lines).

As in the case of the Ni Watts bath + WS_2 dispersions, particle size distribution experiments of the diluted Ni Watts bath + hBN dispersions agree to some extent with the visual appearance of the Watts electrolytes as prepared containing 15 g/L of hBN particles, pointing again to the combined ultrasound/mechanical agitation as the best conditions to disperse hBN particles in the Ni Watts bath. In this case, the results from the visual appearance of the dispersions were very clear due to the white colour of the hBN particles, which facilitated the observation of the dispersion with time. These visual appearance experiments of the Ni Watts bath + hBN dispersions clearly showed why the combination of ultrasound and mechanical agitation works better than using either ultrasound or mechanical agitation on its own: i) from the 'macrodispersion' point of view, mechanical agitation contributed to achieve a more homogeneous dispersion, preventing the larger agglomerated particles from sinking to the bottom of the beaker, and ii) from the 'microdispersion' point of view, the presence of ultrasound enhanced the de-agglomeration

of agglomerated particles due to the formation of cavitating bubbles and the physical effects inherently related to their presence, allowing finely-dispersed particles to remain well-dispersed in the solution for longer times. Although the particle size distribution experiments conducted on diluted Ni Watts electrolytes containing a low concentration of hBN particles suggest that the combined method was slightly better that the 'mechanical only' method, it must be noted that these results did not reflect the significant difference observed in the 'real' Ni Watts baths containing the 'real' amount of hBN particles. This could be caused by the fact that the laser obscuration was >20% in the dispersions prepared with the combined and the 'ultrasound only' methods. Laser obscuration was in these experiments higher than the recommended range for the laser diffraction-based particle sizing system used (Mastersizer 2000). The use of an even lower concentration of hBN would have allowed experiments to be carried out where laser obscuration would be in the recommended range (between 10% and 20%), but this would have resulted in an even less representative dispersion compared to the Ni Watts bath + hBN dispersion from where Ni/hBN composite coatings would be electrodeposited. In spite of this, the same conclusion as in the case of the Ni Watts bath + WS_2 dispersions can be made for Ni Watts bath + hBN dispersions from the visual appearance and particle size distribution experiments: the best dispersions were achieved when mechanical agitation at 300 rpm was combined with ultrasound at 0.180 W/cm^3.

5.2.3. Ni Watts bath with MoS_2 particles

Figure 5.8 shows the appearance of Ni Watts bath + MoS_2 (D50 ≈ 1.2 μm according to the supplier, Asbury) dispersions prepared by different dispersing methods immediately after the end of the dispersing process. A black dispersion similar to the ones containing WS_2 particles was obtained in all cases, and no visual difference was noticed between the different dispersing conditions (ultrasound at 0.180 W/cm^3, mechanical agitation at 300 rpm, and combined ultrasound/mechanical agitation at 0.180 W/cm^3 – 300 rpm).

Figure 5.8. Appearance of Ni Watts bath + MoS_2 dispersions (15 g/L of MoS_2 particles) immediately after dispersing the particles for 30 minutes in the electrolyte under different conditions: ultrasound at 0.180 W/cm³, mechanical agitation at 300 rpm and combined ultrasound/mechanical agitation at 0.180 W/cm³ – 300 rpm. Images were edited (50% increase in brightness) to show the quality of the dispersion.

After 240 minutes, the dispersion produced under mechanical agitation showed a clearer green colour where a black sludge at the bottom of the beaker was noticed, whereas the dispersions produced under either ultrasound or combined agitation presented a darker green tone. Nevertheless, such difference between the Ni Watts bath + MoS_2 dispersion prepared in absence of ultrasound (mechanical agitation at 300 rpm) and the Ni Watts bath + MoS_2 dispersions prepared in presence of ultrasound (ultrasound at 0.180 W/cm³ and combined ultrasound/mechanical agitation at 0.180 W/cm³ – 300 rpm) was a lot less remarkable than in the dispersions prepared with hBN and WS_2 particles.

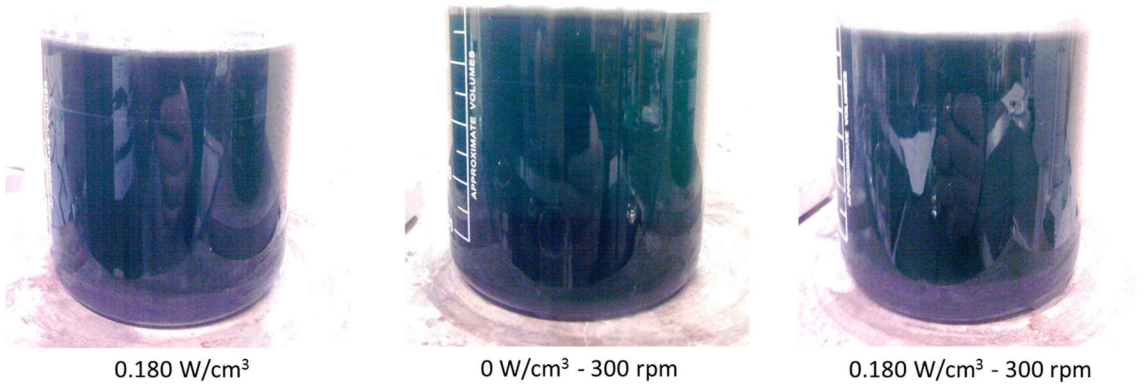

Figure 5.9. Appearance of Ni Watts bath + MoS_2 dispersions (15 g/L of MoS_2 particles) 240 minutes after dispersing the particles for 30 minutes in the electrolyte under different conditions: ultrasound at 0.180 W/cm³,

mechanical agitation at 300 rpm and combined ultrasound/mechanical agitation at 0.180 W/cm^3 – 300 rpm. Images were edited (50% increase in brightness) to show the quality of the dispersion.

Figure 5.10 shows the particle distribution curves estimated from laser diffraction measurements conducted on diluted Ni Watts electrolytes (1 to 100) containing a small quantity of MoS_2 particles (0.1 g/L) and prepared under different conditions. Again, dispersions prepared under mechanical agitation at 300 rpm in absence of ultrasound clearly showed the worst quality in terms of particle size distribution, whereas the combination of ultrasound and mechanical agitation at 0.180 W/cm^3 – 300 rpm yielded the best dispersions with a significant proportion of particles apparently having very small sizes. In all cases, bi-modal curves were obtained, the largest peak being in the same order of magnitude, although the second peak observed in the dispersion prepared with the 'mechanical only' method is very small, compared with the second peaks observed in the data obtained from the dispersions prepared with the other methods. These results suggest that the MoS_2 particles mainly consist of aggregates, which easily agglomerate to form larger agglomerates when dispersed with the 'mechanical only' method. When dispersed with the 'ultrasound only' method, MoS_2 aggregates and particles are de-agglomerated due to the presence of ultrasound, whereas with the combined dispersed method, the MoS_2 aggregates not only benefit from the 'macro' effect of being continuously stirred in the dispersion, but also from the 'micro' effect of the presence of cavitation phenomena, which not only would result in a large de-agglomeration of the agglomerates, but also in the partial de-aggregation of the aggregates.

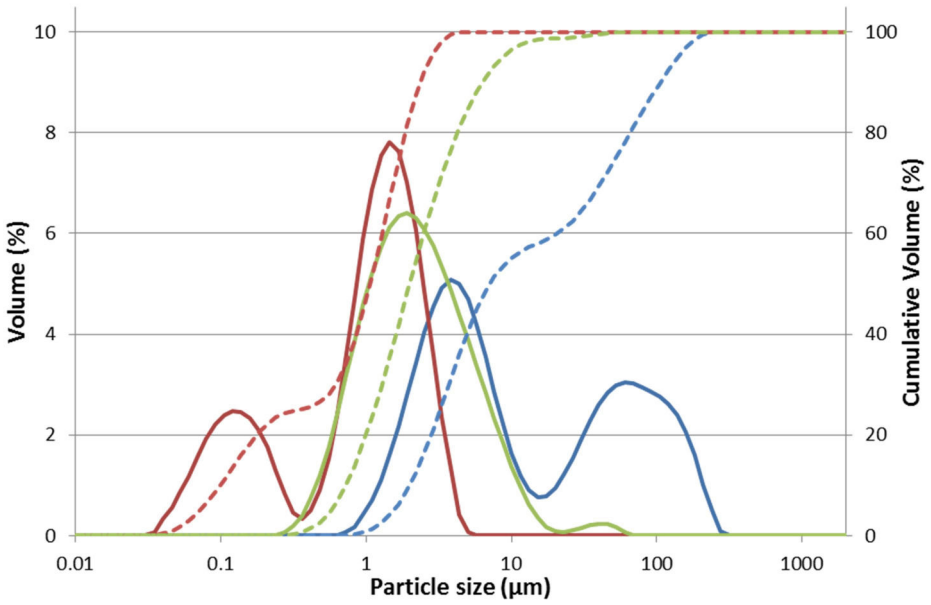

Figure 5.10. Particle size distribution curves (solid line: particle size distribution, dashed line: accumulated particle size distribution) obtained from experiments conducted in diluted Ni Watts bath + MoS_2 dispersions (1 to 100 dilution, 0.1 g/L of MoS_2 particles) where particles where again dispersed for 30 minutes under different conditions: : ultrasound at 0.180 W/cm^3 (green lines), mechanical agitation at 300 rpm (blue lines) and combined ultrasound/mechanical agitation at 0.180 W/cm^3 – 300 rpm (red lines).

As in previous cases, particle size distribution experiments of the diluted Ni Watts bath + MoS_2 dispersions agree to some extent with the visual appearance of the concentrated electrolytes containing 15 g/L of particles, as the combination of ultrasound and mechanical agitation was again the best method to disperse MoS_2 particles in the Ni Watts bath. In this case, the results were qualitatively similar to those observed for the Ni Watts bath + WS_2 dispersions: whereas significant differences were observed in particle size distribution experiments for each of the dispersing methods, visual appearance experiments did not suggest significant differences. As in the case of the Ni Watts bath + WS_2 dispersions this is due to the black colour of the MoS_2 particles, which made it quite difficult to observe a significant visual difference. Regarding the particle size distribution experiments, it must be noted that there were some limitations related to the laser obscuration, as quite large values were measured for the experiments conducted under combined ultrasound/mechanical

agitation conditions (58% versus 38% for the 'ultrasound only' method and 15% for the 'mechanical only' method).

5.2.4. Ni Watts bath with PTFE particles

No satisfactory results were obtained with the PTFE particles (ZONYL MP1100 - PTFE agglomerates with sizes around 1.8 to 4 μm of submicron-sized particles according to the supplier, Du Pont). No dispersion method worked with such particles due to the high hydrophobic behaviour they have. Different approaches could be used to enable the addition of PTFE particles into Ni coatings: i) addition of surfactants to the Ni Watts solution to increase the wettability of the plating solution, and ii) use of commercial PTFE dispersions. Nevertheless, both approaches would involve the modification of the chemical parameters of the current Ni Watts bath where no additives are used, and therefore, they were discarded for the present research project.

5.3. Electrodeposition of Ni-based composite coatings under different agitation conditions

Ni-based composite coatings (around 6 μm thick) containing three different lubricant particles (WS_2, hBN and MoS_2) were electrodeposited under three different agitation conditions (ultrasound at 0.180 W/cm^3, mechanical agitation at 300 rpm, and combined ultrasound/mechanical agitation at 0.180 W/cm^3 – 300 rpm) at 4 A/dm^2 in order to observe which agitation conditions and particles could yield the best Ni composite coatings in terms of visual appearance/surface finish and distribution of finely dispersed particles within the Ni matrix. In all cases, the particles were dispersed prior to the electrodeposition for 30 minutes under combined ultrasound/mechanical agitation at 0.180 W/cm^3 – 300 rpm, as this was the best dispersing method, according to the results reported in Section 5.2.

5.3.1. Ni/WS_2 COMPOSITE COATINGS

Figure 5.11 displays some examples of the Ni/WS_2 composite coatings electrodeposited on Cu substrates under different agitation conditions. Dull, dark grey deposits were obtained when ultrasound was used on its own, while dull, light grey coatings were produced under combined ultrasound/mechanical agitation. In both cases, sludgy deposits of fine powder were observed in the upper edge of the samples, particularly under combined ultrasound/mechanical agitation. No acceptable Ni/WS_2 composite coatings were electrodeposited under mechanical agitation in absence of ultrasound, as particles agglomerated on the surface of the Cu substrate and blocked the active area of the cathode during plating. This layer of agglomerated WS_2 particles was hard to remove by rinsing with deionised water, although it would fall off the substrate quite easily once dried.

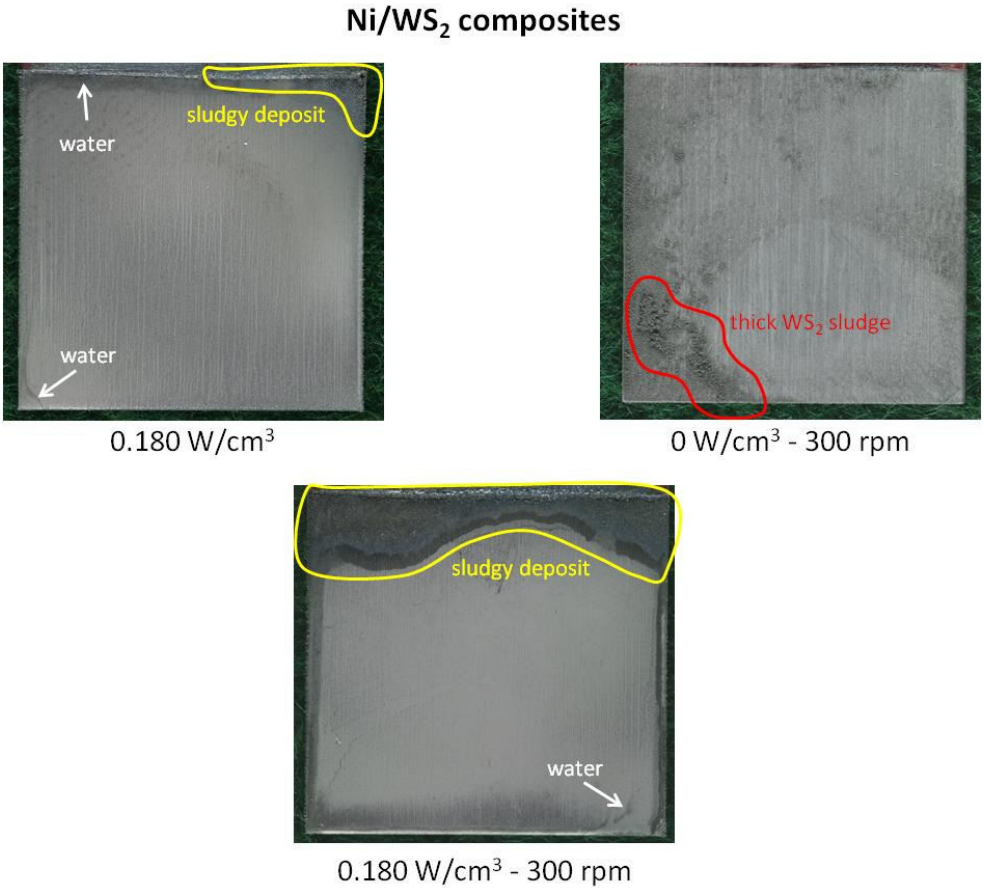

Figure 5.11. Examples of Ni/WS_2 composite coatings electrodeposited on Cu substrates under different conditions: ultrasound at 0.180 W/cm^3, mechanical agitation at 300 rpm and combined ultrasound/mechanical

agitation at 0.180 W/cm³ – 300 rpm. Moisture (water) stains can also be seen near the edges in some of the samples. Electrodeposition time: 14 minutes. Current density: 4 A/dm².

Cross-sections of Ni/WS_2 composite coatings produced under ultrasound and combined ultrasound/mechanical agitation conditions were further examined as shown in Figure 5.12, whereas cross-sections of the composite coatings produced under mechanical agitation were not further evaluated because the deposits came off the Cu substrate while cutting, mounting and polishing the samples for their evaluation. Deposits with the expected thickness (around 5-7 µm) containing many WS_2 particles were produced under ultrasound on its own, whereas significantly thinner composite coatings (around 2-3 µm) with much lower WS_2 content were electrodeposited under combined ultrasound/mechanical agitation.

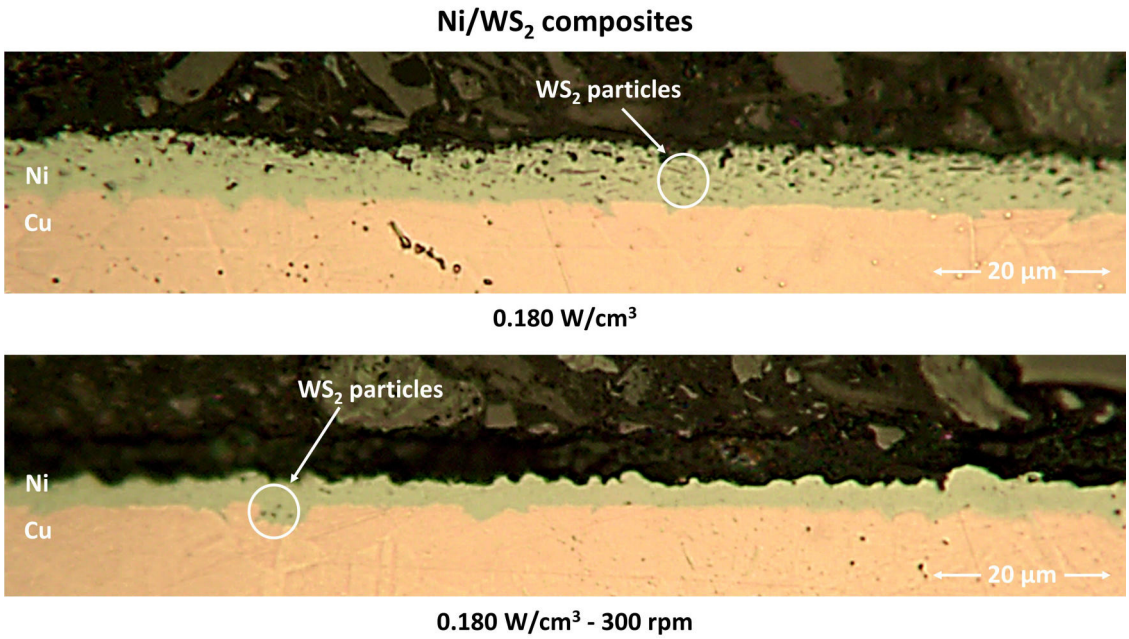

Figure 5.12. Examples of cross-section images of Ni/WS_2 composite coatings electrodeposited on Cu substrates under different plating conditions: ultrasound at 0.180 W/cm³, mechanical agitation at 300 rpm and combined ultrasound/mechanical agitation at 0.180 W/cm³ – 300 rpm. Electrodeposition time: 14 minutes. Current density: 4 A/dm².

Further evaluation of the cross-section of Ni/WS_2 composites produced under ultrasound was conducted by SEM BSE analysis, confirming the high rate of incorporation of WS_2 particles with different sizes into the coating (Figure 5.13).

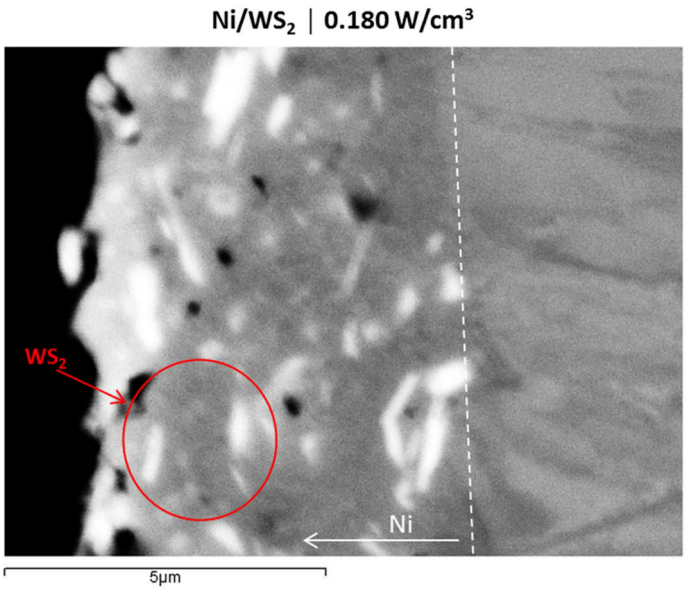

Figure 5.13. SEM BSE images of the cross-section of Ni/WS_2 composite coatings electrodeposited on Cu substrates under ultrasound at 0.180 W/cm^3. Electrodeposition time: 14 minutes. Current density: 4 A/dm^2.

The results observed for electrodeposition experiments carried out under mechanical agitation and under combined ultrasound/mechanical agitation agree to some extent with some results from similar contemporary studies carried out by García-Lecina et al. [9], who tried to incorporate inorganic fullerene-like WS_2 nanoparticles ($IF\text{-}WS_2$) into Ni coatings also electrodeposited from a Watts bath. In the latter, initial trials to produce $Ni/IF\text{-}WS_2$ composite coatings showed that, at low concentrations (0.1-1.0 g/L) of $IF\text{-}WS_2$ nanoparticles in the bath, irregular Ni deposits were obtained with no incorporation of $IF\text{-}WS_2$ nanoparticles, whereas at high concentrations (0.1-1.0 g/L) of $IF\text{-}WS_2$ nanoparticles, a black film would be covering the whole surface of the cathode. Said black film consisted of loosely adhered $IF\text{-}WS_2$ nanoparticles which would be easily removed after ultrasonic rinsing. The authors also noted that no presence of Ni was detected in these black films, suggesting that, under those conditions, the $IF\text{-}WS_2$ nanoparticles are deposited by electrophoretic forces, inhibiting the electrodeposition of Ni. The only way for them to overcome all these issues

was to add a surfactant, cetyl trimethylammonium bromide (CTAB), to the Watts bath. Once CTAB was added to the Watts bath, the presence of ultrasound had a general enhancing effect in terms of particle incorporation, grain refinement and mechanical properties of the Ni/IF-WS_2 composite coatings. In the present study CTAB was not necessary to obtain a good particle dispersion in the coating because the WS_2 particles used in the present research project are 1-2 orders of magnitude larger than the IF-WS_2 nanoparticles used by García-Lecina et al. [9] (particle size around 40-120 nm forming clusters with a size up to 600 nm). As they stated in their paper, the '*smaller the agglomerated WS_2 particle groups, the higher the opportunity for attraction by the electric field*' [9], which would explain to some extent why they struggled to get an acceptable Ni/IF-WS_2 composite coating from an additive-free Watts bath. But the fact that the best Ni/WS_2 composite coatings in terms of surface finish, thickness and particle incorporation were electrodeposited under ultrasound on its own, a condition not considered by García-Lecina et al. in their study [9], suggests that the way the ultrasonic field is set and how it may interact with the stirring of the electrolyte also has a critical impact on the quality of the electrodeposited composite coatings. In this sense, mechanical agitation seemed to counteract the effect of ultrasound in terms of particle incorporation. This could be due to the nature of the fluid flow set when stirring with the overhead stirrer: as the flow is parallel to the surface of the cathode, particles near the surface of the substrate may be 'removed' from there, reducing the concentration of the particles in the cathode-electrolyte interface, resulting in a lower incorporation of particles into the coating. The fact that only the very small WS_2 particles were incorporated into the coatings would be in agreement with this consideration. Cavitating bubbles near the surface would also be affected, being less effective in those areas near the cathode surface. In addition, a less effective ultrasonic field in the surroundings of the substrate would also provoke agglomeration of some of the large WS_2 particles, which would in part block the surface of the substrate, and hence the thinner deposits obtained under ultrasound/mechanical agitation. This would also be in agreement with the fact that the

sludgy areas observed around at upper edge in samples electrodeposited under ultrasound/mechanical agitation were far more extended than in the deposits produced under ultrasound.

In summary, the results obtained during the present research show that, when mechanical agitation was employed during the plating process, poor quality coatings were obtained due to the formation of large agglomerated particles onto the surface of the Cu substrate, blocking the cathode and preventing the electrodeposition of an acceptable Ni/WS_2 coating, The combination of ultrasound and mechanical agitation during the electroplating process improved the quality of the coatings, although thin deposits were produced in this case with not many particles present, possibly due to partial blockage of the surface of the Cu substrate by large agglomerates formed due to the counter-effect that stirring may have on the formation of cavitating bubbles near the cathode-electrolyte interface. Much better coatings were obtained when ultrasound on its own was used during the electrodeposition, as great amounts of particles were co-deposited with Ni. Due to this, the Ni/WS_2 composite coatings produced under ultrasound that presented an apparently uniform thickness and particle distribution were selected for further characterization and evaluation due to the promising features they showed, becoming a potential option to replace current Ni interlayers employed in bronze-based bearings.

5.3.2. Ni/hBN composite coatings

Figures 5.14 displays the surface finish and of Ni/hBN composite coatings produced under ultrasound, mechanical agitation or combined ultrasound/mechanical agitation. A good surface finish was observed in all the deposits, and no apparent difference was noticed in the composite coatings electrodeposited under different plating conditions.

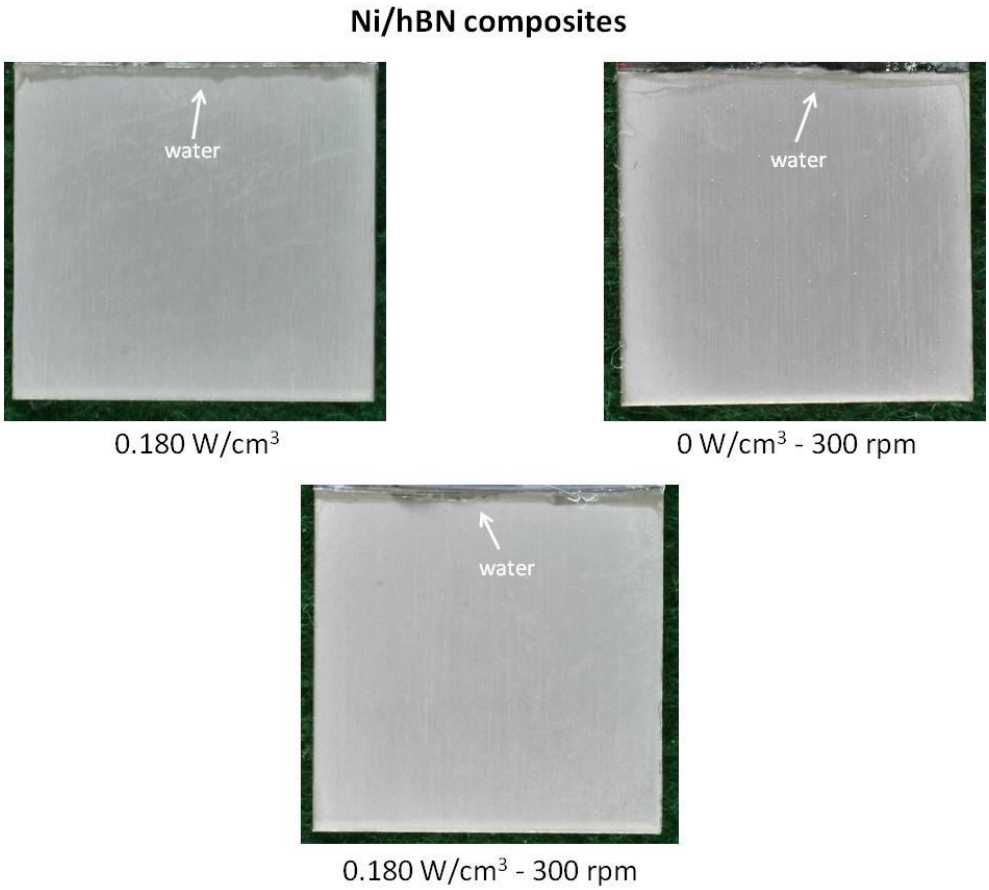

Figure 5.14. Examples of Ni/hBN composite coatings plated on Cu substrates under different conditions: ultrasound at 0.180 W/cm^3, mechanical agitation at 300 rpm and combined ultrasound/mechanical agitation at 0.180 W/cm^3 – 300 rpm. Moisture (water) stains can also be seen near upper edges of the samples. Electrodeposition time: 14 minutes. Current density: 4 A/dm^2.

The cross-section of the Ni/hBN composite coatings produced is displayed in Figure 5.15. Coatings plated under mechanical agitation presented large agglomerates with a less homogeneous distribution of the hBN particles, whereas finer particles were clearly noticed in the deposits electrodeposited under ultrasonic and combined conditions. Nevertheless, coatings plated under ultrasound on its own presented far more particles than the ones plated under combined ultrasound/mechanical agitation. Again, it seemed that the stirring of the Ni bath with the overhead stirrer counteracted the effect of ultrasound in terms of particle incorporation, as in the case of the Ni/WS_2 composite coatings previously reported. In this case though, although the 'removal' of particles from the cathode-electrolyte interface due to the fluid flow developed near the surface of the Cu substrate by the

overhead stirrer would also occur, deposition and blocking of the cathode surface due to the agglomeration of the hBN particles did not take place as in the case of the Ni/WS_2 composite coatings, and all the Ni/hBN composite coatings presented the same thickness with no dependence on the agitation conditions used during the electrodeposition. This would be mainly due to the different physical-chemical properties of the surface of the particles such as the electrokinetic potential and charge of the particles. These differences were already pointed out in Section 5.2, as hBN particles took much shorter times to agglomerate and sink than the WS_2 particles. The difference in charge is suggested by the fact that the WS_2 particles were strongly attracted to the cathode to an extent where they completely block the surface of the Cu substrate in absence of ultrasound, whereas the particle content in the Ni/hBN composite coatings seemed much lower.

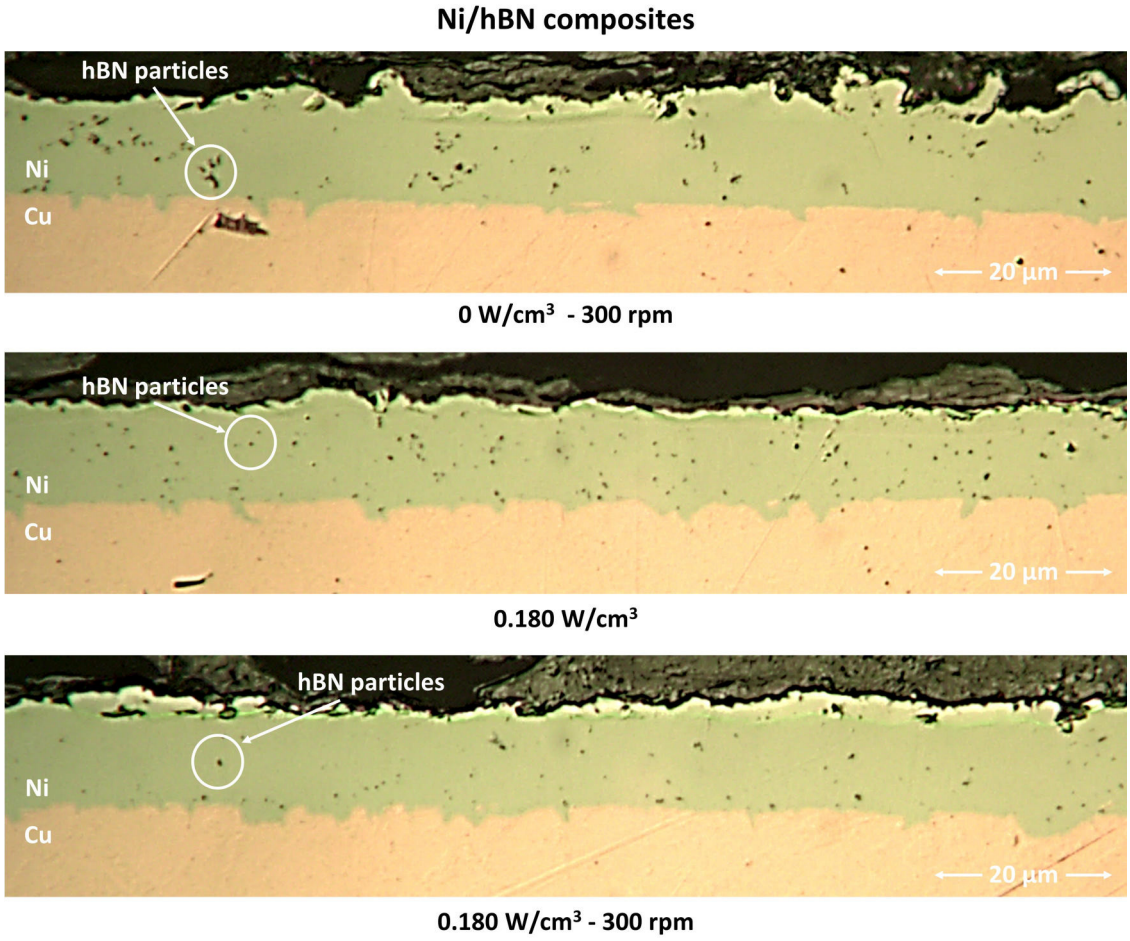

Figure 5.15. Examples of cross-section images of Ni/hBN composite coatings plated on Cu substrates under different plating conditions: ultrasound at 0.180 W/cm³, mechanical agitation at 300 rpm and combined

ultrasound/mechanical agitation at 0.180 W/cm³ – 300 rpm. Coatings shown here were electrodeposited for longer times (24 minutes) in order to achieve thicker coatings for easier observation of the particles. Current density: 4 A/dm².

The cross-sections of the Ni/hBN deposits were further analysed by SEM BSE analysis (Figure 5.16), showing that the distribution of the hBN particles (dark spots in the images) followed the same trends previously observed in the cross-section images obtained with the optical microscope: large agglomerated particles under mechanical agitation and finer particles under combined ultrasound/mechanical agitation and ultrasound on its own, the latter being the best condition to produce Ni coatings with a more uniform distribution of finely dispersed hBN particles.

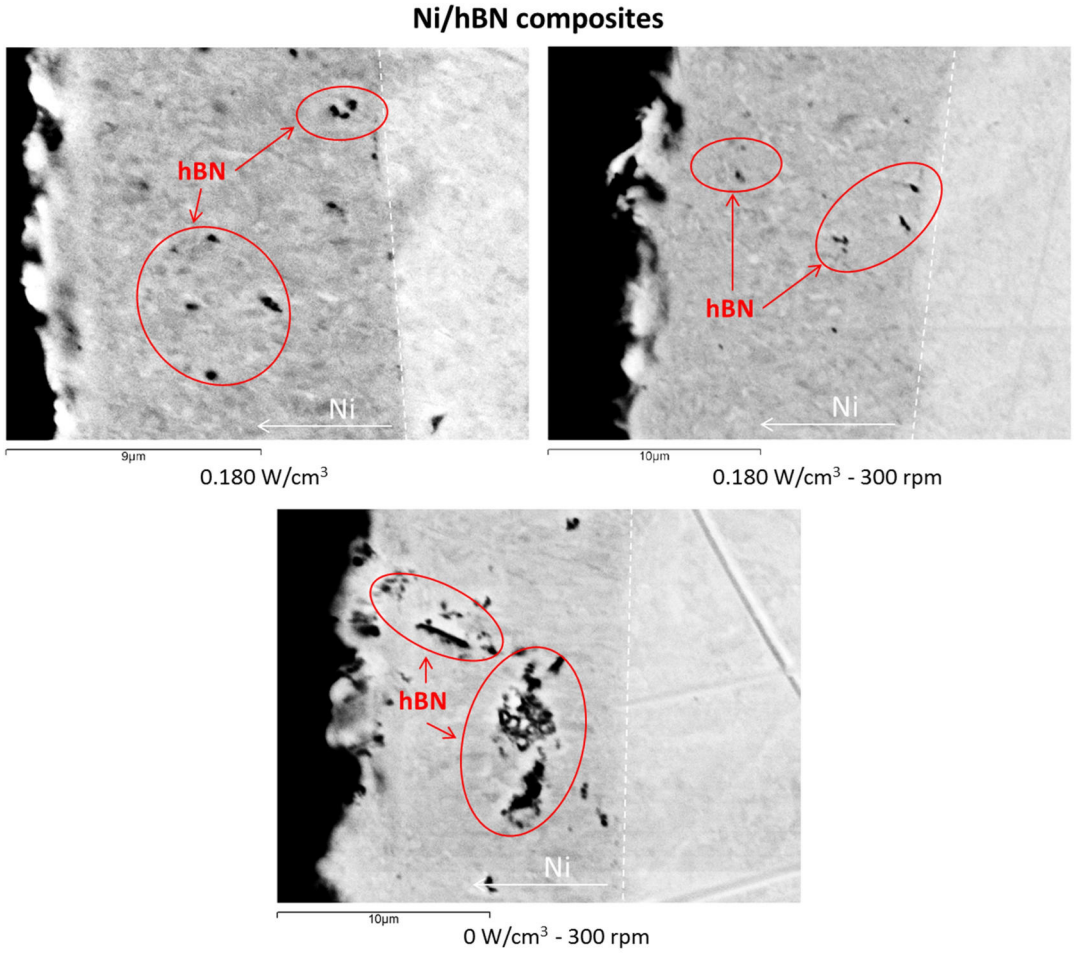

Figure 5.16. SEM BSE analysis of the cross-section of Ni/hBN composite coatings plated on Cu substrates under different plating conditions: ultrasound at 0.180 W/cm³, mechanical agitation at 300 rpm and combined ultrasound/mechanical agitation at 0.180 W/cm³ – 300 rpm. Coatings shown here were electrodeposited for

longer times (24 minutes) in order to achieve thicker coatings for easier observation of the particles. Current density: 4 A/dm^2.

In summary, Ni/hBN coatings presented a more uniform surface finish than Ni/WS_2 coatings and this was not affected by the agitation/dispersion conditions used. The main reason for this was the relatively low incorporation of hBN particles in all cases. Regarding the dispersion of the hBN particles, aggregated hBN particles with a poor distribution were incorporated under mechanical agitation in the absence of ultrasound, while finely divided particles were clearly seen in the coatings produced under ultrasound. Related to this, the presence of hBN particles was far more evident when ultrasound was used on its own than when it was combined with mechanical agitation, as previously observed for the Ni/WS_2 composite coatings. In addition, a more uniform distribution of the hBN in the Ni matrix was achieved with ultrasound alone. Therefore, Ni/hBN composite coatings electroplated under ultrasound were also selected as a potential option to replace current Ni diffusion layers in bronze-based bearings.

5.3.3. Ni/MoS_2 COMPOSITE COATINGS

Ni/MoS_2 composite coatings were (Figure 5.17) also electrodeposited from a Watts bath containing 15 g/L of particles under the three different conditions employed for the previous particles. Poor quality coatings with large black areas were obtained under ultrasound and combined ultrasound/mechanical agitation, while a thick layer of a compacted sludgy deposit completely covered the surface of the substrate when plating was conducted under mechanical agitation. This layer of sludge was quite hard to remove, even after drying the coating.

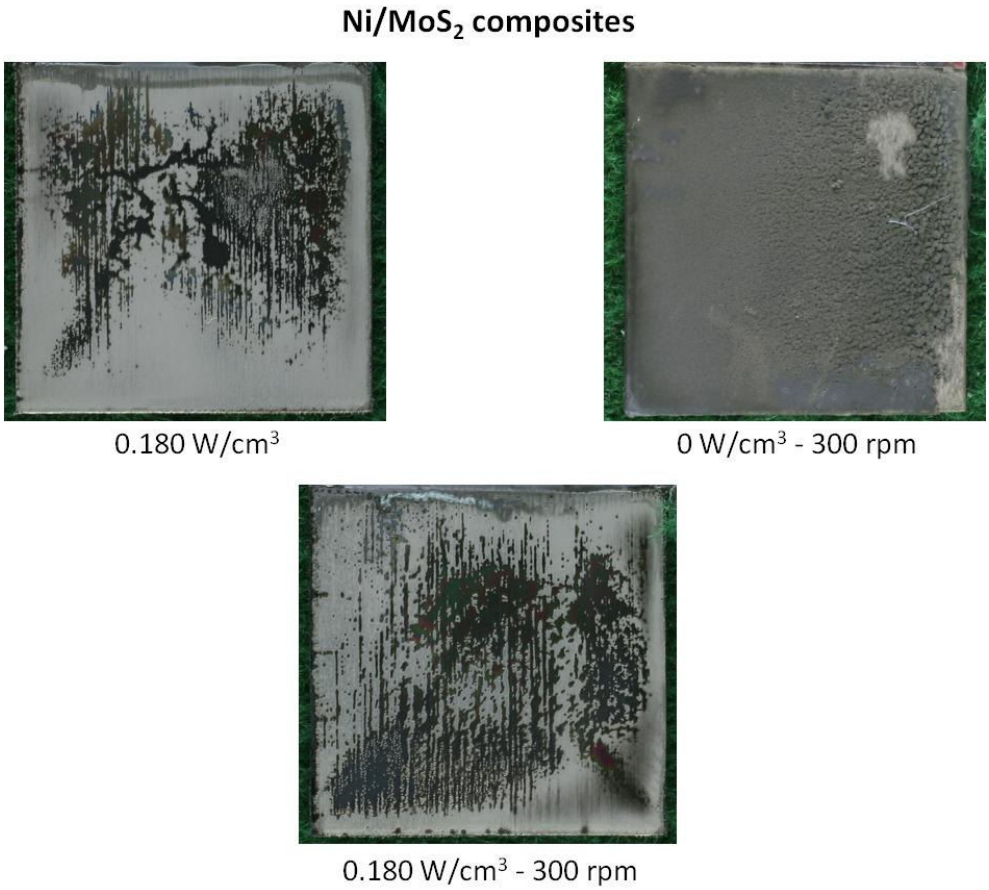

Figure 5.17. Examples of Ni/MoS_2 composite coatings electrodeposited on Cu substrates under different conditions: ultrasound at 0.180 W/cm^3, mechanical agitation at 300 rpm and combined ultrasound/mechanical agitation at 0.180 W/cm^3 – 300 rpm. Moisture (water) stains can also be seen near upper edges of some of the samples. Electrodeposition time: 14 minutes. Current density: 4 A/dm^2.

Figure 5.18 displays the cross-section of Ni/MoS_2 composite coatings plated under ultrasound and combined ultrasound/mechanical agitation. As in the case of the Ni/WS_2 composite coatings produced under mechanical agitation, cross-sections of the Ni/MoS_2 composite coatings electrodeposited under the same conditions were not evaluated because the deposits would partially come off during cutting and mounting, generating a lot of debris while polishing the samples, and therefor making it difficult to obtain a clear picture with the optical microscope. The deposits plated under ultrasound presented poor adhesion and were quite fragmented, as large particles would get between the substrate and the coating, breaking the coating in certain places. Coatings plated under combined conditions had an

even lower quality, as some spots with sludgy deposits were observed, along with some plated areas.

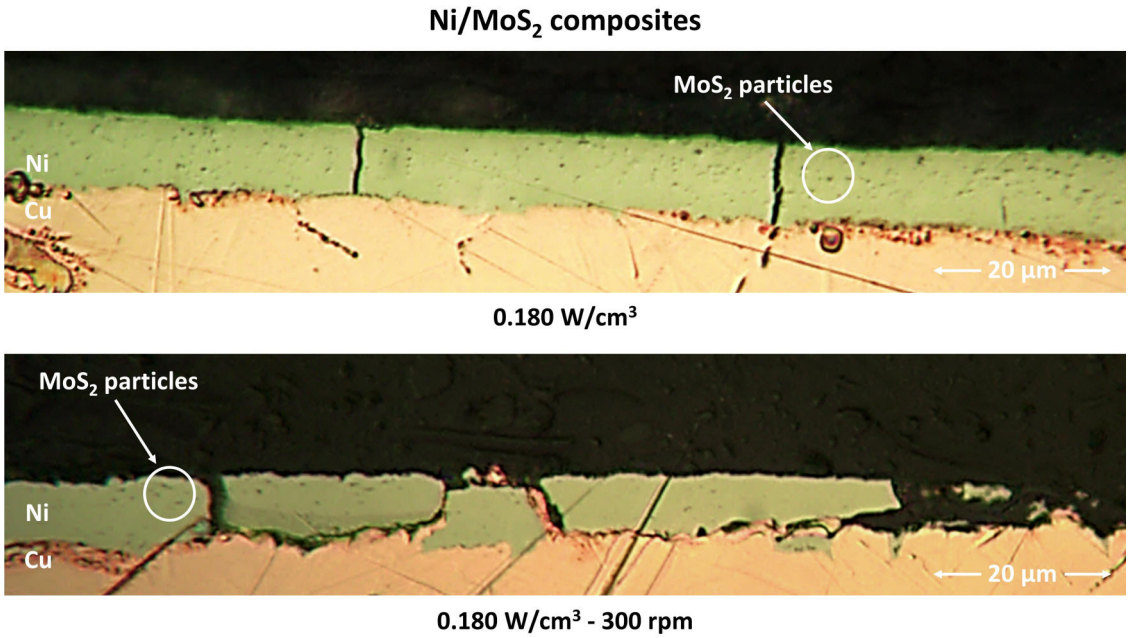

Figure 5.18. Examples of cross-section images of Ni/MoS_2 composite coatings electrodeposited on Cu substrates under different plating conditions ultrasound at 0.180 W/cm^3 and combined ultrasound/mechanical agitation at 0.180 W/cm^3 – 300 rpm. Coatings shown here were electrodeposited for longer times (24 minutes) in order to achieve thicker coatings for easier observation of the particles. Current density: 4 A/dm^2.

In both ultrasound and combined ultrasound/mechanical agitation conditions, only the smallest particles were incorporated in those areas where a Ni/MoS_2 composite coating was successfully deposited. However, as no composite coatings with a good quality were obtained under any of the different plating conditions used (mechanical agitation, ultrasound, and combined mechanical agitation/ultrasound), it was decided that the commercial MoS_2 particles used would not be considered for further experimental work.

5.4. Characterization of Ni/WS_2 and Ni/hBN composite coatings electrodeposited under ultrasound

Out of the nine composite coatings described in section 5.3, only the Ni/WS_2 and Ni/hBN composite coatings (around 6 µm thick) electrodeposited under ultrasound at 0.180 W/cm^3

were selected for further characterization due to the promising features that these two composite materials presented in terms of thickness uniformity, homogeneous particle distribution and reasonable particle incorporation. In this case, the two selected composite materials were characterised with different techniques: Glow Discharge – Optical Emission Spectroscopy (GD-OES) to estimate the particle content, X-Ray Diffraction (XRD) to evaluate the effect that the incorporation of particles into the Ni coatings had on the crystal orientation of the deposit, Focused Ion Beam – Scanning Electron Microscopy (FIB-SEM) to analyse the surface morphology and crystal structure of the composite coatings, and microhardness tests to evaluate the hardness of the deposits.

5.4.1. PARTICLE CONTENT

Figure 5.19 displays data from GD-OES analysis performed on Ni/WS_2 and Ni/hBN composite coatings electrodeposited under ultrasound as a depth profile of the concentration of the different elements present in the sample expressed in percentage by weight. The graphs show that the Ni/WS_2 composite coatings apparently presented higher particle content in terms of weight percentage, up to 1 order of magnitude in some areas, than the Ni/hBN composite coatings electrodeposited on Cu under the same conditions (15 g/L of particles in the bath, ultrasound at 0.180 W/cm^3, etc.). In terms of the distribution of particles within the coating, the Ni/WS_2 composites presented three different areas: i) a superficial layer with a high WS_2 particle content near the surface, ii) the bulk coating with a lower yet constant concentration of WS_2 particles, and iii) a region near the coating-substrate interface where the particle content doubles that of the bulk coating. The GD-OES depth profiles obtained for the Ni/hBN composites point to a slightly different trend: i) a superficial layer with high hBN particle content and ii) a lower concentration of particles which progressively increases towards the coating-substrate interface, where it reaches the highest particle content. The higher particle content observed in the superficial layer in both composites can be attributed to the adherence of some of the particles in the electrolyte to

the surface of the coating once the electrodeposition process is completed, a phenomenon widely observed in other electrodeposited composite coatings studies with GD-OES analysis [10,11].

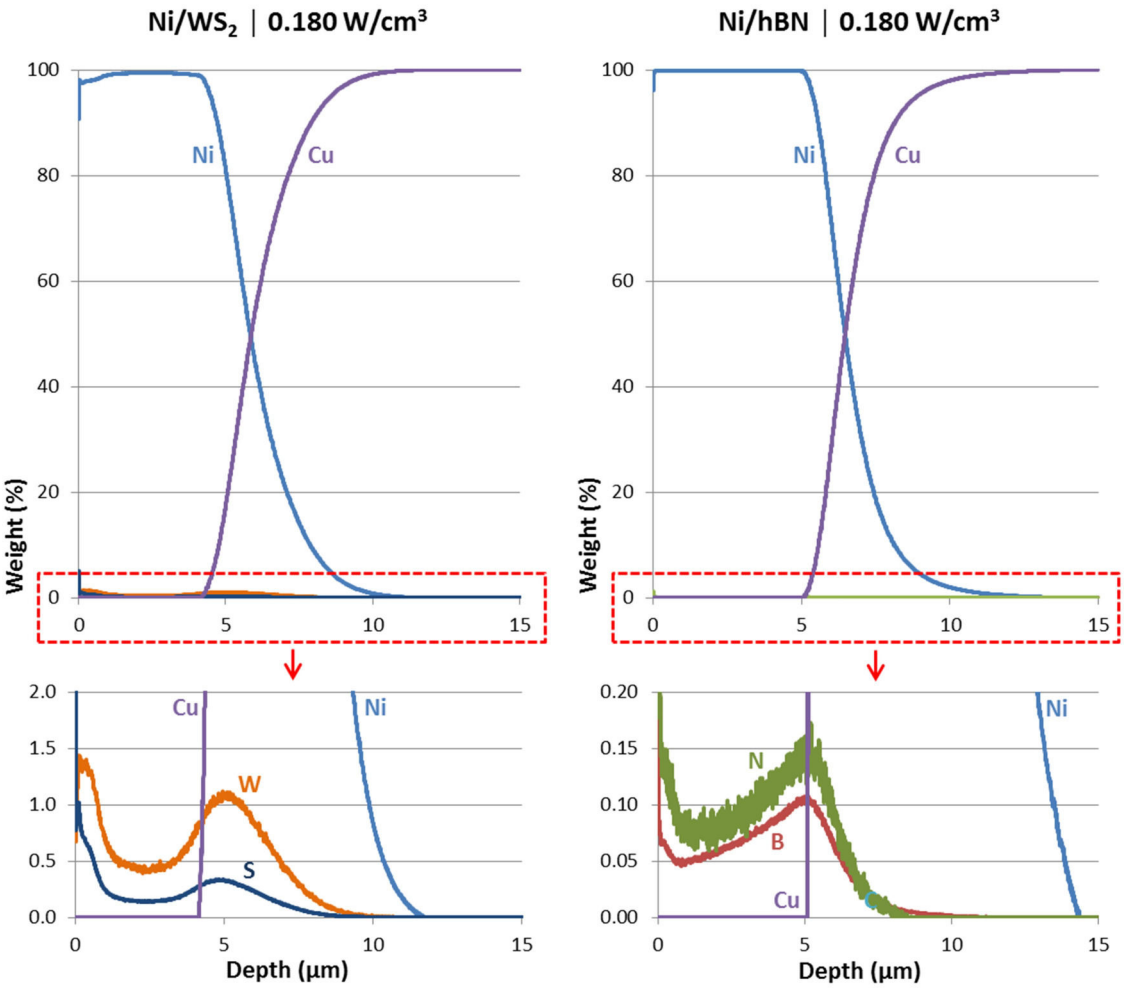

Figure 5.19. GD-OES depth profiles of the presence of different atoms (Ni, Cu, W, S, B, and N) in a Ni/WS_2 composite coating (left) and a Ni/hBN composite coating (right) electrodeposited under ultrasound at 0.180 W/cm^3. Electrodeposition time: 14 minutes. Current density: 4 A/dm^2. The detection of Ni far beyond the actual thickness of the coatings is due to the characteristic interface broadening generally observed in GD-OES depth profile measurements

The differences observed between the Ni/WS_2 and Ni/hBN composite coatings in terms of particle content in weight percentage and distribution within the coating would be related to the hypothetically higher values of electrokinetic potential and higher charge of the WS_2 particles, as already suggested by the dispersion and electrodeposition experiments previously commented. WS_2 particles would be more attracted to the surface of the cathode

than the hBN particles under the same electrodeposition conditions, resulting in a higher incorporation of particles into the coating immediately after the electrodeposition starts, followed by a constant ´replenishment´ of WS_2 from the bulk solution to the cathode-electrolyte interface, and hence a constant content of WS_2 particles in the bulk coating. Such conditions would not be completely achieved in the case of the hBN particles, as these particles would not be as 'attracted' to the cathode surface as the WS_2 particles, and hence the progressive decrease of particle content from the coating-substrate interface towards the bulk coating (if the attraction/incorporation of particles was treated as a 'traditional' electrochemical reaction, the incorporation of WS_2 particles would be considered as a kinetic/mixed-controlled process, whereas the incorporation of hBN particles would be considered as a mass transport-controlled process). It must be noted though the difference in density of the different particles, which is 7500 kg/m^3 for the WS_2 particles and 2300 kg/m^3 for the hBN particles according to the supplier (M K Impex Corp). This actually implies that, when one takes into account the difference of density of the different particles, the difference in terms of particle content between the Ni/WS_2 and the Ni/hBN composite coatings is not as high as it seems when only considering the particle content in weight percentage.

From these GD-OES results, the estimated average particle content in the Ni/WS_2 and Ni/hBN composite coatings was around 1.0 % by weight of WS_2 particles and 0.2 % by weight of hBN particles, respectively. There are not many other studies available in the literature which can be compared to the particle content results included in the present study. Regarding Ni/hBN composite coatings, no particle content measurements were included in previous studies by Pompei et al. [12] which focused on similar coatings electrodeposited from a sulphamate bath. Regarding Ni/WS_2 composite coatings, relatively high particle content (4.5-6.5 % by weight) was measured by García-Lecina et al. [9] on their Ni/IF-WS_2 composite coatings electrodeposited under ultrasound. Nevertheless, IF-WS_2 particle content was measured in their case with an energy-dispersive X-ray spectroscopy

(EDS) detector coupled with a Scanning Electron Microscopy (SEM) system. EDS analysis, even if it is performed on the cross-section of the coatings, may not be a technique as precise as GD-OES when measuring the particle content in composite coatings. This would be of particular importance when the particles are as small as the IF-WS_2 particles and aggregates that García-Lecina et al. incorporated into their Ni coatings [9], which were not larger than 600 nm. Related to this issue, the same Ni/WS_2 composite coatings here presented which exhibited a particle content around 1.0 % by weight when measured by GD-OES routinely showed a particle content around 10 % by weight, one order of magnitude higher, when measured by EDS (WS_2 particle content of 12 % was measured on the cross-section shown in Figure 5.13). This apparent lack of precision of EDS analysis for the evaluation of particle content in a composite coating when compared with GD-OES methods would be related to the nature of the technique: where EDS relies on the interaction of the X-ray emission of the sample being bombarded with an electron beam during SEM analysis, GD-OES is based on the direct analysis of the composition of the coating by analysing the intensity of the light emitted by the plasma discharge as the coating is being sputtered from the surface of the substrate.

5.4.2. CRYSTAL ORIENTATION

Figure 5.20 displays the 2θ scans conducted for both composite coatings. While the Ni/hBN presented high peaks for (111) and (200) crystal planes in a similar way to those previously observed for the pure Ni deposits electrodeposited under different conditions included in Section 4.4.1, the Ni/WS_2 deposits showed a significant decrease in the intensity of the (200) planes when compared to height of the peak observed for the (111) planes. In addition, a relative increase was observed for the (220), (311) and (222) crystal planes when compared with the intensity of the (111) planes for the Ni/WS_2 composites coatings. The 2θ scans also showed the presence of the WS_2 particles embedded in the Ni matrix, as (006)

and (008) crystal planes associated to the presence of WS_2 were quite noticeable (Figure 5.21).

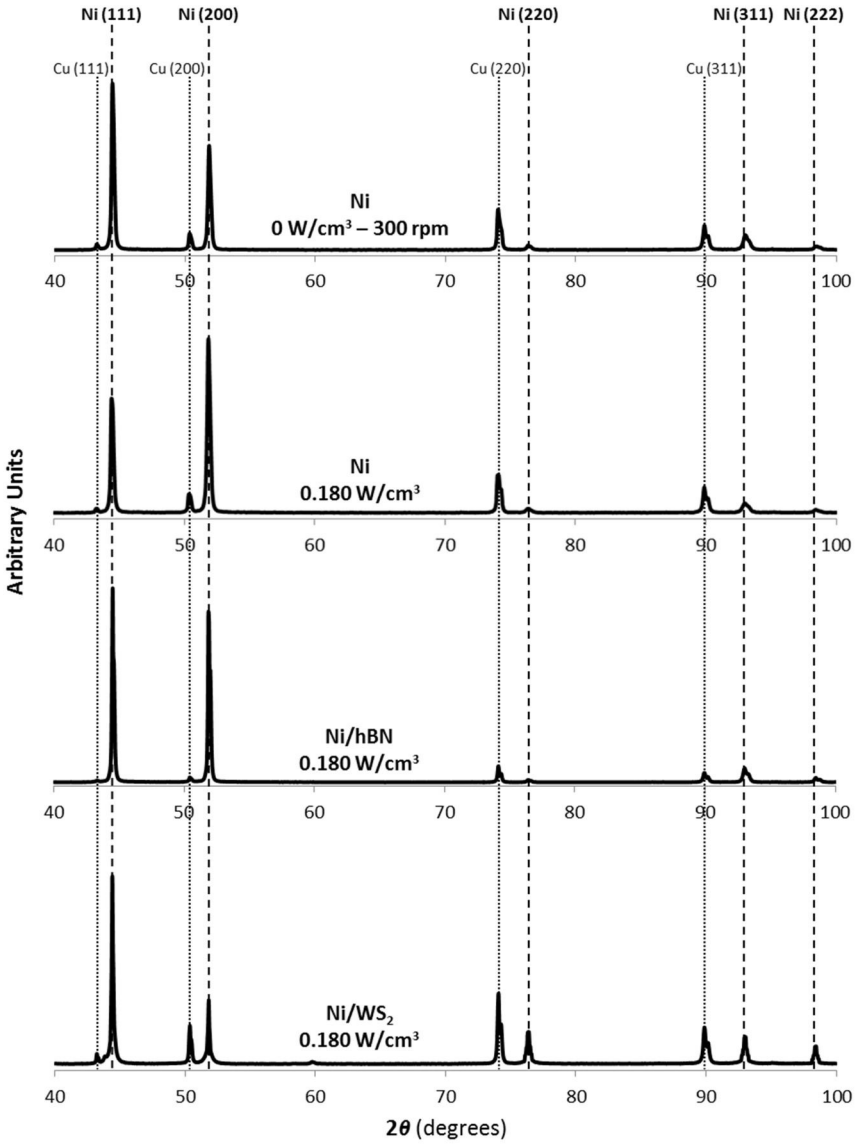

Figure 5.20. XRD spectra of Ni/hBN and Ni/WS_2 composite coatings electrodeposited under ultrasound at 0.180 W/cm³ on Cu substrates. XRD spectra for pure Ni coatings electrodeposited under either mechanical agitation at 300 rpm or ultrasound at 0.180 W/cm³ are included for comparison purposes. Electrodeposition time: 14 minutes. Current density: 4 A/dm².

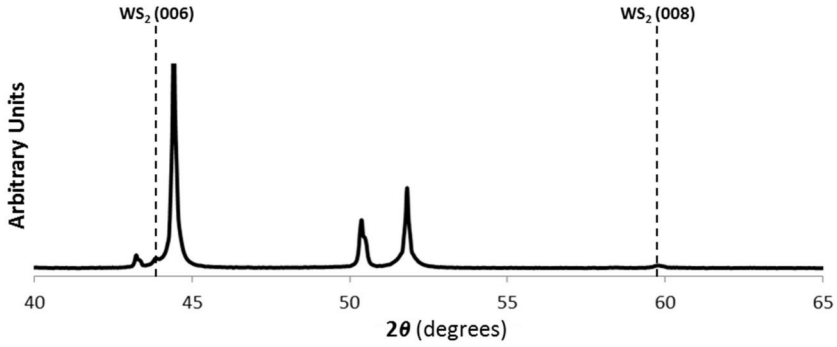

Figure 5.21. Zoomed XRD spectra of a Ni/WS_2 composite coating electrodeposited under ultrasound at 0.180 W/cm^3 on Cu substrates. Scan rate = 0.1 degree/s. (006) and (008) crystal planes associated to the presence of WS_2 are highlighted. Electrodeposition time: 14 minutes. Current density: 4 A/dm^2.

$RTC_{(hkl)}$ coefficients were again estimated for the Ni/hBN and Ni/WS_2 composites electrodeposited under ultrasound at 0.180 W/cm^3 (Figure 5.22) according to the RTC method developed by Bérubé and L'Espérance [13] (detailed explanation of the RTC method has already been included in Section 4.2.2). For the Ni/hBN composite, a small decrease in $RTC_{(200)}$ and $RTC_{(222)}$ was noticed compared to those of Ni deposits produced under ultrasound at the same ultrasonic power, along with a more significant increase in $RTC_{(111)}$ (almost a 100% increase compared to that of the Ni deposit). However, $RTC_{(hkl)}$ coefficients were completely different for the Ni/WS_2 composites, where $RTC_{(222)}$ > 40% while the other $RTC_{(hkl)}$ coefficients would remain below 20%, with $RTC_{(200)}$ presenting the lowest value, as opposed to what was observed for the Ni/hBN composite and all the Ni deposits included in Section 4.4.1 where $RTC_{(200)}$ coefficients always presented the highest values. The very high value of $RTC_{(222)}$ and very low value of $RTC_{(200)}$ are caused, as previously explained in Section 4.2.2, by the own nature of the RTC method, and is a consequence of the high intensities observed for (111) and (200) crystal planes and the very low intensities measured for (220), (311) and (222) crystal planes in a standard Ni powder sample with random orientation [14].

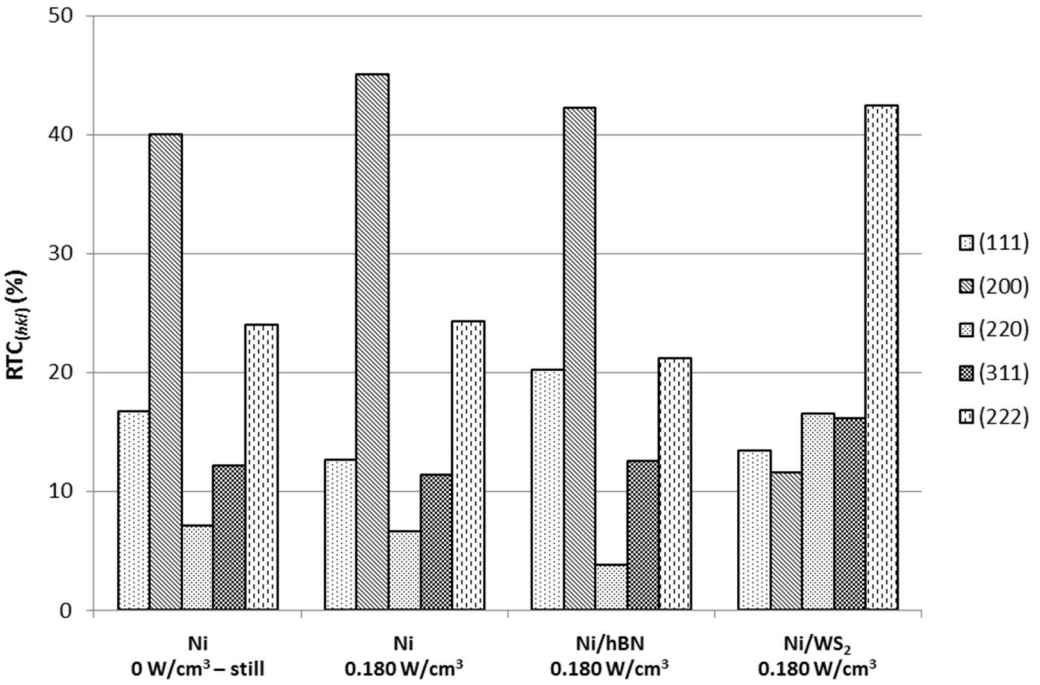

Figure 5.22. $RTC_{(hkl)}$ coefficients estimated for (111), (200), (311) and (222) Ni crystal planes observed in Ni/hBN and Ni/WS_2 coatings electrodeposited on Cu under ultrasound at 0.180 W/cm^3. $RTC_{(hkl)}$ coefficients corresponding to pure Ni coatings electrodeposited under either mechanical agitation at 300 rpm or ultrasound at 0.180 W/cm^3 are included for comparison purposes. Electrodeposition time: 14 minutes. Current density: 4 A/dm^2.

$RTC_{[hkl]}$ were again estimated for the Ni/hBN and Ni/WS_2 composites (Figure 5.23) as shown in Section 4.2.2 As expected from the $RTC_{(hkl)}$ coefficients previously included in Figure 5.23, a small decrease in $RTC_{[100]}$ and small increase in $RTC_{[211]}$ was observed for the Ni/hBN composite compared with the $RTC_{[hkl]}$ coefficients observed for the Ni deposits produced under ultrasound at 0.180 W/cm^3. The increase in $RTC_{[211]}$ and decrease in $RTC_{[100]}$ were far more remarkable for the Ni/WS_2 composite, which clearly showed a strong [211] preferred orientation ($RTC_{[211]}$ > 70%). A significant increase in the presence of crystals with a [110] orientation was also noticed for this composite ($RTC_{[110]}$ > 15%).

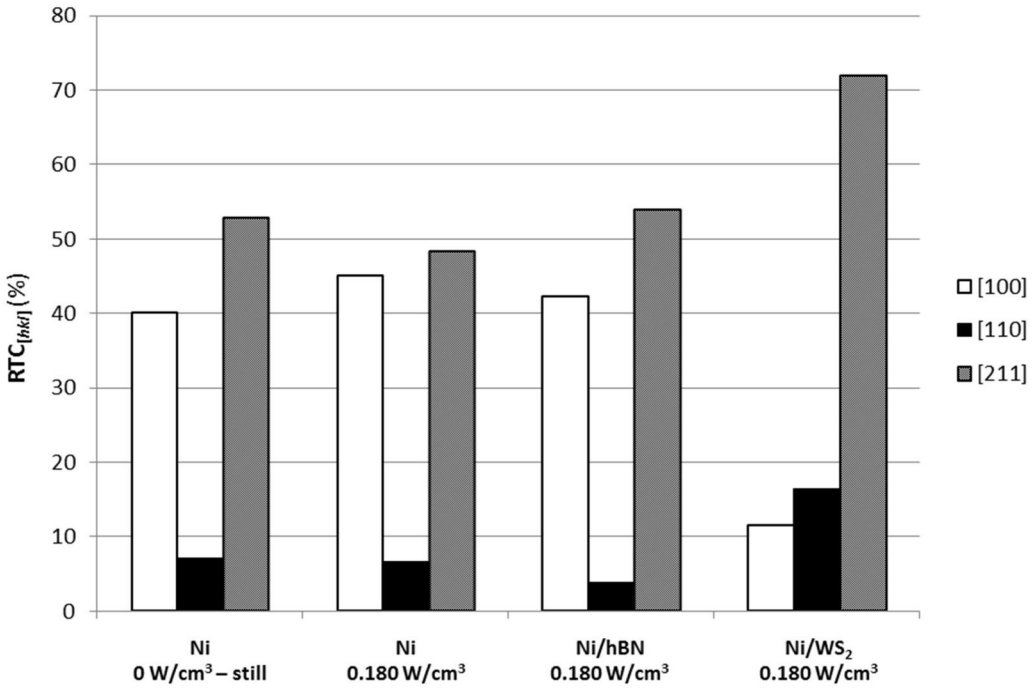

Figure 5.23. $RTC_{[hkl]}$ coefficients estimated for [100], [110], and [211] Ni crystal planes observed in Ni/hBN and Ni/WS_2 coatings electrodeposited on Cu under ultrasound at 0.180 W/cm^3. $RTC_{(hkl)}$ coefficients corresponding to pure Ni coatings electrodeposited under either mechanical agitation at 300 rpm or ultrasound at 0.180 W/cm^3 are included for comparison purposes. Electrodeposition time: 14 minutes. Current density: 4 A/dm^2.

As previously reported in Section 4.2.2, an increase in $RTC_{[100]}$ and decrease in $RTC_{[211]}$ coefficients was observed for electrodeposited Ni coatings under ultrasound at high powers compared to Ni deposits produced under mechanical agitation and silent/still conditions, suggesting that less inhibiting species were present in the cathode-electrolyte interface according to the so-called 'inhibition effect' [15-18] previously explained in Section 4.2.2. However, this situation changed when either hBN or WS_2 particles were added to the Ni Watts bath and composite coatings were produced under the same ultrasonic conditions, especially in the case of the Ni/WS_2 coatings, for which $RTC_{[211]} \approx 7 \times RTC_{[100]}$. The results observed for the Ni/hBN and Ni/WS_2 composite coatings agree with previous observations made by Pompei et al. [12] and García-Lecina et al. [9], respectively, as in both previous studies the incorporation of either hBN or IF-WS_2 particles resulted in an increase in the relative intensity of XRD peaks for (111), (311) and (222) crystal planes associated to a [211] growth direction compared to the peak for the (200) crystal plane related to the [100]

orientation. Again, such higher presence of Ni crystals growing in the [211] direction indicates an increase in precipitated and/or colloidal $Ni(OH)_2$ in the cathode-electrolyte interface due to the alkalization of the interface by either an increase in the hydrogen evolution on the surface of the cathode or the adsorption of atomic hydrogen [17]. As hydrogen evolution on the surface of the cathode was not noticed when preparing both Ni/hBN and Ni/WS_2 composite coatings under ultrasound, the most probable cause for the increase of the proportion of [211] textures in both coatings was the adsorption of atomic hydrogen.

Considering that the Ni/WS_2 composite coatings apparently presented a higher particle content in terms of weight percentage, and that these coatings also presented a more remarkable change in the crystal orientation than the Ni/hBN composite coatings, the results not only suggest that the WS_2 particles have a greater effect than the hBN particles on the orientation of the crystals due to either higher incorporation or different physical and chemical properties of the particles, but also that the atomic hydrogen was adsorbed on the surface of the particles rather than on the surface of the cathode. In this sense, Pavlatou and Spyrellis [19] have suggested that the presence of particles may have an effect on the orientation of the crystals by affecting the electrolyte composition by adsorption of atomic hydrogen. The adsorption results in a local alkalization of the cathode-electrolyte interface, leading to the crystallization of Ni crystals with a [211] preferred orientation. A similar increase in the proportion of crystals with a [211] preferred orientation has also been observed by other authors for different particles dispersed in a Ni Watts bath. McNormack et al. [20] noticed that, the higher the concentration of Y_2O_3, the more remarkable was the change of growth mode from [100] to [211] of the Ni coatings they were producing. Similar results have been previously obtained by other authors for Ni/SiC [21-23] and Ni/Al_2O_3 [24] composite coatings from different electrolytes. It must be noted though that the adsorption of other inhibiting species may also occur. Spanou et al. [25] reported that further addition of TiO_2 particles into a Ni Watts bath would lead to an increase of the proportion of Ni

crystals growing in the [100] direction, suggesting that the formation of precipitated/colloidal $Ni(OH)_2$ on the surface of the cathode was reduced due the presence of the particles in the cathode-electrolyte interface. They attributed the modification of the textural modifications to the adsorption of the inhibiting species on the surface of the TiO_2 particles. This adsorption activity of the particles may also be affected by other operational parameters such as the current density [26].

5.4.3. SURFACE MORPHOLOGY AND MICROSTRUCTURE

Tilted FIB-SEM images of Ni/WS_2 and Ni/hBN composite coatings electrodeposited under ultrasound at 0.180 W/cm^3 are shown in Figures 5.25 and 5.26, respectively (Figure 5.24 shows a Ni deposit, also electrodeposited under ultrasound at the same power, for comparison purposes). Nodule-shaped structures similar to those previously observed in the Ni deposits included in Section 4.2.3 were noticed in some areas of the surface of the Ni/hBN composite coatings. However, a completely different surface morphology with no signs of either nodular structures or grooves was observed for the Ni/WS_2 coatings.

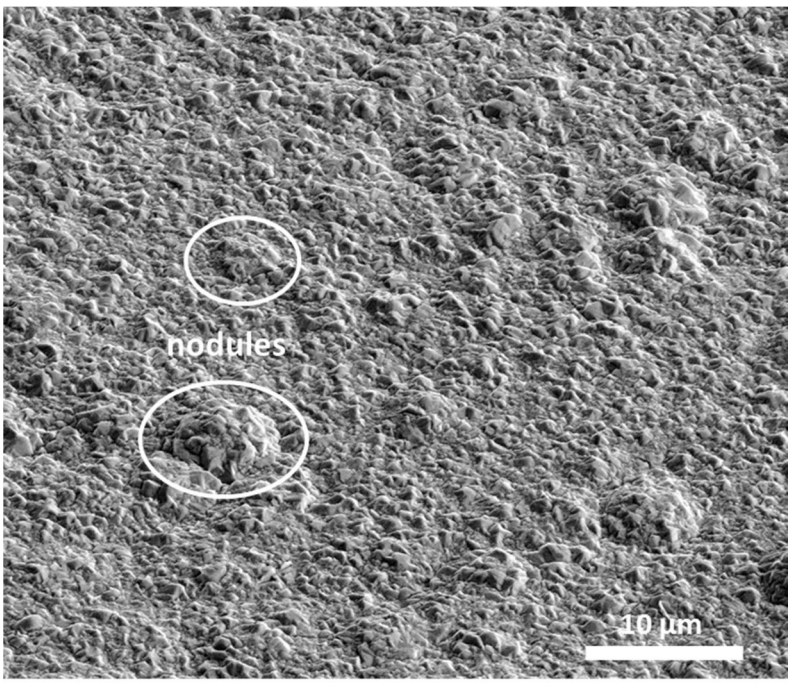

Figure 5.24. Tilted FIB-SEM image of the surface of a Ni coating electrodeposited under ultrasound at 0.180 W/cm^3. Electrodeposition time: 14 minutes. Current density: 4 A/dm^2.

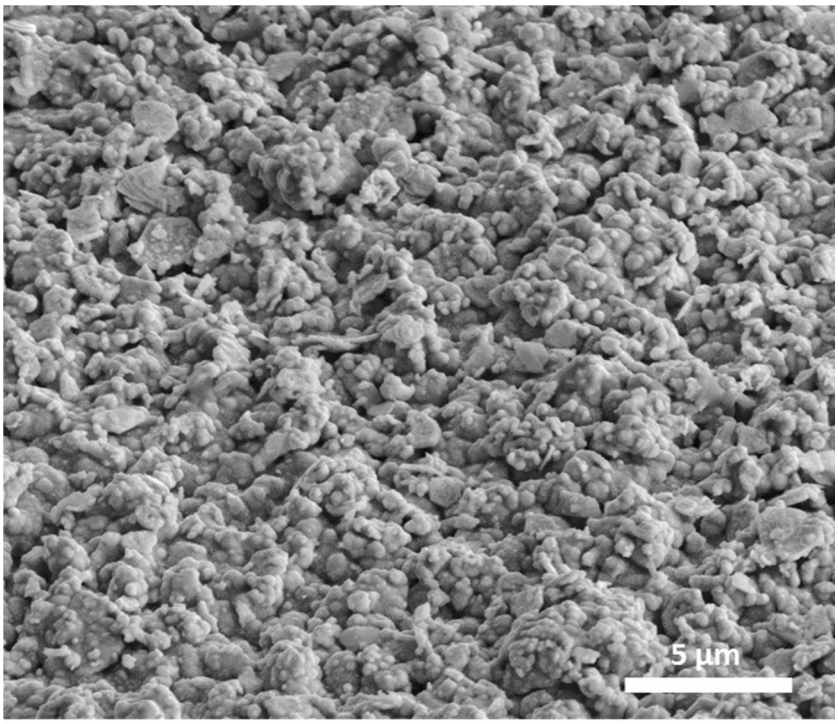

Figure 5.25. Tilted FIB-SEM image of the surface of a Ni/WS_2 composite coating electrodeposited under ultrasound at 0.180 W/cm^3. Electrodeposition time: 14 minutes. Current density: 4 A/dm^2.

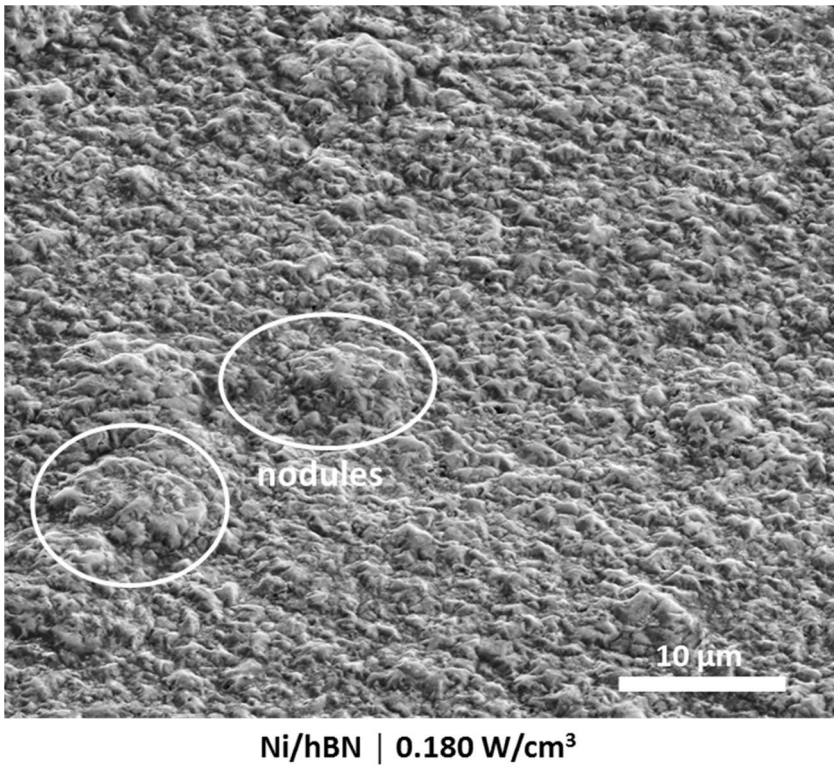

Figure 5.26. Tilted FIB-SEM image of the surface of a Ni/hBN composite coating electrodeposited under ultrasound at 0.180 W/cm^3. Electrodeposition time: 14 minutes. Current density: 4 A/dm^2.

High-magnification FIB-SEM images of Ni/WS_2 and Ni/hBN composite coatings are also displayed in Figures 5.28 and 5.29, respectively, while Figure 5.27 shows a Ni deposit electrodeposited under ultrasound for comparison purposes. As previously pointed out, the surface structure of the Ni/WS_2 composite coatings differed significantly from the surface morphology observed for pure Ni deposits plated under different conditions included in Section 4.2.3. No structures similar to that of crystals with [100], [110] or [211] orientations reported elsewhere [19,25,27,28] were noticed. Instead, a random distribution of spherical and irregular structures was observed, suggesting that WS_2 particles near the surface of the coating were covered by thin Ni layers as in the Ni/Mo composite coatings observed by Kubistzal et al. [29]. A similar structure was also noticed by Mohajeri et al. [30] for their Ni/WC coatings. In the latter, the authors suggested that the particles and the metal were deposited on the surface of the cathode, and Ni gradually grew on the particles to cover the gap between the grains. Nevertheless, despite the similarities of the morphology of both Ni/WS_2 and Ni/Mo composites, the sphere-like structures of the deposits containing WS_2 particles were about one order of magnitude smaller. In addition, Ni/WS_2 composite coatings were more compact, as the Ni/Mo deposits presented deep narrow pores and the Ni/WC coatings also had significant gaps and holes over the surface. Overall, the surface morphology of the Ni/WS_2 composite coatings was quite similar to that of the Ni/IF-WS_2 deposits produced by García-Lecina et al. [9]. For the Ni/hBN composite coatings deposited under ultrasound, although it was harder to associate the structure of the Ni crystals to the different orientations they may have compared to the crystals observed in the Ni deposits characterized in Section 4.2.3, some Ni grains presented morphologies similar to that of crystals with [100] orientation reported by other authors [19,25,27,28].

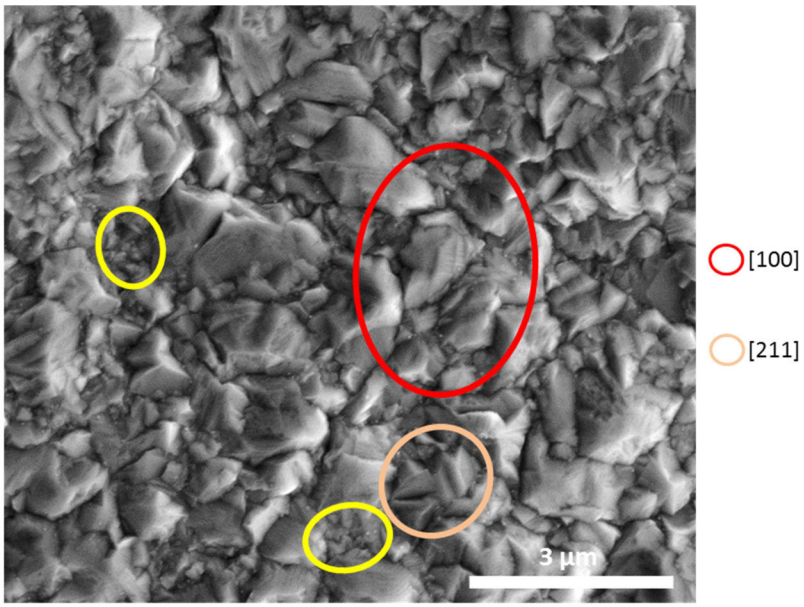

Figure 5.27. High magnification FIB-SEM image of the surface of a Ni coating electrodeposited under ultrasound at 0.180 W/cm^3. Electrodeposition time: 14 minutes. Current density: 4 A/dm^2. Some of the crystals with a surface morphology similar to that of Ni crystals with different orientations reported by other authors [19,25,27,28] are highlighted with different colours.

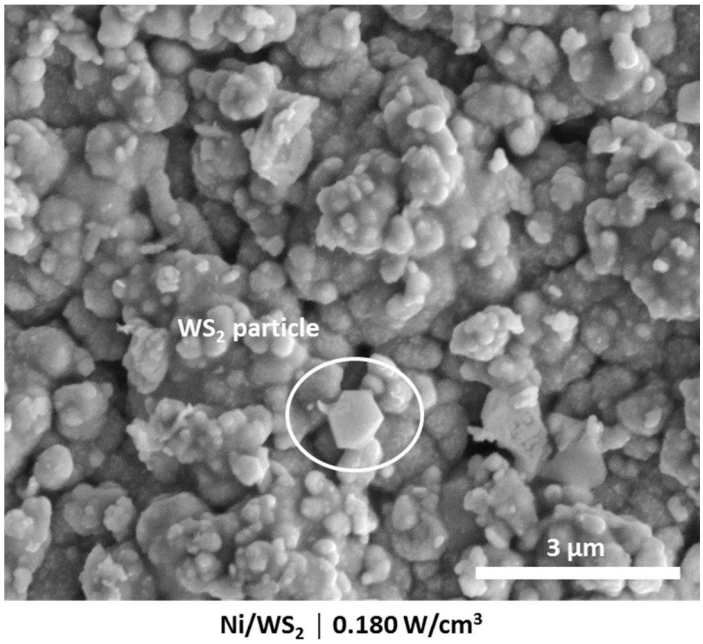

Figure 5.28. High magnification FIB-SEM image of the surface of a Ni/WS_2 composite coating electrodeposited under ultrasound at 0.180 W/cm^3. Electrodeposition time: 14 minutes. Current density: 4 A/dm^2.

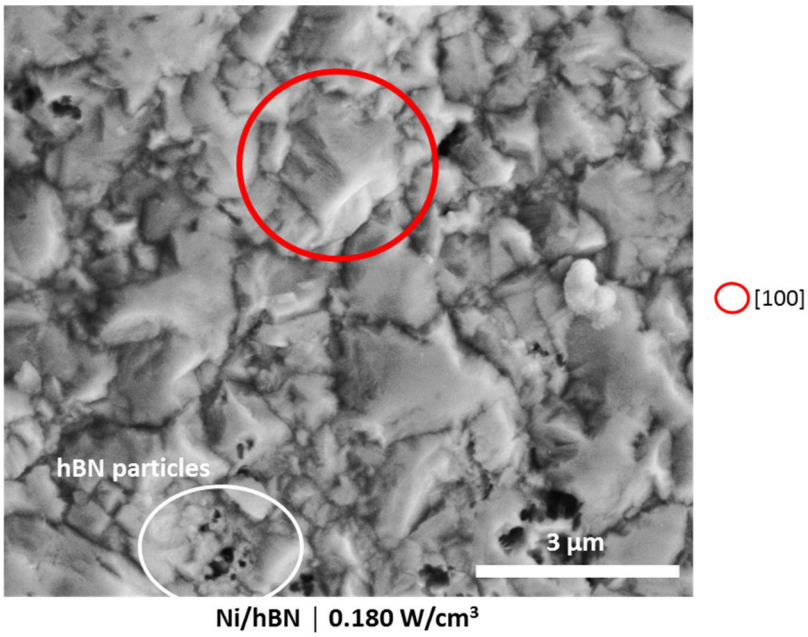

Figure 5.29. High magnification FIB-SEM image of the surface of a Ni/hBN composite coating electrodeposited under ultrasound at 0.180 W/cm^3. Electrodeposition time: 14 minutes. Current density: 4 A/dm^2. Some of the crystals with a surface morphology similar to that of Ni crystals with different orientations reported by other authors [19,25,27,28] are highlighted with different colours.

The cross-section of the Ni/WS_2 and Ni/hBN composite coating electrodeposited under ultrasound at 0.180 W/cm^3 was further analysed by FIB-SEM to observe the effect of the incorporation of the particles into the coatings (Figure 5.30). An apparently nano-crystalline structure of Ni with many WS_2 particles intercalated in the metal matrix was observed for the Ni/WS_2 composite coatings instead of the columnar structure observed in Ni deposits produced in absence of ultrasound and the fragmented structure of Ni deposits produced under ultrasound. hBN particles seemed to have little effect on the grain size and the microstructure of the deposit, as Ni columnar crystals were still visible in the Ni/hBN composite coatings. These composite coatings presented a similar structure to that observed in Ni deposits produced under ultrasound, although the structure of the composite coating seemed slightly less fragmented that that of the pure Ni deposit.

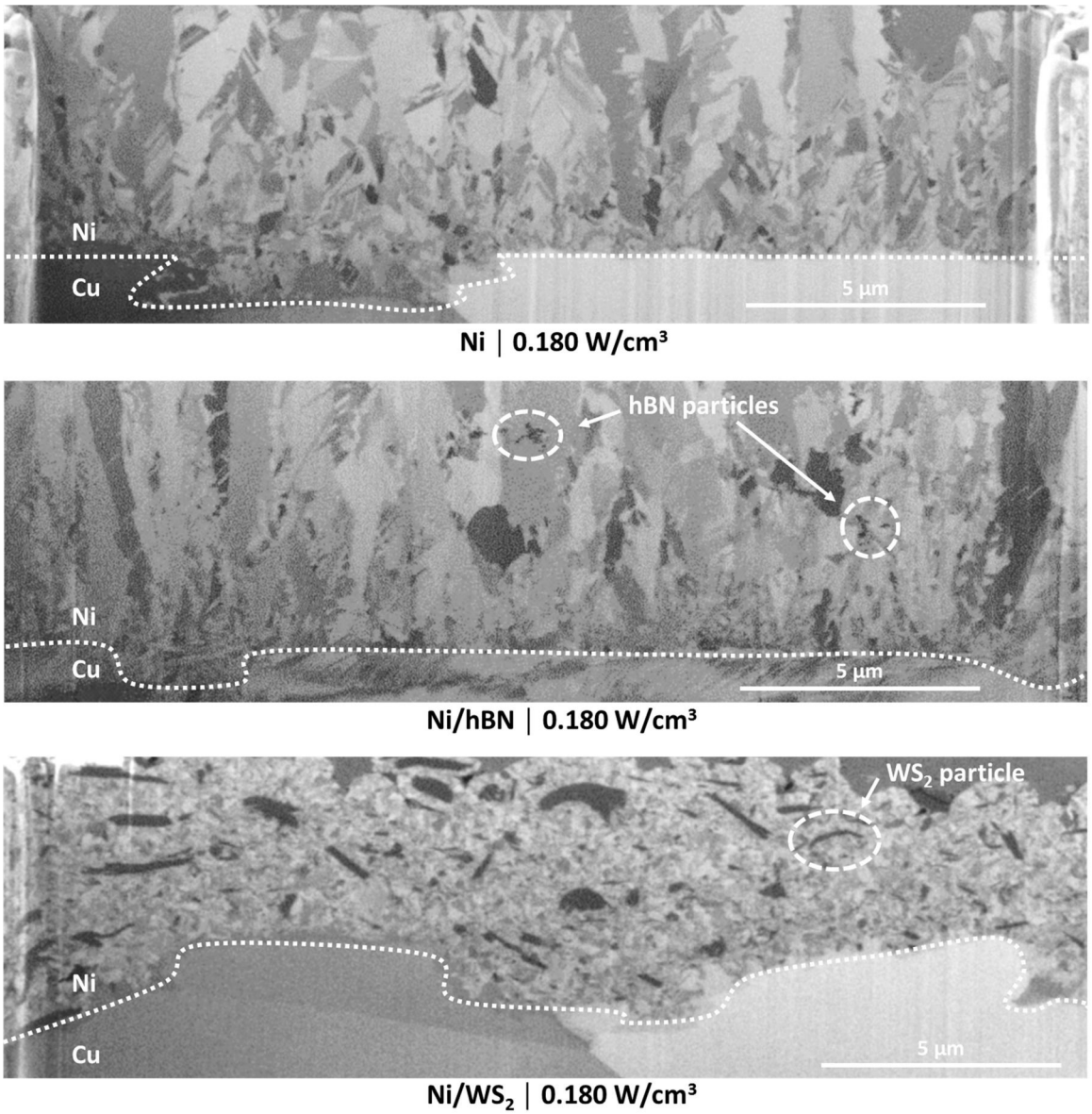

Figure 5.30. FIB-SEM images of the cross-section of Ni/hBN and Ni/WS_2 composite coatings electrodeposited under ultrasound at 0.180 W/cm³. Images of Ni coatings electrodeposited under ultrasound at 0.180 W/cm³ are included for comparison purposes. Electrodeposition time: 14 minutes. Current density: 4 A/dm².

The grain-refinement effect of particles once incorporated into electroplated coatings, which results in finer surface morphology and smoother finish, has been extensively reported in the past, not only when the electrodeposition is carried out in silent conditions [31,32], but also in the presence of ultrasound [22,33,34]. This effect was also pointed out by García-Lecina et al. [9] in their study focused on the electrodeposition of Ni/IF-WS_2 composite coatings under ultrasound. Nevertheless, not very clear evidence of this grain-refinement effect of particles is usually presented in the studies available in the literature, as in most

cases researchers rely on either SEM images of the surface or XRD data (e.g. Scherrer equation [35]) to demonstrate the refinement of the grain size. Lampke et al. [36] did show the effect that both ultrasound and the addition of TiO_2 nanoparticles to the plating solution had on the grain size and structure by EBSD analysis, although in their case the modification of the crystal structure was not as significant as the grain refinement achieved for the Ni/WS_2 composite coatings shown in Figure 5.30. The crystal structure displayed in said figure for the Ni/WS_2 composite coatings electrodeposited under ultrasound constitutes, to the best knowledge of the author, the most significant proof ever reported of the grain refinement effect achieved by the incorporation of particles into electrodeposited Ni coatings.

5.4.4. HARDNESS

Microhardness tests of the Ni/hBN and Ni/WS_2 composite coatings produced under ultrasound at 0.180 W/cm^3 were performed to evaluate the effects of the incorporation of the particles and the modification in the microstructure of the composite coatings. Compared to pure Ni deposits, the Ni/WS_2 composite coatings showed a higher hardness (360 HV). However, different results were obtained for the Ni/hBN composites, as lower values (around 265 HV) were measured for this coatings.

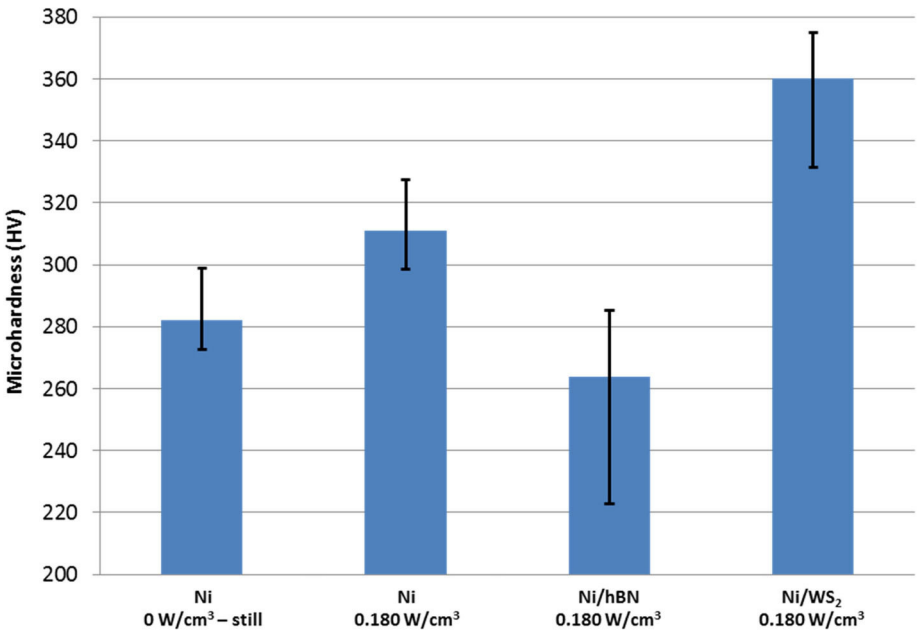

Figure 5.29. Microhardness values measured in the central area of Ni/hBN and Ni/WS_2 composite coatings (6-7 μm) produced under ultrasound at 0.180 W/cm³ (pure Ni coatings electrodeposited under silent/still conditions and ultrasound at 0.180 W/cm³ previously reported in Section 4.3.4 are included for comparison). Electrodeposition time: 14 minutes. Current density: 4 A/dm². Hardness test parameter: load = 2 g-force, load time = 10 seconds.

The grain size is the controlling factor in the hardness of electroplated coatings [37]. Therefore, it should not be a surprise that the incorporation of WS_2 particles into the Ni coatings resulted in an increase in the hardness of the material to around 16% higher than what was observed for pure Ni deposits plated under ultrasound at the same ultrasonic power (0.180 W/cm³) and around 27% higher than what was observed for pure Ni deposits plated under silent/still conditions after observing the outstanding effect that these particles have on refining the grain size of Ni deposits. Nevertheless, it seemed a relatively small increase compared to what should be expected of a Ni matrix with an apparent nano-crystalline structure. Other authors have reported a greater increase in the hardness of Ni coatings with embedded particles. For example, Xue et al. [38] observed an increase from ≈260 HV for pure Ni deposits to ≈620 HV for Ni/CeO_2 coatings produced under ultrasound, while García-Lecina et al. [22] noted an increase from ≈250 HV for pure Ni deposits to ≈460 HV for Ni/Al_2O_3 composites, also plated under ultrasound. An even greater increase in

hardness for Ni/Al_2O_3 coatings was observed by Feng et al. [39] for deposits produced in a solution where Al_2O_3 particles were dispersed with ultrasound prior to the electrodeposition (from ≈280 HV for pure Ni to ≈580 HV for Ni/Al_2O_3 coatings). The enhancement in hardness reported in the present work for the Ni/WS_2 deposits is, however, comparable to the results obtained by other authors for Ni deposits containing SiC (from ≈320 HV for pure Ni to ≈380 HV for Ni/SiC composite coatings plated under ultrasound [40]) and TiO_2 particles (from ≈240 HV for pure Ni to ≈350 HV for Ni/TiO_2 [41]; from ≈5.5 GPa for pure Ni to ≈7.5 GPa for Ni/TiO_2 [42]). It must be noted that, in the work presented here, inherently soft, lubricant WS_2 particles were employed instead of the hard particles used elsewhere, and that a counter-effect on the hardness of the deposit due to the 'softness' of the particles may be expected, meaning that the cause for the hardness increase observed in the Ni/WS_2 composites is the significant grain refinement achieved. Related to this, Sivandipoor and Ashrafizadeh [43] noticed a 60 % decrease in hardness in their electroless plated Ni-P coatings when WS_2 particles were incorporated into the deposit, Balaji et al. [44] observed a progressive reduction in hardness when increasing the proportion of PTFE particles in electrodeposited bronze, and Stanovic and Gojo [45] reported that, while the addition of hard particles such as Al_2O_3, SiC and B_4C increased the hardness of electrodeposited Cu, the incorporation of soft particles such as MoS_2, $BaSO_4$ and graphite lead to a reduction in the hardness of the coatings compared to pure Cu deposits. The increase of hardness in Ni/IF-WS_2 composite coatings reported by García-Lecina et al. [9] was also ascribed to the microstructural changes and grain refinement, although in this case the authors were not able to provide any evidence of the grain refinement effect as strong as the FIB-SEM cross-section images displayed in Figure 5.29. The 'softening' effect brought about by the addition of soft lubricant particles is quite evident in the Ni/hBN composite coatings. For these coatings, despite the modification of the structure of the deposits in terms of a more fragmented structure with less and thinner Ni columnar crystals and more refined grains, the presence of soft hBN particles led to a reduction in the microhardness of

around 6% compared to pure Ni coatings plated under silent/still conditions. Pompei et al. [12] reported different data that may contradict the results presented here, as they obtained Ni/hBN composite coatings with hardness values of around 500 HV. Nevertheless, they used a commercial surfactant to refine the grain size, already obtaining an increase in hardness from 280 HV to 400 HV before incorporating the particles into their coatings.

5.5. CONCLUSIONS

The results obtained in the first stage of the study indicate that, for WS_2, hBN and MoS_2 particles, the lowest quality dispersions were produced under mechanical agitation at 300 rpm, while the best quality dispersions were achieved when combining ultrasound at 0.180 W/cm^3 and mechanical agitation at 300 rpm. The dispersion of PTFE particles was not successful due to the highly hydrophobic nature of the particles.

Ni/WS_2 composite coatings with good surface finish were electrodeposited on Cu substrates when ultrasound at 0.180 W/cm^3 was used during the plating process, while low quality composite coatings were produced under mechanical agitation at 300 rpm and combined ultrasound/mechanical agitation. FIB-SEM analysis showed that the thin Ni/WS_2 composite coatings produced under ultrasound presented a completely different structure compared to pure Ni coatings, as spherical and irregular textures were seen on the surface and a nano-crystalline structure was observed in cross-section images. Such a change in the microstructure of the Ni matrix led to an increase in hardness of 27 % compared to pure Ni plates under silent/still conditions. The thin Ni/WS_2 composite coatings produced under ultrasound could therefore be a good candidate to replace current Ni diffusion barriers, not only because of the expected improvement in the tribological properties due to the presence of the particles and the significant refinement of the grain size, but also because such significant change in the microstructure resulting in very small crystals could lead to the production of more effective and thinner diffusion barrier layers in bronze-based bearings.

For all these reasons, the Ni/WS_2 composite coatings electrodeposited under ultrasound at 180 W/cm^3 will be further evaluated in the next chapters.

Ni/hBN coatings plated with a good surface finish were electrodeposited on Cu substrates with no dependence on the plating conditions employed. However, the most uniform dispersion of the particles in the coatings was achieved by using ultrasound at 0.180 W/cm^3 during the plating process, as aggregates were incorporated into the deposits produced under mechanical agitation at 300 rpm and low particle content was observed in the coatings plated under combined ultrasound/mechanical agitation. FIB-SEM images of the surface of Ni/hBN composite coatings produced under ultrasound showed that the deposits presented a similar structure compared to pure Ni coatings, as structures resembling Ni crystals growing in [100] and [211] directions were observed. Further FIB-SEM analysis of the cross-section of the coatings indicated that a fragmented structure consisting of thin Ni columns and more refined grains similar to that of pure Ni deposits produced under ultrasound at 0.180 W/cm^3. Despite the changes in the microstructure, Ni/hBN composites were slightly softer than the softest pure Ni deposit produced. Nevertheless, this decrease in hardness would not be significant in the application of the coating as a diffusion barrier in bearings, as an enhancement in the tribological properties is mainly expected due to the presence of the lubricant particles. Therefore, the Ni/hBN composite coatings produced under ultrasound at 180 W/cm^3 could also be a suitable option to replace current Ni interlayers and will be further evaluated in the next chapters.

Regarding the incorporation of MoS_2 particles into Ni deposits, no acceptable composite coatings were produced due to the low-quality surface appearance that these coatings exhibited, and therefore, this particle was also discarded as an option for the production of Ni-based composite coatings acting as a diffusion barrier in bearings.

5.6. REFERENCES

[1] S. Alfihed, M. Hossain, A. Alharbi, A. Alyamani, F.H. Alharbi, J. Mater. 2013 (2013) 603648.

[2] Ioffe Physical Technical Institute of Russia, New Semiconductor Materials: Characteristics and Properties Database, BN – Boron Nitride. http://www.ioffe.rssi.ru/SVA/NSM/Semicond/BN/basic.html#hexagonal

[3] L. Tian, Q.-L. Zhou, K. Zhao, Y.-L. Shi, D.-M. Zhao, S.-Q. Zhao, H. Zhao, R.-M. Bao, S.-M. Zhu, Q. Miao, C.-L. Zhang, Chin. Phys. B 20 (2011) 010703.

[4] G. Eshel, G.J. Levy, U. Mingelgrin, M. J. Singer, Soil Sci. Soc. Am. J. 68 (2004) 736.

[5] C. Murphy, Nanoparticle Sizing – Think of a number, Nanotechnology and the Coatings Industry Seminar at The Nottingham Belfry Hotel, October 2013.

[6] S. Alfihed, M. Hossain, A. Alharbi, A. Alyamani, F.H. Alharbi, J. Mater. 2013 (2013) 603648.

[7] M. Camargo, PhD Thesis (unpublished), Technische Universität Ilmenau (Germany), 2014.

[8] R.N. Kelly, F.M. Etzler, What is wrong with laser diffraction? - A critical review of current laser diffraction methods for particle size analysis. http://www.donner-tech.com/whats_wrong_with_ld.pdf

[9] E. García-Lecina, I. García-Urrutia, J.A. Díez, J. Fornell, E. Pellicer, J. Sort, Electrochim. Acta 114 (2013) 859.

[10] M. Camargo, I. Díaz, U. Schmidt, A. Bund, Galvanotechnik 103 (2012) 48.

[11] D. Alberts, B. Fernández, T. Frade, A. Gomes, M.I. da Silva Pereira, R. Pereiro, A. Sanz-Medel, Talanta 84 (2011) 572.

[12] E. Pompei, L. Magagnin, N. Lecis, P.L. Cavallotti, Electrochim. Acta 54 (2009) 2571.

[13] L. Ph. Bérubé, G. L'Espérance, J. Electrochem. Soc. 136 (1989) 2314.

[14] Inorganic Crystal Structure Database code 64989, Fachinformationszentrum Karlsruhe (Germany) and National Institute of Standards and Technology (United States of America).

[15] J. Amblard, M. Froment, N. Spyrellis, Surf. Technol. 5 (1977) 205.

[16] J. Amblard, M. Froment, Faraday Symp. Chem. Soc. 12 (1977) 136.

[17] J. Amblard, I. Epelboin, M. Froment, G. Maurin, J. Appl. Electrochem. 9 (1979) 233.

[18] J. Amblard, M. Froment, G. Maurin, N. Spyrellis, E. Trevisan-Souteyrand, Electrochim. Acta 28 (1983) 909.

[19] E.A. Pavlatou, N. Spyrellis, Russ. J. Electrochem. 44 (2008) 745.

[20] A.G. McCormack, M.J. Pomeroy, V.J. Cunnanez, J. Electrochem. Soc. 150 (2003) C356.

[21] E.A. Pavlatou, M. Stroumbouli, P. Gyftou, N. Spyrellis, J. Appl. Electrochem. 36 (2006) 385.

[22] E. García-Lecina, I. García-Urrutia, J.A. Díez, M. Salvo, F. Smeacetto, G. Gautier, R. Seddon, R. Martin, Electrochim. Acta 54 (2009) 2556.

[23] S. Özkan, G. Hapçı, G. Orhan, K. Kazmanlı, Surf. Coat. Technol. 232 (2013) 734.

[24] H. Gül, F. Kiliç, S. Aslan, A. Alp, H. Akbulut, Wear 267 (2009) 976.

[25] S. Spanou, E.A. Pavlatou, N. Spyrellis, Electrochim. Acta 54 (2009) 2547.

[26] F. Erler, C. Jakob, H. Romanus, L. Spiess, B. Wielage, T. Lampke, S. Steinhaüser, Electrochim. Acta 48 (2003) 3063.

[27] S. Spanou, E.A. Pavlatou, J. Appl. Electrochem. 40 (2010) 1325.

[28] A. Vicenzo, P.L. Cavalloti, Russ. J. Electrochem. 44 (2008) 716.

[29] J. Kubisztal, A. Budniok, A. Lasia, Int. J. Hydrogen Energ. 32 (2007) 1211.

[30] S. Mohajeri, A. Dolati, S. Rezagholibeiki, Mater. Chem. Phys. 129 (2011) 746.

[31] M. Lekka, D. Koumoulis, N. Kouloumbi, P.L. Bonora, Electrochim. Acta 54 (2009) 2540.

[32] C.T.J. Low, R.G.A. Wills, F.C. Walsh, Surf. Coat. Technol. 201 (2006) 371.

[33] C. Cai, X.B. Zhu, G.Q. Zheng, Y.N. Yuan, X.Q. Huang, F.H. Cao, J.F. Yang, Z. Zhang, Surf. Coat. Technol. 205 (2011) 3448-3454.

[34] F.-f. Xia, M.-h.Wu, F. Wang, Z.-y. Jia, A.-l. Wang, Curr. Appl. Phys. 9 (2009) 44-47.

[35] P. Scherrer, Bestimmung der Größe und der inneren Struktur von Kolloidteilchen mittels Röntgenstrahlen, in: Nachrichten von der Gesellschaft der Wissenschaften zu Göttingen, Mathematisch-Physikalische Klasse, 1918, pp 98-100.

[36] T. Lampke, D. Dietrich, A. Leopold, G. Alisch, B. Wielage, Surf. Coat. Technol. 202 (2008) 3967.

[37] C.T. Walker, R. Walker, Electrodepos. Surf. Treat. 1 (1973) 457.

[38] Y.-J. Xue, J.-S. Li, W. Ma, M.-D. Duan, M.-M. Lan, Int. J. Surf. Sci. Eng. 4 (2010) 202.

[39] Q. Feng, T. Li, H. Yue, K. Qi, F. Bai, J. Jin, Appl. Surf. Sci. 254 (2008) 2262.

[40] C. Zanella, M. Lekka, P.L. Bonora, Surf. Eng. 26 (2010) 511.

[41] S. A. Lajevardi, T. Shahrabi, V. Hasannaeimi, Mater. Corros. 62 (2011) 29.

[42] J. Li, Y. Sun, X. Sun, J. Qiao, Surf. Coat. Technol. 192 (2005) 331.

[43] I. Sivandipoor, F. Ashrafizadeh, Appl. Surf. Sci. 263 (2012) 314.

[44] R. Balaji, M. Pushpavanam, K.Y. Kumar, K. Subramanian, Surf. Coat. Technol. 201 (2006) 3205.

[45] V.D. Stankovic, M. Gojo, Surf. Coat. Technol. 81 (1996) 225.

6. PERFORMANCE OF NI-BASED COATINGS ACTING AS TRIBOLOGICALLY-ACTIVE LAYERS

6.1. OVERVIEW

The present chapter includes the tribological analysis of the three different Ni-based coatings described in Chapters 4 and 5 that were selected for further tribological evaluation in order to compare their performance with benchmark Ni deposits prepared under

mechanical agitation: pure Ni deposits and Ni/hBN and Ni/WS_2 composite coatings, the three of them electrodeposited under ultrasound at 0.180 W/cm^3.

As described in Chapter 1, although journal bearings are designed to operate under 'hydrodynamic' lubrication, current trends in modern engine design may cause journal bearings to run under 'mixed-film' and 'boundary' lubrication, potentially resulting in local loss and removal of the overlay by wear, corrosion or other mechanisms, leading to the exposure of the Ni diffusion barrier. These areas of the surface of the bearing where the Ni barrier is exposed would also operate under those same conditions. For this reason, two different types of scratch tests were performed on the electroplated Ni-based coatings studied:

1. Lubricated scratch tests where lubrication was achieved via a single drop of SAE 10 oil immediately before the tests started in order to study the performance of the electrodeposited Ni-based coatings under 'mixed-film'/'boundary' lubrication where the sliding contacting bodies are supported on a combination of asperity-asperity contact points and fluid regions between asperities [1].
2. Non-lubricated scratch tests where no lubricant was used in order to study the performance of the electrodeposited Ni-based coatings under dry 'boundary' lubrication where asperity-asperity contact points fully support the load [2].

6.2. LUBRICATED SCRATCH TESTS

6.2.1. NI COATINGS ELECTRODEPOSITED UNDER MECHANICAL AGITATION

Figure 6.1 displays Coefficient of Friction (CoF) curves obtained during the lubricated scratch test performed on a Ni deposit electrodeposited under mechanical agitation at 300 rpm. Lowest CoF values were measured during the first scratch, progressively increasing with each new scratch until a steady CoF value around 0.3 was achieved. From the third scratch, the signal measured showed a significant amount of 'noise'. A closer look at the CoF

curves revealed that the apparent noise was not such, as a very distinctive repetition of cycles alternating a 'concave down' increase followed by a sudden drop of CoF was clearly observed. Such repeated feature observed in the CoF curves corresponding to scratches 3 to 10 is a very strong indication of 'stick-slip' motion [3]. In stick-slip motion, the test ball virtually stops sliding (maximum observed in each cycle) and then experiences rapid sliding which progressively slows down until it reaches the point where very slow, almost imperceptible sliding motion occurs again [1]. Despite this, no signs of coating failure were seen in the recorded Acoustic Emission (AE) signal (Figure 6.2).

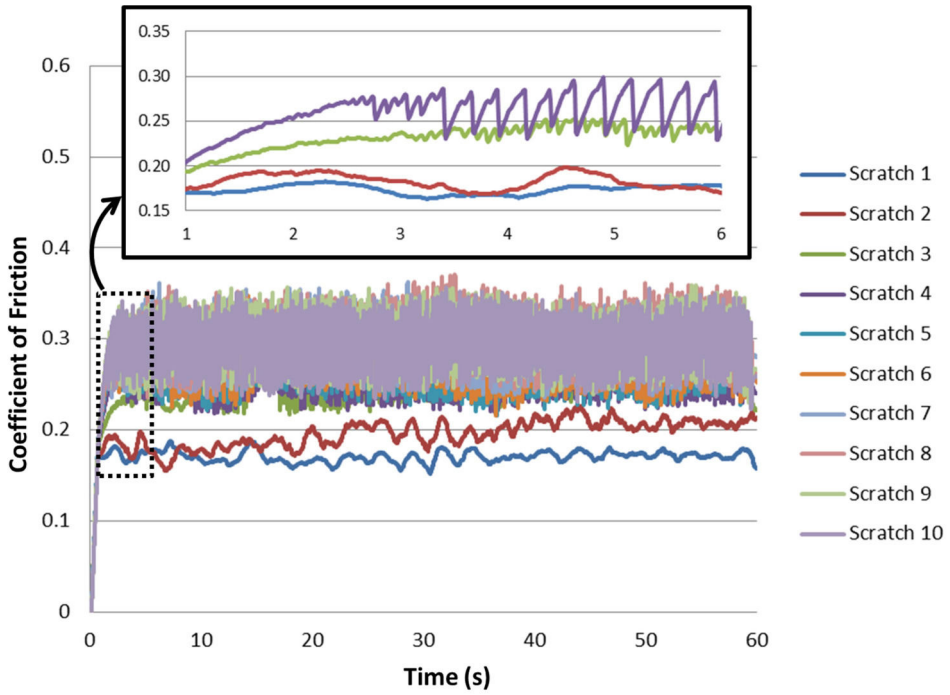

Figure 6.1. CoF measured during a lubricated scratch test (10 continuous scratches) performed on a Ni coating electrodeposited under mechanical agitation at 300 rpm. Zoomed-in graph shows when stick-slip motion started to occur (only scratches 1 to 4 are shown for better visibility).

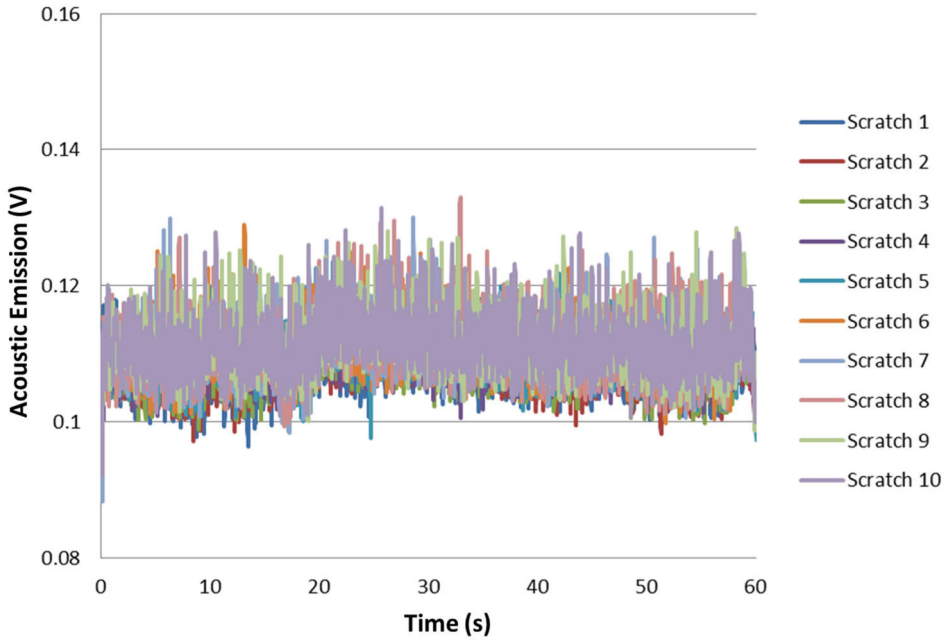

Figure 6.2. Acoustic emission recorded during a lubricated scratch test (10 continuous scratches) performed on a Ni coating electrodeposited under mechanical agitation at 300 rpm.

Figure 6.3 A displays the test ball after the lubricated scratch test was performed on the Ni coating produced under mechanical agitation, showing that a small transfer of material occurred from the coating to the ball during the scratch test, while Figures 6.3 B and C displays the wear track left on the tested sample after the scratch test, where little accumulation of debris forming ridges on both sides of the wear track was observed. All these features suggest that ploughing-like abrasive wear occurred during the test, where repeated sliding and accumulation of plastic flow at the surface of the coating resulted in the formation and growth of the 'wear lump' observed in the test ball [4].

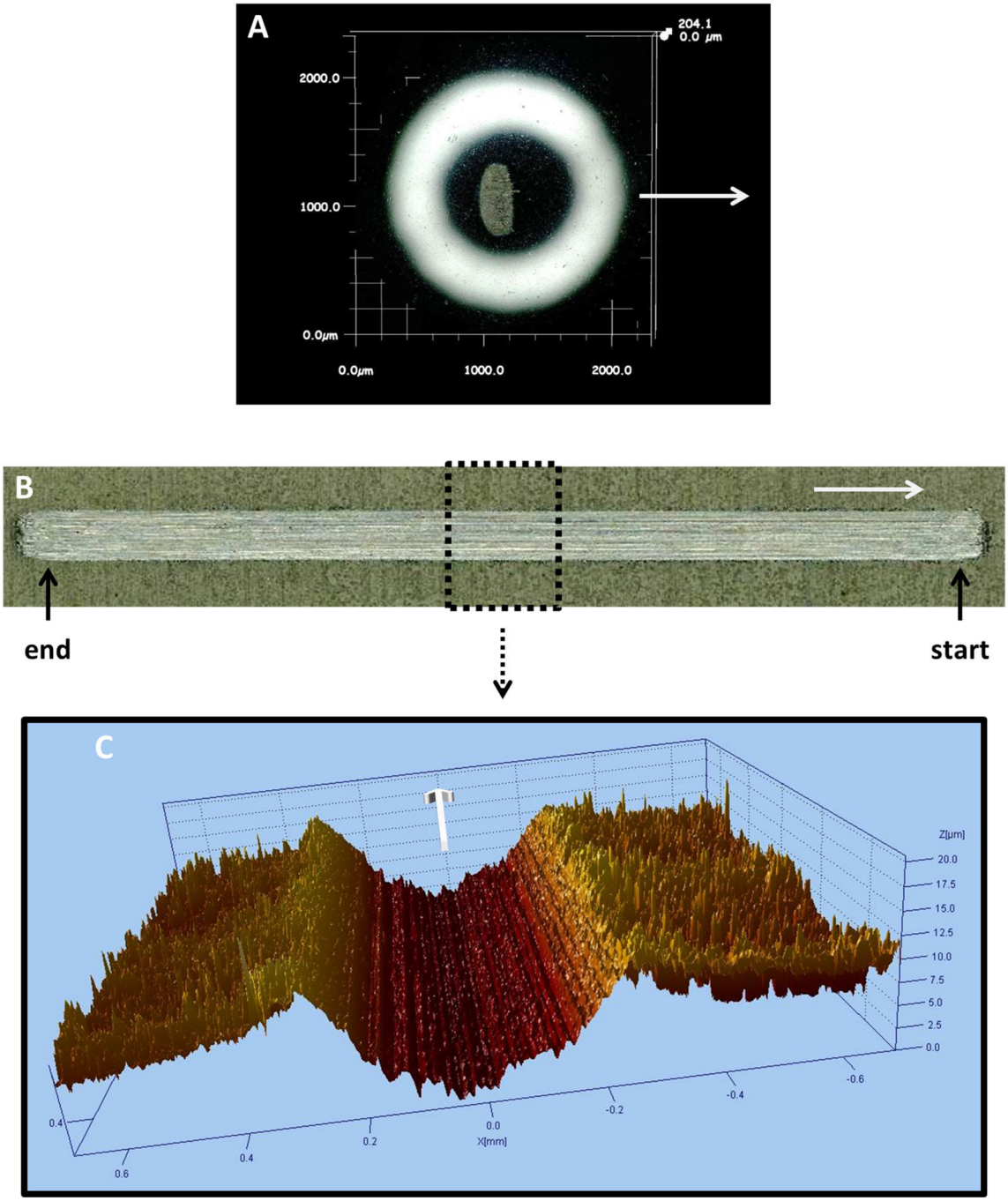

Figure 6.3. Images of the test ball and the wear track left by the test ball on a Ni coating electrodeposited under mechanical agitation at 300 rpm after a lubricated scratch test: (A) test ball, (B) wear track left on the sample, (C) 3D depth profile on the middle area of the wear track left on the sample obtained by white light interferometry. The white arrows point the direction of the sample motion.

6.2.2. Ni coatings electrodeposited under ultrasound

Figure 6.4 displays CoF values measured during the scratch test carried out on a Ni deposit electrodeposited under ultrasound. As in the case of the Ni coatings electrodeposited under mechanical agitation in absence of ultrasound, the lowest CoF values were measured during the first scratch, and progressively increased with each consecutive scratch until a steady CoF value was achieved in the fourth scratch, with CoF values settled around 0.3 for the rest of the test. Again, 'stick-slip' motion occurred during the test, in this case from the second half of the second scratch test onwards, while no signs of coating failure were noticed in AE signal (Figure 6.5).

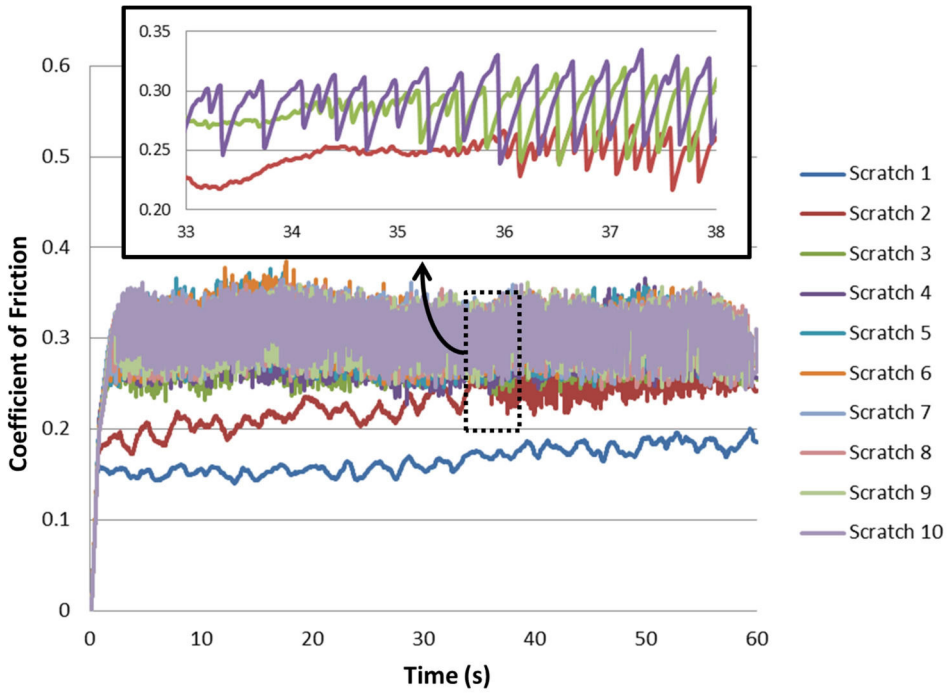

Figure 6.4. CoF measured during a lubricated scratch test (10 continuous scratches) performed on a Ni coating electrodeposited under ultrasound at 0.180 W/cm^3. Zoomed-in graph shows when stick-slip motion started to occur (only scratches 1 to 4 are shown for better visibility).

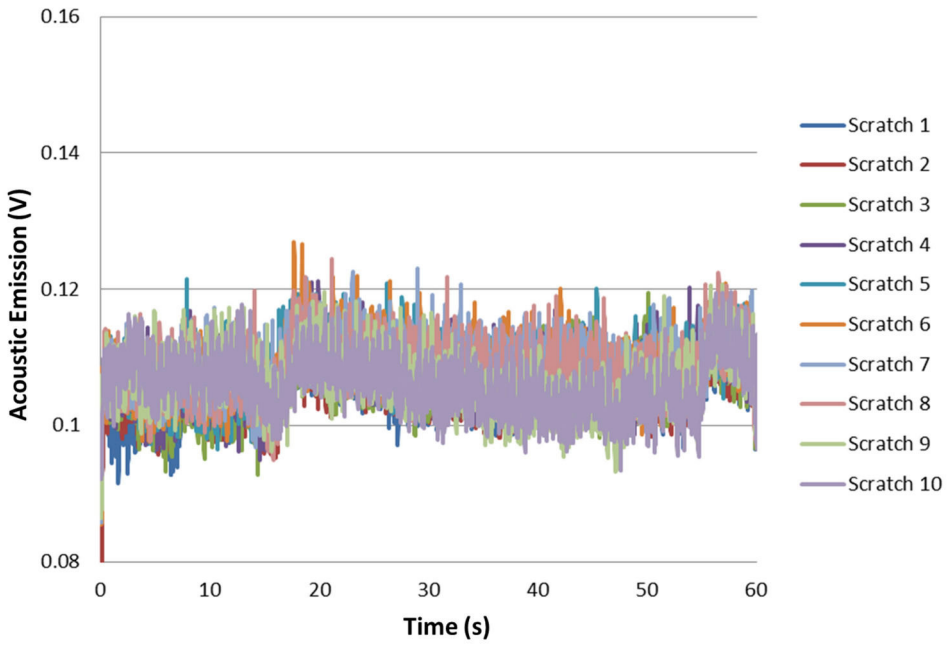

Figure 6.5. Acoustic emission recorded during a lubricated scratch test (10 continuous scratches) performed on a Ni coating electrodeposited under ultrasound at 0.180 W/cm^3.

The different features observed in the test ball (small transference of material from the coating to the ball) and the wear track (little accumulation of worn-out material forming ridges on both sides) left on the Ni coating electrodeposited under mechanical agitation after the lubricated scratch test were again noticed in the ball and the sample coated with the ultrasonically-assisted electrodeposited Ni coating (Figure 6.6), suggesting also in this case that ploughing-like abrasive wear was the main wear mechanism.

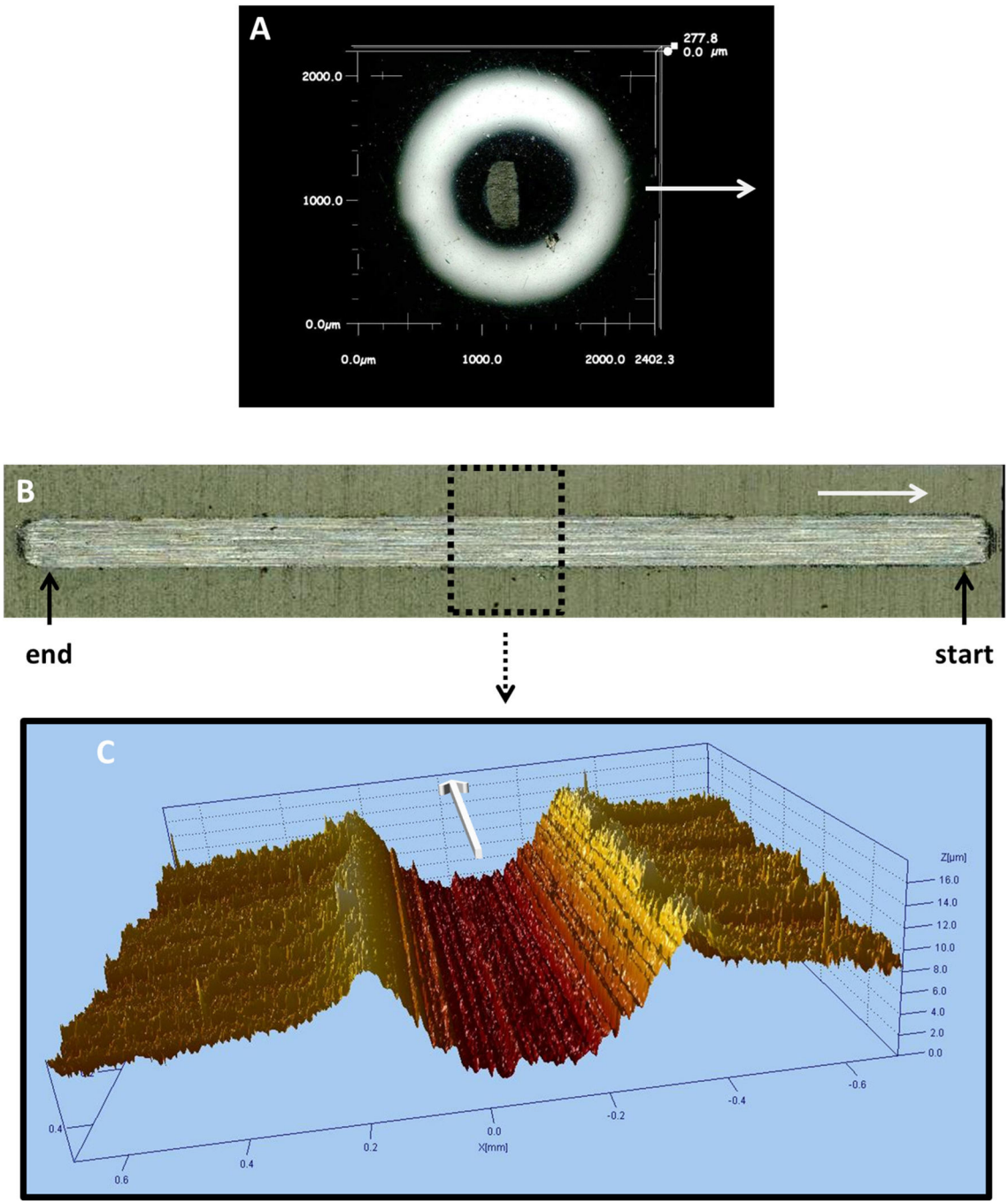

Figure 6.6. Images of the test ball and the wear track left by the test ball on a Ni coating electrodeposited under ultrasound at 0.180 W/cm^3 after a lubricated scratch test: (A) test ball, (B) wear track left on the sample, (C) 3D depth profile on the middle area of the wear track left on the sample obtained by white light interferometry. The white arrows point the direction of the sample motion.

6.2.3. Ni/hBN COMPOSITE COATINGS ELECTRODEPOSITED UNDER ULTRASOUND

Figure 6.7 displays CoF values measured during the scratch test performed on a Ni/hBN composite coating electrodeposited under ultrasound at 0.180 W/cm^3. As in previous cases, the lowest CoF values were measured during the first scratch, and a progressive increase in CoF was observed with consecutive scratches until a steady CoF value around 0.3 was achieved in the fourth scratch, showing again the same characteristic features of stick-slip motion from the final part of the second scratch onwards. As in previous cases, no signs of coating failure were observed in the AE signal (Figure 6.8).

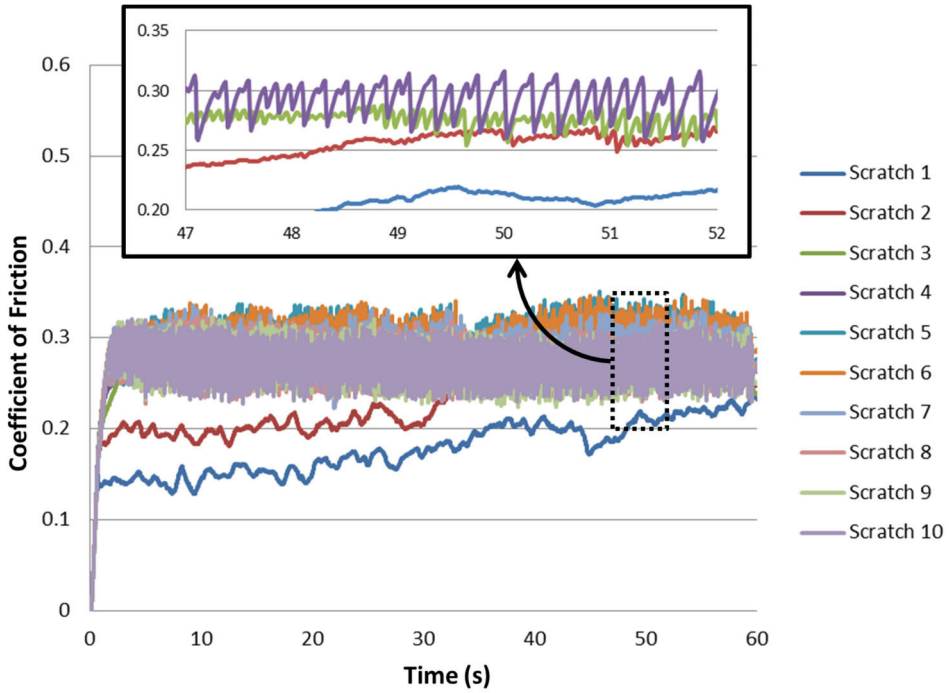

Figure 6.7. CoF measured during a lubricated scratch test (10 continuous scratches) performed on a Ni/hBN composite coating electrodeposited under ultrasound at 0.180 W/cm^3. Zoomed-in graph shows when stick-slip friction started to occur (only scratches 1 to 4 are shown for better visibility).

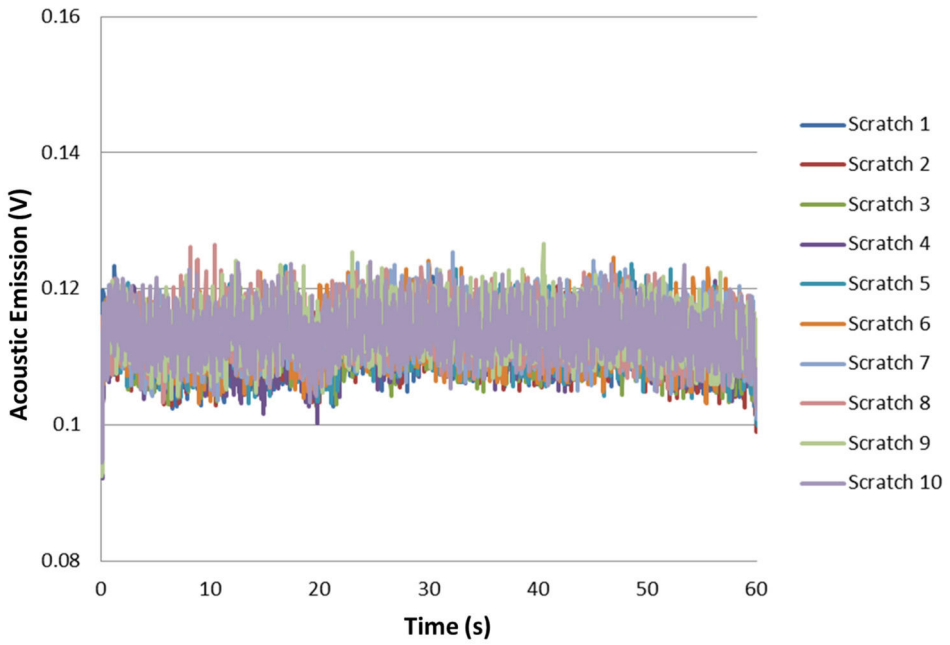

Figure 6.8. Acoustic emission recorded during a lubricated scratch test (10 continuous scratches) performed on a Ni/hBN composite coating electrodeposited under ultrasound at 0.180 W/cm^3.

The features observed in the test ball and the wear track left on the Ni/hBN composite coating after the scratch test were again very similar to those previously noticed for the pure Ni deposits electrodeposited under either mechanical agitation or ultrasound. A small amount of the coating material was transferred from the sample to the ball during the scratch test (Figure 6.9 A), and a wear track with little accumulation of debris on the sides was observed on the surface of the tested sample (Figure 6.9 B and C), indicating again that the ploughing-like abrasive mode was the wear mechanism.

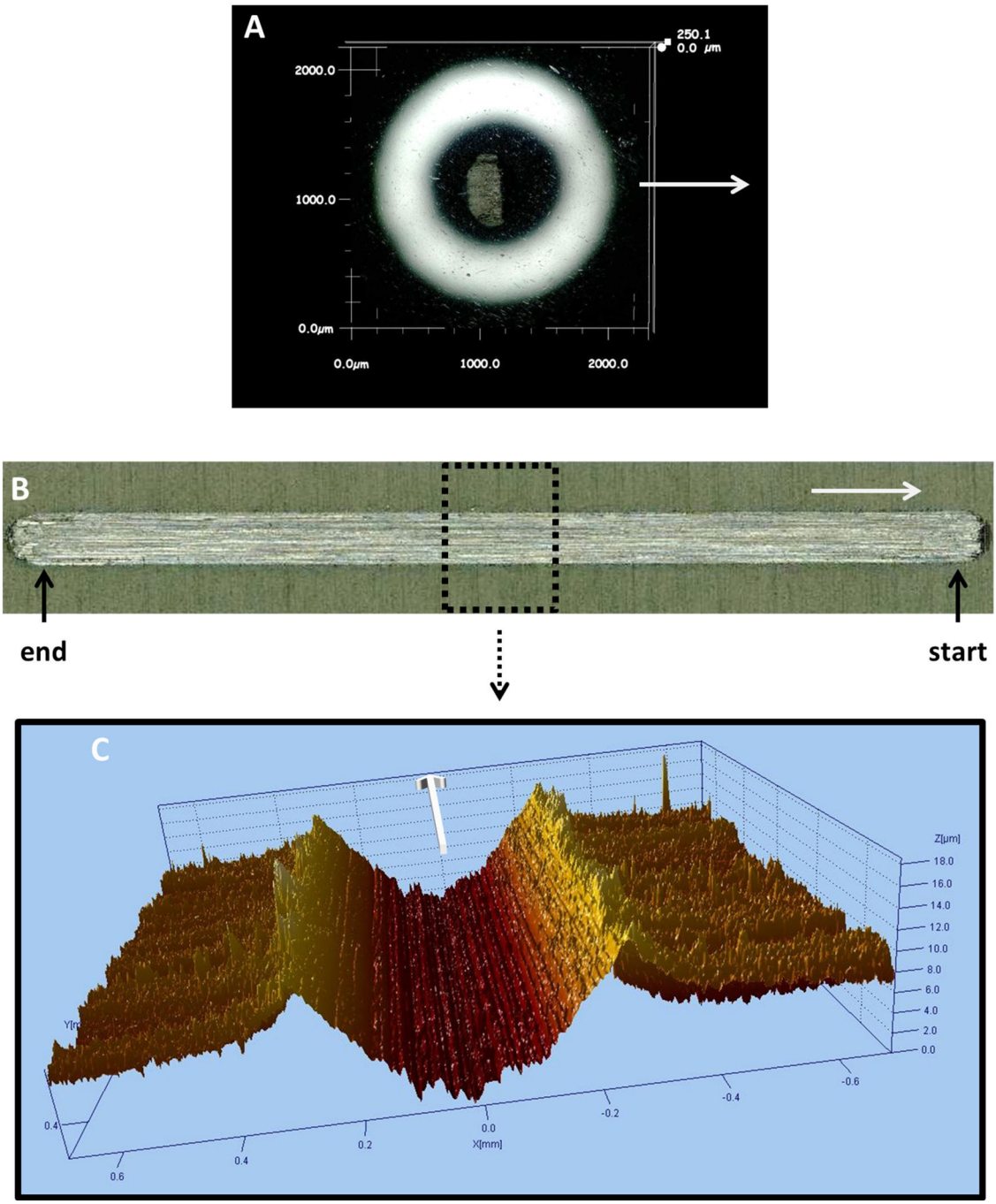

Figure 6.9. Images of the test ball and the wear track left by the test ball on a Ni/hBN composite coating electrodeposited under ultrasound at 0.180 W/cm^3 after a lubricated scratch test: (A) test ball, (B) wear track left on the sample, (C) 3D depth profile on the middle area of the wear track left on the sample obtained by white light interferometry. The white arrows point the direction of the sample motion.

6.2.4. Ni/WS_2 COMPOSITE COATINGS ELECTRODEPOSITED UNDER ULTRASOUND

Figure 6.10 displays the CoF values measured during the lubricated scratch test performed on a Ni/WS_2 composite coating electrodeposited under ultrasound at 0.180 W/cm^3. The lowest CoF values were again measured during the first scratch. In this case though, CoF values slowly increased with each new scratch until a steady CoF value around 0.24 was achieved in the sixth scratch, being up to 20% lower than the CoF values measured for the other Ni-based coatings. As opposed to what was observed for the other Ni-based coatings tested, CoF curves did not indicate the occurrence of stick-slick motion in this case. Again, no signs of coating failure were seen in the recorded AE signal (Figure 6.11).

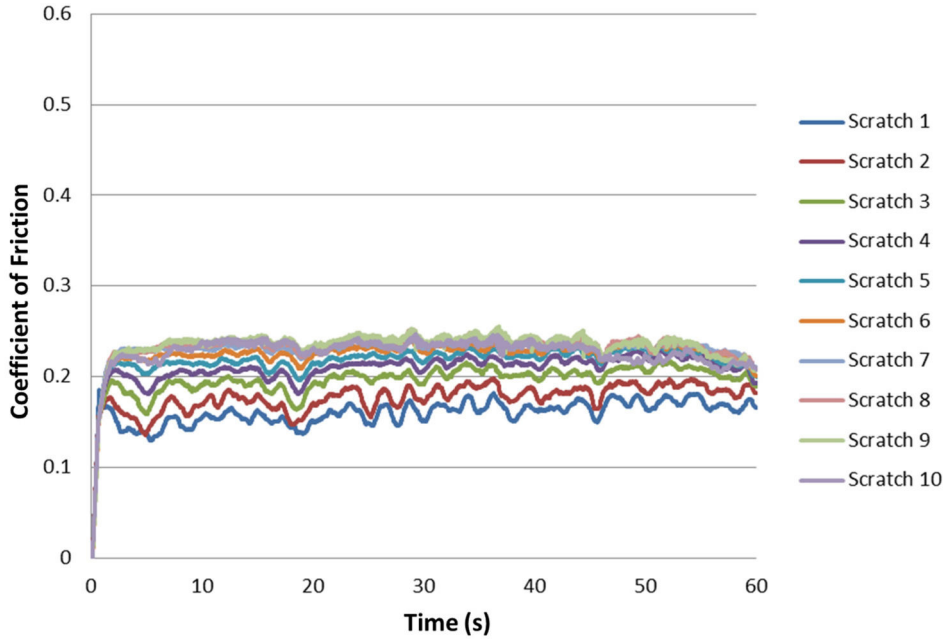

Figure 6.10. CoF measured during a lubricated scratch test (10 continuous scratches) performed on a Ni/WS_2 composite coating electrodeposited under ultrasound at 0.180 W/cm^3.

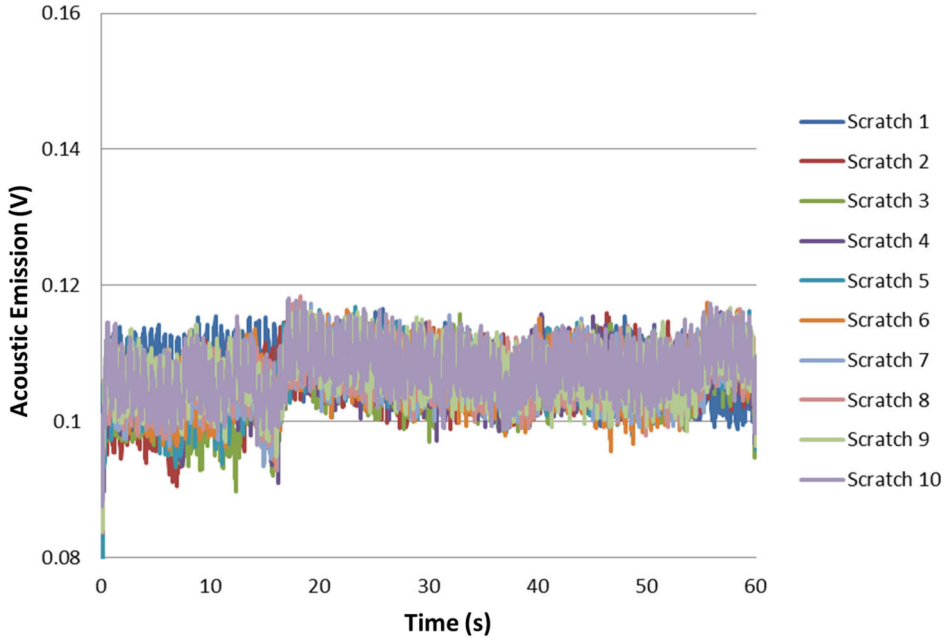

Figure 6.11. Acoustic emission recorded during a lubricated scratch test (10 continuous scratches) performed on a Ni/WS_2 composite coating electrodeposited under ultrasound at 0.180 W/cm^3.

A small transfer of material from the coating to the ball was again observed in the test ball used for the test (Figure 6.12 A). In this case though, the contact area of the wear lump attached to the test ball presented a smooth black surface which suggests the formation of a very thin tribofilm. Compared with the other Ni-based coatings, a smaller amount of worn-out material accumulated on the sides of the wear track, which now presented a smoother appearance with low wear at the end of the wear track (Figure 6.12 B and C).

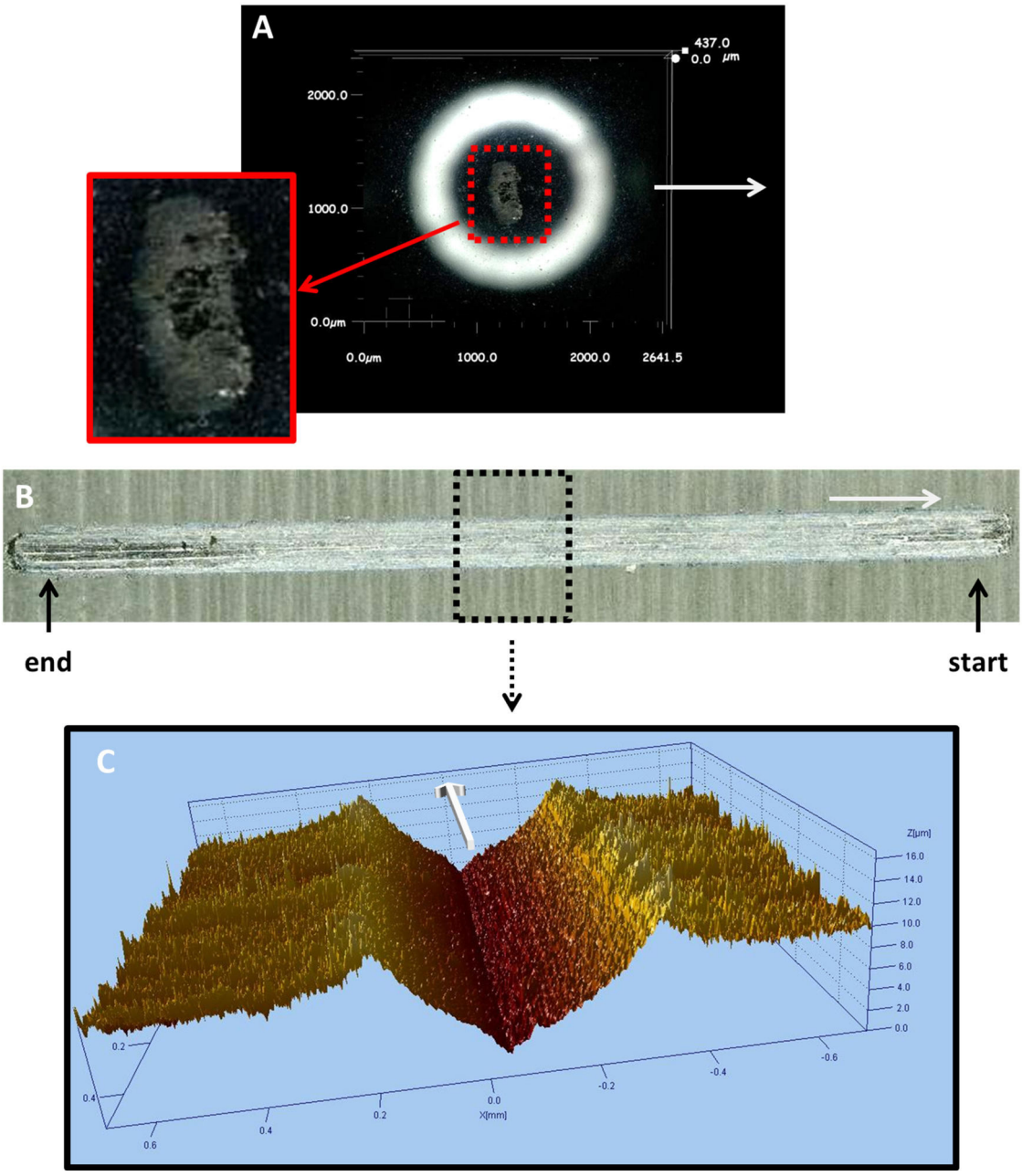

Figure 6.12. Images of the test ball and the wear track left by the test ball on a Ni/WS_2 composite coating electrodeposited under ultrasound at 0.180 W/cm^3 after a lubricated scratch test: (A) test ball, (B) wear track left on the sample, (C) 3D depth profile on the middle area of the wear track left on the sample obtained by white light interferometry. The white arrows point the direction of the sample motion. Zoomed-in image of the test ball shows the black film covering the contact surface of the test ball.

6.2.5. SUMMARY AND DISCUSSION OF RESULTS

Figure 6.13 displays the average CoF values of each scratch (bars depict the maximum CoF value measured during each scratch) for the different Ni-based coatings tested under lubricated conditions. The Ni/hBN composite coating electrodeposited under ultrasound and the Ni deposits produced under either mechanical agitation or ultrasound exhibited very similar behaviour, not only in terms of the average CoF values estimated, but also in terms of the stick-slip motion developed during the course of the tests. In all the tests performed on these coatings, stick-slip motion routinely started during the second half of the second scratch or early on the third scratch. Stick-slip motion occurred as a result of the combination of Ni-Ni sliding contact in the presence of the lubricant. Ni-Ni sliding contact took place due to the formation and growth of a wear lump on the ball by the repeated sliding action of the ball on the tested sample. Lower CoF values and no signs of stick-slip motion were observed during the first scratch for the Ni/hBN composite coating and both Ni deposits as no material had been transferred from the coating to the ball yet. High friction is expected in those situations where Ni-Ni sliding contact occurs, whereas low friction is expected where a lubricant film forms between the sliding surface and the counter-part, and hence the stick-slip phenomenon observed for these coatings. This would be partly due to the generally poor tribological performance of the Ni-based coatings, but also due to the mixed-lubrication regime expected in a tribosystem such as the one studied here (test ball/lubricant/Ni-based coating), especially once there has been a transfer of material from the coating to the test ball. When this transfer of material occurs, the load is then borne partly by the lubricant film and partly by the asperities present in the surface of the test ball and the wear track formed in the coating [5]. Regarding stick-slip motion, such phenomenon is quite often observed as a cause/consequence of seizure failure of coating systems in bearings, which is likely to occur when the Ni interlayer is exposed in bronze-based bearings [6], leading to catastrophic failure of the tribological system [7]. Nevertheless, as

observed in the respective AE curves, no critical coating failure was noticed during the scratch tests of both Ni deposits and the Ni/hBN composite coatings.

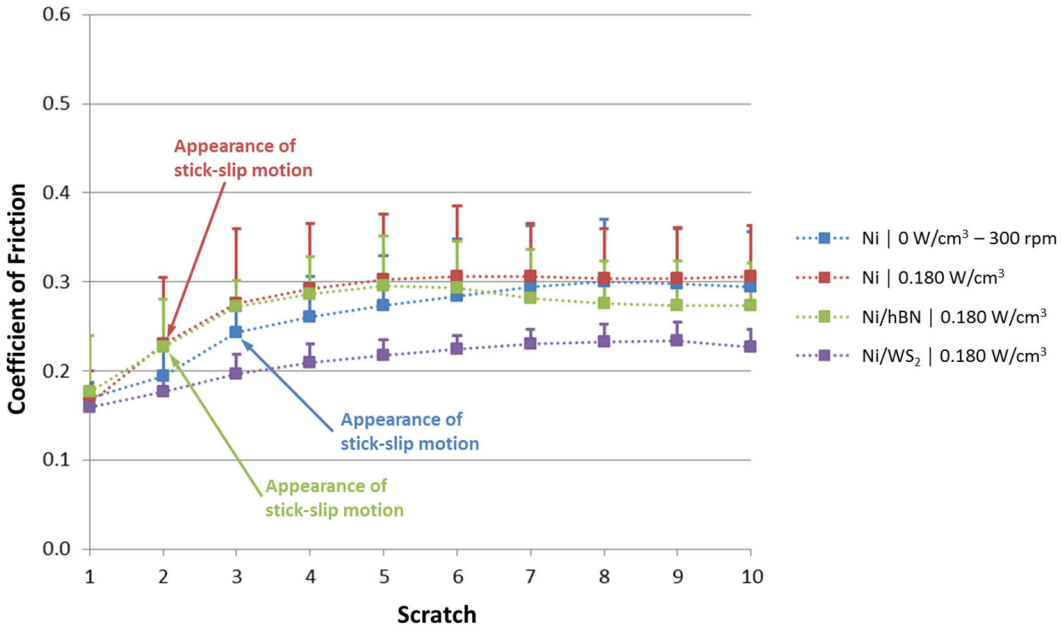

Figure 6.13. Average CoF estimated from a lubricated scratch test (10 continuous scratches) performed on different Ni-based coatings. Bars indicate maximum CoF values recorded during each scratch.

The Ni/WS_2 composite coatings electrodeposited under ultrasound exhibited a very different behaviour, not only in terms of CoF, which was 20% lower, but also in terms of the sliding motion, as smooth sliding occurred with no signs of the stick-slip phenomenon previously reported for the other Ni-based coatings tested. The causes for this beneficial presence of the WS_2 particles in lubricated tribosystems are diverse: i) rolling friction [8], ii) WS_2 particles acting as spacers, preventing the contact between the asperities in both metal surfaces [8], iii) third body material transfer (i.e. gradual transference of layers of WS_2 onto the metal surfaces during repeated sliding) [9] and iv) the gradual formation of a thin WS_2 film after continuous and repeated sliding [10]. In the latter referenced study, a thin black WS_2 film gradually formed on the metal surface. A thin black film also formed on the contact surface of the test ball used for the scratch test performed on the Ni/WS_2 composite coating (Figure 6.12 A), suggesting the formation of a thin WS_2 film which would protect the contact surface and restrict the rise of the friction force, decreasing the influence of asperity contact and improving the tribological performance of the system under mixed lubrication [11].

The differences in terms of tribological performance between the Ni/WS_2 composite coatings and the rest of the Ni-based coatings are not only related to the CoF curves obtained during the tests, but also to the appearance of the wear tracks left on the different samples tested. Figure 6.14 displays the cross-sectional depth profile measured at the middle of each wear track in order to compare the depth of each wear track and the debris accumulated on the sides of the track. As expected from the appearance of the 3D depth profiles previously shown, the Ni/WS_2 composite coating presented the smoothest wear track, showing a significantly lower accumulation of debris forming small ridges on each side of the wear track. It is also worth pointing out that, taking into account the thickness of the coatings (≈6 μm in all cases), the final scratches partially took place over the Pb-bronze substrate, especially in both Ni deposits and the Ni/hBN composite coating, where only a small portion of the test ball would be in contact with the Pb-bronze substrate in the Ni/WS_2 composite coating.

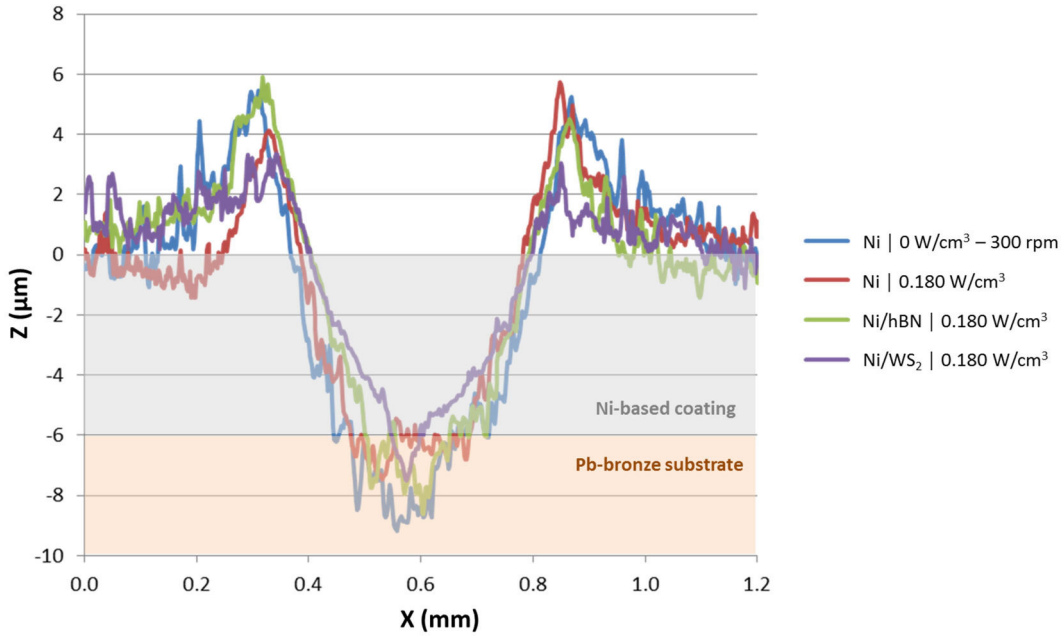

Figure 6.14. Cross-sectional depth profile measured at the middle of the wear track left by the test ball during a lubricated scratch test (10 continuous scratches) performed on different Ni-based coatings. Data from 3D depth profiles obtained by white light interferometry.

In order to have a better idea of the wear resistance of each coating, two parameters were estimated from the depth profiles shown in Figure 6.15: $\Delta \mathbf{V}_g$, which is defined as the wear

track volume per unit sliding distance, and $\Delta \mathbf{V}_r$, which is defined as the ridge volume per unit sliding distance (Figure 6.15). Table 6.1 shows $\Delta \mathbf{V}_g$ and $\Delta \mathbf{V}_r$ values estimated for the four different Ni-based coatings evaluated in the present study. Although these $\Delta \mathbf{V}_g$ and $\Delta \mathbf{V}_r$ values are a rough estimation and therefore should be carefully considered, they give a qualitative idea of the wear resistance of the different Ni-based coatings developed during the present project compared to the original Ni coating electrodeposited under mechanical agitation. In this sense, the Ni coating electrodeposited under mechanical agitation showed by far the highest $\Delta \mathbf{V}_r$ and $\Delta \mathbf{V}_g$ values, which suggests that this coating material would exhibit the worst wear resistance among the different coatings tested. The Ni coating electrodeposited under ultrasound and the Ni/hBN composite coating exhibited very similar behaviour in terms of the volume of the ridges and the wear suffered by both samples, and this could be related to the similar crystal structure both coatings have (combination of columnar crystals and more refined grains). As expected, the Ni/WS_2 presented the lowest $\Delta \mathbf{V}_r$ and $\Delta \mathbf{V}_g$ values, which suggest a higher wear resistance for said coating compared with the other three Ni-based coatings tested.

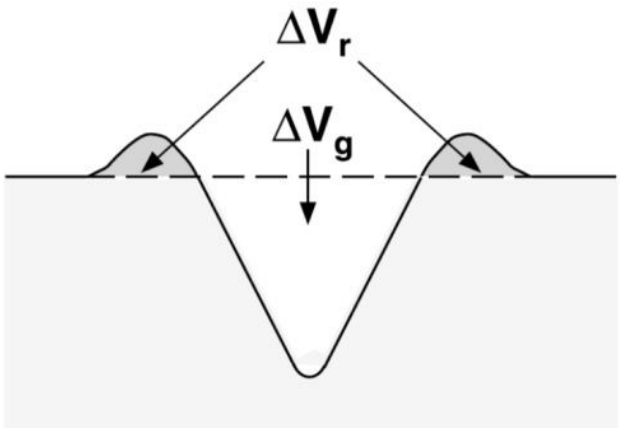

Figure 6.15. Schematic diagram of the cross-sectional profile of the wear track formed by abrasive wear showing $\Delta \mathbf{V}_r$ and $\Delta \mathbf{V}_g$. Adapted from [4].

Table 6.1. ΔV_r and ΔV_g values estimated from cross-sectional depth profiles measured at the middle of the wear track left by the test ball during lubricated scratch tests (10 continuous scratches) performed on different Ni-based coatings.

	ΔV_g (μm^2)	ΔV_r (μm^2)
Ni | 0 W/cm³ – 300 rpm	2431	1220
Ni | 0.180 W/cm³	1941	823
Ni/hBN | 0.180 W/cm³	1908	904
Ni/WS_2 | 0.180 W/cm³	1506	478

In this case though, the enhanced wear resistance of the Ni/WS_2 composite coatings would not be a direct result of the presence of the WS_2 particles, but a result of the extremely refined grain size of these coatings and the consequent enhanced hardness. Related to this, non-annealed electroless deposited Ni-P/WS_2 composite coatings studied by Sivandipoor and Ashrafizadeh [12] presented a lower hardness due to the 'softening' effect of the WS_2 particles in the coating. Although significantly lower CoF values were measured for these Ni-P/WS_2 composite coatings compared to regular electroless deposited Ni-P coatings, the latter exhibited a much higher wear resistance due to their higher hardness (all these non-annealed electroless coatings were amorphous, implying that no grain refinement caused by the incorporation of particles could have an effect on grain size and hardness and therefore affect the tribological response). In addition, although grain refinement (down to the nano-scale) and consequent increase in hardness in electrodeposited Ni may not significantly improve CoF [13], it clearly has an enhancing effect on wear resistance [13,14]. All of this suggests that, whereas the lower CoF values and absence of stick-slip motion observed in the Ni/WS_2 composite coatings presented in this thesis would therefore be a consequence of the presence of the WS_2 particles, the apparently higher wear resistance would be related to the significantly smaller grain size and consequent higher hardness which is achieved by incorporating the WS_2 particles into coating.

In summary, the Ni/WS_2 composite coating exhibited the best tribological performance under lubricated conditions, as this coating material not only showed the lowest CoF and the highest wear resistance, but also prevented the occurrence of stick-slip motion which was routinely observed for the other coatings evaluated under the same conditions. This feature is of critical importance, as stick-slip motion is a major cause/consequence of bearing failure (e.g. seizure) in bearings where the Ni interlayer is exposed. Regarding the Ni/hBN composite coating, its tribological performance under lubricated conditions was rather unsatisfactory, as it showed similar behaviour in terms of CoF than the original Ni coating electrodeposited under mechanical agitation with apparently little improvement in terms of wear resistance. There could be different reasons for this: i) the little amount of hBN particles incorporated (around 0.2 % by weight, as mentioned in Section 5.4.1 in Chapter 5) and ii) the low tribological efficiency of such particles. Although hBN powder is routinely reported as an effective solid lubricant, previous works with electrodeposited Ni/hBN composite coatings showed no change in terms of CoF and some improvement in terms of wear resistance compared with pure Ni deposits [15], agreeing with the results obtained in the lubricated scratch tests carried out in the present study. The Ni coating electrodeposited with ultrasound showed similar performance under lubricated conditions, i.e. no improvement in terms of CoF and little enhancement of the wear resistance, which would be mainly related to the modification of the microstructure by ultrasound and the resulting small increase in hardness, as reported in Section 5.4.4.

6.3. NON-LUBRICATED SCRATCH TESTS

6.3.1. NI COATINGS ELECTRODEPOSITED UNDER MECHANICAL AGITATION

Figure 6.16 displays CoF curves obtained during a non-lubricated scratch test performed on a Ni deposit electrodeposited under mechanical agitation at 300 rpm. Although reasonably low CoF values were measured during scratch 1, very high CoF values (up to 0.56) were observed in scratch 2, which showed a very chaotic trend with no clear average CoF value. Scratches 3 and 4 yielded CoF curves showing an intermediate behaviour between scratches 1 and 2, and the system seemed to settle down from scratch 5 onwards. Some parts of the CoF curves (scratch 3 onwards) also showed signs of stick-slip motion which in the case of solid-solid contact with absence of a lubricant are mainly due to changes in the area of contact and surface temperature [3]. AE signal was also recorded during the non-lubricated scratch test (Figure 6.17) showing in this case very clear signal peaks indicating critical failure of the coatings on different scratches. The first indication was noticed at the very end of scratch 1 (probably due to the removal of part of the coating or the deposition of part of the wear lump attached to the test ball when the ball was arising before returning to the starting point to start the third scratch), followed by a very strong signal peak in scratch 3. It was, at this latter point, where significant coating failure occurred, as the system seemed to start settling down from that point. Once the system had settled down, CoF values remained between 0.2 and 0.3.

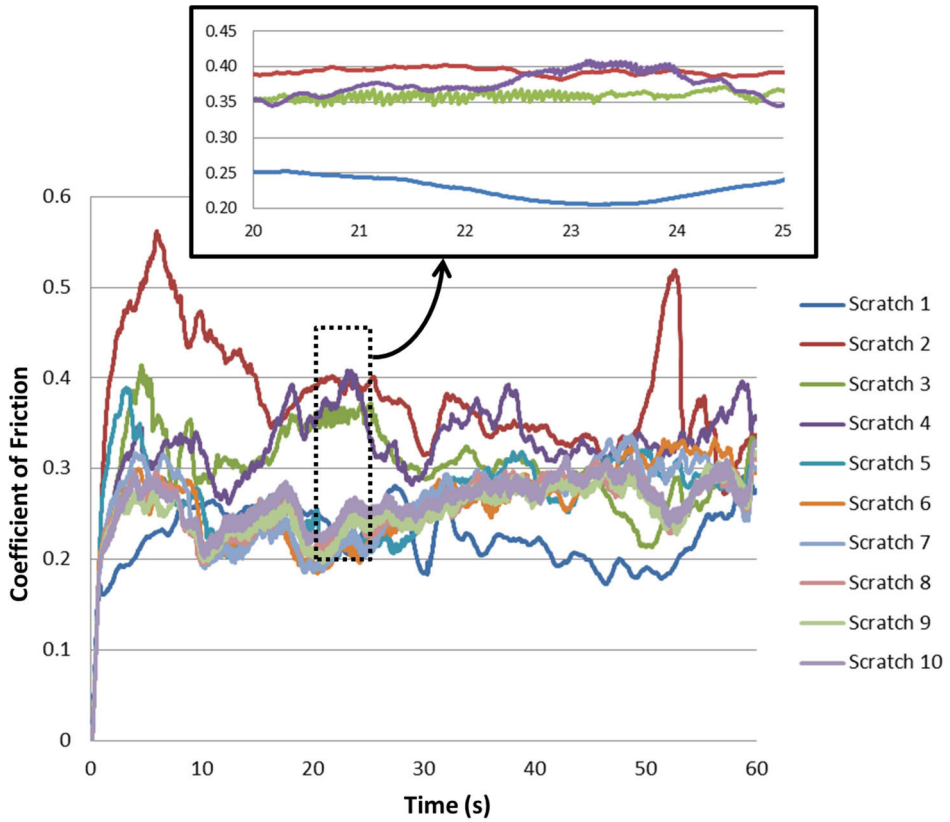

Figure 6.16. CoF measured during a non-lubricated scratch test (10 continuous scratches) performed on a Ni coating electrodeposited under mechanical agitation at 300 rpm. Zoomed-in graph shows when stick-slip friction started to occur (only scratches 1 to 4 are shown for better visibility).

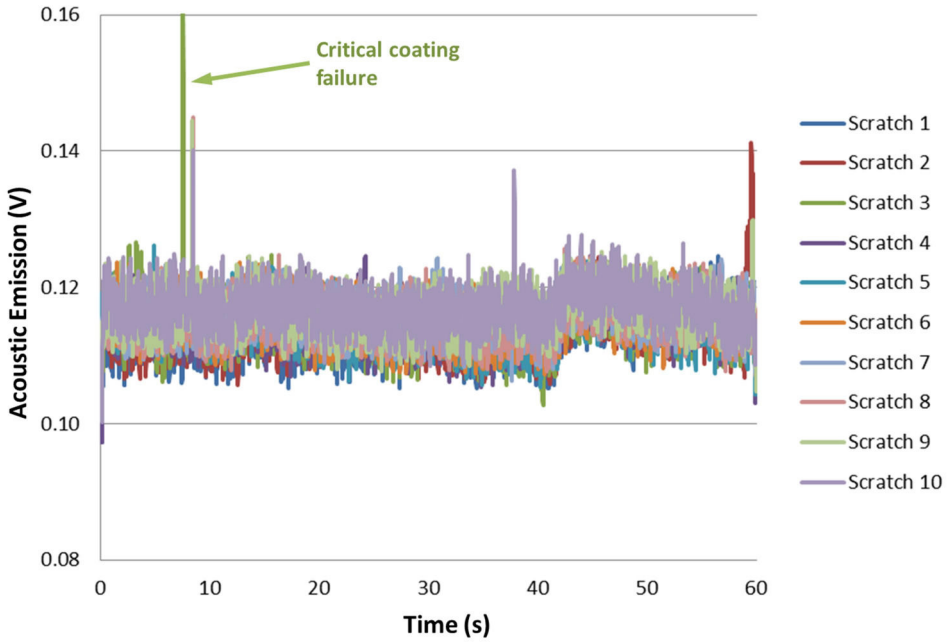

Figure 6.17. Acoustic emission recorded during a non-lubricated scratch test (10 continuous scratches) performed on a Ni coating electrodeposited under mechanical agitation at 300 rpm.

Figure 6.18 A displays the test ball after the non-lubricated scratch test performed on the Ni coating electrodeposited under mechanical agitation. Compared to the lubricated test, the transfer of material from the coating to the ball was far more significant, showing very distinctive ridges and asperities on the surface of the wear lump attached to the test ball. These distinctive asperities match perfectly with the deep scratches observed on the surface of the wear track left on the tested sample after the non-lubricated scratch test (Figures 6.19 B and C), which now was much rougher and irregular and presented a greater amount of debris on the sides of the track forming greater ridges than the wear track left after the lubricated scratch test. The matching between the asperities formed on the wear lump and the surface of the wear track suggests that these hard abrasive asperities were formed by work hardening, phase transitions, and third-body formation at the contact interface during repeated and continuous sliding [4]. All these features indicate that ploughing-alike abrasive wear was again occurring during the non-lubricated scratch test. A different matter is the presence of flat flakes around the ridges and in the wear track and test ball. These flakes would originate from deformed surface material caused by heavy sliding contact [16]:

1. As Ni-Ni contact occurs under non-lubricated conditions, strong 'adhesion' between the 'softer' areas of the surface of the wear lump in the test ball and the surface of the wear track might be expected due to high material compatibility.
2. Tangential shear under compression when strong adhesive bonding takes place generates 'slips' along slip planes in the contact region, resulting in the formation of flake-like shear tongues [4].

Some of these flakes would adhere to the surface of the wear lump during continuous sliding, and hence the larger wear lumps observed in the scratch test performed in the absence of lubrication. In addition, a large amount of accumulated, plastically-deformed debris was left at the end of the wear track, growing after each scratch due to partial removal of the debris attached to the wear lump in the ball and the accumulation of flakes in that area. These later features are characteristic of adhesive wear [4], which would gain

much more importance in this case when no lubricant was used. This means that combined abrasive-adhesive wear would be the wear mechanism during the non-lubricated scratch test, as opposed to pure abrasive wear observed in the lubricated tests.

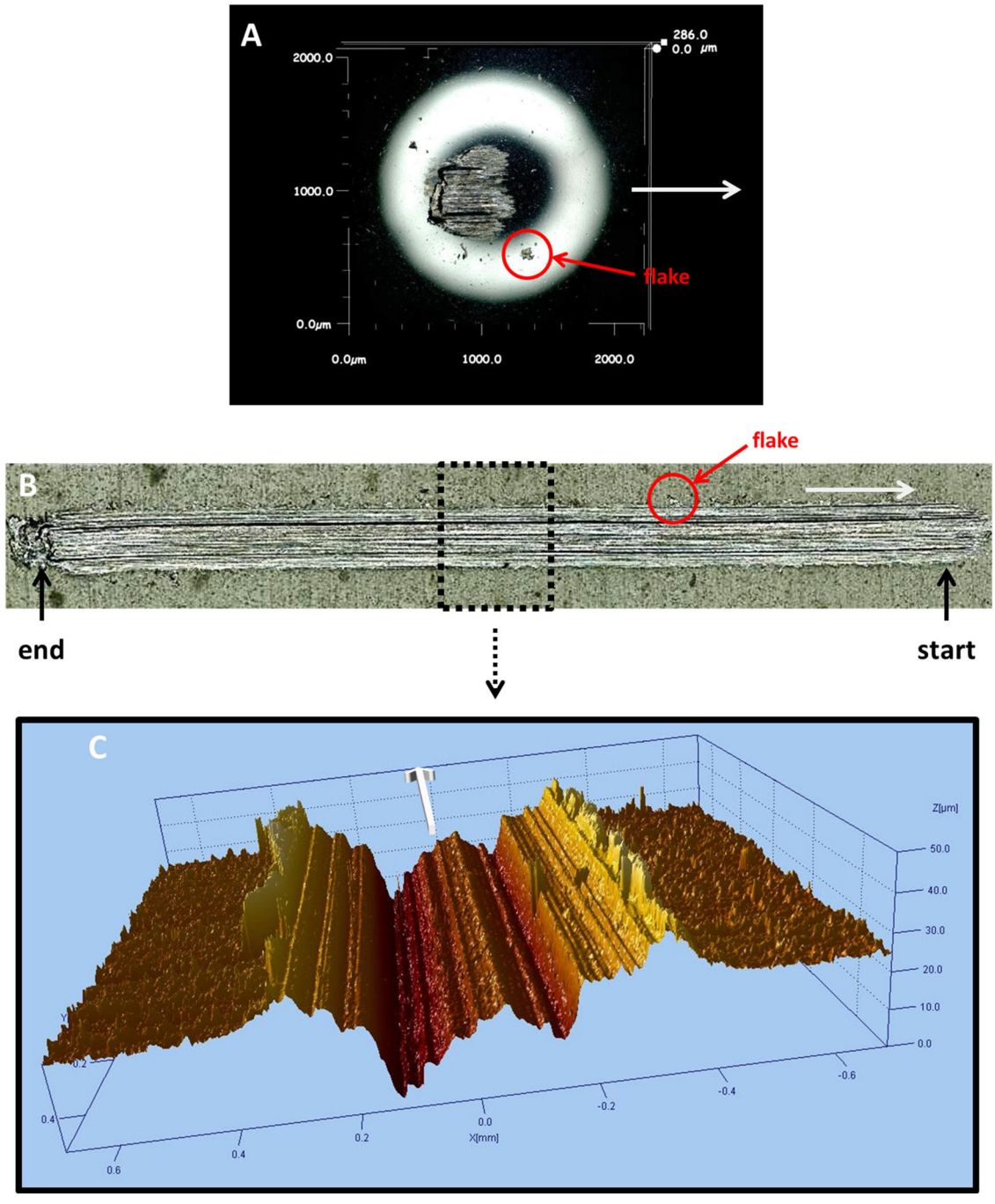

Figure 6.18. Images of the test ball and the wear track left by the test ball on a Ni coating electrodeposited under mechanical agitation at 300 rpm after a non-lubricated scratch test: (A) test ball, (B) wear track left on the sample, (C) 3D depth profile on the middle area of the wear track left on the sample obtained by white light interferometry. The white arrows point the direction of the sample motion.

6.3.2. Ni coatings electrodeposited under ultrasound

Figure 6.19 displays CoF curves measured during the non-lubricated scratch test carried out on a Ni deposit electrodeposited under ultrasound. As in the previous case, fairly low CoF values depicting a smooth curve was recorded during scratch 1. Higher CoF values were measured during scratch 2, where initial signs of stick-slip motion were again noticed, although in this case the CoF curve was not as chaotic as the same scratch recorded for the Ni coating electrodeposited under mechanical agitation. This situation changed in scratch 3, where very high CoF values (up to 0.54) and a very chaotic curve were observed. The same behaviour was observed during scratch 4 until the coating apparently failed after 10-15 seconds, as shown in the AE signal recorded (Figure 6.20). After that, the system seemed to start settling down, with CoF values around 0.2 from scratch 6 onwards.

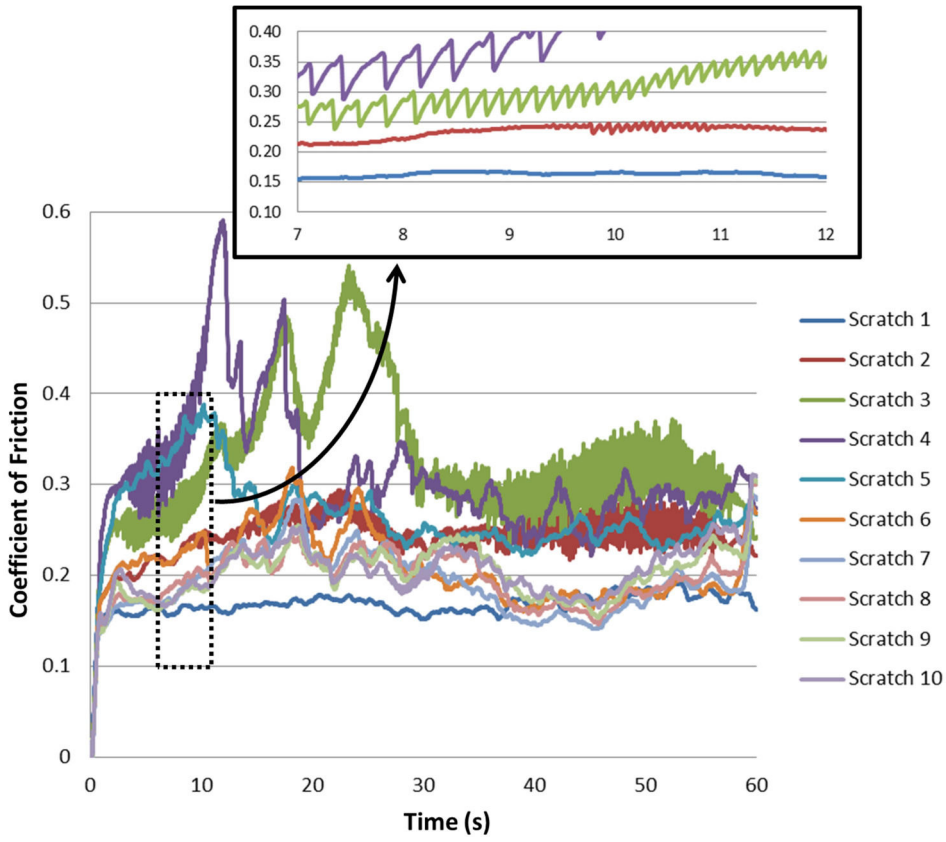

Figure 6.19. CoF measured during a non-lubricated scratch test (10 continuous scratches) performed on a Ni coating electrodeposited under ultrasound at 0.180 W/cm³. Zoomed-in graph shows when stick-slip friction started to occur (only scratches 1 to 4 are shown for better visibility).

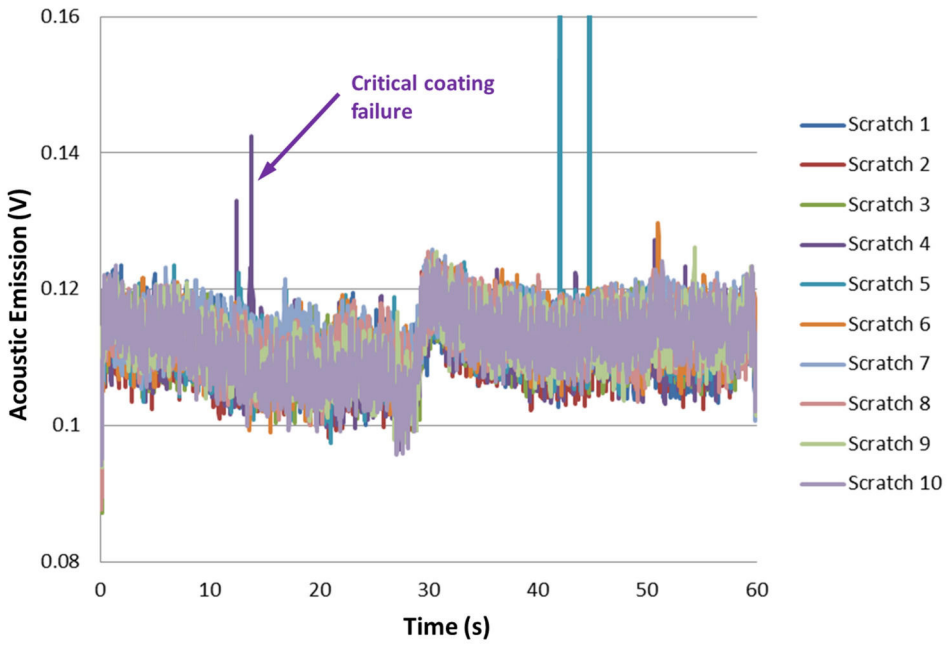

Figure 6.20. Acoustic emission recorded during a non-lubricated scratch test (10 continuous scratches) performed on a Ni coating electrodeposited under ultrasound at 0.180 W/cm^3.

The features observed in the test ball and the wear track left on the sample plated with the Ni coating electrodeposited under mechanical agitation after the non-lubricated scratch test were also observed in the ball and the sample coated with the Ni coating electrodeposited under ultrasound (Figure 6.21). A large transfer of material from the coating to the ball was again noticed in the test ball, where great asperities formed on the surface of the wear lump matched the scratches observed on the surface of the wear track. The wear track was again very rough, presenting large ridges on its sides and a significant number of flat flakes over the track itself and around the ridges. Some of these flakes were also attached to the test ball. A large amount of accumulated debris was also left at the end of the wear track. As in the previous case, combined abrasive-adhesive wear would be the wear mechanism.

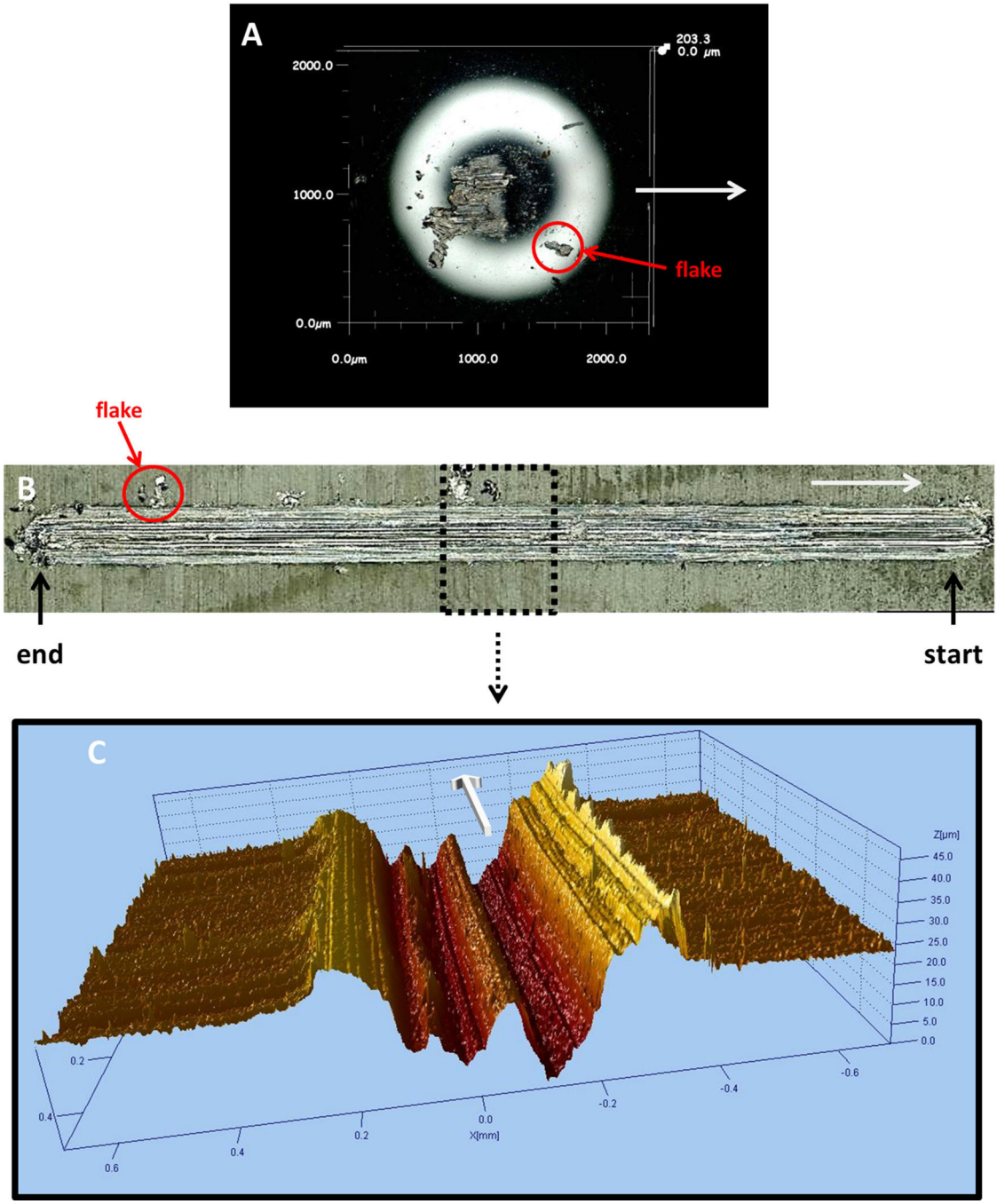

Figure 6.21. Images of the test ball and the wear track left by the test ball on a Ni coating electrodeposited under ultrasound at 0.180 W/cm^3 after a non-lubricated scratch test: (A) test ball, (B) wear track left on the sample, (C) 3D depth profile on the middle area of the wear track left on the sample obtained by white light interferometry. The white arrows point the direction of the sample motion.

6.3.3. Ni/hBN COMPOSITE COATINGS ELECTRODEPOSITED UNDER ULTRASOUND

Figure 6.22 displays the CoF curves recorded during a non-lubricated scratch test performed on a Ni/hBN composite coating electrodeposited under ultrasound at 0.180

W/cm³. Again, low CoF values depicting a smooth curve were measured during scratch 1. CoF values did not fluctuate as much as in previous cases, and CoF values decreased during the second half of scratches 2-4, possibly due to the action of the hBN particles, which could have more influence when no lubricant was used. The CoF values measured during scratch 5 seemed to follow the same trend of previous scratches until a significant drop in CoF was observed after 10-15 seconds, when a first AE signal peak was observed (Figure 6.23), possibly due to coating failure. After that point, CoF values went down during the rest of the scratches as the tribosystem settled down and CoF values around 0.2-0.25 were measured from scratch 6 onwards. Before the reported coating failure, no stick-slip motion was observed, and only some signs of stick-slip motion were observed at the end of scratch 5 once the coating had already failed (see zoomed-in graph in Figure 6.22).

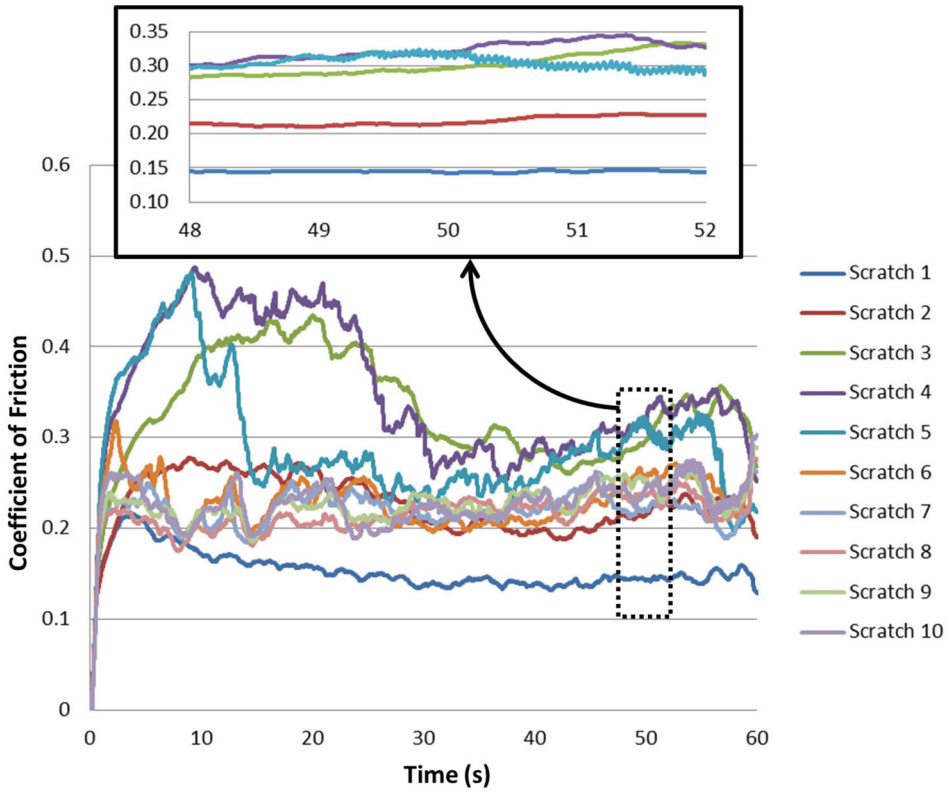

Figure 6.22. CoF measured during a non-lubricated scratch test (10 continuous scratches) performed on a Ni/hBN composite coating electrodeposited under ultrasound at 0.180 W/cm³. Zoomed-in graph shows when stick-slip friction started to occur (only scratches 1 to 5 are shown for better visibility).

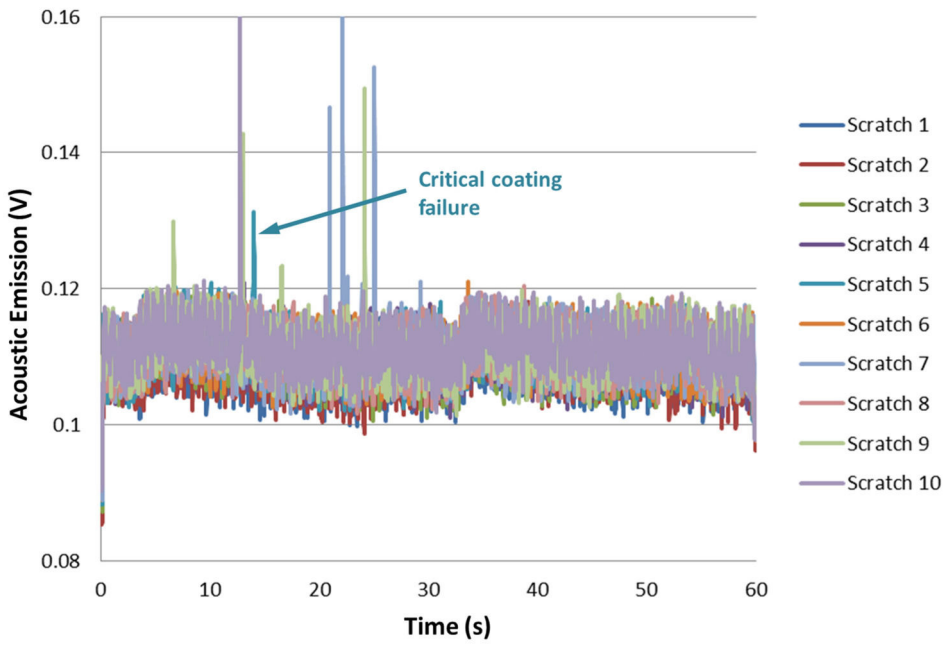

Figure 6.23. Acoustic emission recorded during a non-lubricated scratch test (10 continuous scratches) performed on a Ni/hBN composite coating electrodeposited under ultrasound at 0.180 W/cm^3.

The features observed in the test ball and the wear track left on the Ni/hBN composite coating (Figure 6.24) after the non-lubricated scratch test were again very similar to those previously observed for both Ni coatings electrodeposited under either mechanical agitation or ultrasound. A large amount of the coating material was again transferred from the sample to the ball during the scratch test. Again, great asperities matching the scratches formed on the surface of the wear track were observed. A rough wear track was presenting large ridges on its sides was left on the tested sample after the test. As in previous cases, a significant number of flat flakes were noticed over the wear track, around the ridges enclosing the wear track and on the test ball. In addition, a significant accumulation of debris was clearly notice at the end of the wear track. As in previous cases, combined abrasive-adhesive wear would again be the wear mechanism.

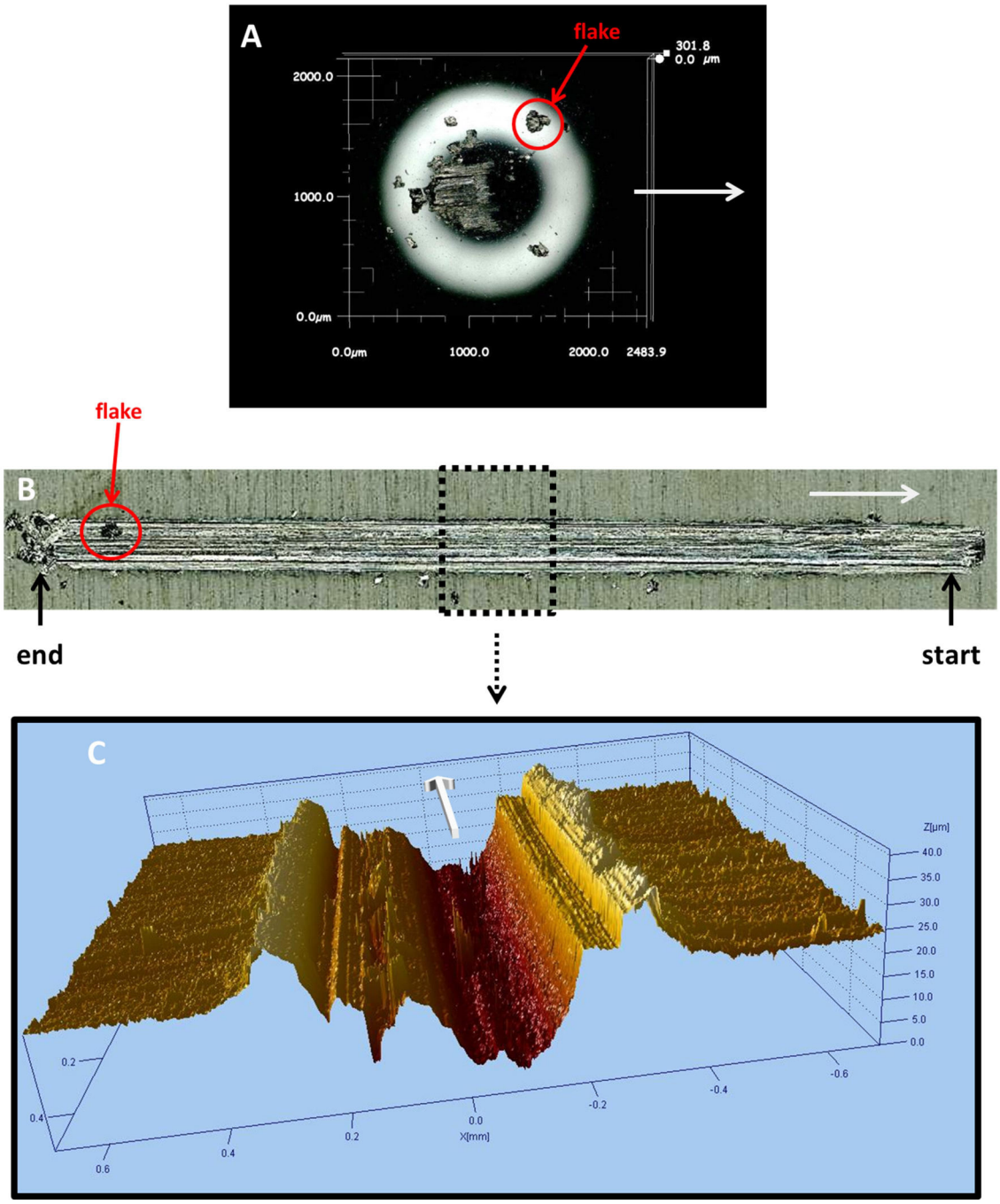

Figure 6.24. Images of the test ball and the wear track left by the test ball on a Ni/hBN composite coating electrodeposited under ultrasound at 0.180 W/cm^3 after a non-lubricated scratch test: (A) test ball, (B) wear track left on the sample, (C) 3D depth profile on the middle area of the wear track left on the sample obtained by white light interferometry. The white arrows point the direction of the sample motion.

6.3.4. Ni/WS_2 COMPOSITE COATINGS ELECTRODEPOSITED UNDER ULTRASOUND

Figure 6.25 displays CoF values measured during the non-lubricated scratch test carried out on a Ni/WS_2 composite coating electrodeposited under ultrasound at 0.180 W/cm^3. In this

case, the CoF curves obtained were fairly constant, ranging CoF values between 0.15 and 0.3 during the whole experiment with no signs of stick-slip motion. As opposed to what was observed for the other Ni-based coatings evaluated under non-lubricated conditions, no signs of coating failure were seen in the recorded AE signal (Figure 6.26).

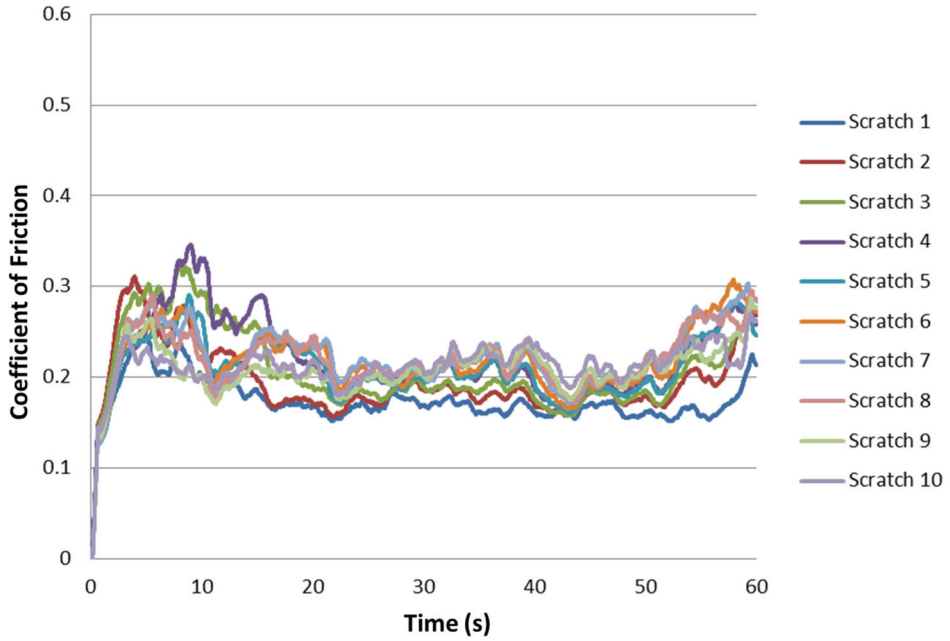

Figure 6.25. CoF measured during a non-lubricated scratch test (10 continuous scratches) performed on a Ni/WS_2 composite coating electrodeposited under ultrasound at 0.180 W/cm^3.

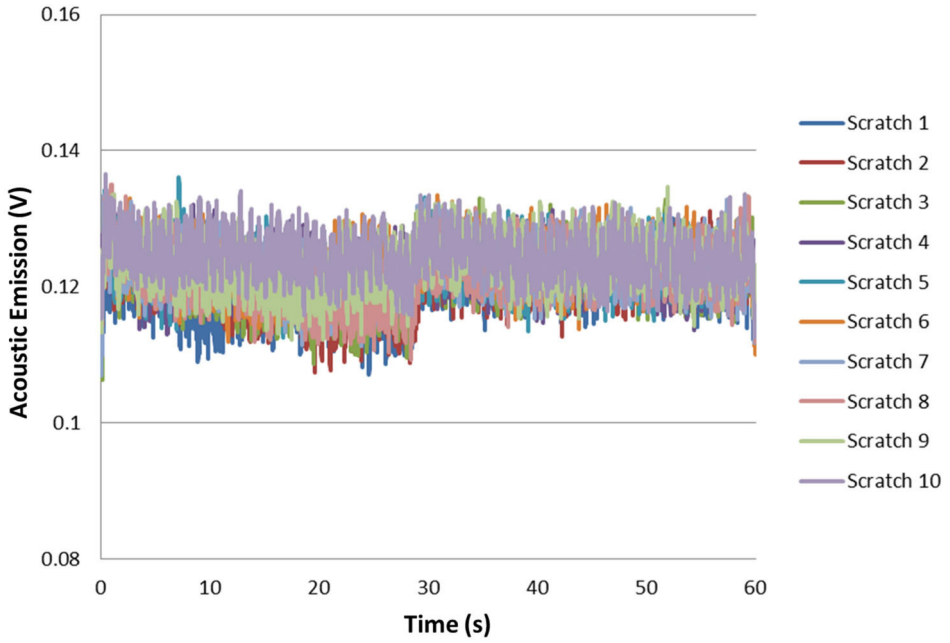

Figure 6.26. Acoustic emission recorded during a non-lubricated scratch test (10 continuous scratches) performed on a Ni/WS_2 composite coating electrodeposited under ultrasound at 0.180 W/cm^3.

A reasonably large wear lump was observed in the test ball used during the non-lubricated scratch test (Figure 6.27 A), although in this case the amount of material transferred from the ball to the coating was not as significant as in the non-lubricated tests performed on the samples coated with the other Ni-based coatings. A smaller amount of worn-out material forming ridges on both sides of the wear track was observed in the sample coated with the Ni/WS_2 composite coating (Figure 6.27 B and C). Little accumulation was also noticed at the end of the wear track, as opposed to the larger amount of debris that was observed on the other Ni-based coatings tested under the same non-lubricated conditions. Although the surface of the wear track left after the non-lubricated scratch test was not as smooth as the one left after the lubricated test as some scratches were clearly seen in this case, it was far more rounded than the wear track left in the samples coated with the other Ni-based coatings. In addition, just a few flat flakes were noticed around the ridges in the wear track and in the test ball after the test. Compared to the test ball used in the lubricated scratch test performed on the same composite coating where a black thin film had formed during the test, no apparent signs of the formation of a thin WS_2 film were noticed on the surface of the wear lump in the test ball use for the non-lubricated scratch test. These results show that, although a combination of abrasive-adhesive wear also occurred during the non-lubricated scratch test performed on the Ni/WS_2 composite coating electrodeposited under ultrasound at 0.180 W/cm^3, the 'adhesive' component was far less significant than the 'abrasive' one in the resulting wear mechanism, and hence a smaller wear lump formed on the surface of the test ball and far less severe wear of the coating/substrate system occurred due to the presence of the WS_2 particles within the Ni matrix.

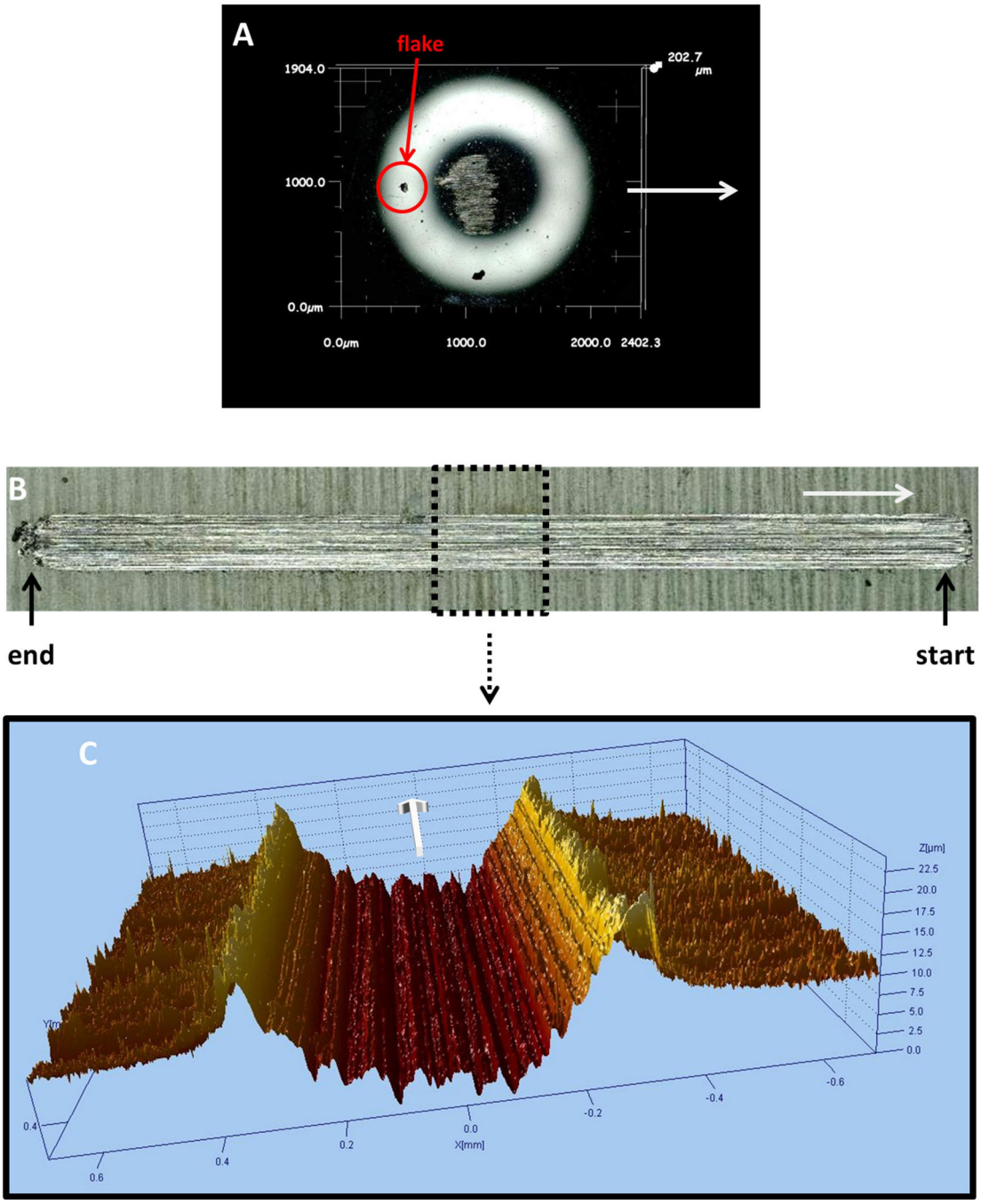

Figure 6.27. Images of the test ball and the wear track left by the test ball on a Ni/WS_2 composite coating electrodeposited under ultrasound at 0.180 W/cm^3 after a lubricated scratch test: (A) test ball, (B) wear track left on the sample, (C) 3D depth profile on the middle area of the wear track left on the sample obtained by white light interferometry. The white arrows point the direction of the sample motion.

6.3.5 SUMMARY AND DISCUSSION OF RESULTS

Figure 6.27 displays the average CoF values of each scratch (bars depict the maximum CoF value measured during each scratch) for the different Ni-based coatings tested under non-lubricated conditions. After the initial scratch, high CoF values were observed for the Ni/hBN composite coating electrodeposited under ultrasound and the Ni deposits produced under either mechanical agitation or ultrasound. These three materials eventually failed after a few scratches: Ni coatings electrodeposited under ultrasound routinely failed during scratch 3, while the Ni deposits and the Ni/hBN composite coatings electrodeposited under ultrasound generally failed during scratches 4 and 5, respectively. In all cases, coating failure was preceded by the highest average CoF value, which would be measured in the scratch prior to the one where coating failure was actually noticed. Stick-slip motion also occurred before or during the failure event, being potentially the cause and/or consequence of coating failure by seizure of the coating and the transfer/welding of the coating material to the test ball, which agrees with the significantly larger wear lumps that formed on the contact surface of the test balls used for testing both Ni deposits and Ni/hBN composite coatings. Nevertheless, there were some differences between these three coatings:

- Stick-slip motion was far more significant and occurred more often in the Ni deposits produced under ultrasound. This could be related to the more fragmented structure that these coatings present, i.e. combination of columnar crystals with refined grains, as the ball would slide in areas with higher proportion of small grains ('stick'), whereas 'adhesive' forces would slow down the motion of the ball in areas richer on columnar grains ('slip'). In addition, stick-slip motion was generally observed before coating failure was signified by the AE signal, meaning that stick-slip motion would probably be the cause of seizure failure of the Ni coating electrodeposited under ultrasound.
- For both the Ni deposit produced under mechanical agitation and the Ni/hBN composite coating electrodeposited under ultrasound stick-slip motion was not as

severe as for the Ni coating electrodeposited under ultrasound, and it occurred once coating failure had already been pointed out by AE signal. This means that, for said coatings, stick-slip motion was a consequence of seizure of both coatings rather than being the cause.

- A small contribution of the presence of the hBN particles could be noticed in the performance of the Ni/hBN composite coatings, as the incorporation of these particles into the Ni coating seemed to 'stabilise' the tribological performance of the coating (CoF curves recorded prior to the failure event were not as chaotic as those recorded for both Ni deposits electrodeposited under either mechanical agitation or ultrasound) and retard to some extent the seizure failure of the coating.

In all three previous cases (Ni/hBN composite coating electrodeposited under ultrasound and Ni deposits produced under either mechanical agitation or ultrasound), different phenomena would contribute to the occurrence of stick-slip motion and/or seizure failure of the coating such as changes in the area of contact and surface temperature [3], which would be expected where very similar/compatible materials are in contact with absence of lubrication as in non-lubricated Ni-Ni contact. Combined abrasive-adhesive wear was the wear mechanism, resulting in severe wear of the samples coated with the Ni/hBN composite coatings electrodeposited under ultrasound and the Ni deposits produced under either mechanical agitation or ultrasound.

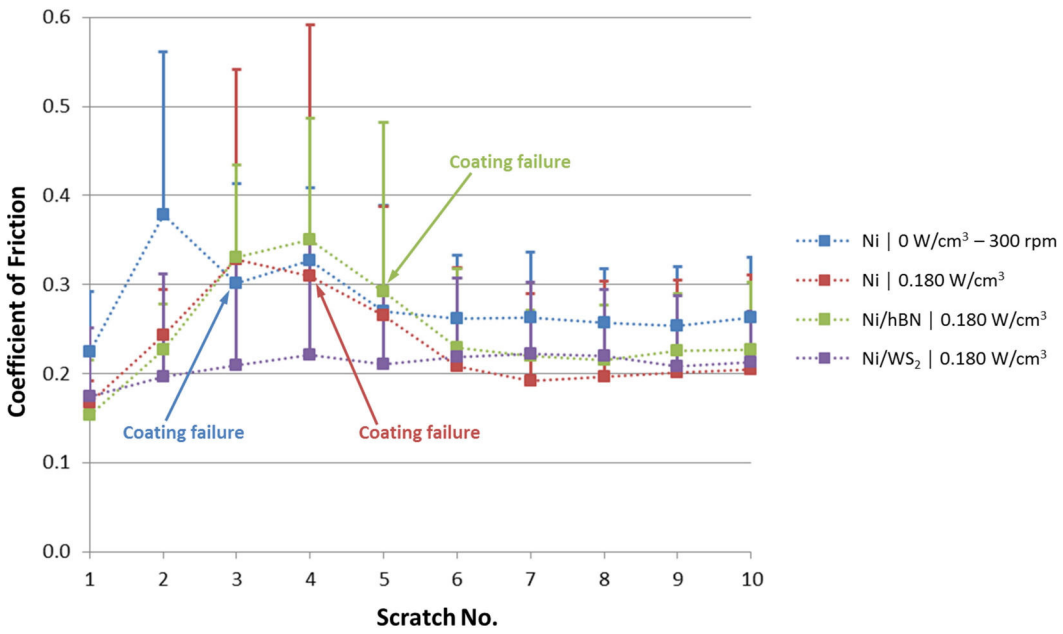

Figure 6.28. Average CoF estimated from a non-lubricated scratch test (10 continuous scratches) performed on different Ni-based coatings. Bars indicate maximum CoF values recorded during each scratch.

Compared with the Ni/hBN composite coatings electrodeposited under ultrasound and the Ni deposits produced under either mechanical agitation or ultrasound, the Ni/WS_2 composite coatings electrodeposited under ultrasound exhibited a very different behaviour, not only due to the reasonably smooth and constant CoF values measured during the tests and the absence of stick-slip motion, but also due to the fact that the Ni/WS_2 composite coatings did not fail during any of the non-lubricated scratch tests performed on these coatings. The main reason for this would again be the presence of the WS_2 particles. Nevertheless, no thin WS_2 film apparently formed on either the wear track or the test ball used. In addition, asperities still formed on the surface of the wear lump in the test ball, resulting in the appearance of scratches in the wear track. This leads to the assumption that, in this case, WS_2 particles would act as a lubricant lowering CoF by rolling friction mechanisms as suggested by Rapoport et al. [8]. Rolling friction mechanisms provided by IF-WS_2 nanoparticles were also suggested by García-Lecina et al. [17] after non-lubricated tribological tests (ball-on-disc tests conducted under very low loads of 1 N) performed on ultrasound-assisted electrodeposited Ni/IF-WS_2 composite coatings, where some of the IF-WS_2 particles incorporated into the coating would be released, serving as spacers and

preventing asperity contact between the mating surfaces. A different friction mechanism, also under non-lubricated conditions, was suggested by Sivandipoor and Ashrafizadeh for their electroless deposited Ni–P/WS_2 composite coatings (pin-on-disc tests also conducted under very low loads of 1 N), as they reported the formation of a WS_2-rich film forming discrete regions along the surface of the wear track left on the tested coatings [12]. No clear evidence of such films was noticed in the non-lubricated tests performed on the Ni/WS_2 composite coatings developed during the present research project. Nevertheless, the potential presence and contribution of these WS_2-rich regions on the surface of the wear track must not be discarded, and more detailed studies should be carried out in order to fully understand the friction mechanisms that may take place when WS_2 particles are incorporated into Ni coatings used as tribologically active layers in non-lubricated tribological systems, as all of the more fundamental research dealing with the friction mechanisms in systems with the presence of WS_2 particles is mainly focused on the use of nano-size WS_2 particles in lubricated systems [8-11,18].

Significant differences were observed in terms of transference of material from coating to test ball and appearance of wear track left after non-lubricated scratch tests for the Ni/WS_2 composite coatings compared to the other three Ni-based coatings. Related to this, the comparison of the cross-sectional depth profile measured at the middle of each wear track left after non-lubricated scratch tests performed on the four Ni-based coatings tested (Figure 6.29) shows that, whereas very irregular wear tracks showing very deep scratches (up to 24 μm deep) were observed for both Ni deposits produced under either mechanical agitation or ultrasound and the Ni/hBN composite coatings electrodeposited under ultrasound, a reasonably smoother wear track with far less deeper and irregular scratches (up to 11 μm deep) was always left on the samples coated with the Ni/WS_2 composite coating electrodeposited under ultrasound. The cause for the depth achieved in both Ni deposits and Ni/hBN composite coatings is the abrasive action of the hard Ni asperities formed on the large wear lumps formed covering the contact surface of the test balls. As a

result, the test ball ended up sliding mainly over the Pb-bronze substrate in the samples coated with both Ni deposits and the Ni/hBN composite coating, and hence the decrease in CoF values down to 0.2-0.25 once the coating failed and the tribosystem settled down. For the Ni/WS_2 composite coating though, the ball was still partially sliding over the coating after 10 scratches with relatively constant CoF around 0.2-0.22.

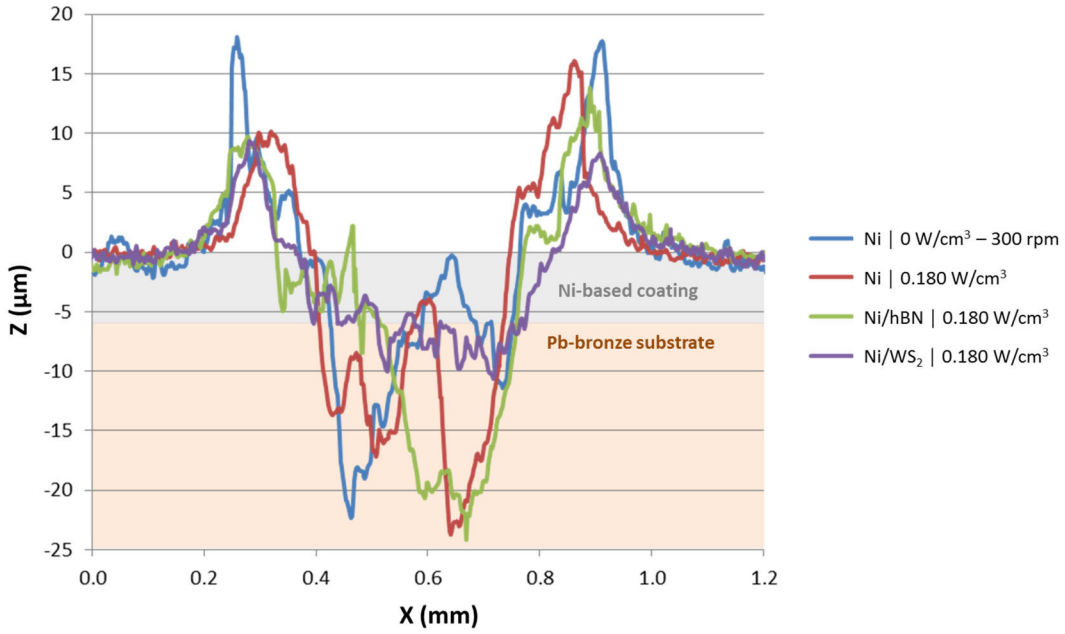

Figure 6.29. Depth profile measured at the middle of the wear track left by the test ball during a non-lubricated scratch test (10 continuous scratches) performed on different Ni-based coatings. Data from 3D depth profiles obtained by white light interferometry.

$\Delta \mathbf{V}_g$ and $\Delta \mathbf{V}_r$ values were again estimated from the depth profiles measured in the middle of the wear tracks left after the non-lubricated scratch tests performed on the four different Ni-based coatings evaluated in the present study (Table 6.2). As expected, the Ni/WS_2 composite coating presented the lowest $\Delta \mathbf{V}_r$ and $\Delta \mathbf{V}_g$ values, which again indicate a higher wear resistance that the other three Ni-based coatings tested under non-lubrication. Regarding the other coatings, $\Delta \mathbf{V}_r$ and $\Delta \mathbf{V}_g$ values did not show a coherent trend, as opposed to the analogous values previously estimated for the same coatings after the lubricated scratch tests. The main reason for this is the relatively high error of the $\Delta \mathbf{V}_r$ and $\Delta \mathbf{V}_g$ values estimated, which are significantly underestimated for both Ni deposits and the Ni/hBN

composite coating due to the abrasive-adhesive nature of wear during the non-lubricated scratch tests, as opposed to the pure abrasive wear observed during the lubricated scratch tests (calculation of $\Delta \mathbf{V}_r$ and $\Delta \mathbf{V}_g$ as a rough estimation of the wear resistance is only suggested when abrasive wear mechanism is predominant [4]). Regarding this, $\Delta \mathbf{V}_r$ values were underestimated for both Ni deposits and the Ni/hBN composite coating due to the inaccurate estimation of the debris volume, as the large amount of debris accumulated at the end of the wear tracks observed in the Ni/hBN composite coating and both Ni deposits is not accounted for. $\Delta \mathbf{V}_g$ values were also difficult to estimate from the depth profile due to the nature of the wear track left on the samples coated with both Ni deposits and the Ni/hBN composite coating (very rough and uneven wear track with large and deep scratches), as opposed to the relatively easy estimation of those same values for the Ni/WS_2 composite coating, which presented a far more regular and even depth profile.

Table 6.2. $\Delta \mathbf{V}_r$ and $\Delta \mathbf{V}_g$ values estimated from cross-sectional depth profiles measured at the middle of the wear track left by the test ball during non-lubricated scratch tests (10 continuous scratches) performed on different Ni-based coatings.

	$\Delta \mathbf{V}_g$ (μm^2)	$\Delta \mathbf{V}_r$ (μm^2)
Ni | 0 W/cm³ – 300 rpm	3190	2572
Ni | 0.180 W/cm³	4346	2371
Ni/hBN | 0.180 W/cm³	4595	2066
Ni/WS_2 | 0.180 W/cm³	2709	1342

In summary, the results observed during the non-lubricated scratch are analogous to the results previously obtained from the lubricated tests, as the Ni/WS_2 composite coating again exhibited the best tribological performance under non-lubricated conditions. In this case, besides exhibiting the lowest CoF and the highest wear resistance, the Ni/WS_2 composite coating was the only coating material that did not show any signs of critical coating failure

or seizure, as the rest of the Ni-based coatings evaluated under non-lubricated conditions failed during the scratch tests carried out.

6.4. CONCLUSIONS

The results previously discussed indicate that, whereas Ni deposits and Ni/hBN composite coatings electrodeposited under ultrasound show a tribological performance similar to that of Ni coatings electrodeposited under mechanical agitation equivalent to those currently used as barrier layer coatings in bronze-based bearings for medium-speed diesel engines, Ni/WS_2 composite coatings electrodeposited under ultrasound exhibited a remarkable enhancement of the tribological performance under either lubricated and non-lubricated conditions. Under lubricated conditions, a thin WS_2 film grows on the surface of the wear lump formed on the test ball after repeated and continuous sliding action, not only resulting in a lower coefficient of friction, but also in the prevention of stick-slip motion that would lead to seizure failing of the coating. Under non-lubricated conditions, although no clear evidence of the formation of a thin WS_2 film on the surface of the wear lump were noticed, reasonably smooth sliding was achieved due to the potential release and presence of WS_2 particles in the contact, which would then act as spacers preventing asperity contact between the test ball and the surface of the tested samples. For non-lubricated conditions, the incorporation of WS_2 into Ni coatings not only results in a lower coefficient of friction of the coating, but also in the prevention of seizure failure of the coating, as Ni/WS_2 was the only composite coating material that did not seize during the non-lubricated scratch tests. The performance here reported for ultrasound-assisted electrodeposited Ni/WS_2 composite coatings under lubricated and non-lubricated conditions would be of critical importance in bronze-based bearings where the Ni-based interlayer is exposed under mixed-film and boundary lubrication, as the Ni/WS_2 composite coating would ensure a remarkably smoother transition without seizure from sliding over the overlay coating (before the interlayer is exposed) to sliding over the lining material.

6.5. REFERENCES

[1] K.C. Ludema, Friction, in: B. Bhushan (Ed.), Modern Tribology Handbook, CRC Press, Boca Raton-London-New York-Washington D.C., 2000.

[2] S.M. Hsu, R.S. Gates, Boundary lubrication and boundary lubriating films, in: B. Bhushan (Ed.), Modern Tribology Handbook, CRC Press, Boca Raton-London-New York-Washington D.C., 2000.

[3] F.P. Bowden, D. Tabor, The friction and lubrication of solids, Oxford University Press, Oxford, 1954 (reprinted as part of Oxford Classic Series 2001).

[4] K. Kato, K. Adachi, Wear Mechanisms, in: B. Bhushan (Ed.), Modern Tribology Handbook, CRC Press, Boca Raton-London-New York-Washington D.C., 2000.

[5] H.A. Spike, Lubr. Sci. 9 (1997) 221.

[6] X. Ni, H.S. Cheng, Seizure failure of copper-lead with overlay and aluminum-tin connecting rod bearings, Tribology Transactions 39 (1996) 121-129.

[7] Q. Wang, Seizure failure of journal-bearing conformal contacts, Wear 210 (1997) 8-16.

[8] L. Rapoport, Yu. Bilik, Y. Feldman, M. Homyonfer, S.R. Cohen, R. Tenne, Nature 387 (1997) 791.

[9] Y. Golan, C. Drummond, M. Homyonfer, Y. Feldman, R. Tenne, J. Israelachvily, Adv. Mater. 11 (1999) 934.

[10] L. Rapoport, M. Lvovsky, I. Lapsker, V. Leshinsky, Y. Volovik, Y. Feldman, A. Zak, R. Tenne, Adv. Eng. Mater. 3 (2001) 71.

[11] L. Rapoport, V. Leshchinsky, I. Lapsker, Yu. Volovik, O. Nepomnyashchy, M. Lvovsky, R. Popovitz-Biro, Y. Feldman, R. Tenne, Wear 255 (2003) 785.

[12] I. Sivandipoor, F. Ashrafizadeh, Appl. Surf. Sci. 263 (2012) 314.

[13] L. Wang, Y. Gao, T. Xu, Q. Xue, Mater. Chem. Phys. 99 (2006) 96.

[14] D.H. Jeong, F. Gonzalez, G. Palumbo, K.T. Aust, U. Erb, Scripta Mater. 44 (2001) 493.

[15] E. Pompei, L. Magagnin, N. Lecis, P.L. Cavallotti, Electrochim. Acta 54 (2009) 2571.

[16] W.A. Glaeser, Wear Debris Classification, in: B. Bhushan (Ed.), Modern Tribology Handbook, CRC Press, Boca Raton-London-New York-Washington D.C., 2000.

[17] E. García-Lecina, I. García-Urrutia, J.A. Díez, J. Fornell, E. Pellicer, J. Sort, Electrochim. Acta 114 (2013) 859.

[18] M. Ratoi, V.B. Niste, J. Walker, J. Zekonyte, Tribol. Lett. 52 (2013) 81.

7. PERFORMANCE OF Ni/WS_2 COMPOSITE COATINGS ACTING AS DIFFUSION BARRIER LAYERS

7.1. OVERVIEW

In previous chapters, three different materials were depicted as suitable candidates to replace electrodeposited Ni coatings currently used as diffusion barrier layers in bronze-based bearings: i) Ni deposits produced under ultrasound at 0.180 W/cm^3, ii) Ni/WS_2 composites electrodeposited under ultrasound at 0.180 W/cm^3, and iii) Ni/hBN composite coatings electrodeposited under ultrasound at 0.180 W/cm^3. Tribological tests then showed that, whereas Ni deposits and Ni/hBN composite coatings electrodeposited under ultrasound exhibited a tribological performance very similar to that of standard Ni coatings electrodeposited under mechanical agitation, Ni/WS_2 composite coatings electrodeposited under ultrasound exhibited a significantly enhanced tribological performance. To conclude the PhD research project here presented, the performance of the ultrasound-assisted

electrodeposited Ni/WS_2 composite coatings acting as diffusion barrier layers was evaluated and compared with the standard Ni coating electrodeposited under mechanical agitation. This comparison was established using two different responses: i) adhesion or 'bonding strength' and ii) 'resistance to diffusion'.

7.2. ADHESION TESTS

Good adhesion/bonding properties are one of the basic requirements that a diffusion barrier layer must meet. Bonding failure due to poor adhesion of either the overlay to the Ni/WS_2 composite coating or the Ni/WS_2 composite coating to the lining in a demanding environment such as an internal combustion engine where high loads are exerted could end up in a critical failure of the engine. Related to this, qualitative 'knife and tape' adhesion tests [1] were routinely performed on the different coatings and samples produced during the research project, indicating in all cases no signs of de-attachment of the electroplated Ni coatings from the substrate. Nevertheless, quantitative adhesion or 'bonding' tests were also performed with an in-house method to evaluate the improvement/decline of the bonding properties of real bearing systems with Ni/WS_2 diffusion barrier layers (more information about this method is found in Appendix D). The main purpose was to evaluate if there was any undesired effect in terms of bonding/de-attachment between the Sn-Cu overlay electroplated on top of a Ni/WS_2 diffusion barrier compared to the same electroplated on a benchmark Ni diffusion barrier similar to that currently found in real bearings. The reason for this is that Ni/WS_2 diffusion barriers are far more likely to present a 'dirtier' surface due to the presence WS_2 particles loosely attached to the surface (GD-OES data and FIB-SEM images in Chapter 5 apparently indicated so) than the standard Ni diffusion barriers, and this could indeed result in poor bonding between the diffusion barrier layer and the overlay electrodeposited on top.

The bonding tests were performed on samples simulating real bearing systems which consisted of:

1. A steel backing
2. A Pb-bronze lining deposited over the steel backing
3. A diffusion barrier layer (either Ni coatings electrodeposited under mechanical agitation or Ni/WS_2 composite coatings electrodeposited under ultrasound) over the Pb-bronze lining
4. A Sn-Cu overlay electrodeposited over the diffusion barrier layer

Figure 7.1 displays the results of the bonding tests performed in samples simulating real bearing systems where the two different Ni-based coatings evaluated (Ni deposits produced under mechanical agitation and Ni/WS_2 composite coatings electrodeposited under ultrasound) were used as diffusion barrier layers. For samples tested as plated, 'failure' loads (i.e. load measured immediately before bonding failure occurred in the overlay system) achieved in the samples with a Ni/WS_2 diffusion barrier layer were slightly higher (≈17.5 MPa) than the failure load measured in samples with a Ni diffusion barrier layer (≈15.5 MPa). For samples heat-treated at 130 °C for 500 hours, a significant increase was observed in the failure load measured in samples with a Ni/WS_2 diffusion barrier layer (≈22.4 MPa), whereas it remained the same in samples with a Ni diffusion barrier layer (≈15.0 MPa).

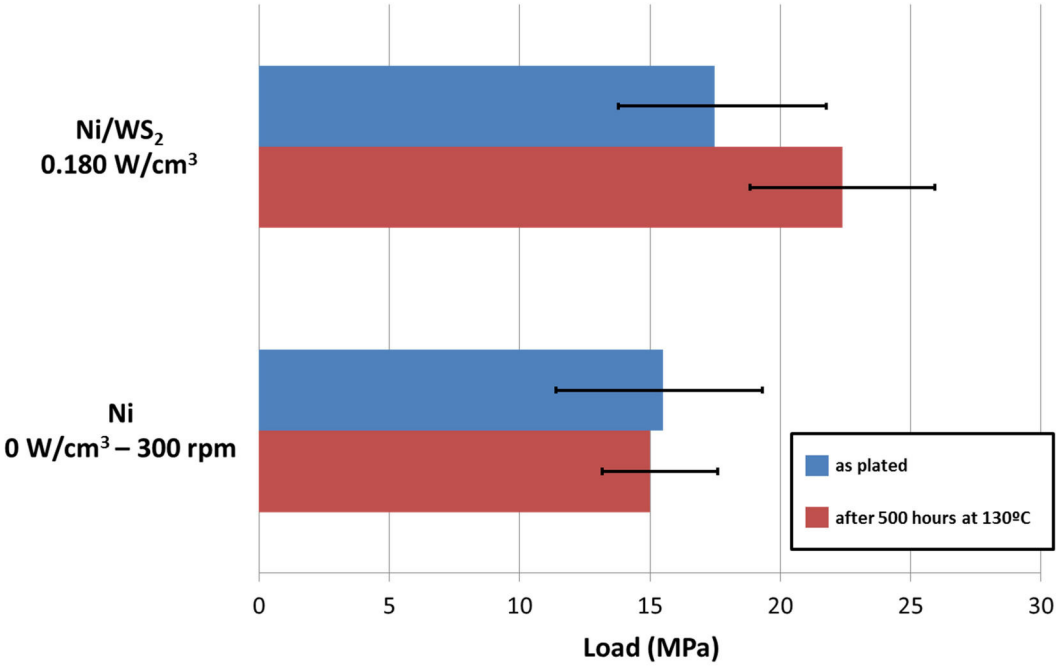

Figure 7.1. Load measured immediately before bonding failure of overlay systems in samples simulating real bearing systems as plated and after being heat-treated for 500 hours at 130°C. Samples consisted of a steel backing, a Pb-bronze lining deposited over the steel backing, a Ni-based diffusion barrier layer (either a Ni electrodeposit produced under mechanical agitation or a Ni/WS_2 composites electrodeposited under ultrasound) over the lining, and an electrodeposited Sn-Cu overlay on top.

The surface of both sample and dolly was also investigated after each bonding test in order to elucidate where the main bonding failure was taking place (Figures 7.2 and 7.3 for samples with Ni and Ni/WS_2 diffusion barrier layers, respectively). For the samples tested as plated, the Sn-Cu overlay was covering most of the surface of the samples with a few areas where the diffusion barrier layer was exposed due to the removal of the Sn-Cu overlay, which was transferred to the dolly. The same trends in the transfer of Sn-Cu overlay material from the sample to the dolly and the partial exposure of the diffusion barrier layer were also observed in the surface of the samples tested after being heat-treated. In this case though, the amount of Sn-Cu overlay material transferred from sample to dolly and the area of the diffusion barrier layer exposed were generally smaller.

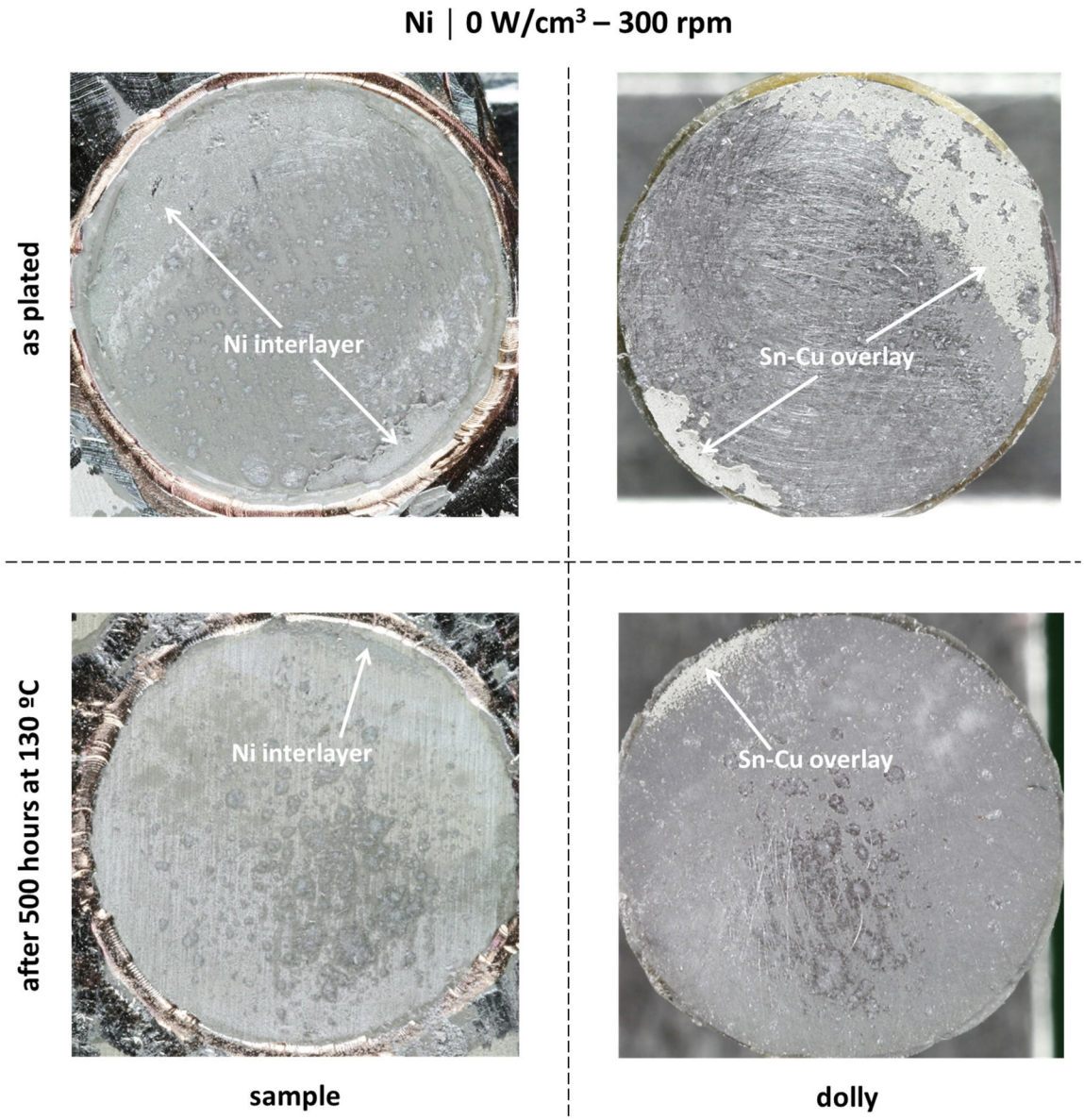

Figure 7.2. Images of the surface of samples and dollies after bonding tests performed on samples simulating real bearing systems consisting of a steel backing, a Pb-bronze lining deposited over the steel backing, a Ni diffusion barrier layer electrodeposited over the lining under mechanical agitation at 300 rpm, and an electroplated Sn-Cu overlay on top.

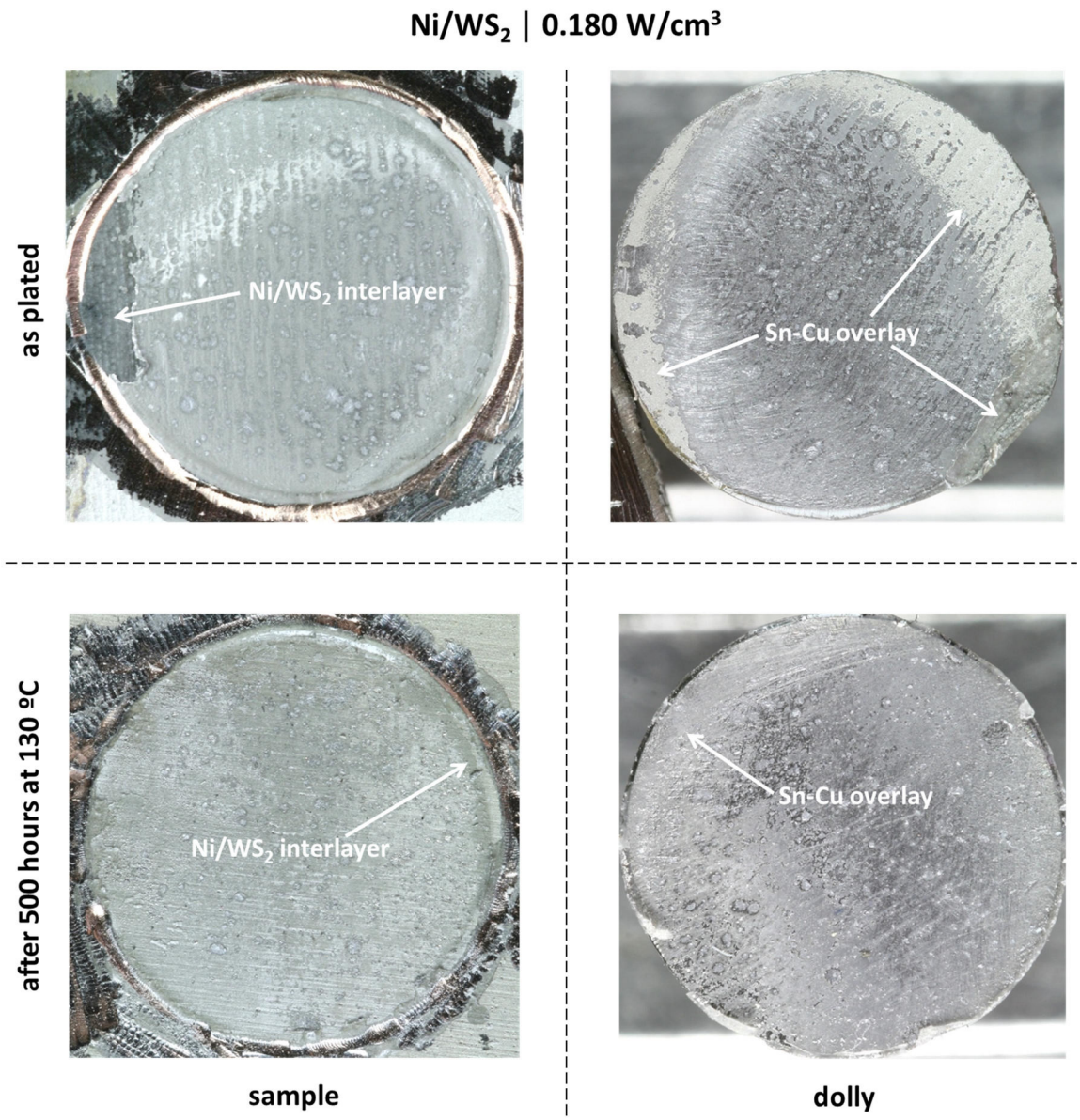

Figure 7.3. Images of the surface of samples and dollies after bonding tests performed on samples simulating real bearing systems consisting of a steel backing, a Pb-bronze lining deposited over the steel backing, a Ni/WS_2 diffusion barrier layer electrodeposited over the lining under ultrasound at 0.180 W/cm^3, and an electrodeposited Sn-Cu overlay on top.

Good adhesion between the diffusion barrier layer and the Pb-bronze lining was achieved in all cases with no dependence on the Ni-based coating applied as diffusion barrier layer, as no bonding failure between the Pb-bronze lining and the diffusion barrier layer was ever observed during the bonding tests. Failure was mainly noticed within the Sn-Cu overlay and between the adhesive glue used to attach the dolly to the surface of the sample tested and the Sn-Cu overlay, although the diffusion barrier layer was partially exposed in some

regions of the tested samples, meaning that bonding between the overlay and the diffusion barrier layer eventually failed in those areas. These regions where the diffusion barrier layer was exposed were small compared to the rest of the tested surface, indicating that good adhesion between the overlay and the diffusion barrier layer was generally achieved regardless of the Ni-based coating used as the diffusion barrier layer. Very distinctive and reasonably large areas of the diffusion barrier layers were exposed in the samples tested as plated, whereas very small areas of the diffusion barrier layers were hardly noticed in the surface of samples tested after heat treatment. The main reason for this difference would be the formation of an intermetallic SnCuNi layer between the Sn-Cu overlay and the diffusion barrier layer, which would strengthen the adhesion of the Sn-Cu overlay and the diffusion barrier. Depending on the 'nature' of the SnCuNi intermetallic layer formed, which is further explained in the next section, an improvement on the strength of the overall overlay system could also be expected, as observed on the samples with a Ni/WS_2 diffusion barrier layer tested after being heat-treated.

It is fair to question to some extent the 'meaningfulness' of the results and discussion included in the previous pages if one considers that most of the bonding occurred between the glue and the Sn-Cu overlay and within the Sn-Cu overlay itself. Nevertheless, the objective of the tests was to check whether the Ni/WS_2 diffusion barriers would be more likely to present bonding issues and consequent de-attachment of the overlay due to a potentially 'dirtier' surface. And the answer to this would be that the Ni/WS_2 composite coatings are as suitable to be used as diffusion barriers in bearings with Sn-Cu overlays as the standard Ni coatings currently used for this application.

7.3. DIFFUSION TESTS

The basic task of a diffusion barrier layer in a journal bearing is to slow down the diffusion and the formation of intermetallic compounds that would occur in bronze-based bearings where a Pb-based or a Sn-based overlay is electrodeposited. For this purpose, diffusion tests

were performed on samples simulating real bearing systems which again consisted of a steel backing, a Pb-bronze lining deposited over the steel backing, a diffusion barrier layer (either Ni coatings electrodeposited under mechanical agitation or Ni/WS_2 composite coatings electrodeposited under ultrasound) electrodeposited over the Pb-bronze lining, and a Sn-Cu overlay electrodeposited over the diffusion barrier layer.

Figure 7.5 displays FEG-SEM cross-section images of samples simulating real bearing systems where the two different Ni-based coatings evaluated (Ni deposits produced under mechanical agitation and Ni/WS_2 composite coatings electrodeposited under ultrasound) were used as diffusion barrier layers. In both types of samples, the diffusion barrier layer (thickness around 5 μm) was clearly visible over the Pb-bronze substrate with a Sn-Cu overlay on top where the Cu was present in the overlay as part of SnCu intermetallic phases dispersed within the Sn matrix.

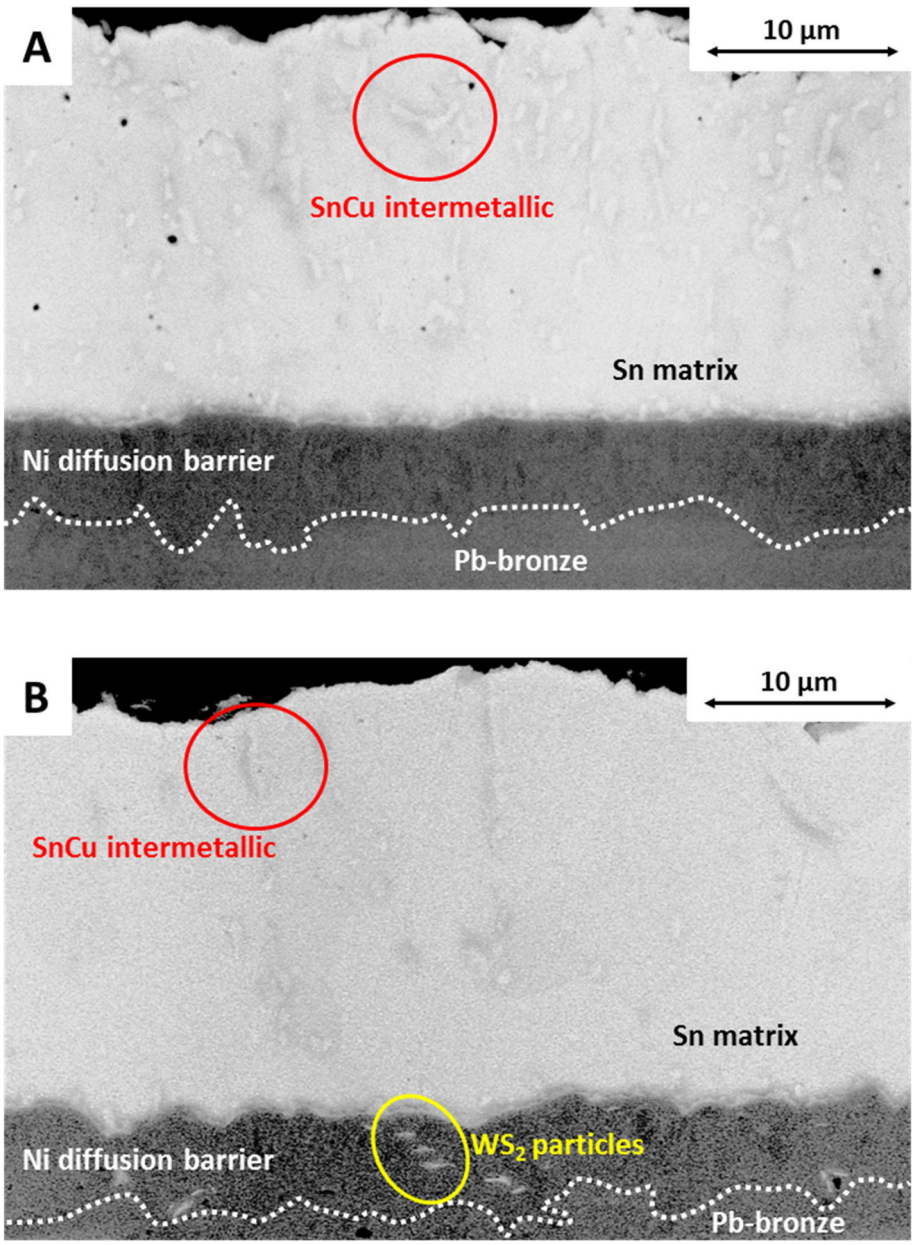

Figure 7.5. FEG-SEM cross-section images of samples simulating real bearing systems as plated. Samples consisted of a steel backing, a Pb-bronze lining deposited over the steel backing, a Ni-based diffusion barrier layer (either a Ni deposit produced under mechanical agitation or a Ni/WS_2 composites electrodeposited under ultrasound) over the lining, and an electroplated Sn-Cu overlay on top.

After 1000 hours at 130 °C (Figure 7.6), the SnCu intermetallic phases present within the Sn matrix in the Sn-Cu overlay coalesced forming larger SnCuNi intermetallic phases (small traces of Ni were detected in such intermetallic phases, indicating the migration of Ni from the diffusion barrier) within the overlay. A SnCuNi intermetallic layer formed between the diffusion barrier layer and the Sn-Cu overlay. Said SnCuNi intermetallic layer was

significantly thicker in samples with a Ni/WS_2 diffusion barrier electrodeposited under ultrasound at 0.180 W/cm^3 (Figure 7.6 B), as a very thin SnCuNi intermetallic layer formed in samples with a Ni diffusion barrier layer electrodeposited under mechanical agitation at 300 rpm (Figure 7.6 A). These results indicate that the resistance to diffusion of the Ni coating had decline once the WS_2 particles had been incorporated into the Ni matrix. In both cases, the SnCuNi intermetallic layer exhibited the so-called 'scallop'-like structure, similar to that of Cu_6Sn_5 intermetallic layers commonly formed in those cases where lead-free solders such as Sn-Cu or Sn-Ag-Cu are electrodeposited on Cu substrates [2-5]. In the present work though, as the 'real' substrate of the Sn-Cu overlay was a Ni-based coating, other possible intermetallic compounds should be considered. For this reason, EDS analysis was performed in the SnCuNi intermetallic layers to roughly estimate the composition of the SnCuNi intermetallic layer. In the case of the samples with Ni diffusion barrier layer, the molar composition of the SnCuNi intermetallic layer after 1000 hours at 130 °C was roughly around 45% of Sn, 44% of Cu and 11% of Ni. A significantly different molar composition was reported for the thicker SnCuNi intermetallic layer formed in samples with Ni/WS_2 diffusion barrier layers after 1000 hours at 130 °C (57% of Sn, 28% of Cu and 15% of Ni).

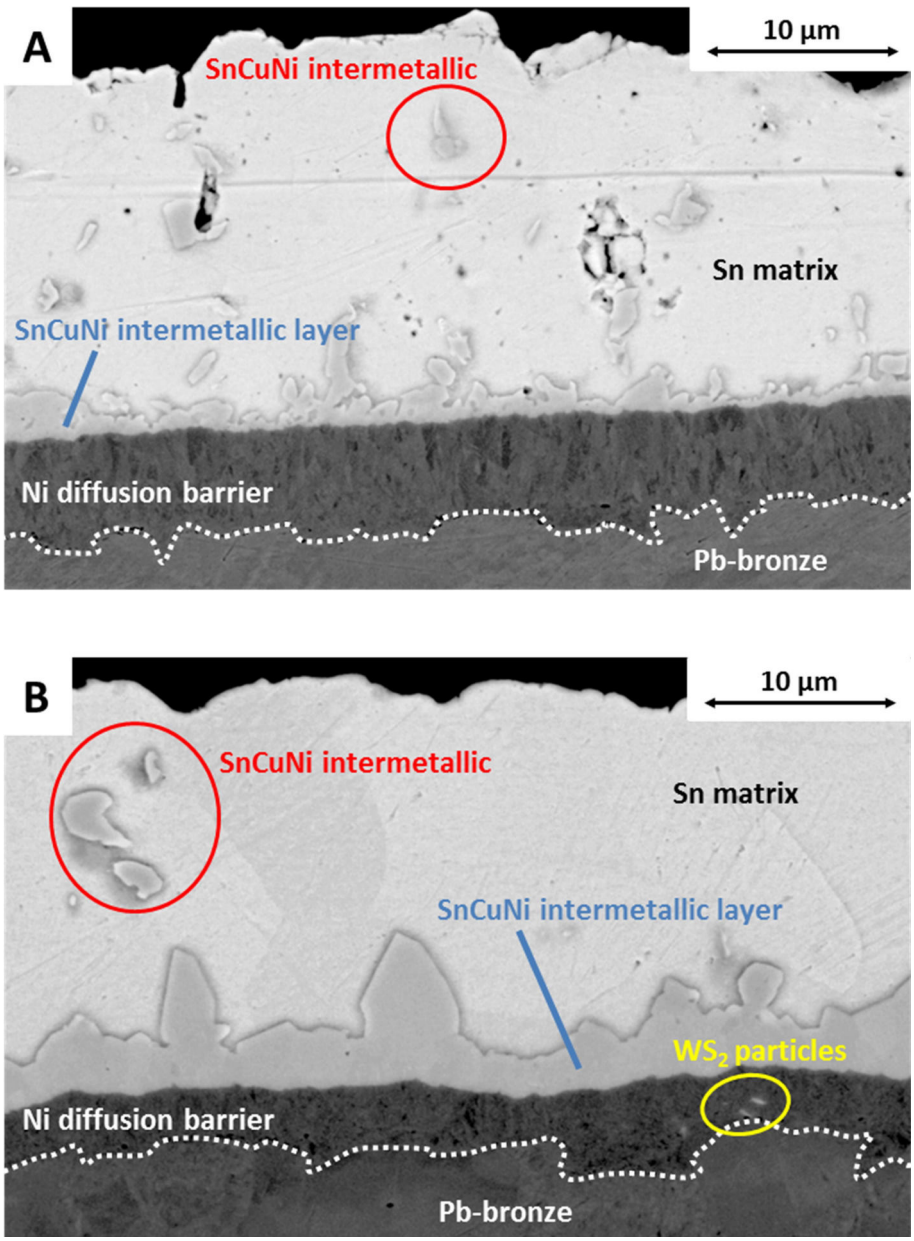

Figure 7.6. FEG-SEM cross-section images of samples simulating real bearing systems after 1000 hours at 130 °C. Samples consisted of a steel backing, a Pb-bronze lining deposited over the steel backing, a Ni-based diffusion barrier layer (either a Ni deposit produced under mechanical agitation or a Ni/WS_2 composites electrodeposited under ultrasound) over the lining, and an electroplated Sn-Cu overlay on top.

After 3000 hours at 130 °C (Figure 7.7), the SnCuNi intermetallic layer grew further in both types of samples. Nevertheless, whereas a significant increase in thickness was observed for the SnCuNi intermetallic layer in samples with the Ni diffusion barrier electrodeposited under mechanical agitation at 300 rpm with the consequent reduction in thickness of the diffusion barrier (Figure 7.7 A), the increase in thickness noticed for the SnCuNi

intermetallic layer in samples with the Ni/WS_2 diffusion barrier electrodeposited under ultrasound at 0.180 W/cm^3 and reduction in thickness of the diffusion barrier (Figure 7.7 B) was not as significant as it had been in the first 1000 hours. Some voids or cavities located in the grain boundaries of the scallop-like structures present in the SnCuNi intermetallic layer and in the interface between the intermetallic layer and the Sn matrix, especially in the samples with a Ni/WS_2 diffusion barrier layer where significantly larger scallop-like structures were observed in the SnCuNi intermetallic layer. The location of such cavities suggests that these are a consequence of the so-called Kirkendall effect [6], i.e. atomic diffusion through a vacancy mechanism due to the different diffusion rates of the metals present in the system [7]. Regarding the intermetallic compounds present in the SnCuNi intermetallic layers formed in both types of samples, while the molar composition of the intermetallic layer in samples with Ni diffusion barriers after 3000 hours at 130 °C was around 57% of Sn, 14% of Cu and 29% of Ni, the molar composition of the intermetallic layer in samples with Ni/WS_2 diffusion barrier layers was 58% of Sn, 9% of Cu and 33% of Ni.

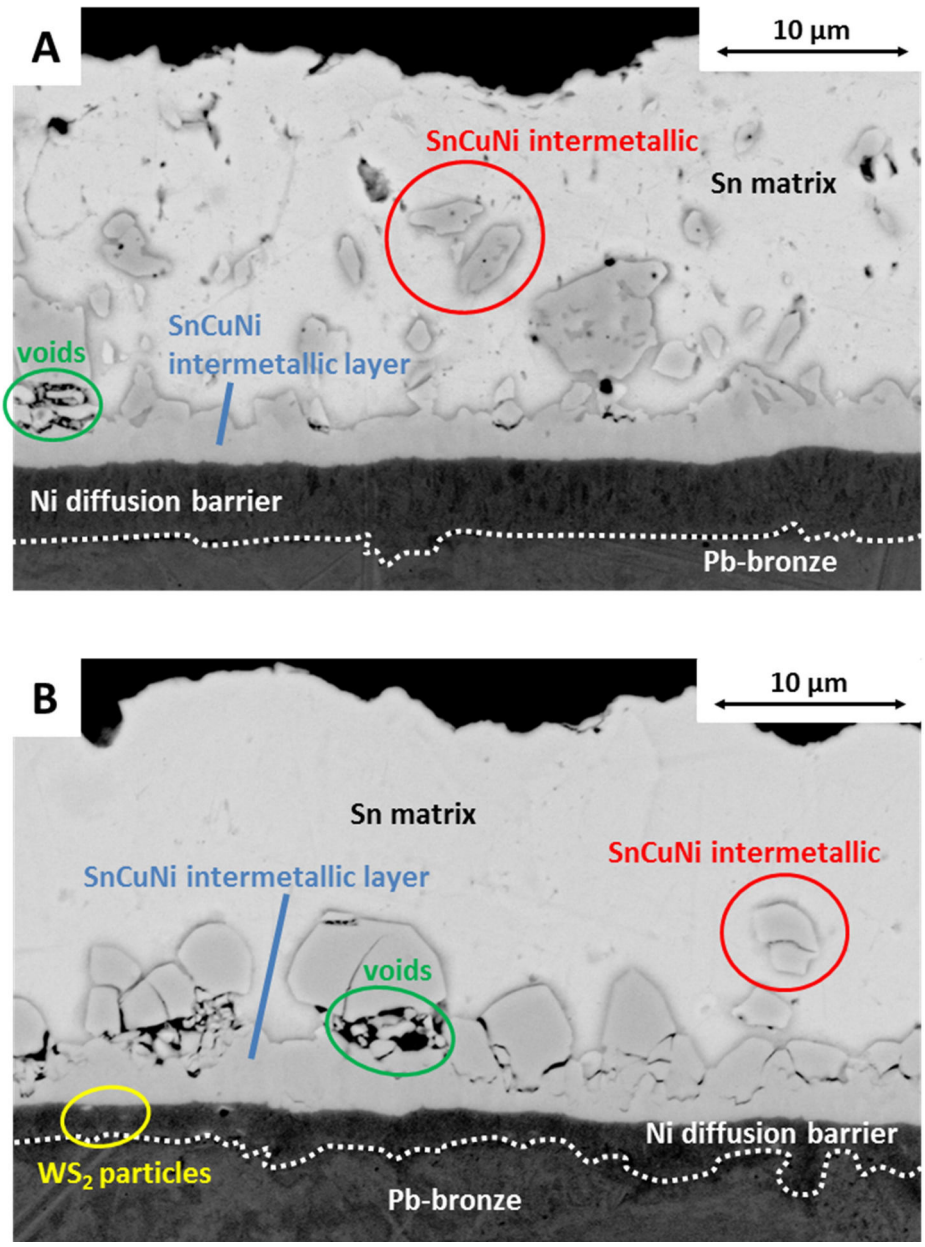

Figure 7.7. FEG-SEM cross-section images of samples simulating real bearing systems after 3000 hours at 130 °C. Samples consisted of a steel backing, a Pb-bronze lining deposited over the steel backing, a Ni-based diffusion barrier layer (either a Ni deposit produced under mechanical agitation or a Ni/WS_2 composites electrodeposited under ultrasound) over the lining, and an electroplated Sn-Cu overlay on top.

The thickness of the SnCuNi intermetallic layer was measured in all the samples to have a better idea of the growth of the layer during the heat treatment. Figure 7.8 displays the evolution of the thickness of the intermetallic layer vs. heat-treatment time for samples with either a Ni or a Ni/WS_2 diffusion barrier layer. The measurements confirmed the initial considerations made with the observation of the FEG-SEM cross-section images: the thicker

intermetallic layer was always observed in samples with a Ni/WS_2 diffusion barrier layer. It must be noted though, that even if the electrodeposition of a Ni/WS_2 interlayer results in the formation of the SnCuNi intermetallic layer at a higher rate, the intermetallic growth would still be much slower that in the absence of a Ni diffusion layer, as a Cu_6Sn_5 + Sn_3Cu intermetallic layer in a system consisting of Sn deposited on Cu would reach a thickness around 5 μm at a similar temperature (135 °C) in less than 500 hours [8-10]. Regarding the maximum thickness observed in the scallop-like structures observed in the SnCuNi intermetallic layer (thin bars in Figure 7.8), the values observed for all the different samples, especially after 3000 hours, indicate how large these structures may be.

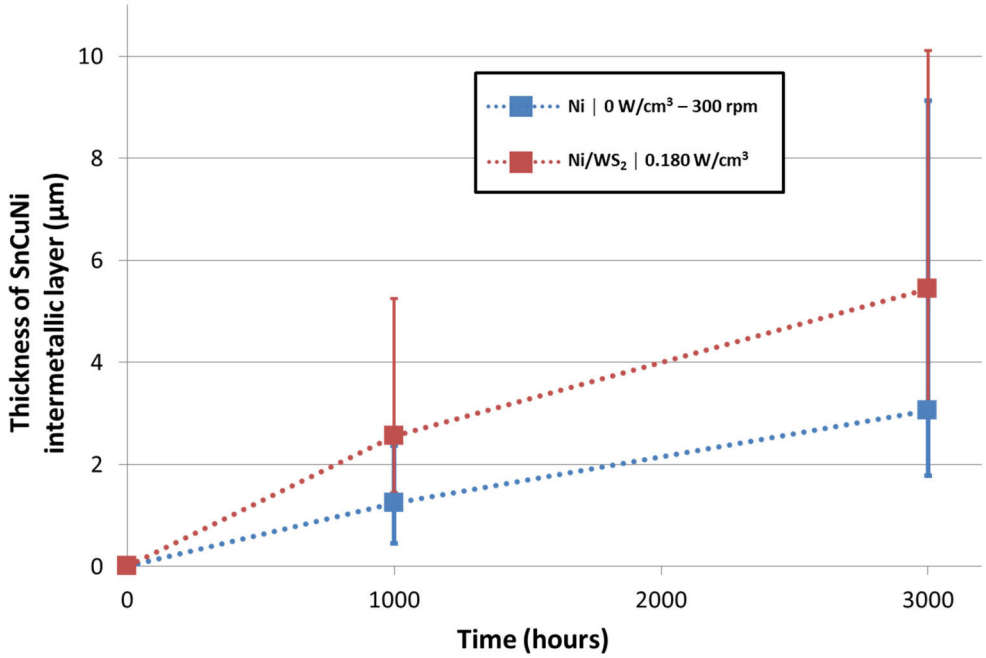

Figure 7.8. Thickness of the SnCuNi intermetallic layer vs. heat-treatment time for samples simulating real bearing systems. Samples consisted of a steel backing, a Pb-bronze lining deposited over the steel backing, a Ni-based diffusion barrier layer (either a Ni deposit produced under mechanical agitation or a Ni/WS_2 composites electrodeposited under ultrasound) over the lining, and an electroplated Sn-Cu overlay on top.

The reduction in thickness of the diffusion barrier layers during heat treatment was also evaluated by measuring its thickness in the tested samples. Figure 7.9 displays the reduction in the thickness of the diffusion barrier layer vs. heat-treatment time for samples with either a Ni or a Ni/WS_2 diffusion barrier layer a better comparison. After 1000 hours, no significant

reduction of the diffusion barrier layer was noticed in the samples with a Ni barrier layer. This was completely different in the samples where a Ni/WS_2 composite coatings was used as a diffusion barrier layer, as a significant reduction of the interlayer was observed in these samples. After 3000 hours, a more significant reduction of the diffusion barrier layer was noticed in the samples with a Ni barrier layer (around 1.2 μm). In the case of the samples with a Ni/WS_2 diffusion barrier, although the diffusion barrier layer was further reduced after 3000 hours, the 'loss' of barrier layer seemed to slow down compared to previous measurements after 1000 hours.

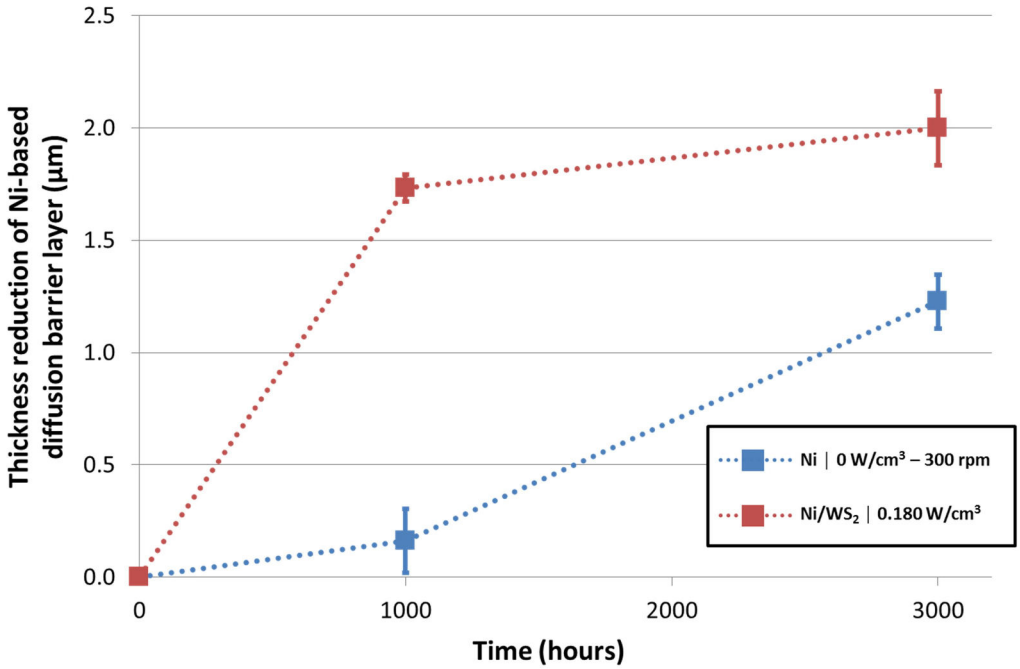

Figure 7.9. Reduction of the thickness of the interlayer vs. heat-treatment time for samples simulating real bearing systems. Samples consisted of a steel backing, a Pb-bronze lining deposited over the steel backing, a Ni-based diffusion barrier layer (either a Ni deposit produced under mechanical agitation or a Ni/WS_2 composites electrodeposited under ultrasound) over the lining, and an electroplated Sn-Cu overlay on top.

The results obtained during the diffusion tests not only indicate how fast the SnNiCu intermetallic layer forms and grows in samples with different Ni-based diffusion barrier layers, but also the nature of the intermetallic compounds formed, which are of high importance in order to understand how the intermetallic forms and how it could affect the

bearing overlay system in real applications. In this sense, the mechanism for the formation of the SnCuNi intermetallic layer would be as follows [11]:

1. Migration of Cu from the Sn-Cu overlay towards the overlay-diffusion barrier layer interface.
2. Formation of a Cu_6Sn_5 layer in the overlay-diffusion barrier layer interface.
3. Diffusion of Ni into the Cu_6Sn_5 intermetallic layer to substitute Cu in Cu_6Sn_5 intermetallic compounds resulting in an overall $(Cu,Ni)_6Sn_5$ layer.
4. Depletion in Cu from overlay as the $(Cu,Ni)_6Sn_5$ layer grows. Continuous supply of Ni from the barrier layer results in a gradual transformation of $(Cu,Ni)_6Sn_5$ into $(Ni,Cu)_3Sn_4$ where Ni_3Sn_4 progressively becomes the main phase of the intermetallic layer.

The mechanism of the formation and growth of the SnCuNi intermetallic layer described above agrees with the results obtained from the samples with the Ni diffusion barrier electrodeposited under mechanical agitation at 300 rpm: as previously reported, the molar composition of the SnCuNi intermetallic layer after 1000 hours at 130 °C was around 45% of Sn, 44% of Cu and 11% of Ni, which is consistent with the predominance of a $(Cu,Ni)_6Sn_5$ layer [12], as observed by Ho et al. [13] in their study with Sn-Ag-Cu solders with high Cu content (up to 3%) reacting with Ni (Cu content in the overlays deposited in the present work was around 3-5%). In the present case, the SnCuNi intermetallic layer would consist of 80% of Cu_5Sn_6 phases and 20% of Ni_5Sn_6 phases. However, the molar composition of the SnCuNi intermetallic layer after 3000 hours at 130 °C was around 58% of Sn, 32% of Cu and 10% of Ni, more consistent with the predominance of $(Ni,Cu)_3Sn_4$ (37% of Cu_3Sn_4 phases and 67% of Ni_3Sn_4 phases). Regarding this, Wong et al. [14] found that, after the depletion of Cu in their Sn-Ag-Cu solder deposited on Ni, further annealing treatment gradually transformed the $(Cu,Ni)_6Sn_5$ phase into a $(Ni,Cu)_3Sn_4$ phase.

For the samples with the Ni/WS_2 diffusion barrier electrodeposited under ultrasound at 0.180 W/cm^3, the formation and growth of the SnCuNi intermetallic layer seemed to occur

very fast. The transformation of $(Cu,Ni)_6Sn_5$ into $(Ni,Cu)_3Sn_4$ would also start sooner due to the earlier depletion of Cu in the overall overlay system, as suggested by the molar composition of the intermetallic layer after 1000 hours at 130 °C (58% of Sn, 32% of Cu and 10% of Ni) which already indicated the existence of a $(Ni,Cu)_3Sn_4$ intermetallic layer (76% of Cu_3Sn_4 phases and 24% of Ni_3Sn_4 phases). Further heat treatment at 130 °C up to 3000 hours resulted in a Ni-enrichment of the $(Ni,Cu)_3Sn_4$ intermetallic layer, where now the proportion of the Ni_3Sn_4 phase would be higher (21% of Cu_3Sn_4 phases and 79% of Ni_3Sn_4 phases).

Considering the crystal structure of the Ni and Ni/WS_2 diffusion barrier layers reported in Chapters 4 and 5, it is possible to correlate the overall diffusion in the system, i.e. growth and nature of the SnCuNi intermetallic layer and reduction in thickness of the Ni-based diffusion barrier layer, with the microstructure of the latter: whereas slower diffusion of the barrier layer and intermetallic growth was observed in coatings where diffusion barrier layer consisted of Ni columnar crystals (Ni diffusion barrier layers electrodeposited under mechanical agitation at 300 rpm), a much faster increase of the intermetallic layer with a more significant reduction of the diffusion barrier layer was noticed when no columnar crystals are present and the Ni matrix structure apparently consists of refined nano-size grains (Ni/WS_2 diffusion barrier layers electrodeposited under ultrasound at 0.180 W/cm^3). These results suggest that grain boundary diffusion is predominant over lattice diffusion, and therefore, by reducing the grain size, the overall diffusion is increased. Although no similar studies have been found in the literature regarding diffusion and intermetallic growth in electroplated Sn-Cu on Ni-based coatings with refined grain size, there are some experimental works that indicate that, by reducing the grain size from a coarse structure to a nano-crystalline structure, grain boundary diffusion of metals such as Cu in Ni can be increased by 4-5 orders of magnitude [15].

The results included in the present work imply that, from the diffusion barrier point of view, the change in microstructure of the Ni interlayer due to the incorporation of particles with the assistance of ultrasound is not beneficial in terms of preventing and/or reducing the diffusion with the Sn-Cu interlayer, as the overall diffusion process is increased when using Ni/WS_2 diffusion barrier layers deposited under ultrasound. Nevertheless, such increase in the overall diffusion process observed by refining the grain size and reducing or preventing the formation of columnar crystals may be of interest where functional SnCu (Cu_6Sn_5, Cu_3Sn_4) or SnNi (Ni_6Sn_5, Ni_3Sn_4) intermetallic compounds are sought for different bearing applications [16,17]. Related to this, the thermally-induced formation of a thick Ni_3Sn_4 intermetallic layer on bronze-based bearings with sputtered SnCu overlays has already shown an improvement in the performance of such bearings due to the general increase in strength achieved by the presence of such intermetallic phase [18]. This general increase in strength due to the quicker formation and growth would actually explain why, in the adhesion tests shown earlier in this chapter, an slight increase in the load measured immediately before bonding failure was achieved in samples simulating real bearing systems with a Ni/WS_2 diffusion barrier layer electrodeposited under ultrasound at 0.180 W/cm^3.

7.4. CONCLUSIONS

Adhesion tests showed that a good adhesion between the diffusion barrier layer and the Pb-bronze lining was always achieved in samples simulating real bearing materials with both standard Ni and Ni/WS_2 diffusion barrier layers. Although failure was mainly observed between the Sn-Cu overlay and the glue, relatively small areas of the diffusion barrier layers were exposed in all the samples tested due to localized bonding failure between the Ni-based diffusion barrier and the Sn-Cu coating deposited on top. Nevertheless, the areas of the diffusion barrier layer that were exposed after the adhesion tests were less prominent in samples heat-treated for 500 hours at 130 °C. Moreover, an increase in the load measured

immediately before adhesion failure occurred was observed in samples with the Ni/WS_2 diffusion barrier layer, most probably due to the nature and thickness of the SnCuNi intermetallic formed in the overlay-barrier layer interface after being heat-treated for 500 hours at 130 °C.

Diffusion tests showed that the formation and growth of the SnCuNi intermetallic in the overlay-barrier layer interface at 130 °C occurred faster in samples where a Ni/WS_2 diffusion barrier layer was used, as opposed to samples with a Ni diffusion barrier layer where diffusion was lower, resulting in a thinner SnCuNi intermetallic layer. Faster diffusion in samples with a Ni/WS_2 diffusion barrier layer apparently resulted in an accelerated transformation of $(Cu,Ni)_6Sn_5$ phases into $(Ni,Cu)_3Sn_4$ phases in the SnCuNi intermetallic layer. In spite of this, diffusion slowed down in samples with the Ni/WS_2 diffusion barrier layer, and this would occur once the $(Cu,Ni)_6Sn_5$ phases had completely transformed into $(Ni,Cu)_3Sn_4$ phases and the relative proportion of Ni_3Sn_4 would increase compared to Cu_3Sn_4. The immediate conclusion is that, compared to standard Ni diffusion barrier layers, Ni/WS_2 diffusion barrier layers in bronze-based bearings failed in preventing/retarding diffusion. Nevertheless, the nature and growth of the intermetallic compounds that would form when the Ni/WS_2 barrier layer is used opens new options and possibilities due to the improvement in strength that may be achieved with such intermetallic phases. An indication for this would be the increase in the load necessary to achieve bonding failure observed in the adhesion tests performed on heat-treated samples with a Ni/WS_2 diffusion barrier layer.

7.5. REFERENCES

[1] ASTM Standard D6677-07, Standard test method for evaluating adhesion by knife, 2012.

[2] W. Wang, Z. Wang, A. Xian, J. Shang, J. Mater. Sci. Technol. 23 (2007) 85.

[3] W. Peng, E. Monlevade, M.E. Marques, Microelectron. Reliab. 47 (2007) 2161.

[4] G. Zeng, S. Xue, L. Zhang, L. Gao, W. Dai, J. Luo, J. Mater. Sci. Mater. Electron. 21 (2010) 421.

[5] F. Gao, J. Qu, Mater. Lett. 73 (2012) 92

[6] A.D. Smigelkas, E.O. Kirkendall, Trans. AIME 171 (1947) 130.

[7] H. Nakajima, JOM 49 (1997) 15.

[8] D.A. Unsworth, C.A. Mackay, Trans. Inst. Met. Finish. 51 (1973) 85.

[9] P.J. Kay, C.A. Mackay, Trans. Inst. Met. Finish. 54 (1976) 70.

[10] M. Jordan, The electrodeposition of tin and its alloys, Eugen G. Leuze Publishers, Saulgau-Ŵürtt, 1995.

[11] Y. Zhang, Daido Metal Internal Report: Intermetallics on Sn-Cu-Ni system, 2008

[12] A. Zribi, A. Clark, L. Zavalij, P. Borgesen, E.J. Cotts, J. Electron. Mater. 30 (2001) 1157.

[13] C.E. Ho, R.Y. Tsai, Y.L. Lin, C.R. Kao, J. Electron. Mater. 31 (2002) 584.

[14] C.K. Wong, J.H.L. Pang, J.W. Tew, B.K. Lok, H.J. Lu, F.L. Ng, Y.F. Sun, Microelectron. Reliab. 48 (2008) 611.

[15] Y.R. Kolobov, G.P. Grabovetskaya, M.B. Ivanov, A.P. Zhilyaev, R.Z. Valiev, Scripta Mater. 44 (2001) 873.

[16] H.-U. Huhn, P Spahn, D. Wiebach, A. Adam, F. Niegel, DE patent 19963385, 1999

[17] S. Takayanagi, Y. Zhang, H. Asakura, Y. Kagohara, US patent 2012064365, 2012.

[18] A. Adam, G. Andler, G. Arnold, The progression of engine bearing overlays, SAE World Congress, Detroit, March 2002. Paper 2002-01-1316.

8. FINAL REMARKS

8.1. CONCLUSIONS

During the present PhD research project, it has been demonstrated how ultrasound may affect the electrodeposition of Ni coatings and Ni-based composite coatings with embedded lubricant particles from an additive-free Watts bath. Regarding pure Ni deposits, ultrasonic power did not only affect the surface finishing of the coatings, but also the crystal orientation and the surface morphology and microstructure to some extent, resulting in an increase in hardness of the deposits by both grain refinement and work hardening. Regarding the Ni-based composite coatings with lubricant particles, whereas the combination of ultrasound with mechanical agitation was the best method to disperse the lubricant particles in the Ni Watts bath, ultrasound on its own yielded the best composite coatings in terms of higher incorporation and uniform distribution of finely dispersed particles within the Ni coatings. Due to their more promising characteristics, Ni/WS_2 and Ni/hBN composite coatings electrodeposited under ultrasound were further evaluated in

terms of particle content, crystal orientation, surface morphology and crystal structure and hardness. WS_2 content in Ni/WS_2 composite coatings was around five times greater than hBN content in Ni/hBN composite coatings. Ni/WS_2 composite coatings also presented a more significant change in crystal orientation, surface morphology, crystal structure and grain size, being the latter the main cause for the significant improvement in hardness observed in said composite coatings. No significant effect of ultrasound was observed on the chemical parameters and lifespan of the Watts bath used, being this an important consideration for future scale-up and long term use.

The evaluation of the tribological performance of the different Ni-based coatings studied indicated that, whereas the use of ultrasound on its own or the incorporation of hBN particles did not have any effect on the tribological performance of electrodeposited Ni coatings, Ni/WS_2 Composite coatings showed a significant enhancement of the tribological performance when operating in both mixed-film and boundary lubrication regimes. Under mixed-film lubrication, the incorporation of WS_2 particles not only resulted in a significant improvement of the Coefficient of Friction (CoF), but also in the prevention of undesired stick-slip motion that would end up causing coating failure by seizure. The latter was quite evident under boundary lubrication, as the Ni/WS_2 composite coatings were the only ones that did not show any signs of coating failure during the tribological tests, as opposed to the other Ni-based coatings tested.

When the Ni/WS_2 composite coating that exhibited an enhanced tribological performance was used as a diffusion barrier layer in samples simulating real bearing materials, diffusion was accelerated compared with samples where a standard Ni barrier layer was used. Nevertheless, this accelerated diffusion also affected the nature of the intermetallic phases present in the intermetallic layer formed, as the transformation of $(Cu,Ni)_6Sn_5$ phases into $(Ni,Cu)_3Sn_4$ phases also occurred earlier. Once this was achieved, diffusion seemed to slow down. The formation of $(Cu,Ni)_6Sn_5$ and $(Ni,Cu)_3Sn_4$ phases is in fact beneficial due to the

overall improvement in strength that is achieved when said intermetallic phases are present in bearing overlay systems. This would explain why, during the adhesion tests performed, an slight increase in the load measured immediately before adhesion failure was observed in samples with a Ni/WS_2 diffusion barrier after heat treatment.

8.2. CURRENT AND FUTURE WORKS

8.2.1. FUNDAMENTAL STUDIES

Many interesting questions have arisen during the PhD research presented herein that have not been answered due to the applied nature of the research project between DIBE and Coventry University. The effect of ultrasound on the crystal orientation of pure Ni deposits constitutes an example of this. Prior literature on the topic has established the inhibition effect due to the presence of certain chemical species in the cathode-electrolyte interface. The results included in the present thesis clearly established that ultrasound does have a significant effect on the crystal orientation of the Ni grains, apparently counteracting the effect of electrolyte stirring. In the present thesis, it was assumed that ultrasound should therefore have a different effect on the inhibiting species that may be present in the cathode-electrolyte interface. In this sense, different effects could be attributed to the presence of ultrasound (reduction of local alkalization in the surface of the cathode, disturbance of the formation of a double layer structure on the electrode surface, etc.), and future studies are being planned to shed more light on this issue.

Another example is the tribological performance of the Ni/WS_2 composite coatings electrodeposited under ultrasound. Although these composite coatings exhibited an enhanced tribological performance under lubricated and non-lubricated conditions, the fact that a black film was forming in the former whereas Ni asperities seemed to remain 'unprotected' in the latter should also receive more attention in order to better explain the different tribological mechanisms that improved the overall tribological performance of the

Ni/WS_2 with and without a liquid lubricant. In this sense, deeper and more fundamental tribological studies, combined with advanced surface characterization techniques (TEM, XPS, AFM, etc.) will be carried out in the near future.

The final example could be Chapter 7 in its entirety. In this sense, further and more precise diffusion tests with advance analytical methods (e.g. GD-OES, XPS or Auger electron spectroscopy for depth profiling of the composition and EBSD on the cross-section of samples for phase identification) on real bearings with the Ni/WS_2 composite coatings will be carried out in order to properly estimate the diffusion kinetics and mechanism [1], not only in the overlay-diffusion barrier layer interface, but also in the overlay, as Cu content may also be critical in the formation of the different intermetallic phases [2]. Combining these studies with further mechanical testing (Sapphire fatigue and wear tests, as well as further adhesion tests) would give a better understanding of how the intermetallic compounds formed in the SnNiCu intermetallic layer will evolve after long time operation (i.e. +20000 hours) of real bearings with new overlay systems with a Ni/WS_2 diffusion barrier layer.

8.2.2. SCALE UP OF ULTRASONIC-ASSISTED ELECTRODEPOSITION OF Ni/WS_2 DIFFUSION BARRIERS

The ultrasound-assisted electrodeposited Ni/WS_2 composite coatings presented herein showed an improved tribological performance when compared with standard Ni coatings and interesting properties in terms of diffusion and formation and growth of intermetallic phases. These coatings have therefore become a promising option for bronze-based bearings, not necessarily as diffusion barrier layers, but as effective diffusion intermediate layers in new bearing overlay systems under current development. For this reason, current work is mainly focused in scaling the ultrasound-plating process up to pilot scale.

The results included in Chapter 5 showed how the effect of ultrasound during the electrodeposition of Ni/WS_2 composite coatings in terms of particle de-agglomeration and incorporation into the coating could be counteracted by mechanically stirring the solution. Nevertheless, flow circulation may be mandatory in a larger scale to renew the electrolyte near the surface of the cathode under certain conditions. In addition, an uneven ultrasonic field over a large cathode area may result in non-uniform distribution of the properties of the coatings due to the distribution of pressure antinodes and nodes along the surface of the cathode [3] in an analogous way to the antinode marks observed in the Ni anodes shown in Chapter 4. For this reason, a strong effort is being made to properly design the location and set the ultrasonic parameters of the submersible ultrasonic transducers in large plating tanks. This would allow us to optimize the ultrasonic field near the surface of the bearings during the electrodeposition of the Ni/WS_2 composite coatings. In this sense, Finite Element Methods (FEM) has proved to be a powerful tool in the simulation of the ultrasonic field inside sonochemical reactors [4]. Therefore, FEM models defined to couple the vibration of solids coupled with the acoustic field [5,6] accounting for linear [7] and non-linear [8,9] acoustic cavitation are being used to simulate and optimize the ultrasonic field inside the electroplating tanks.

8.2.3. Continuous improvement of electrodeposited Ni-based composite coatings for bearing applications

Although current and future work is mainly focused in scaling the ultrasound-plating process of Ni/WS_2 coatings to pilot scale, some efforts are also being put into improving and developing Ni-based composite coatings with other particles.

Regarding Ni/hBN composite coatings, current research showed that particle incorporation under ultrasound was low, and even the increase in the concentration of particles in the bath or the use of surfactants would not significantly improve particle incorporation in the coating and therefore its tribological performance in terms of CoF values [10] (very recent

trials performed doubling the concentration in the Watts bath, 30 g/L, did not result in different performance in lubricated and non-lubricated scratch tests as showed in Chapter 6 for Ni/hBN composite coatings electrodeposited under ultrasound from a Watts bath with 15 g/L of particles). For this reason, hBN has been discarded for future work.

Regarding Ni/MoS_2 composite coatings, Ni and Ni-alloy coatings containing MoS_2 with an adequate surface finish and a good deposit quality are quite difficult to produce by electrodeposition methods, as reported by Cardinal et al. [11], who were unsuccessful in producing Ni-W/MoS_2 composite coatings with what would be considered an acceptable quality for bearing applications (uniform thickness, low roughness and no porosity). In the present research context, apart from the use of other commercial MoS_2 particles with a narrow particle size distribution (and therefore a higher cost), other options could be considered in order to produce a satisfactory Ni/MoS_2 composite coating in further studies. For example, brush plating could improve the quality of the coating [12], although such plating process would not be feasible for the electroplating of bearings. Another approach could be the incorporation of MoS_2 particles coated with other materials, as suggested by Huang and Xiang [13]. In their work, the authors coated the MoS_2 particles with Al_2O_3 prior to the electrodeposition of the Ni deposits. Their Ni/WS_2 coatings without the Al_2O_3-coated particles presented an undesired dendritic structure and poor adhesion to the substrate, whereas the Ni deposits produced with the Al_2O_3-coated MoS_2 particles had a better structure with a good tribological performance. However, these authors needed a surfactant, CTAB, to reduce particle agglomeration in the plating bath.

The use of surfactants in the electrodeposition of Ni/PTFE composite coatings is essential due to the highly hydrophobic nature of PTFE, as the use ultrasound on its own or combined with mechanical agitation was unsuccessful in dispersing particles in the Watts bath. Even in this case, the use of ultrasound may significantly improve the dispersion of PTFE particles with very little addition of the surfactant, reducing the concentration of the surfactant

required to wet the particles, and therefore minimizing the disadvantages associated to their use in current DIBE's plating lines. In this sense, work started very recently has proven quite effective so far, not only in terms of the incorporation of well-dispersed PTFE particles into electrodeposited Ni coatings (Figure 8.1), but also in terms of the tribological performance of said coatings in lubricated (Figure 8.2) and non-lubricated (Figure 8.3) scratch tests as those included in Chapter 6.

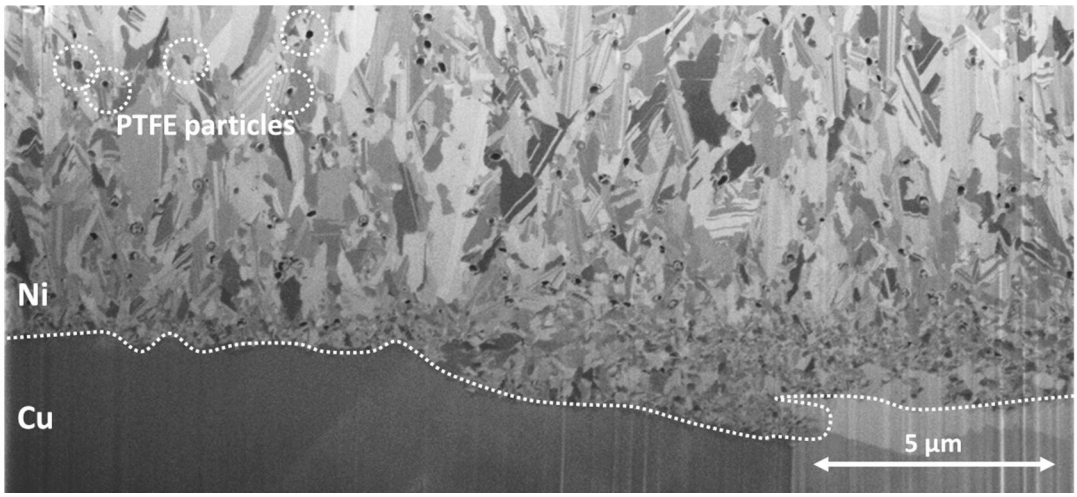

Figure 8.1. FIB-SEM image of the cross-section of a Ni/PTFE composite coating electrodeposited from a Ni Watts bath under current development.

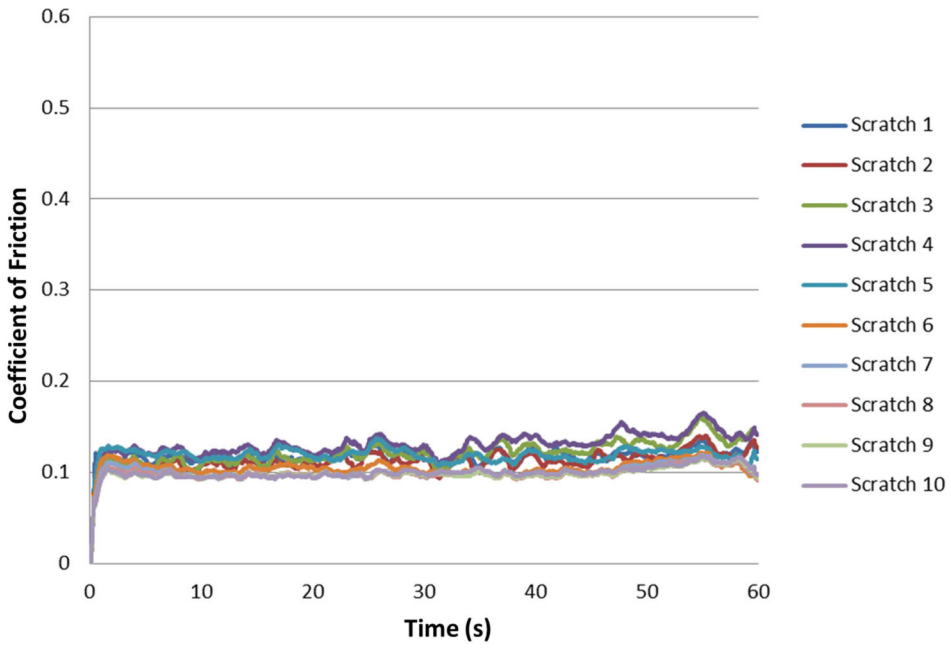

Figure 8.2. CoF measured during a lubricated scratch test (10 continuous scratches) performed on a Ni/PTFE composite coating electrodeposited from a Ni Watts bath under current development.

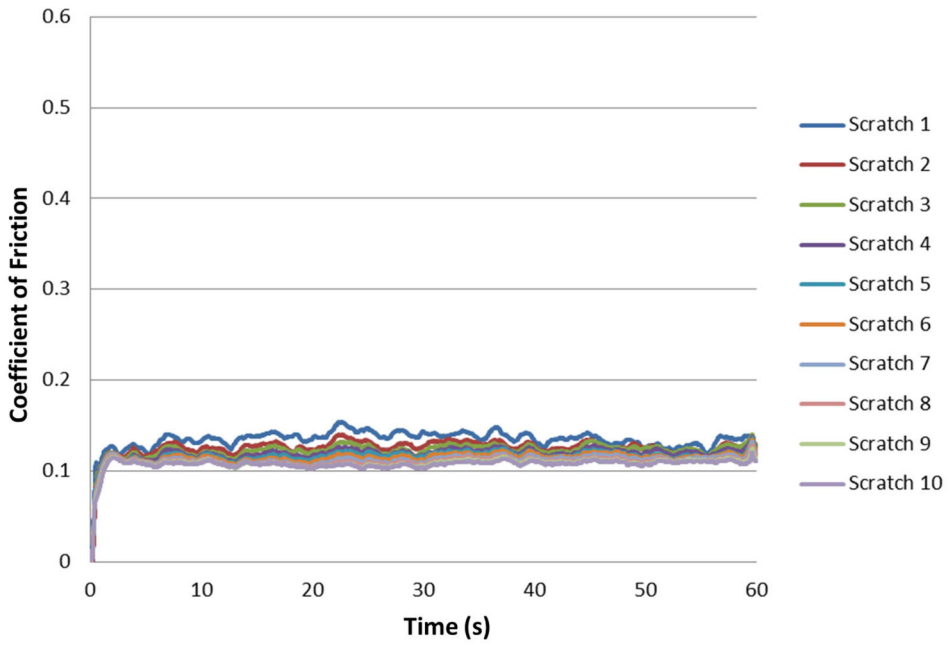

Figure 8.3. CoF measured during a non-lubricated scratch test (10 continuous scratches) performed on a Ni/PTFE composite coating electrodeposited from a Ni Watts bath under current development.

8.3. REFERENCES

[1] R.W. Balluffi, J. Electron. Mater. 21 (1992) 527.

[2] C.E. Ho, S.C. Yang, C.R. Kao, J. Mater. Sci. Mater. Electron. 18 (2007) 155.

[3] F. Touyeras, J.Y. Hihn, X. Bourgoin, B. Jacques, L. Hallez, V. Branger, Ultrason. Sonochem. 12 (2005) 13.

[4] I. Tudela, V. Sáez, M.D. Esclapez, M.I. Díez-García, P. Bonete, J. González-García, Ultrason. Sonochem. 21 (2014) 909.

[5] O. Louisnard, J. Gonzalez-Garcia, I. Tudela, J. Klima, V. Sáez, Y. Vargas-Hernández, Ultrason. Sonochem. 16 (2009) 250.

[6] I. Tudela, V. Sáez, M.D. Esclapez, P. Bonete, H. Harzali, F. Baillon, J. González-García, O. Louisnard, Chem. Eng. J. 171 (2011) 81.

[7] J. Jordens, A. Honings, J. Degrève, L. Braeken, T. Van Gerven, Ultrason. Sonochem. 20 (2013) 1345.

[8] O. Louisnard, Ultrason. Sonochem. 19 (2012) 56.

[9] O. Louisnard, Ultrason. Sonochem. 19 (2012) 66.

[10] E. Pompei, L. Magagnin, N. Lecis, P.L. Cavallotti, Electrochim. Acta 54 (2009) 2571.

[11] M.F. Cardinal, P.A. Castro, J. Baxi, H. Liang, F.J. Williams, Surf. Coat. Technol. 204 (2009) 85.

[12] X.-H. Zhang, J.-J. Liu, B.-L. Zhu, Wear 157 (1992) 381.

[13] F. Erler, C. Jakob, H. Romanus, L. Spiess, B. Wielage, T. Lampke, S. Steinhaüser, Electrochim. Acta 48 (2003) 3063.

APPENDIX A. CALIBRATION OF THE QS12 ULTRASONIC BATH/0.6 L BEAKER SYSTEM

A.1. OVERVIEW

The present Appendix describes the methodology followed to estimate the ultrasonic output power (i.e. 'effective' ultrasonic power and cavitation activity) in the QS12 ultrasonic bath/0.6 L beaker system, and the results obtained. In this sense, calibration of the ultrasonic power was performed by calorimetry [1], a calibration method widely used in Sonochemistry and Sonoelectrochemistry [2-6].

A.2. THEORETICAL BACKGROUND

The calorimetric method is derived from an energy conservation and dissipation equation with the combination of the theorem of kinetic energy and the first principle of thermodynamics [7]:

$$\iiint_V \rho_\mathrm{l} C_{v,\mathrm{l}} \frac{\mathrm{d}\langle T\rangle}{\mathrm{d}t} = P_{diss} + \dot{Q} \tag{A.1}$$

where V is an arbitrary volume of irradiated liquid, ρ_l is the density of the liquid, $C_{v,\mathrm{l}}$ is the specific heat capacity at constant volume of the liquid, $\langle T\rangle$ is the local temperature of the liquid averaged over one or more acoustic periods, t is time, P_{diss} is the power dissipated by the formation, growth and collapse of the bubbles in the liquid and $\dot{Q}$ is the (algebraic) heat gained or lost by volume V. In the calorimetric method, V is taken as the whole volume of irradiated liquid, which must be sufficiently stirred to ensure its homogeneity so $\langle T\rangle$ becomes the temperature T of the whole liquid, which is monitored in the liquid immediately after ultrasound is switched on. At $t = 0$, heat cannot escape due to thermal inertia, and therefore $\iiint_V \rho_\mathrm{l} C_{v,\mathrm{l}} \frac{\mathrm{d}\langle T\rangle}{\mathrm{d}t}$ matches P_{diss}. This allows the estimation of the power dissipated by the bubbles, and hence the 'effective' ultrasonic power which results in cavitation activity in the reactor, by just obtaining the initial slope of the temperature vs. time curve as follows [8]:

$$P_{diss} = m\, C_{p,\mathrm{l}} \left(\frac{\mathrm{d}T}{\mathrm{d}t}\right)_{t=0} \tag{A.2}$$

where m is the mass of the liquid, $C_{p,\mathrm{l}}$ is the specific heat capacity at constant pressure of the liquid and $\left(\frac{\mathrm{d}T}{\mathrm{d}t}\right)_{t=0}$ is the initial slope of the T vs. t curve.

A.3. Experimental set-up

The same experimental set-up used for the electrodeposition experiments was also used for the calorimetric method of the QS12 ultrasonic bath/0.6 L beaker system. A 0.6 L beaker containing 0.5 L of deionised water was immersed in the Q12 ultrasonic bath in the centre of the bath at a certain depth (11 cm between the bottom of the beaker and the surface of the water) with a certain water level (2 cm between the edge of the ultrasonic bath and the surface of the water). Deionised water was used in the calibration due to the lack of physical data of the Watts electrolyte in terms of ρ_l and $C_{p,\mathrm{l}}$, while $T_{t=0}$ was always around 14.6 ºC

(room temperature) for all the experiments due to the extremely complex experimental set-up required to maintain the liquid in the beaker and the water bath at 50 ºC in an adiabatic state. Immediately after switching on the ultrasonic transducers in the bath, T was recorded as a function of t during 180 s at intervals of 30 s while the ultrasonic bath was operated at different output powers (60%, 80% and 100%).

A.4. RESULTS

Three calibration experiments were conducted at each ultrasonic output power (60%, 80% and 100%) as shown in Figure A.1. $\left(\frac{\mathrm{d}T}{\mathrm{d}t}\right)_{t=0}$ was estimated by 5th-degree polynomial curve fitting, and then P_{diss} was calculated according to Equation (A.2). For ultrasonic output powers of 60%, 80% and 100%, the estimated ultrasonic power was 0.011, 0.124 and 0.180 W/cm^3, respectively.

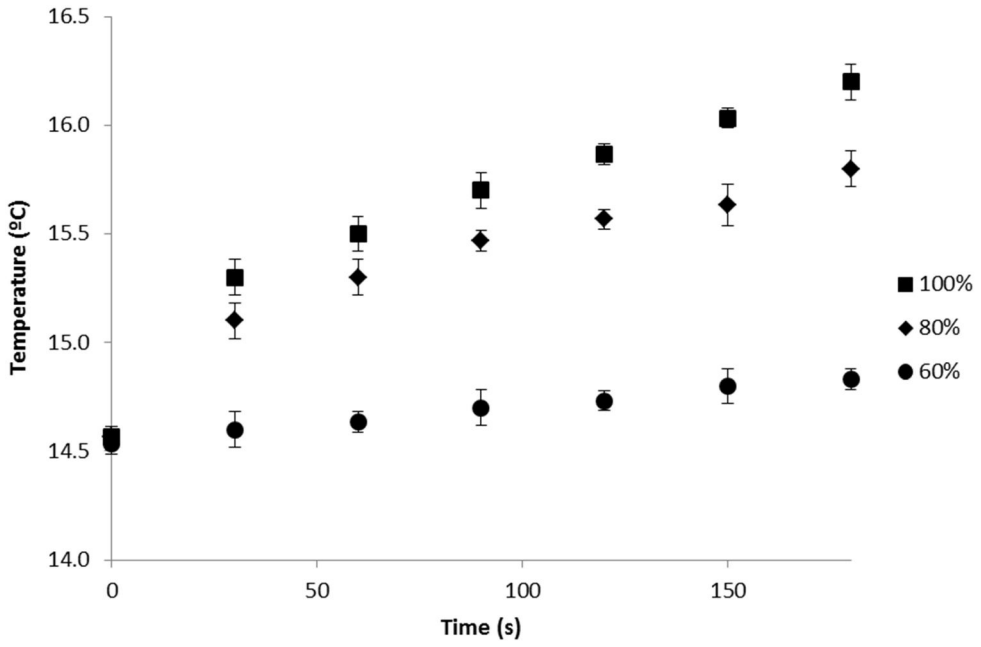

Figure A.1. Evolution of T vs. t time in 0.5 l of deionised water contained in a 0.6 l beaker containing submersed in an Ultrawave QS12 ultrasonic bath.

A.5. REFERENCES

[1] T.J. Mason, Practical sonochemistry: User's guide to applications in chemistry and chemical engineering, Ellis Horword Ltd., Chichester, 1991.

[2] A. Tiehm, K. Nickel, M. Zellhorn, U. Neis, Water Res. 35 (2001) 2003.

[3] H. Li, L. Pordesimo, J. Weiss, Food Res. Int. 37 (2004) 731.

[4] V. Sáez, A. Frías-Ferrer, J. Iniesta, J. González-García, A. Aldaz, E. Riera, Ultrason. Sonochem. 12 (2005) 59.

[5] H.-Y.Zheng, M.-Z. An, J. Alloy. Compd. 459 (2008) 548.

[6] M.D. Esclapez, V. Sáez, D. Milán-Yáñez, I. Tudela, O. Louisnard, J. González-García, Ultrason. Sonochem. 17 (2010) 1010.

[7] O. Louisnard, J. González-García, Acoustic cavitation, in: H. Feng, G. Barbosa-Canovas, J. Weiss (Eds.), Ultrasound technologies for food and bioprocessing, Springer, New York-Dordrecht-Heidelberg-London, 2011.

[8] Ratoarinoro, F. Contamine, A.M. Wilhelm, J. Berlan, H. Delmas, Ultrason. Sonochem. 2 (1995) S43.

APPENDIX B. EXPERIMENTAL PROCEDURES FOR THE ANALYSIS OF THE CHEMICAL PARAMETERS OF THE NI WATTS BATH

B.1. OVERVIEW

As indicated in Chapter 3 and shown in Chapter 4, a short experimental stability study was conducted in the Ni Watts bath irradiated at different ultrasonic powers with the aim to observe any change in the pH or the concentration of $NiSO_4.6H_2O$, $NiCl_2.6H_2O$ and H_3BO_3 that could suggest the modification of the chemical parameters of the Watts bath due to the chemical effects of ultrasound (e.g. radical formation) after being irradiated for various hours.

The present Appendix describes the different experimental procedures to monitor the chemical parameters of the Watts electrolyte used during said experimental stability study. These analytical procedures are DIBE's standard methods to analyse the concentration of $NiSO_4.6H_2O$, $NiCl_2.6H_2O$ and H_3BO_3 and the pH of the Watts bath employed in the manufacturing line [1].

B.2. EXPERIMENTAL PROCEDURES

B.2.1. TITRIMETRIC DETERMINATION OF $NiCl_2.6H_2O$

Chemicals required:

- 10% K_2CrO_4 solution.
- 0.1N (0.1M) $AgNO_3$ solution.

Procedure:

1. Pipette a 2 mL sample of the Ni plating solution into a 250 mL conical flask and dilute to 100 mL with deionised water.
2. Add 2 mL of 10% K_2CrO_4 solution and swirl to mix.
3. Titrate with 0.1N $AgNO_3$ solution until a reddish colour just develops. Record the volume used (V in mL).
4. Calculation:

$$\frac{V \text{ mL of 0.1N } AgNO_3}{2 \text{ mL of Ni Watts bath}} \times \frac{0.1 \text{ moles of } AgNO_3}{1000 \text{ ml of 0.1N } AgNO_3} \times \frac{1 \text{ mol of } NiCl_2.6H_2O}{2 \text{ mol of } AgNO_3} \times \frac{237.69 \text{ g of } NiCl_2.6H_2O}{1 \text{ mol of } NiCl_2.6H_2O} \times \frac{1000 \text{ mL Ni Watts bath}}{1 \text{ L Ni Watts bath}} = \text{content of } NiCl_2.6H_2O \text{ in g/L}$$

B.2.2. TITRIMETRIC DETERMINATION OF $NiSO_4.H_2O$

Chemicals required:

- Ammonia solution 0.88 G†.
- Murexide indicator (0.1 g of murexide to 50 g NaCl).

† Designates that it is a saturated solution of ammonia in water. The density of a saturated solution is 0.88 g cm^{-3}.

- EDTA 0.1 M solution (EDTA di-sodium salt).

Procedure:

1. Pipette a 2 mL sample of the Ni plating solution into a 250 mL conical flask and dilute to 100 mL with deionised water.
2. Transfer flask to the fume cupboard, add 20 mL of the ammonia solution and swirl to mix.
3. Using a spatula, add a drop size quantity of murexide indicator to the flask and mix thoroughly.
4. Titrate with 0.1 M EDTA to a violet/blue end point. Record the volume used (V in mL).
5. Calculation:

$$\frac{V \text{ mL of 0.1M EDTA}}{2 \text{ mL of Ni Watts bath}} \times \frac{0.1 \text{ moles of EDTA}}{1000 \text{ ml of 0.1M EDTA}} \times \frac{1 \text{ mol of } Ni^{2+}}{1 \text{ mol of EDTA}} \times \frac{1 \text{ mol of } NiSO_4.6H_2O}{1 \text{ mol of } Ni^{2+}} \times$$

$$\frac{262.85 \text{ g of } NiSO_4.6H_2O}{1 \text{ mol of } NiSO_4.6H_2O} \times \frac{1000 \text{ mL Ni Watts bath}}{1 \text{ L Ni Watts bath}} - \text{content of } NiCl_2.6H_2O \text{ in g/L} \times$$

$$\frac{1 \text{ mol of } NiCl_2.6H_2O}{237.69 \text{ g of } NiCl_2.6H_2O} \times \frac{262.85 \text{ g of } NiSO_4.6H_2O}{1 \text{ mol of } NiSO_4.6H_2O} = \text{content of } NiSO_4.6H_2O \text{ in g/L}$$

B.2.3. TITRIMETRIC DETERMINATION OF H_3BO_3

Chemicals required:

- Analysis solution: to 300 mL of glycerol, add 30 g of sodium citrate and make up to 500 mL with deionised water. Stir until completely dissolved.
- Phenolphthalein solution: 1 g of phenolphthalein in 100 mL of methanol.

Procedure:

1. Pipette a 1 mL sample of the Ni plating solution into a 250 mL conical flask.
2. Add 25 mL of Boric Acid Mixture, 8 drops of Phenolphthalein and swirl to mix.
3. Swirl the flask continuously whilst titrating with 0.1N Sodium Hydroxide to a blue-pink end-point. Record the volume used (V in mL).
4. Calculation:

$$\frac{V \text{ mL of 0.1N NaOH}}{1 \text{ mL of Ni Watts bath}} \times \frac{0.1 \text{ moles of NaOH}}{1000 \text{ mL of 0.1N NaOH}} \times \frac{1 \text{ mol of } H_3BO_3}{1 \text{ mol of NaOH}} \times \frac{61.8 \text{ g of } H_3BO_3}{1 \text{ mol of } H_3BO_3} \times$$

$$\frac{1000 \text{ mL Ni Watts bath}}{1 \text{ L Ni Watts bath}} = \text{content of } H_3BO_3 \text{ in g/L}$$

B.2.4. Determination of pH

Equipment required:

- HI-8424 pH meter supplied by Hanna Instruments.

Procedures:

1. Submerge the tip of the electrode and the temperature probe four centimetres into the sample to be tested. The value displayed in the screen, once it stabilizes after 30-60 seconds, is the pH.

B.3. References

[1] C. Tratt, Laboratory Instruction 704, Daido Industrial Bearings Europe, 2011.

APPENDIX D. EXPERIMENTAL PROCEDURES FOR GRINDING AND POLISHING RESIN MOUNTS CONTAINING CU SAMPLES WITH ELECTRODEPOSITED COATINGS

C.1. OVERVIEW

The present Appendix describes the procedures followed to grind and polish resin mounts containing all of the different samples that were characterised by different methods (optical microscope imaging, microhardness tests, FEG-SEM) during the present PhD project. These procedures were developed in-house, and are routinely used internally at the R&D department in Daido Metal Europe for evaluating different properties of electroplated coatings.

C.2. EXPERIMENTAL PROCEDURES

C.2.1. PROCEDURE FOR GRINDING AND POLISHING MOUNTS WITH NI-COATED SAMPLES

The equipment used for grinding and polishing mounts with Ni-coated samples was:

- 20DVT semi-auto polishing machine (Met Prep Ltd)
- SiC grinding cloths: P120, P240, P400 and P1200 (Struers Ltd)
- Polishing cloths: MD-Plan, MD-Dac, MD-Chem (Struers Ltd)
- Water-based diamond suspensions: 9 μm, 3 μm and Op-Chem (Met Prep Ltd)

The next table describes all the parameters of the different grinding and polishing stages of the procedure:

	Time (s)	Cloth disc	Rotation speed (RPM)	Force (N)	Polishing media
Grinding	120	P120	300	30	Water
	120	P240	300	30	Water
	60	P400	300	25	Water
	60	P1200	300	25	Water
Polishing	180	MD-Plan	150	30	9 μm diamond suspension
	240	MD-Dac	150	25	3 μm diamond suspension
	120	MD-Chem	150	15	OP-Chem

C.2.2. PROCEDURE FOR GRINDING AND POLISHING MOUNTS WITH NI-COATED SAMPLES AND A SN-CU OVERLAY ON TOP

The equipment used for grinding and polishing mounts with Ni-coated samples with a Sn-Cu overlay was:

- 20DVT semi-auto polishing machine (Met Prep Ltd)

- SiC grinding cloths: P240, P500 and P1200 (Struers Ltd)
- Polishing cloths: MD-Plan, MD-Mol, MD-Nap and MD-Chem (Struers Ltd)
- Water-based diamond suspensions: 9 μm, 3 μm and Op-Chem (Met Prep Ltd)

The next table describes all the parameters of the different grinding and polishing stages of the procedure:

	Time (s)	Cloth disc	Rotation speed (RPM)	Force (N)	Polishing media
Grinding	60	P240	300	30	Water
	60	P500	300	30	Water
	60	P1200	300	30	Water
Polishing	150	MD-Plan	150	35	9 μm diamond suspension
	150	MD-Mol	150	30	3 μm diamond suspension
	600	MD-Nap	150	10	1 μm diamond suspension
	120	MD-Chem	150	20	OP-Chem

APPENDIX D. EXPERIMENTAL PROCEDURES FOR CONDUCTING ADHESION TESTS

D.1. OVERVIEW

As indicated in Chapter 3 and shown in Chapter 7, a study of adhesion performance of selected Ni-based coatings (Ni coatings deposited under mechanical agitation at 300 rpm and Ni/WS_2 composite coatings electrodeposited under ultrasound at 0.180 W/cm^3) acting as diffusion barrier layers was performed.

The present Appendix describes the procedure [1] to carry out these tests. This procedure was developed in-house, and is routinely used internally at the R&D department in Daido Metal Europe for new coating developments.

D.2. EXPERIMENTAL PROCEDURES

D.2.1. PROCEDURE FOR PREPARING ADHESION TEST SAMPLES

1. Cut test samples in pieces with sides measuring at least 1.5 cm long and remove all the burs.
2. Use 500grit polishing paper to roughen the test face of the test dollies.
3. Clean the test samples and dollies in an ultrasonic bath with Isopropyl alcohol (IPA) for 10 minutes.
4. Pre-heat the test samples and dollies in an oven at 150 °C for 10 minutes to evaporate traces of IPA.
5. After removing the test samples and dollies from the oven, spread a micro-spatula full of DenaTite powdered glue over the test sample. Put the test samples back in the oven for another 10 minutes at 150°C to allow the glue to melt and to reduce the size of air-pockets in the melted glue.

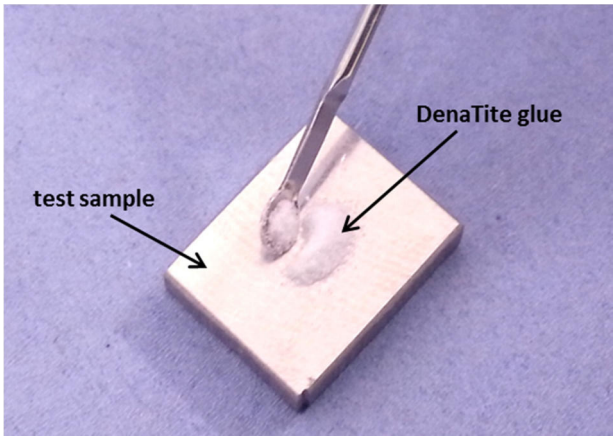

Figure D.1. Image showing where the DenaTite glue is spread over the surface of the test sample.

6. Remove the test samples from the oven one-by-one and place a dolly over the melted glue, make sure that there are no large air pockets visible in the melted glue. Put the assembled test sample and dolly in the sample fixture shown below and tighten the two fly-nuts with a moderate force (melted glue will ooze out around the dolly).

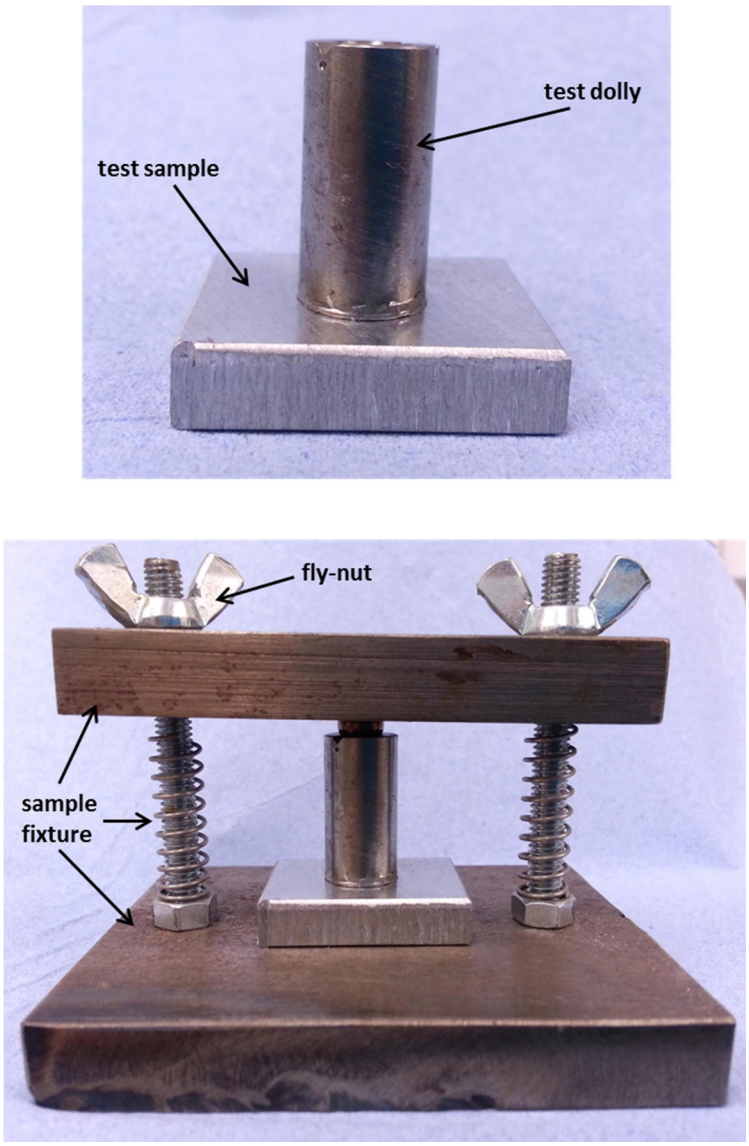

Figure D.2. Image showing the assembled test sample and dolly and the sample fixture.

7. Put the whole sample fixture back in the oven at 130 °C for 15 hours to cure the bonding glue.
8. Take the sample fixture out of the oven and leave it to cool down at room temperature. Once cool, take the assembled test sample and dolly out of the sample fixture and gently remove the excess glue and the coating from around the dolly right down to the substrate with a de-burring drill tool.

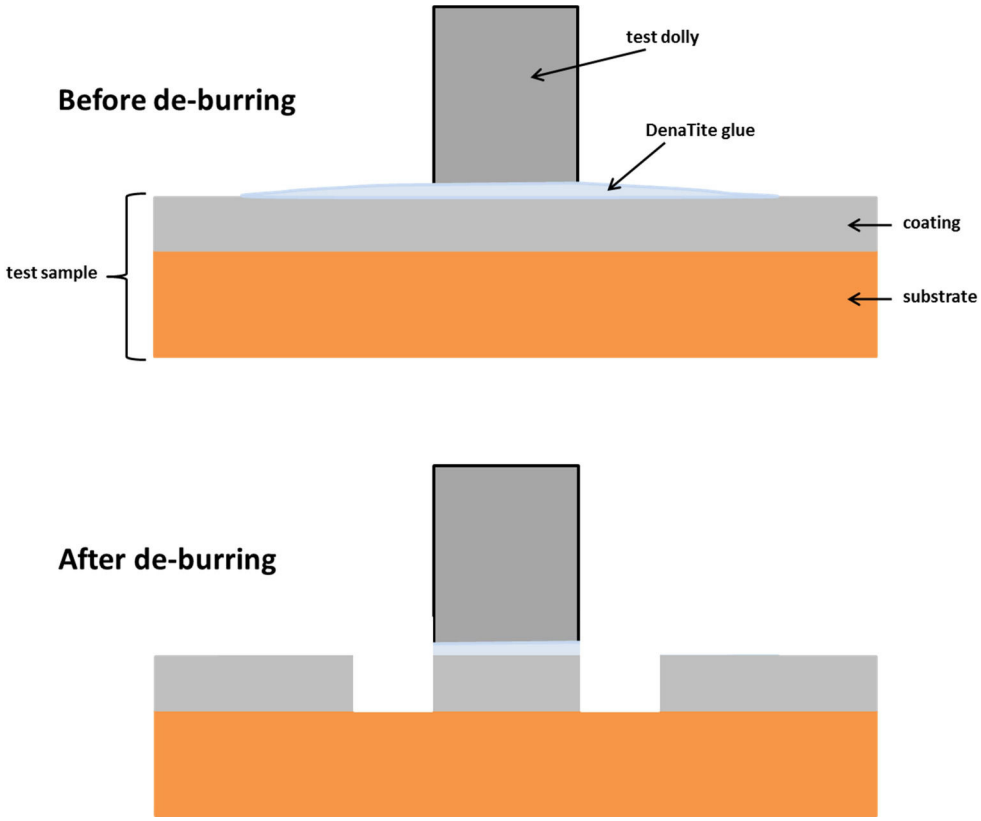

Figure D.3. Diagram showing the cross-section of a assembled test sample and dolly before and after de-burring once the DenaTite glue is cured.

D.2.2. PROCEDURE TO PERFORM PULL TEST

1. Mount the assembled test sample and dolly in the housing, making sure that the test sample is mounted flat in the housing. Fix the housing with the base of the Hounsfield Tensile test machine. Use one end of a M6 stud to screw into the dolly attached to the test sample. The other end of the stud is screwed into a spigot which is then attached with the moving end of the tensile test machine.

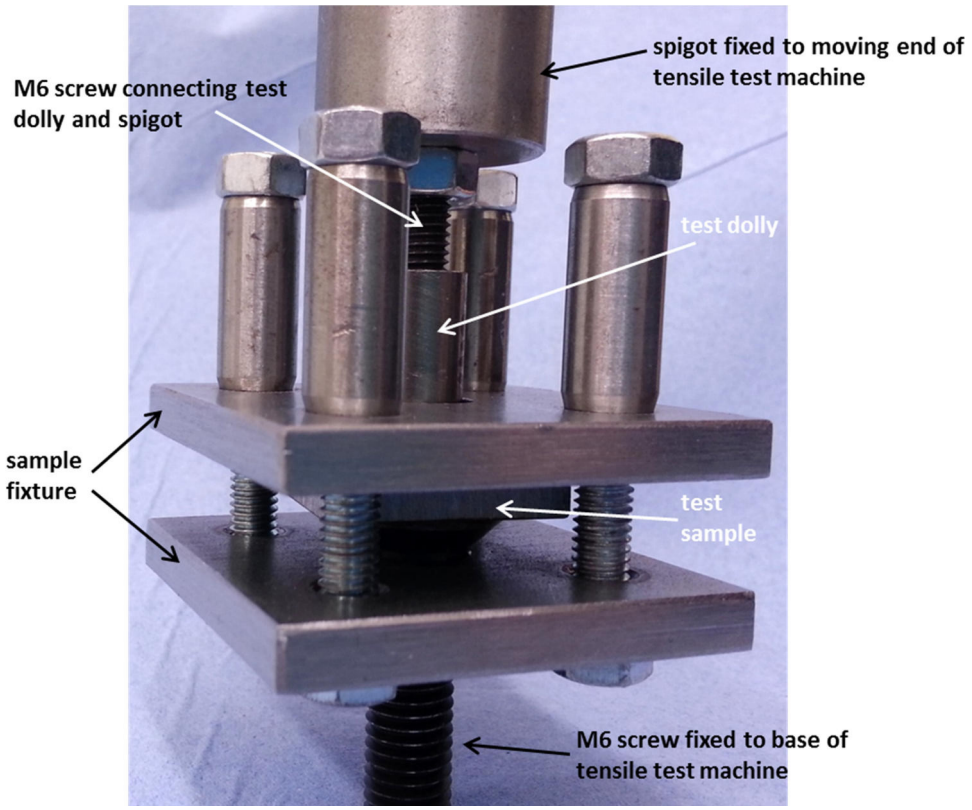

Figure D.4. Image showing the assembled test sample and dolly fixed in the housing that is then connected to the Hounsfield 5000 tensile test machine before the start of the bonding test.

2. ZERO the displacement and force reading on the test machine scale, and then START the test. Now the moving end of the machine will start to pull away from the housing. The pulling displacement is 3mm/minute.

   The machine will stop when the dolly is snapped away from the sample showing the glue or coating failure. The snapped Load reading will be displayed in the screen.

3. Calculate the failure stress (MPa or N/mm^2) by divide the load reading (N) by the area of the dolly (mm^2).

D.3. REFERENCES

[1] M. Pal, Laboratory Instruction EIS-016, Daido Metal EHQ R&D, 2012.

APPENDIX E. DISSEMINATION OF RESULTS

One patent has been recently filed in Great Britain as a result of the research here presented. The patent deals with the production of bearings with improved interlayers:

- I. Tudela, Y. Zhang, M. Pal, A.J. Cobley, G. Burmistroviene, T.J. Mason, Ian Kerr, A plain bearing with improved composite interlayer, Patent Application 1411143.9, 2014.

An invited review paper prepared during the writing stage of the thesis has been published in Surface & Coatings Technology. This review paper is focused on the electrodeposition of metal-based composite coatings with embedded particles under ultrasound:

- I. Tudela, Y. Zhang, M. Pal, I. Kerr, A.J. Cobley, Ultrasound-assisted electrodeposition of composite coatings with particles, Surf. Coat. Technol. 259 (2014) 363-373.

A research paper focused on the effect of ultrasound on the electrodeposition of thin Ni coatings based on the results and discussion has also been recently published in Surface & Coatings Technology:

- I. Tudela, Y. Zhang, M. Pal, I. Kerr, T.J. Mason, A.J. Cobley, Ultrasound-assisted electrodeposition of nickel: Effect of ultrasonic power on the characteristics of thin coatings, Surf. Coat. Technol. 264 (2015) 49-59.

And another two papers have been submitted. These two papers are focused on the electrodeposition and tribological performance of the novel Ni-based composite coatings with lubricant particles developed during the present PhD project:

- I. Tudela, Y. Zhang, M. Pal, I. Kerr, A.J. Cobley, Ultrasound-assisted electrodeposition of thin Ni-based composite coatings with soft particles, submitted to Surface & Coatings Technology.
- I. Tudela, Y. Zhang, M. Pal, I. Kerr, A.J. Cobley, Preliminary study of the tribological performance of novel nickel-based composite coatings with lubricant particles, submitted to Wear.

The results and discussions contained in this thesis have also been disseminated in the next conferences:

- I. Tudela, Yi Zhang, Madan Pal, Ian Kerr, A.J. Cobley, Sonoelectrodeposition of novel thin nickel-based composite coatings with lubricant particles, Electrochem 2014, Loughborough (United Kingdom), September 7th – 9th, 2014.
- I. Tudela, Yi Zhang, Madan Pal, Ian Kerr, A.J. Cobley, Initial evaluation of the tribological performance of novel nickel-based composite coatings with lubricant particles, 6th UK-China Symposium on Tribology, Southampton (United Kingdom), August 31st – September 2nd, 2014.
- I. Tudela, A.J. Cobley, T.J. Mason, Ultrasound-assisted electrodeposition of nickel from a Watts bath: Effects of ultrasonic power on the structure and mechanical properties of thin deposits, Electrochem 2012, Dublin (Ireland), September 2nd – 4th, 2012.